In presenting the dissertation as a partial fulfillment of the requirements for an advanced degree from the Georgia Institute of Technology, I agree that the Library of the Institute shall make it available for inspection and circulation in accordance with its regulations governing materials of this type. I agree that permission to copy from, or to publish from, this dissertation may be granted by the professor under whose direction it was written, or, in his absence, by the Dean of the Graduate Division when such copying or publication is solely for scholarly purposes and does not involve potential financial gain. It is understood that any copying from, or publication of, this dissertation which involves potential financial gain will not be allowed without written permission.

James D. Wright, Jr.

3/17/65
b

A STUDY OF CLUTCHES FOR USE IN A CLUTCH-OPERATED POWER SCREW ACTUATOR FOR SPACE APPLICATIONS

A THESIS

Presented to

The Faculty of the Graduate Division

by

James Glynn Wright, Jr.

In Partial Fulfillment

of the Requirements for the Degree

Doctor of Philosophy

in the School of Mechanical Engineering

Georgia Institute of Technology

February, 1968

A STUDY OF CLUTCHES FOR USE IN A CLUTCH-OPERATED

POWER SCREW ACTUATOR FOR SPACE APPLICATIONS

Approved:

Chairman

Date approved by Chairman: 3-6-68

ACKNOWLEDGMENTS

The author dedicates this thesis to his wife, Odessa, whose love, encouragement, and sacrifices made the attainment of this goal possible.

To Dr. Eugene Harrison, faculty advisor, the author expresses sincere appreciation for his encouragement, advice, and interest throughout the various phases of the work. It was through Dr. Harrison's efforts that the project was begun and the necessary financial aid was made available.

The author also wishes to thank the National Aeronautics and Space Administration for the financial assistance which made this work possible. Special thanks are extended to Messrs. Mike Kalange, Jim Smith, and Charles Cornelius of the NASA Astrionics Laboratory, Marshall Space Flight Center, Huntsville, Alabama, for their cooperation and help in several stages of the project work.

Thanks also to the Curtiss-Wright Corporation and its representative, Mr. Gabriel, for their aid in setting up the actuator tests herein described.

Three fellow students, Bob Anderson, Craig Depken, and Bill Jones, are also deserving of thanks for the work they did in the initial phase of the project. The efforts of many members of the staff of the School of Mechanical Engineering helped to make the author's stay at Georgia Tech a pleasant one. Notable among these are Mrs. Whitt and Mr. Doyal. Miss Wright and Professor Foster were also very helpful. The author also wishes to thank Mr. Cavalli, Mr. Davis, Mrs. Campbell, Mr. Bannister,

Mr. Collins, Mr. Kiebel, and Mr. Stokes.

A word of thanks is due to Mr. Fred Dixon of the Georgia Tech Engineering Experiment Station for his help in solving many problems related to analog computer hardware.

The constructive comments and time given by the members of the thesis committee, Dr. S. L. Dickerson and Dr. R. P. Webb, are gratefully acknowledged.

Finally, the author wishes to express his deepest gratitude to his parents for guidance in his early life and their never ending faith and encouragement.

TABLE OF CONTENTS

Appendix Page

LIST OF TABLES

LIST OF ILLUSTRATIONS

Figure Page

Clutch-Actuator Simulation Data
(8 in./sec. Actuation Rate)

Magnetic-Particle Clutch-Actuator

Friction-Disc Clutch-Actuator

Figure Page

Figure Page

Figure Page

Figure Page

Figure Page

NOMENCLATURE

a_o, a_1, a_2, a_3, a_4	Constant coefficients defined on p. 36
a	Constant specifying deadband in nonlinear characteristic for a wrap-spring clutch
A_1	Amplitude of sinusoidal reference signal in analog computer circuit
A_2	Magnitude of step reference signal in analog computer circuit
b_o, b_1, b_2, b_3, b_4	Constant coefficients defined on p. 103
b	Rotary viscous damping coefficient
b_a	Lumped rotary viscous friction of actuator drive train
b_e	Equivalent lumped viscous friction of engine gimbal referred to the actuator output
b_{vs}	Lumped viscous friction of vehicle structure at the actuator-to-vehicle attachment point
b(E)	Imaginary part of describing function, K_{eq}
C	Capacitance
C_2	Rate feedback coefficient
$C_{2'}$	10 C_2. Potentiometer setting
d_o, d_1, d_2, d_3, d_4	Constant coefficients defined on p. 36
d	Constant specifying hysteresis in nonlinear characteristic for a wrap-spring clutch
db	Decibels
DB	One-half of total engine gimbal system position deadband
DB'	$DB + DB_{\alpha}$. Effective deadband
DB_s	Distance required to decelerate the engine mass to rest from some initial velocity

DB_{TD}	Deadband required because of brake engagement time delay
$DB_{\dot{\alpha}}$	$C_2\dot{\alpha}$. Contribution to system deadband due to rate feedback
e	2.71828. Constant
e	Voltage
E	Amplitude of sinusoidal error assumed in the development of the describing function
F	Disturbing force
F_d	Equivalent force due to thrust vector offset referred to the actuator output
g(E)	Real part of describing function, K_{eq}
G_1, G_2, G_3	Transfer functions defined on p. 28
G_4, G_5	Transfer functions defined on pp. 102 and 103
G_{10}, G_{12}	Transfer functions defined on pp. 37 and 38
G	Constant. Gain in analog circuit of Figure 35, as discussed on p. 93
$G_I, G_{II}, G_{III}, G_{IV}$	Transfer functions defined on pp. 38 and 39
H	Equivalent hysteresis
IM	Imaginary part of $-1/K_{eq}(E)$
J	Moment of inertia
J_a	Lumped moment of inertia of actuator drive train and screw
k	Constant
K_1, K_2, K_3	Constants defined on p. 28
K	Gain in proportional clutch system
K_a	Actuator stiffness
K_c	Slope of torque build-up characteristic in Chapter VI

K_e	$\frac{K_a K_{es} K_{vs}}{K_a K_{vs} + K_{vs} K_{es} + K_{es} K_a}$
K_{eq}	$g(E) + j\, b(E)$. Describing function
K_{es}	Structural stiffness at the actuator-to-engine attachment point
K_p	$\frac{K_a K_{es}}{K_a + K_{es}}$
K_{p3}	$\frac{K_{es} K_{vs}}{K_{es} + K_{vs}}$
K_{vs}	Structural stiffness at the actuator-to-vehicle attachment point
K'	R_f/R_i. Operational amplifier gain in magnetic particle clutch-actuator simulation
K''	Gain related to potentiometer setting in magnetic-particle clutch-actuator simulation
K.E.	Kinetic energy
m_o, m_1, m_2, m_3	Constant coefficients defined on p. 105
m_a	Actuator mass
m_e	Equivalent mass of gimballed engine referred to actuator output
m_s	Mass of power screw
M	Limit on output of operational amplifier
n_1, n_2	Number of teeth on input and output gears, respectively, assumed in defining effective gear ratio, N (see Figure 49).
N	$n_1 P/n_2$. Effective gear ratio between clutch output and power screw
O_2	Operational amplifier output voltage
P_d	Gearing pitch circle diameter
P	Pitch of power screw

P_d	Clutch power dissipation
$P_{d_{avg.}}$	Average clutch power dissipation
$P_{d_{max.}}$	Peak clutch power dissipation
P_o	Actuator power output
P_l	Power loss in actuator drive train
P.E.	Potential energy
R	Maximum actuation rate
R_i	Input resistor for an operational amplifier programmed as a summer
R_f	Feedback resistor for an operational amplifier programmed as a summer
$R\alpha$	Actuator output reference position
$R\alpha_r$	"Real" actuator output reference position
r	Moment arm of the actuator force about the gimbal point
RE	Real part of $-1/K_{eq}(E)$
s	Laplace operator
t	Time
t_b	Torque build-up time assumed in torque characteristic of Chapter VI
t_c	Computer time
t_o	Transport delay time
T_m,TM	Maximum clutch torque capability
T_v	Drag torque due to viscous friction
TBU	Torque build-up
TD	Torque time delay

TQ	Torque
TQ_{ss}	Steady-state torque
TQD	Torque decay
U(t)	Unit step function
$\alpha, \dot{\alpha}$	Actuator extension and extension rate, respectively
α_i	"Ideal" actuator extension as defined on p. 81
$\dot{\alpha}_i, \ddot{\alpha}_i$	Extension rate and acceleration, respectively, for the "ideal" actuator
α_r	"Real" actuator extension as defined on p. 81
$\dot{\alpha}_r$	Extension rate for the "real" actuator
β_a	Displacement of the actuator-to-engine attachment point
$\beta_e, \dot{\beta}_e, \ddot{\beta}_e$	Displacement, velocity, and acceleration, respectively, of the rocket engine
$\dot{\beta}_{e_{max.}}$	Maximum engine rate
β_i	$\beta_s + \alpha_i$. Variable used in derivation of equations of motion
$\beta_s, \dot{\beta}_s, \ddot{\beta}_s$	Displacement, velocity and acceleration, respectively, of the actuator-to-vehicle attachment point
Δ	$K_a \Delta_1$
Δ_1	Determinant defined by Equation (3.24)
$\Delta\alpha_r$	Variation of α_r about a given locked-actuator value
$\Delta\beta_e$	Variation of β_e about a given locked-actuator value
$\Delta\beta_{e_d}$	Engine displacement occurring after the onset of brake torque build-up while decelerating the load to rest
ε	Control loop error
ε'	$R\alpha - \alpha$

ζ_a	Actuator damping ratio
ζ_e	Engine damping ratio
$\theta, \dot{\theta}, \ddot{\theta}$	Clutch output position, velocity and acceleration, respectively
$\dot{\theta}_{max.}$	Maximum clutch output rate
$\dot{\theta}_i$	Rate of clutch input member
τ	Time constant
ω	Frequency, rad./sec.
ω_{na}	Natural frequency of actuator with rocket engine fixed
ω_{ne}	Natural frequency of rocket engine in simple model of Chapter VI

SUMMARY

The primary objective of the reported research was to conduct a study of clutch-operated power screw actuators to determine their suitability for rocket engine gimbal control functions. A secondary objective was to present methods for analyzing engine gimbal control systems incorporating actuators of that type.

Initially, a survey of available clutch-types was made to determine their qualifications relative to space applications. Comparison of the characteristics of the various clutch-types resulted in the selection of three that have the greatest potential for employment in engine gimbal systems: magnetic-particle, friction-disc, and wrap-spring. Each of these clutch-types has qualifications that are desirable for the intended application. Generally, the shortcomings of one type are the strong points of another. A study of system dynamics under the influence of the three different clutch-types was deemed necessary for further comparison.

During the first stage of the dynamic study, a four degree-of-freedom mathematical model was developed to simulate an engine gimbal system employing clutch-operated power screw actuators. Two of the four degrees of freedom resulted from the inclusion of springs in the model to account for structural compliances at the actuator-to-vehicle and actuator-to-engine attachment points. The other two consisted of clutch output motion and engine displacement. Actuation requirements and characteristics for an RL-10 rocket engine gimbal system were selected

as typical requirements in deriving the model. A significant part of the model-development task was the determination of suitable clutch torque characteristics for the clutches of interest.

An additional phase of the dynamic study consisted of a describing function analysis of the engine gimbal system to examine its stability characteristics. That investigation resulted in the choice of actuator extension and actuation rate as the position and rate feedback combination that yielded the best dynamic performance of those considered.

Equations of motion derived from the mathematical model were implemented on an analog computer for a more complete analysis of the engine gimbal system. Each of the three clutch-types selected at the beginning of the study was "installed" in the actuation system to examine its merits relative to the other types. Simulation results showed the magnetic-particle clutch-type to be superior dynamically to the other two types, although they are limited to low power applications (a few hundred watts). The friction-disc clutch-type yielded a smooth response and was quite acceptable, althcugh the necessity for ON-OFF operation imposed some restrictions. The wrap-spring clutch-type was not as desirable dynamically as the other two types because of the oscillatory response attributable to the very rapid torque build-up which characterizes that clutch-type. Cther characteristics of the wrap-spring clutch, however, such as very low torque-to-weight and torque-to-inertia ratios, warrant further investigation of the device for space usage. The conclusion was reached that clutch-operated power screw actuators can provide acceptable dynamic response at low actuation

rates (approximately 4 in./sec. or slower).

Hardware tests were conducted on an existing wrap-spring clutch-actuator to provide a check on the clutch model assumed in the analog computer simulation. Good correlation of simulation and test data was obtained.

Finally, analytical techniques were developed for use in the design of engine gimbal actuation systems incorporating clutch-operated actuators. The most important results were methods for predicting system deadband requirements.

CHAPTER I

INTRODUCTION AND HISTORICAL BACKGROUND

Statement of Intent

Although there have been numerous applications of clutches in automatic flight control systems, little has been published relating techniques for analysis of such systems. This work is concerned with a study of clutches for use in clutch-operated power screw actuators for space applications. The objectives of the study are to determine the suitability of clutch-operated actuators for engine gimbal systems and to present analysis techniques for these systems. Included in the reported results are:

1. A summary and comparison of various clutch-types relative to space application.

2. Development of a mathematical model for an engine gimbal system employing clutch-operated actuators.

3. Analog simulation of the model and performance analysis results.

4. Actuator hardware test results.

5. Analytical design techniques.

Background

The engine gimbal technique for obtaining thrust vector control is currently used on large, liquid-fueled boosters and on some of the upper-stage vehicles, such as the Service Module on the Saturn V of the Apollo project. The concept is well known, is simple, and utilizes a small number of reliable components. This technique may be explained by Figure 1 which depicts the use of an engine gimbal system to achieve attitude control. The control force available is engine thrust times the sine of the gimbal angle, and the control moment is control force times the moment arm from the gimbal point to the vehicle center of gravity. In an actual installation another actuator would be present, and the two would maintain the vehicle attitude commanded by the guidance and flight control system. On some of the larger booster vehicles several gimballed engines are used to develop the required thrust (Saturn V S-IC has five engines--four gimballed and one fixed); two actuators for each engine are controlled as part of a coordinated team by the guidance system.

Most of the control servoactuators used to date have been hydraulically powered, especially those used on the larger boosters whose extreme actuation requirements make the use of hydraulics a necessity. In engine gimbal systems on upper stage vehicles designed for deep-space penetration, however, there is a tendency toward the use of electro-mechanical actuators. Although hydraulic servoactuators have performed quite well in many attitude-control applications, their reliability for deep space functions is questionable. For example, the extremes of temperature and vacuum of deep space require that special

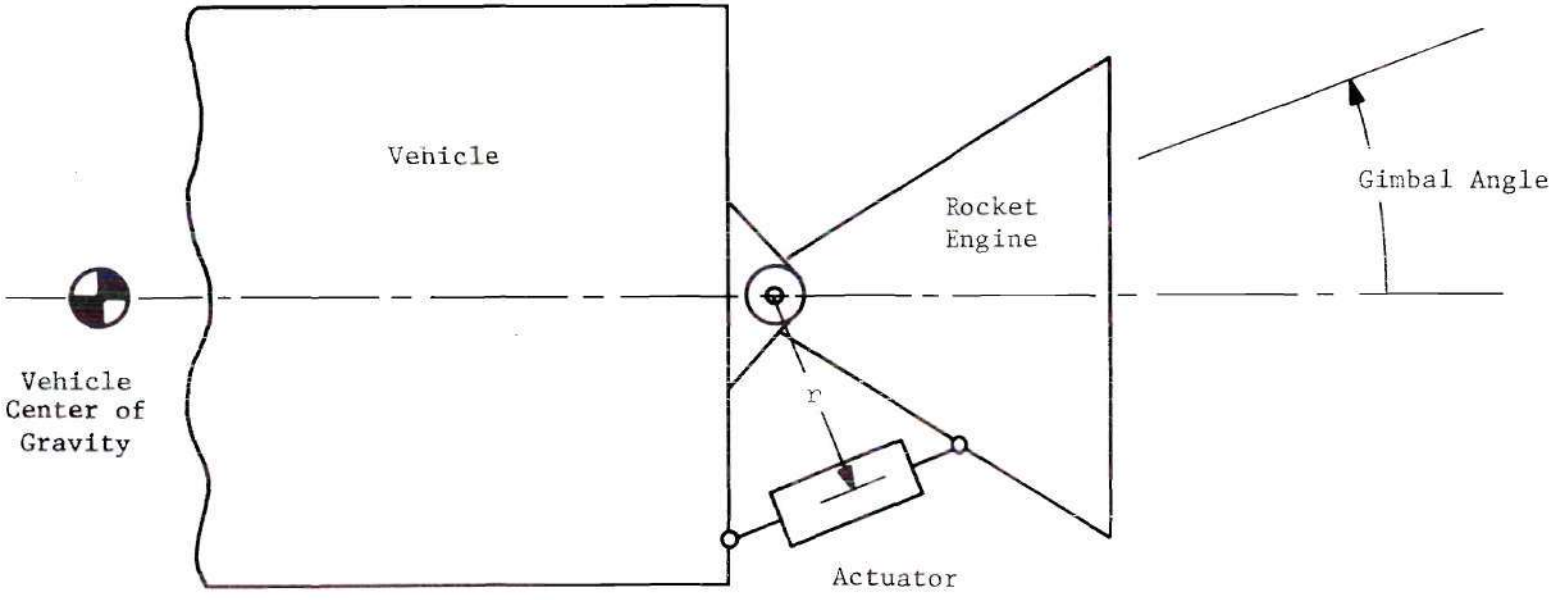

Figure 1. Schematic Representation of an Engine Gimbal System.

attention be given to factors such as the maintenance of suitable fluid viscosities and the prevention of leaks during operating as well as storage periods.

Clutch-Operated Actuator

The clutch-operated actuator under consideration is a descendant of earlier electro-mechanical types which employed only an electric motor, gear train, and power screw. Such devices have functioned reliably for several years in many military as well as commercial applications. In operation the response of this system was limited because the motor had to overcome its own inertia in responding to a new command. In addition, to reverse direction, a reversal of motor rotation was required. The addition of a system of clutches as shown in Figure 2 yields a device with a much-improved response. When the actuator is armed, the motor runs continuously at full speed in one direction, with one or the other of the clutches being caused to engage as required for extension or retraction. A brake is sometimes used to maintain a particular position. Operation of the clutches and brake in an optimum manner is accomplished by the control loop in which the device functions. The limiting factors as far as the response of the actuator is concerned are the engagement and disengagement rates for the clutches; however, the state-of-the-art in clutch manufacture has reached a point where very short engagement and disengagement times are attainable.

In recent years ball screws have been included in actuator designs because of their high efficiency and low hysteresis. A low hysteresis characteristic is important in designing for good frequency response capability.

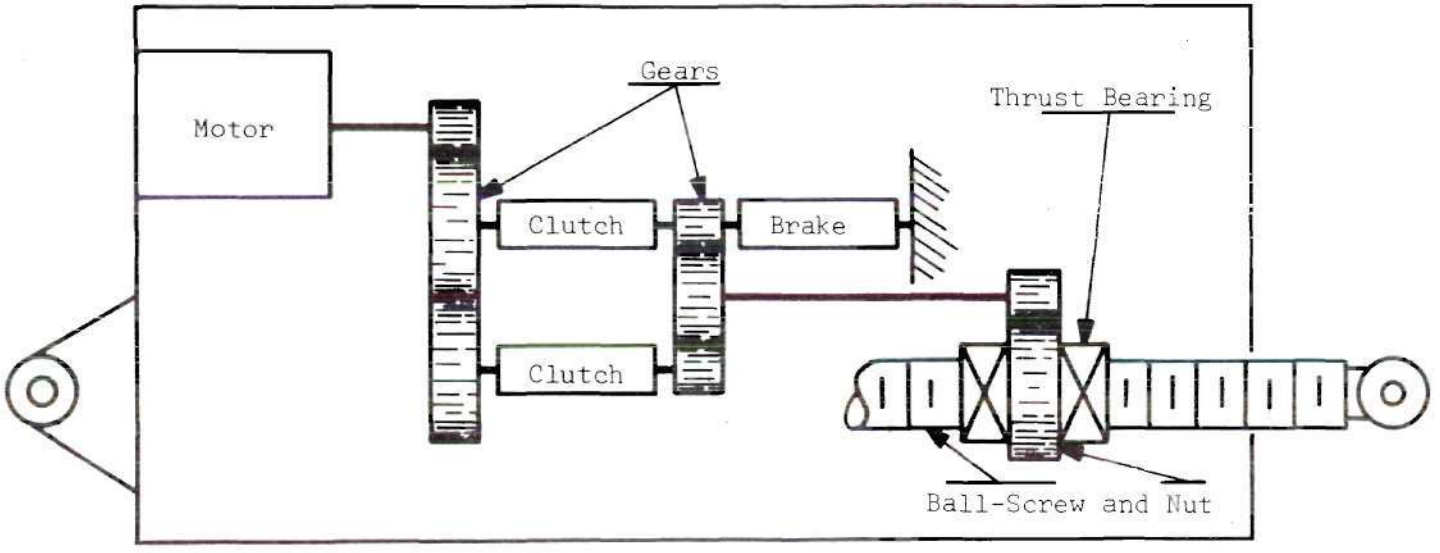

Figure 2. Conceptual Schematic of a Clutch-Operated Power Screw Actuator

Clutch-operated electro-mechanical actuators appear promising as simple, relatively rugged, reliable, high-response devices for deep-space servo functions.

Continuous versus ON-OFF Control. Two types of clutch systems may be employed for control of a servoactuator--those designed for continuous-control and those intended for strictly ON-OFF operation. Clutches in the former system are always engaged to some degree as long as the actuator is armed. This type of operation alleviates two disadvantages of clutch actuators:

1. the time delay in torque build-up which is experienced in engaging a clutch from its unexcited state, and

2. the nonlinearity associated with most clutches.

These disadvantages are depicted graphically in Figures 3 and 4. Linear operation may be achieved as shown in Figure 5, where a composite torque-clutch excitation characteristic has been derived from those for the individual clutches in the system shown in the inset. This technique is similar to that employed in push-pull servo amplifiers. Since the outputs of the two clutches are summed, the nonlinearities cancel, resulting in the linear composite curve shown. By maintaining a bias of clutch excitation, not only is linear operation achieved, but the clutches are in a state of partial engagement so that the time delay on torque buildup is no longer a problem.

However, there are other problems associated with the continuous-control technique. One of these, clutch heating due to the continuous dissipation of power, even under quiescent conditions, requires special attention in the design of space systems because of the reduction in

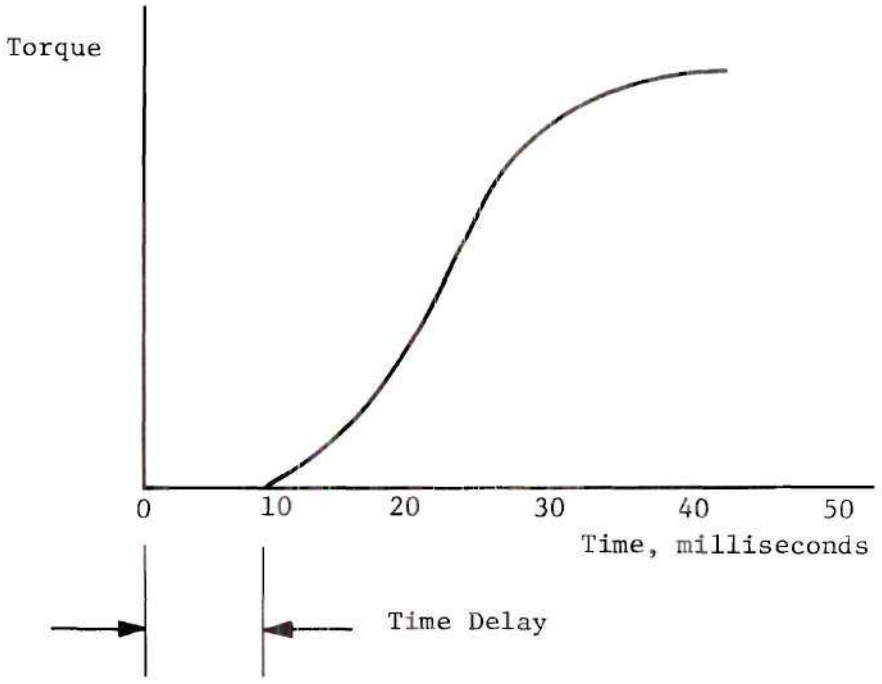

Figure 3. Typical Clutch Response Characteristic

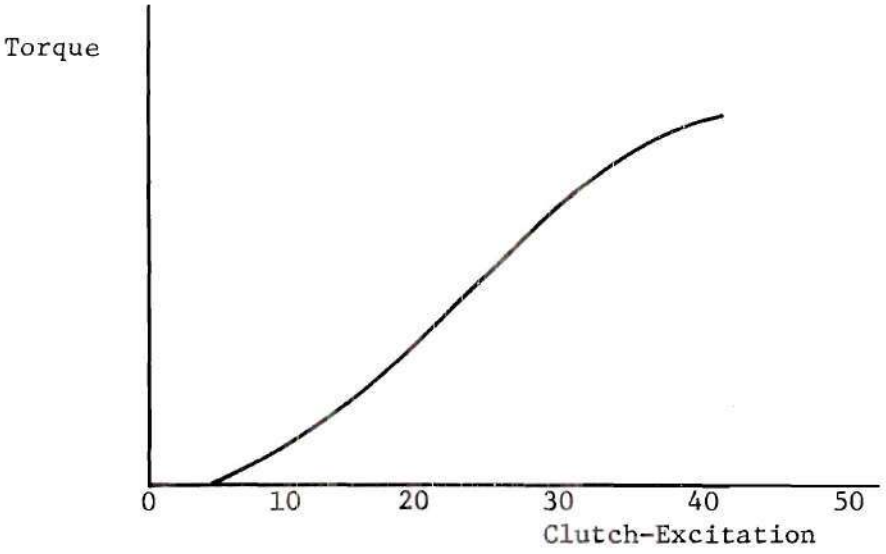

Figure 4. Typical Torque - Clutch Excitation Characteristic

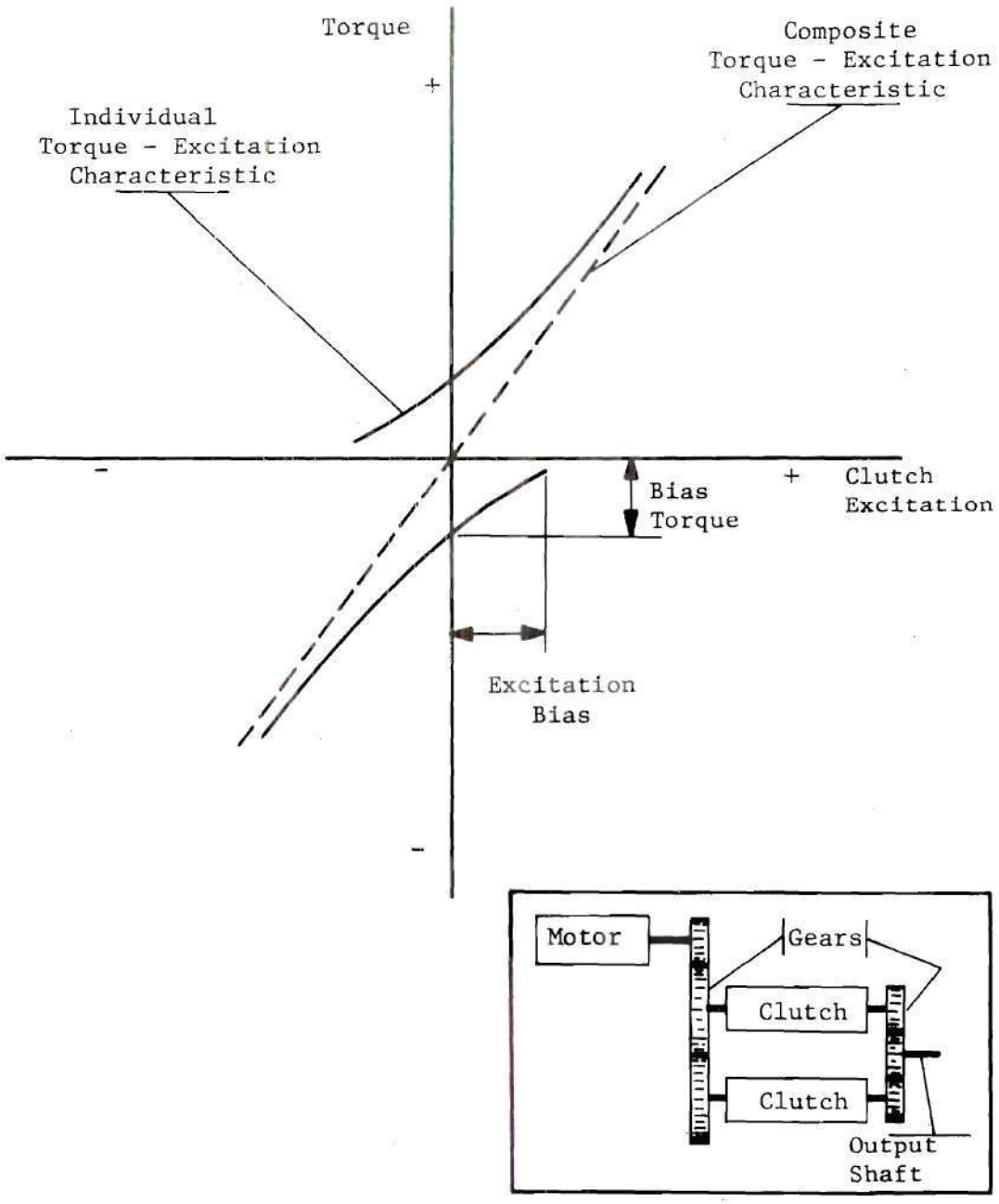

Figure 5. Composite Torque - Clutch Excitation Characteristic.

heat transfer capability in a vacuum. This dissipation of power in clutches is discussed in references (1) and (2), along with some of the heat transfer problems associated with their application in space.

Another disadvantage of continuous-control is that some clutches are not suited for that mode of operation because they wear out very rapidly when subjected to such severe slip conditions; some of the more powerful clutches are therefore eliminated from consideration.

In spite of associated difficulties, the continuous-control technique has been applied in several high-performance actuators. References (3) and (4) are a technical proposal and engineering report on performance data, respectively, for an early version of an engine gimbal actuator for the Service Module on the Apollo moonship. The continuous control operation of these devices offers good frequency response and a constant force-to-clutch excitation gain--both of which are important in satisfying requirements for guidance and flight control systems as presently conceived.

The ON-OFF clutch system in contrast to the continuous system operates with clutches that are completely disengaged at times during the active operation of the actuator. Two immediately obvious disadvantages of this arrangement are those removed by the continuous-control method: clutch engagement time delay and nonlinear torque--clutch excitation characteristic. There are, however, important advantages of the ON-OFF system which may outweigh the above objections. Possible torque-to-weight ratio improvement and increased reliability are among those which may be cited.

CHAPTER II

INITIAL CLUTCH-TYPE COMPARISONS

Literature Survey Goal

This chapter reports the results of a literature survey which was made in order to gather pertinent information regarding clutch characteristics in general and information related to their application in actuation systems for use in space. Various journals and magazines were searched; a number of engineering reports covering actuator designs were found; and clutch manufacturers were contacted for literature describing their products. Reference (5) is a report presenting much of the data on clutch characteristics which was obtained from the manufacturers. It was anticipated that the survey would reveal a variety of clutch-types, many of which would be eliminated by a brief consideration, thus simplifying the overall task of recommending a clutch-type for use in a clutch-operated actuator for deep space.

Clutch Categories

Initial consideration of available clutches revealed that each type may be placed in one of three categories, the division being based on the primary mechanism whereby torque is transmitted: mechanical contact, electromagnetic flux, or fluid. A listing of the devices in each category is given in Table 1.

Table 1. Clutch Categories

Category	
I.	Mechanical Contact
	1. Friction-disc
	2. Wrap-spring
	3. Positive engagement
II.	Electromagnetic Flux
	1. Magnetic-particle
	2. Hysteresis
	3. Eddy Current
III.	Fluid
	1. Hydrostatic--piston-type
	2. Hydrodynamic--fluid coupling, torque converter.

Tests of the clutches in categories I, II, and III were conducted by Anderson, Depken, and Jones, respectively; test results and general characteristics of each clutch type may be found in references (1), (2), and (6). In addition, Anderson (1) discusses clutch heating and conduction heat transfer in a vacuum, where thermal contact conductance becomes an important consideration. Depken (2) also considers clutch heating in space, with emphasis on the radiation heat transfer mechanism.

Factors for Clutch Comparison

In order to establish a basis for comparison of the clutches listed in Table 1, a list of factors pertinent to the selection of a clutch for use in space was prepared. These factors are presented in

Table 2. No single clutch is likely to rate highest in all of these areas; rather, the requirements for a particular application will dictate which of these criteria are critical, and the designer will be forced to live with certain shortcomings in order to satisfy these requirements. There is some overlapping of the criteria in Table 2.

Initial Clutch-Type Eliminations

The method of operation and characteristics of the various clutches listed in Table 1 may be found in the references cited above. Numerous other references listed in this report also describe these devices, often in more detail. Review of the literature shows that some of the clutches listed in Table 1 may be readily discounted as far as deep space application in an engine gimbal actuator is concerned.

Fluid Clutch

One entire category--Fluid Clutches--may be eliminated. Since the object of this study is to find a suitable electro-mechanical substitute for the hydraulic actuation system, nothing would be gained by selecting another fluid-operated device.

Positive Engagement Clutch

In addition, positive engagement clutches may be eliminated, since they cannot be engaged and disengaged under load as required for the actuator application.

Eddy-Current Clutch

Another clutch-type which may be removed from further consideration is the eddy-current clutch. As pointed out in reference (7), the eddy-current device is properly classified as a clutch-coupling since

Table 2. Factors Pertinent to the Selection of a Clutch for Space Application

Item	Factor
1	Control action: Is the device more suitable for proportional or ON-OFF operation?
2	Torque-response characteristic (i) Delay time (ii) Torque build-up time (iii) Torque decay time
3	Maximum torque capability
4	Maximum operating temperature
5	Maximum operating speed
6	Duty cycle
7	Power gain; Output power ÷ control power
8	Torque-to-volume ratio
9	Torque-to-weight ratio
10	Torque-to-inertia ratio
11	Method of actuation
12	Effect of clutching on power train
13	Production of wear products which may contaminate other parts or equipment
14	Effect of space environment on clutch (i) Heat transfer reduction. (ii) Wear increased in vacuum? (iii) Welding or seizure of parts?
15	Reliability
16	Life
17	State-of-the-Art

it is not capable of non-slip operation. This clutch type offers a good speed control capability, but most applications have been in heavy-duty equipment, (7), (8). One serious drawback concerning use of the eddy-current clutch in space is the heating problem. In addition, Figure 6 which was plotted from data in references (8) and (9) shows that the eddy-current clutch has the lowest torque-to-weight ratio of any of the electromagnetic flux clutches considered.

Hysteresis Clutch

A final clutch-type which may be eliminated at this point is the hysteresis clutch. Even though this device offers very smooth operation, close torque control, and fast response when used in continuous control applications, it has the disadvantages of being bulky and heating excessively in continuous slip operation. In addition, if the magnetic coil rotates with the input member, slip rings and brushes are required, creating additional problems where space applications are desired. If the stationary coil variety is used, an additional air gap is inherent in the design, calling for a larger excitation coil or increased coil current, hence, added weight and bulk or control power. To realize a fast response capability, it is necessary to operate the clutch in continuous slip (in ON-OFF operation the hysteresis clutch torque-response is much slower than for the comparable mechanical contact clutch). Even though hysteresis clutches compared to magnetic-particle devices present no seal problems, are more linear, and exhibit smoother performance, a magnetic-particle clutch of the same torque rating, with closely equivalent sensitivity can be supplied in a much smaller and lighter package. Figure 6 shows a comparison between

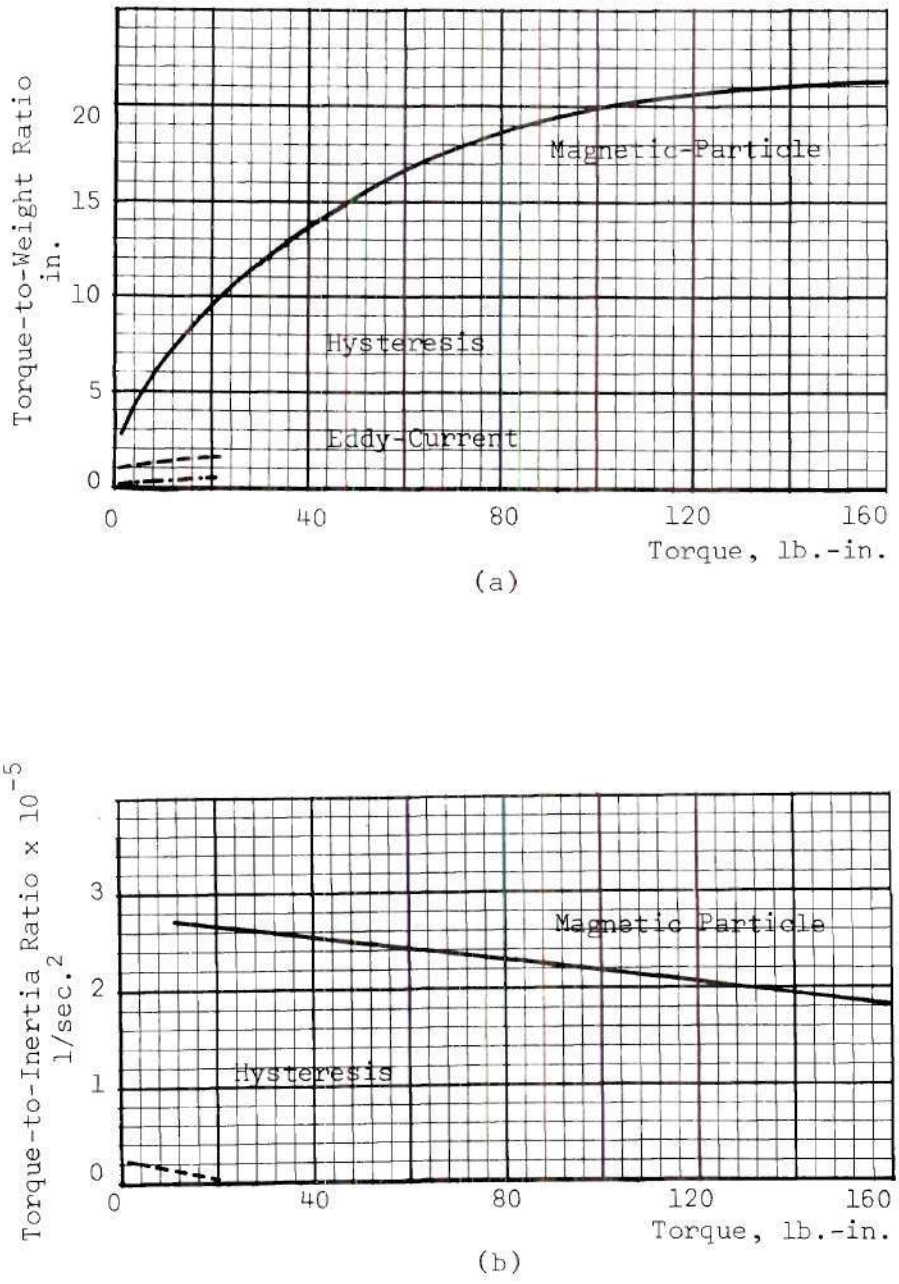

Figure 6. Comparison of Torque-to-Weight Ratio and Torque-to-Inertia Ratio for Three Electromagnetic Flux Clutches

magnetic-particle and hysteresis clutches on the basis of torque-to-weight ratio and torque-to-inertia ratio. The magnetic-particle clutch is decidedly superior in both categories. Furthermore, magnetic-particle clutches offer a much higher amplification ratio. All factors considered, the magnetic-particle clutch has more to offer for the proposed actuator application than the hysteresis clutch.

Remaining Types

With the elimination of the clutches discussed above, three clutch types remain which require serious consideration before a choice may be made: magnetic-particle, friction-disc, and wrap-spring.

Comparison of Remaining Clutch-Types

The final clutch choice depends heavily on the type of actuator control action which the spacecraft guidance and flight control system will permit: proportional (continuous) or ON-OFF. For example, if the control system cannot possibly perform acceptably with an ON-OFF system, the *magnetic-particle* clutch would be the natural choice. This device, when used in a continuous-control fashion, has a very fast response and offers a linear system with good repeatability and low hysteresis. In addition the magnetic-particle clutch has a high power gain and a high torque-to-inertia ratio, offers a small package and electrical control, and provides smooth operation with no wear in continuous slip.*

There are, however, a number of serious shortcomings of the magnetic-particle clutch which should be noted. As discussed earlier,

---

*The particles show signs of wear after many hours of operation, but over the normal duty cycle wear is insignificant.

continuous-control clutch systems have a definite heating problem because of the continuous slip operation. This condition is aggravated in engine gimbal actuation systems by the ever-present requirement for an actuator force to overcome engine disturbance torque which arises from thrust-vector offset, a condition existing in gimballed engine systems because of manufacturing tolerances. If the thrust vector is misaligned with the line through the vehicle center of gravity by a few thousandths of an inch, a disturbance torque results which must be countered by the gimbal control system. The clutches have to maintain a significant torque level at nearly 100 per cent slip, which results in rapid heating.

Another shortcoming is that the magnetic-particle clutch does not have a good path for heat conduction from its working medium to the surroundings. Since the heat is generated within the particles, which have an inherent insulating quality due to the space between particles, these clutches experience extreme internal temperatures. In space where radiation is the only readily available heat transfer mechanism, provisions must be made to remove this heat rapidly. One solution (3), (4), is to provide an artificial atmosphere about the clutches. Another approach is to raise the clutch's maximum temperature limit by improving the magnetic coil insulation. One company reports successful clutch operation at 700°F. with a Teflon-and-ceramic coated wire.

Some further shortcomings of the magnetic-particle clutch are a low power transmissibility (a few hundred watts), slip ring and brush failures in a vacuum, problems with sealing the magnetic powder, and questionable storage capability. Stationary coil models are now avail-

able which are reported to have an improved torque-to-weight ratio, so that slip ring problems may be alleviated. Sealing of the magnetic mixture has been a major problem with the magnetic-particle clutches of the past and one of the factors having most influence on clutch life. Seal failure allows the particle mixture to leak out, causing reduced torque capability, and bearing contamination leading to eventual failure. For deep-space flight, the actuator's storage capability is a factor of great importance, since the device must stand by during periods of coasting or orbital flight and perform readily when required. Settling and lumping of the particle mixture, leading to clutch binding, are possible failure modes which need examination.

In the event that ON-OFF control action can be tolerated by the spacecraft's guidance system, the choice falls between the *wrap-spring* and the *friction-disc* clutches, since the magnetic-particle device has a much slower operation than the other two in the ON-OFF mode. More important, however, is the fact that both of the mechanical contact clutches offer a chance for increasing the actuator system's reliability* compared to that for a continuous-control system employing magnetic-particle clutches. The friction-disc and the wrap-spring clutches are both simple and rugged, offer good storage capability and long life, and may be actuated by a number of means, including electrical or pneumatic (hot or cold gas).

---

*Actuator tests described in Chapter V indicated a tendency to bind in the case of the wrap-spring clutch tested. The cause was unknown, but possibly may have been due to incomplete release by one clutch before the other started its engagement. A rated-load test should be conducted to investigate reliability.

The *friction-disc* clutch is perhaps the simpler and more rugged of the two mechanical contact types. It is capable of high speeds, which permits the use of a smaller, higher-response clutch to deliver the same power as lower-speed devices. In addition, the disc clutch has negligible drag torque, an important factor when considering heat generated in the disengaged clutch.

A number of features, however, may make the friction clutch less desirable than the wrap-spring clutch. One of these features is that the torque transmitted is directly proportional to the product of coefficient of friction and normal force between the clutch plates. Variations of the coefficient of friction in a vacuum environment could drastically alter the actuator's operation. The normal force between clutch plates must be maintained by the actuating medium, so that a significant continuous power input is required while the clutch is engaged. In contrast, the wrap-spring clutch tends to maintain its own engagement once wrap-up is initiated by applying a frictional torque to the end of the spring. To insure continuous engagement during instances when the load may overrun the input and attempt to unwind the spring, it is necessary to maintain the frictional engagement torque at all times. However, the power required for the maintenance of this torque is much less than the input power for any of the other clutch-types of comparable torque capability (10).

Another undesirable feature of the friction clutch is the generation of wear products which may contaminate bearings or other spacecraft equipment. However, Anderson (11) investigated a friction clutch with a ceramic-faced disc which reduced wear and wear products to a minimum.

The unit was cycled (with output fixed) once each second for 14 hours resulting in over 50,000 cycles. The wear was reported to be only 0.0005 inches with no changes in the torque characteristic recorded at the beginning of the test. No vacuum tests were made.

The *wrap-spring* clutch has much to offer for space design. In addition to the advantages mentioned earlier, it has the highest torque-to-inertia, torque-to-volume, and torque-to-weight ratios of all the clutches investigated. Furthermore, it lays claim to the fastest ON-OFF engagement of any of the clutches considered in this study. The wrap-spring clutch also exhibits a higher power gain, i.e., output power ÷ control power, than any other clutch (10).

Some further desirable features of the wrap-spring clutch are an engagement time that is not a function of load condition, increased "gripping" with load resistance, and high power transmissibility.

Wrap-spring clutches are not without shortcomings, however. A number of problem areas, listed and discussed below, need further investigation.

1. Galling or welding of the clutch elements in a vacuum: The effect of the vacuum environment must be determined before reliability predictions can be made. It is possible that the clutch may seize when operated in a vacuum because of welding of the spring to the input shaft. Galling or fretting of the shaft, if indeed a problem at all, could render clutch performance unsatisfactory. This would appear, however, to be a problem which could be solved by the proper combination of materials in the clutch.

2. Possible heating in a vacuum due to rubbing in the clutch's disengaged configuration: Close tolerances inherent in the spring clutch may result in a drag torque which can cause serious heating in space. This problem was experienced in laboratory tests of industrial-type wrap-spring clutches (12); however, much-improved wrap-spring clutches exist in which such heating may not be a problem at all. Kaplan (13) discusses wrap-spring slip clutches.

3. Spring breakage due to clutch-engagement shock loads: Fatigue failure of the springs may occur when the spring clutch is repeatedly engaged. This is a design problem, however, and should be solved by proper attention to design details. Kaplan (14) outlines design methods for calculating the dynamic load capacity of spring clutches. Nevertheless, a testing program is necessary to insure spring reliability, since manufacturing expediences and errors often cause unexpected limiting of component life.

4. Limited speed: Centrifugal effects limit the maximum speed of wrap-spring clutches to low values. Reference (15) presents a design with a clutch speed of 1000 RPM. Slightly higher speeds may be possible.

Need for a Dynamic Study

Consideration of the clutch-types presently available resulted in the preliminary choice of three types--magnetic-particle, friction-disc, and wrap-spring--as those most suitable for use in an actuator for deep space. As discussed earlier in this chapter, each type has qualities which are desirable. However, unsatisfactory dynamic per-

formance with ON-OFF clutch-types was thought a possibility. Therefore, a computer study of the dynamics of a typical engine gimbal control system employing actuators with each of the three remaining clutch-types installed in turn was undertaken to allow a comparison of the operation in each case. Chapter IV presents the details of the computer study. Determination of a mathematical model and an analytical study are described in Chapter III.

CHAPTER III

MATHEMATICAL MODEL AND ANALYTICAL TREATMENT OF THE ENGINE GIMBAL SYSTEM

Introduction

A mathematical model for an engine gimbal system is presented, and the equations of motion which were derived from the model are introduced. In addition, analytical predictions of the performance of an engine gimbal control system employing clutch-operated actuators are presented.

In constructing the above mentioned mathematical model, characteristics and actuation requirements for the RL-10 engine were assumed. The data were contributed by the Astrionics Laboratory, Marshall Space Flight Center, Huntsville, Alabama, and are contained in Tables 5 and 6. Figures 1 and 2 depict the basic forms of gimballed engine and actuator, respectively, which were assumed throughout the work.

Mathematical Model

Figure 7 illustrates the mathematical model employed to simulate an engine gimbal actuation system embodying clutch-operated power screw actuators. Only one actuator is shown in the model, since the motion due to each actuator is, for all practical purposes, independent. The inclusion of spring rates K_a, K_{vs}, and K_{es} to represent the structural stiffness of the actuator and its attachment points on the vehicle and engine, respectively, resulted in the four degree-of-freedom model shown.

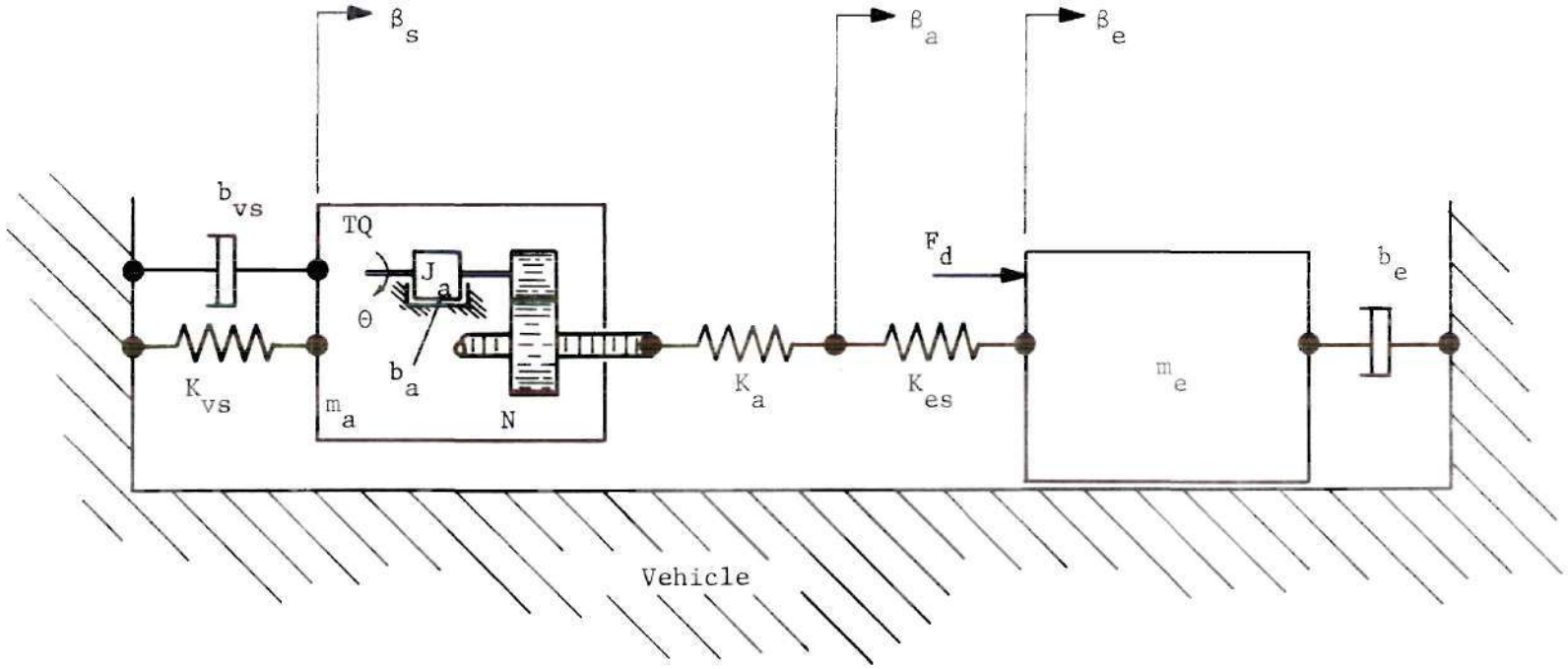

Figure 7. Mathematical Model for an Engine Gimbal System.

Some of the assumptions made in arriving at the model are:

1. All friction is viscous.

2. Torque, TQ, is the sum of the torques developed by both clutches and the brake. Clutch and brake were assumed identical, although this was not necessary.

3. The effect of fuel lines may be neglected.

4. Motor dynamics are neglected in this study, since clutch dynamic effects are being examined. A constant clutch input speed of 100 rad./sec. (approximately 1000 RPM) was assumed throughout.

5. All engine motion and parameters were referred to the actuator output. Thus, engine displacement is linear rather than angular as shown in Figure 1. Conversion to the actual case may be made using the factors in Table 5.

Equations of Motion

Actuator and Gimballed Engine

Using the mathematical model of Figure 7, the following equations of motion were derived:

$$m_a\ddot{\beta}_s + b_{vs}\dot{\beta}_s + (K_{vs} + K_a)\beta_s + K_aN\theta - K_a\beta_a = 0 \qquad (3.1)$$

$$J_a\ddot{\theta} + b_a\dot{\theta} + N^2K_a\theta + N\,K_a\beta_s - N\,K_a\beta_a = TQ \qquad (3.2)$$

$$(K_a + K_{es})\beta_a - K_a\beta_s - K_aN\theta - K_{es}\beta_a = 0 \qquad (3.3)$$

$$m_e\ddot{\beta}_e + b_e\dot{\beta}_e + K_{es}\beta_e - K_{es}\beta_a = F_d \qquad (3.4)$$

where

m_a = actuator mass, $(lb.\text{-}sec.^2)/in.$

m_e = equivalent rocket engine mass, $(lb.\text{-}sec.^2)/in.$

J_a = lumped moment of inertia of the actuator drive train, $lb.\text{-}in.\text{-}sec.^2$

b_{vs} = lumped viscous damping of the vehicle structure, $(lb.\text{-}sec.)/in.$

b_a = lumped viscous damping of the actuator drive train, $lb.\text{-}in.\text{-}sec.$

b_e = equivalent gimbal point viscous friction, $(lb.\text{-}sec.)/in.$

K_a = lumped actuator spring rate, $lb./in.$

K_{vs} = vehicle structure spring rate, $lb./in.$

K_{es} = engine structure spring rate, $lb./in.$

N = effective gear ratio between clutch output and power screw, $in./rad.$

β_s = displacement of the actuator-to-vehicle attachment point, $in.$

$\dot{\beta}_s = \frac{d\beta_s}{dt}$ = velocity of the actuator-to-vehicle attachment point, $in./sec.$

$\ddot{\beta}_s = \frac{d^2\beta_s}{dt^2}$ = acceleration of the actuator-to-vehicle attachment point, $in./sec.^2$

β_a = displacement of the actuator-to-engine attachment point, $in.$

θ = clutch output shaft displacement, $rad.$

$\dot{\theta}$ $\frac{d\theta}{dt}$ = clutch output shaft velocity, $rad./sec.$

$\ddot{\theta} = \frac{d^2\theta}{dt^2}$ = clutch output shaft acceleration, $rad./sec.^2$

β_e = engine displacement, $in.$

$\dot{\beta}_e = \frac{d\,\beta_e}{dt}$ = engine velocity, $in./sec.$

$\ddot{\beta}_e = \frac{d^2\beta_e}{dt^2}$ = engine acceleration, in./sec.^{2}

TQ = clutch output torque, lb.-in.

F_d = equivalent engine disturbance due to thrust-vector offset,* lb.

A detailed derivation of these equations may be found in Appendix A.

For zero initial conditions the Laplace Transform of Equations (3.1) through (3.4) is given by the following:

$$\left[\frac{m_a}{K_a} s^2 + \frac{b_{vs}}{K_a} s + \frac{K_{vs} + K_a}{K_a}\right] \beta_s(s) + \alpha_i(s) - \beta_a(s) = 0 \qquad (3.5)$$

$$\beta_s(s) + \left[\frac{J_a}{N^2 K_a} s^2 + \frac{b_a}{N^2 K_a} s + 1\right] \alpha_i(s) - \beta_a(s) = \frac{TQ(s)}{N K_a} \qquad (3.6)$$

$$-\beta_s(s) - \alpha_i(s) + \left[\frac{K_a + K_{es}}{K_a}\right] \beta_a(s) - \frac{K_{es}}{K_a} \beta_e(s) = 0 \qquad (3.7)$$

$$-\beta_a(s) + \left[\frac{m_e}{K_{es}} s^2 + \frac{b_e}{K_{es}} s + 1\right] \beta_e(s) = 0 \qquad (3.8)$$

where

---

*Thrust-vector offset merely has the effect dynamically of biasing the system displacement. Hence, its effect will be neglected.

$$\alpha_i(s) = N\,\theta(s) = \text{"ideal"}^{*} \text{ actuator extension, in.} \qquad (3.9)$$

Making the substitutions,

$$G_1(s) = \frac{m_e}{K_{es}} s^2 + \frac{b_e}{K_{es}} s + 1 \,, \qquad (3.10)$$

$$G_2(s) = \frac{m_a}{K_a} s^2 + \frac{b_{vs}}{K_a} s + \frac{K_{vs} + K_a}{K_a} \,, \qquad (3.11)$$

$$G_3(s) = \frac{J_a}{N^2 K_a} s^2 + \frac{b_a}{N^2 K_a} s + 1 \,, \qquad (3.12)$$

$$K_1 = \frac{1}{N\,K_a} \,, \qquad (3.13)$$

$$K_2 = \frac{K_a + K_{es}}{K_a} \,, \text{ and} \qquad (3.14)$$

$$K_3 = \frac{K_{es}}{K_a} \,, \qquad (3.15)$$

the final equations of motion are derived:

$$G_2(s)\,\beta_s(s) + \alpha_i(s) - \beta_a(s) = 0 \qquad (3.16)$$

---

*See Chapter V, p. 81, for a definition of the terms "ideal" and "real" actuator.

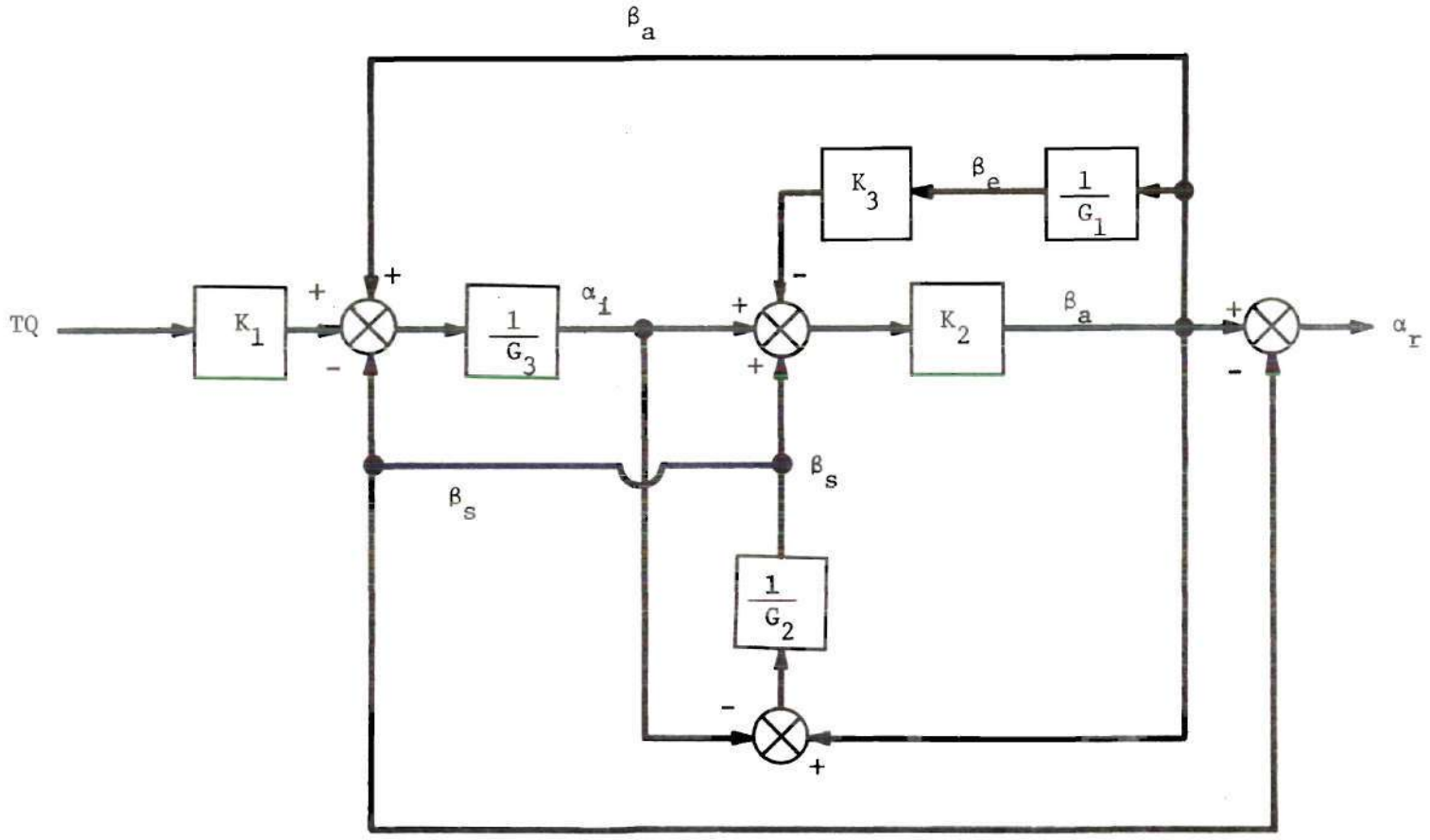

Figure 8. Block Diagram Representation of Engine Gimbal System Equations of Motion.

$$\beta_s(s) + G_3(s)\,\alpha_i(s) - \beta_a(s) = K_1 TQ(s) \tag{3.17}$$

$$-\beta_s(s) - \alpha_i(s) + K_2\beta_a(s) - K_3\beta_e(s) = 0 \tag{3.18}$$

$$-\beta_a(s) + G_1\beta_e(s) = 0 \tag{3.19}$$

Equations (3.16) through (3.19) are represented in block diagram form in Form 8. The relation of "real" actuator extension, α_r, to clutch output torque, TQ, is shown, where

$$\alpha_r = \beta_a - \beta_s \ . \tag{3.20}$$

Describing Function Analysis

A stability analysis of an engine gimbal system employing actuators incorporating ON-OFF clutches was undertaken making use of the Describing Function (DF) technique. One often used approach to the analysis of ON-OFF clutch-actuators has been to assume that the clutch (brake) output member experiences a rate step during engagement. This approximation is quite good where the wrap-spring clutch is involved. A refinement of the approach (15) is to include an equivalent hysteresis which is calculated based on the maximum clutch rate and the time required for clutch engagement. This is illustrated in Figure 9, which shows the equivalent hysteresis (referred to the actuator output), which is calculated by

$$H = R(TD) \ ,$$

where

R = maximum actuation rate, in./sec., and

TD = engagement time delay, sec.

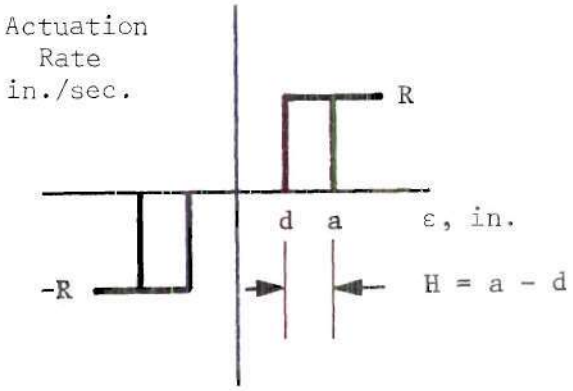

Figure 9. Nonlinear Characteristic for a Wrap-Spring Clutch-Actuator Illustrating Equivalent Hysteresis

In the present analysis, a simple relay characteristic with deadband, in conjunction with a transport delay to represent clutch (brake) engagement time delay was considered a better approximation to a wrap-spring clutch servoactuator. The more general case of a relay characteristic with deadband and hysteresis was examined to include servoamplifier hysteresis. The assumed system is shown in Figure 10, where the simple relay characteristic with deadband may be attained by letting a = d; a typical value for t_o is 5 ms. R represents maximum actuator extension rate, with a value of 8 inches per second being assumed for this analysis. "Ideal" actuator position is considered the input to the gimbal system dynamics. Thus, Equation (3.17) is eliminated, since α_i is "known" in that case.

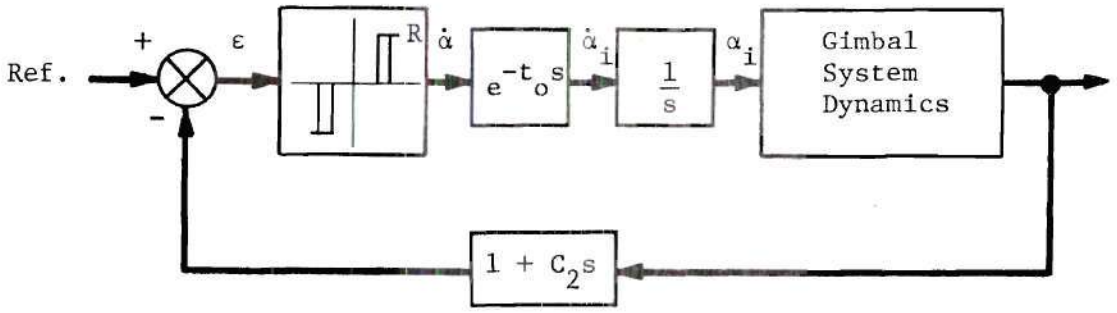

Figure 10. System Assumed for Describing Function Analysis of a Wrap-Spring Clutch Servoactuator

Feedback Pickoffs

Since rate feedback is most easily provided as a means of improving system performance, its effect alone was considered. However, the merits of actuator versus engine pickoffs were investigated. Figure 11 illustrates four feedback cases which were examined: Case I--actuator position and rate; Case II--actuator position and engine rate; Case III--engine position and rate; and Case IV--engine position and actuator rate. For each case the rate feedback coefficient, C_2, was varied from 0 to 0.1 to determine its influence.

Transfer Functions

Before proceeding further with the DF analysis, it is necessary to develop the appropriate linear relations among the variables of interest in the engine gimbal system. From Figures 8 and 11 one may note that transfer functions relating α_r to α_i and β_e to α_i are required to generate the necessary feedback for the four previously-mentioned cases to be analyzed.

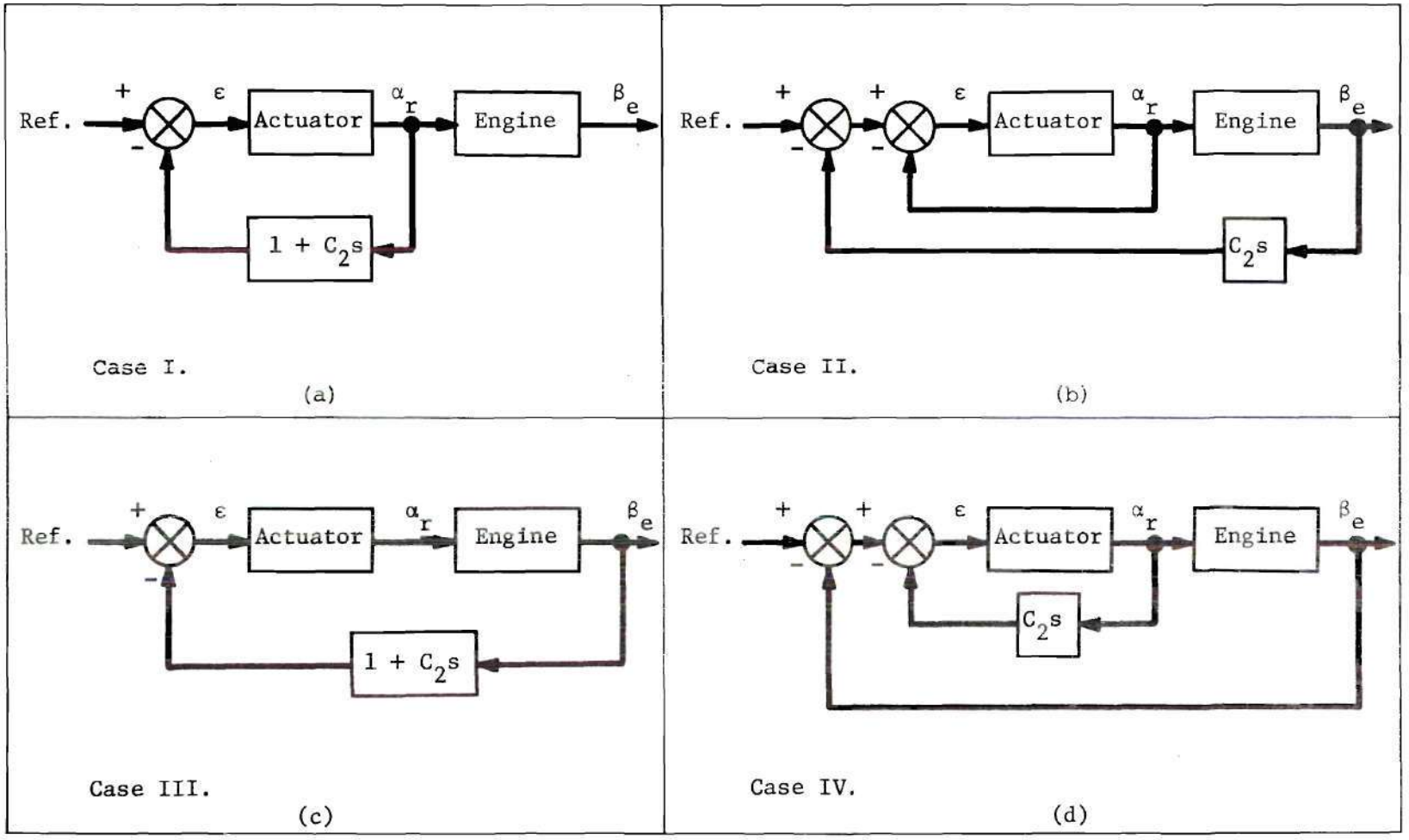

Figure 11. Feedback Configurations Investigated to Determine Relative Merits

Equations (3.16), (3.18), and (3.19) may be written in matrix form as follows:

$$\begin{bmatrix} G_2 & -1 & 0 \\ -1 & K_2 & -K_3 \\ 0 & -1 & G_1 \end{bmatrix} \begin{bmatrix} \beta_s(s) \\ \beta_a(s) \\ \beta_e(s) \end{bmatrix} = \begin{bmatrix} -\alpha_i(s) \\ \alpha_i(s) \\ 0 \end{bmatrix} \tag{3.21}$$

Solving for $\frac{\alpha_r}{\alpha_i}$,

$$\frac{\alpha_r}{\alpha_i} = \frac{\beta_a}{\alpha_i} - \frac{\beta_s}{\alpha_i} \tag{3.22}$$

or

$$\frac{\alpha_r}{\alpha_i} = \frac{\begin{vmatrix} G_2 & -1 & 0 \\ -1 & 1 & -K_3 \\ 0 & 0 & G_1 \end{vmatrix} - \begin{vmatrix} -1 & -1 & 0 \\ 1 & K_2 & -K_3 \\ 0 & -1 & G_1 \end{vmatrix}}{\Delta_1} \tag{3.23}$$

where

$$\Delta_1 = \begin{vmatrix} G_2 & -1 & 0 \\ -1 & K_2 & -K_3 \\ 0 & -1 & G_1 \end{vmatrix} \tag{3.24}$$

Expansion of the determinants involved yields

$$\frac{\alpha_r}{\alpha_i} = \frac{G_1(G_2 + K_2 - 2) - K_3}{\Delta_1} \tag{3.25}$$

where

$$\Delta_1 = G_1(K_2G_2 - 1) - K_3G_2 \tag{3.26}$$

Similarly, solving for $\frac{\beta_e}{\alpha_i}$,

$$\frac{\beta_e}{\alpha_i} = \frac{\begin{vmatrix} G_2 & -1 & -1 \\ -1 & K_2 & 1 \\ 0 & -1 & 0 \end{vmatrix}}{\Delta_1} \tag{3.27}$$

and

$$\frac{\beta_e}{\alpha_i} = \frac{G_2 - 1}{\Delta_1} \tag{3.28}$$

Substituting from Equations (3.10) through (3.15) and making subsequent reductions, the final transfer functions result:

$$\frac{\alpha_r(s)}{\alpha_i(s)} = \frac{A(s)}{\Delta(s)^*} = \frac{a_4s^4 + a_3s^3 + a_2s^2 + a_1s + a_o}{d_4s^4 + d_3s^3 + d_2s^2 + d_1s + d_o} \tag{3.29}$$

---

*$\Delta(s) = K_a\Delta_1(s)$.

where,

$$a_4 = \frac{m_e m_a}{K_{es}}$$

$$a_3 = \frac{m_e b_{vs} + m_a b_e}{K_{es}}$$

$$\left.\begin{aligned} a_2 &= \frac{[m_e(K_{vs} + K_{es}) + b_e b_{vs}]}{K_{es}} + m_a \\ a_1 &= \frac{b_e(K_{vs} + K_{es})}{K_{es}} + b_{vs} \end{aligned}\right| \qquad (3.30)$$

$$a_o = K_{vs}$$

$$d_4 = \left[\frac{K_a + K_{es}}{K_a K_{es}}\right] m_e m_a$$

$$d_3 = \left[\frac{K_a + K_{es}}{K_a K_{es}}\right] (m_e b_{vs} + m_a b_e)$$

$$d_2 = \left[\frac{K_a K_{vs} + K_{vs} K_{es} + K_{es} K_a}{K_a K_{es}}\right] m_e + \left[\frac{K_a + K_{es}}{K_a K_{es}}\right] b_e b_{vs} + m_a$$

$$d_1 = \left[\frac{K_a K_{vs} + K_{vs} K_{es} + K_{es} K_a}{K_a K_{es}}\right] b_e + b_{vs}$$

$$d_o = K_{vs}$$

and

$$\frac{\beta_e(s)}{\alpha_i(s)} = \frac{m_a s^2 + b_{vs} s + K_{vs}}{\Delta(s)} \tag{3.31}$$

For the case where m_a and b_{vs} may be neglected,* Equations (3.29) and (3.31) reduce to

$$\frac{\alpha_r(s)}{\alpha_i(s)} = G_{10}(s) = \left[\frac{K_a(K_{vs} + K_{es})}{K_a K_{vs} + K_{vs} K_{es} + K_{es} K_a}\right] \left[\frac{s^2 + \frac{b_e}{m_e} s}{s^2 + \frac{b_e}{m_e} s + \left(\frac{1}{m_e}\right)\left(\frac{K_{vs} K_{es}}{K_{vs} + K_{es}}\right)}\right] \left[\frac{}{+ \left(\frac{1}{m_e}\right)\left(\frac{K_a K_{vs} K_{es}}{K_a K_{vs} + K_{vs} K_{es} + K_{es} K_a}\right)}\right] \tag{3.32}$$

and

---

*See Chapter IV, page 70.

$$\frac{\beta_e(s)}{\alpha_i(s)} = G_{12}(s) = \left[\frac{K_a K_{vs} K_{es}}{K_a K_{vs} + K_{vs} K_{es} + K_{es} K_a}\right] \qquad (3.33)$$

$$\frac{1}{\left[s^2 + \frac{b_e}{m_e} s + \frac{K_a K_{vs} K_{es}}{K_a K_{vs} + K_{vs} K_{es} + K_{es} K_a}\right]}$$

Case I in Figure 11 (a) may be represented by the block diagram in Figure 12.

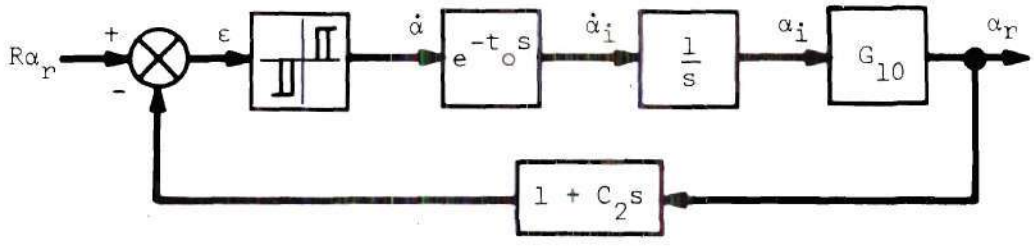

Figure 12. Block Diagram for Case I

To apply the DF technique this block diagram must be reduced to the system in Figure 13, where all frequency-dependent elements are lumped in $G_I(s)$, and the nonlinearity is represented by N. For Case I,

$$G_I(s) = \frac{e^{-st_o}}{s}(1 + C_2 s)G_{10} \qquad (3.34)$$

Similarly for Cases II through IV,

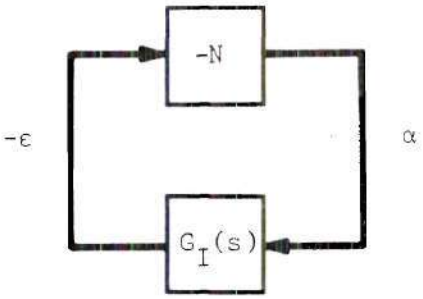

Figure 13. Autonomous System for Describing Function Analysis

$$G_{II} = \frac{e^{-st_o}}{s} (G_{10} + C_2 s\, G_{12}) \tag{3.35}$$

$$G_{III} = \frac{e^{-st_o}}{s} (1 + C_2 s) G_{12} \tag{3.36}$$

$$G_{IV} = \frac{e^{-st_o}}{s} (G_{12} + C_2 s\, G_{10}) \tag{3.37}$$

According to Gibson (16) the describing function $K_{eq}(E)$ in cartesian coordinates is

$$K_{eq}(E) = g(E) + j\, b(E) \tag{3.38}$$

where for the nonlinearity in Figure 9,

$$g(E) = \frac{2R}{\pi E} \left[\sqrt{1 - (a/E)^2} + \sqrt{1 - (d/E)^2}\right] \tag{3.39}$$

$$b(E) = -\frac{2R}{\pi E^2}(a - d) \tag{3.40}$$

and E = amplitude of sinusoidal error, ε, assumed in the development of the describing function.

The basic equation of the DF analysis is

$$G(j\omega) = -\frac{1}{K_{eq}(E)}, \tag{3.41}$$

the satisfaction of which indicates the possibility of sustained system oscillation, or a limit cycle. To check for satisfaction of Equation (3.41) it is necessary only to plot the $G(j\omega)$ curve and the $-1/K_{eq}(E)$ locus and check for any intersections of the two. It is still necessary to determine whether a given intersection represents a stable or an unstable equilibrium point. (This will be discussed subsequently.) Assuming a given intersection represents a stable equilibrium condition, the amplitude of the oscillation is given by the value of E from the $-1/K_{eq}(E)$ plot, while the frequency is the value of ω occurring on the $G(j\omega)$ curve.

For the problem at hand, $G(j\omega)$ is obtained for each of the four cases by substitution of $j\omega$ into the proper one of Equations (3.34) through (3.37). Euler's equation was used to resolve $e^{-j\omega t_o}$ into its real and imaginary components, and then each $G(j\omega)$ function was likewise resolved. A digital computer program was employed to calculate the data required for the plots which are shown in Figures 15 through 18.

The $-1/K_{eq}$ locus data was also calculated by a digital computer. The equation

$$\frac{-1}{K_{eq}} = \frac{-g(E) + jb(E)}{g^2(E) + b^2(E)} \tag{3.42}$$

produced real and imaginary components

$$RE = - \frac{g(E)}{g^2(E) + b^2(E)} \tag{3.43}$$

and

$$IM = \frac{b(E)}{g^2(E) + b^2(F)} \tag{3.44}$$

For the case of a simple relay characteristic with deadband, d = a in Figure 9, and b(E) is zero. For that case

$$K_{eq} = g(E) = \frac{4R}{\pi E} \sqrt{1 - (d/E)^2} \tag{3.45}$$

It is a simple matter to determine the maximum value of the $-1/K_{eq}$ plot by differentiating Equation (3.42) with respect to E. The result is that a maximum occurs for

$$E = \sqrt{2}\ d\ ,$$

and is given by

$$-\frac{1}{K_{eq_{max.}}} = -\frac{\pi d}{2R} \tag{3.46}$$

In the problem of interest

$$d = 0.05 \text{ in.}, \text{ and}$$

$$R = 8 \text{ in./sec.},$$

so that

$$-\frac{1}{K_{eq_{max.}}} = 0.0098 .$$

The entire locus lies on the negative real axis with a maximum occurring at 0.0098.

When hysteresis is included in the nonlinearity, K_{eq} is a complex function of E. Figure 14 shows $-1/K_{eq}$ plotted for three values of the ratio d/a (0.6, 0.8, and 1.0) at two different deadband values (0.05 and 0.075 in.). The data for a deadband of 0.05 in. has been superimposed wholly or partially on Figures 15 through 18. In Figure 15 the effect of increasing hysteresis (i.e., d/a decreasing) can be noted, where for d/a = 0.6 an intersection with the $G(j\omega)$ locus for zero rate feedback occurs, indicating a limit cycle. The frequency and amplitude of oscillation would be approximately 79 rad./sec. and 0.055 in., respectively. For less hysteresis no intersection would occur for zero rate feedback, and no limit cycle would develop for the parameters assumed in this study.

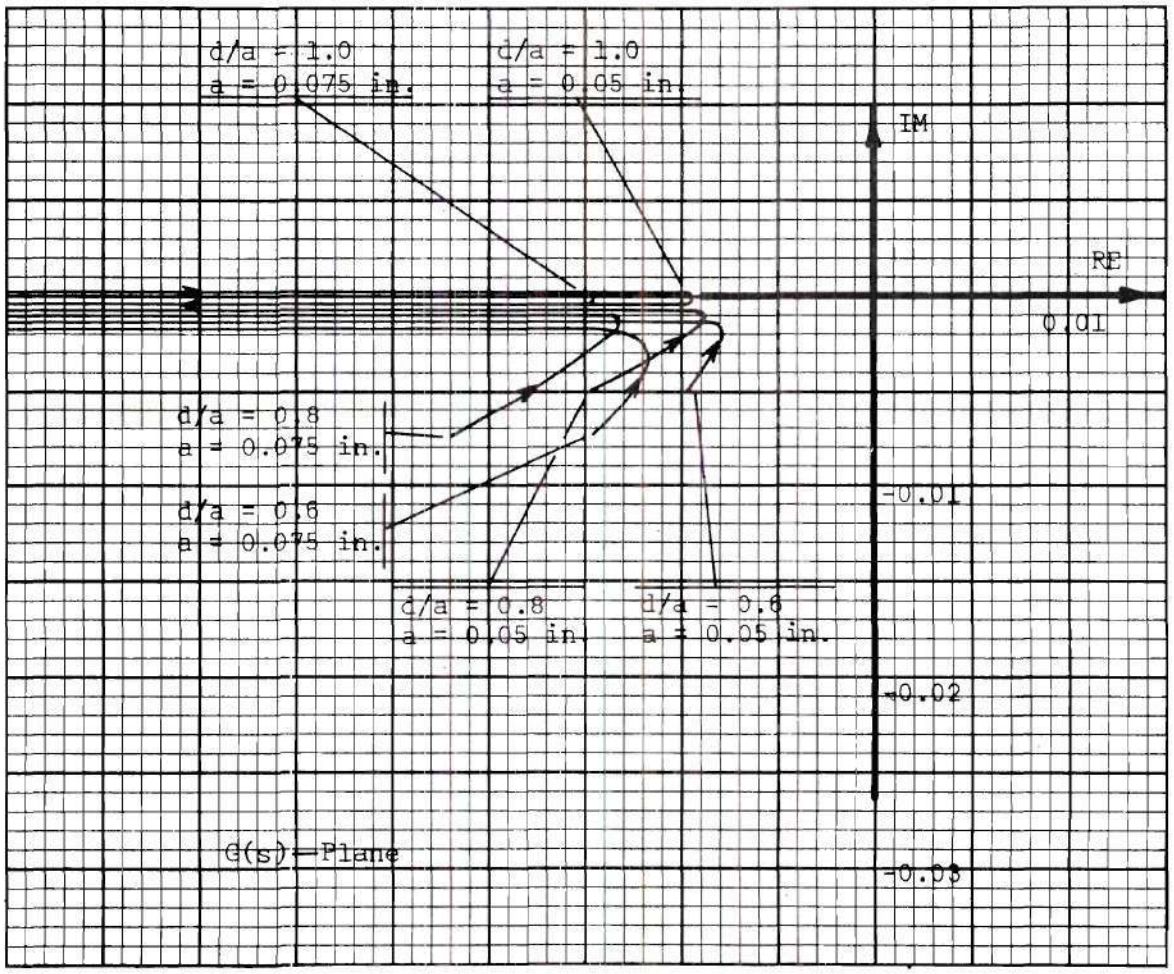

Figure 14. Plot of - $1/K_{eq}(E)$ for the Nonlinearity of Figure 9

Normally the hysteresis in the servoamplifier will be practically negligible, i.e., d/a = 0.9 or better.

A stable equilibrium condition is indicated by the intersection noted above. This can be determined as follows: For an increase in amplitude, E, of limit cycle, the critical point would move to the left of the $G(j\omega)$ curve. In that region the system is stable and oscillations will die out, moving the operating point on the $-1/K_{eq}$ curve back toward the intersection. On the other hand, a decrease in E will move the critical point so that it is enclosed by the $G(j\omega)$ curve. This corresponds to an unstable condition, and the amplitude of oscillation increases, driving the operating point back again toward the intersection. Hence, this discussion shows this intersection of the $G(j\omega)$ curve and the $-1/K_{eq}$ locus to represent a stable equilibrium point, since any changes due to disturbances always result in operation returning to that point. This type of analysis as outlined in reference (17) should be carried out on any given intersection, since it may or may not represent a stable equilibrium condition. For example, in Figure 15 for $C_2 = 0.06$ two intersections of the $-1/K_{eq}$ locus occur for the same value of ω on the $G(j\omega)$ curve. The analysis used above will show the intersection for the lower value of E to be an unstable equilibrium point, while the other indicates sustained oscillation.

Consider Figures 15 through 18 which correspond to Cases I through IV in Figure 11, respectively. Figures 17 and 18 show that the systems of Cases III and IV would limit cycle for all values of

C_2*. Figures 15 and 16 on the other hand indicate that their respective systems would not limit cycle for a limited range of C_2. A maximum value of $C_2 \simeq 0.01$ without limit cycle is indicated from Figure 15 with an even smaller maximum C_2 for Figure 16. Analog computer simulation of Cases I and II, however, showed that no system compensation was possible before limit cycle operation using Case II, but better results were obtained with Case I for which a C_2 varying between 0.025 and 0.04 was reached before limit cycle operation occurred. Since Case I is desirable because of the ease of taking the rate feedback signal from the actuator output, and since it yielded the best results of Cases I through IV as discussed above, the remaining work will be based on that system configuration.

It should be noted that even better results are possible for a reduced actuation rate, since according to Equation (3.46) the maximum value for the $-1/K_{eq}$ plot would occur further out the negative real axis. This would indicate a less oscillatory system in general due to more separation of the $G(j\omega)$ and $-1/K_{eq}$ loci, as well as allowing more rate feedback compensation before limit cycle operation occurred. This observation is supported by comparison of the analog computer data for a wrap-spring clutch-actuator with actuation rates of 8 in./sec. and 4 in./sec. found in Appendices C and D, respectively.

It should also be pointed out that the describing function analysis carried out in this chapter will predict a more oscillatory

---

*In Figure 18 the $G(j\omega)$ plots would be identical to those in Figure 15 for $\omega \to \infty$. This may be seen by comparing Equations (3.34) and (3.37) with $s = j\omega$ as $\omega \to \infty$.

system than actually exists because of the model for the nonlinearity, which includes a rate step. The rate build up is less severe in an actual clutch, although the assumption is reasonably accurate for the wrap-spring clutch as mentioned earlier. The analog simulation which more nearly approximates the real situation is better.

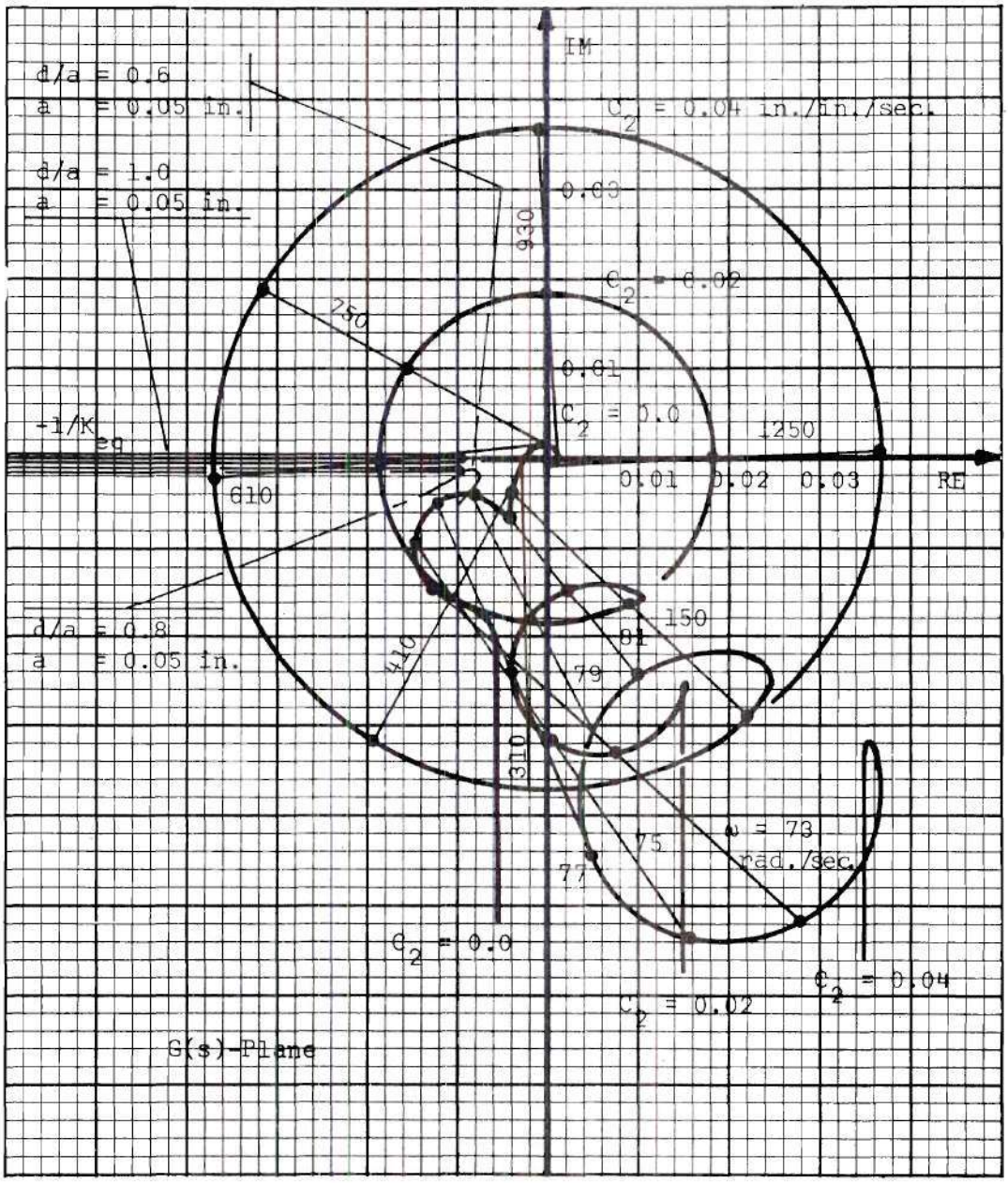

Figure 15. Plot of $G(j\omega)$ and $-1/K_{eq}$ for the Describing Function Analysis of Case I

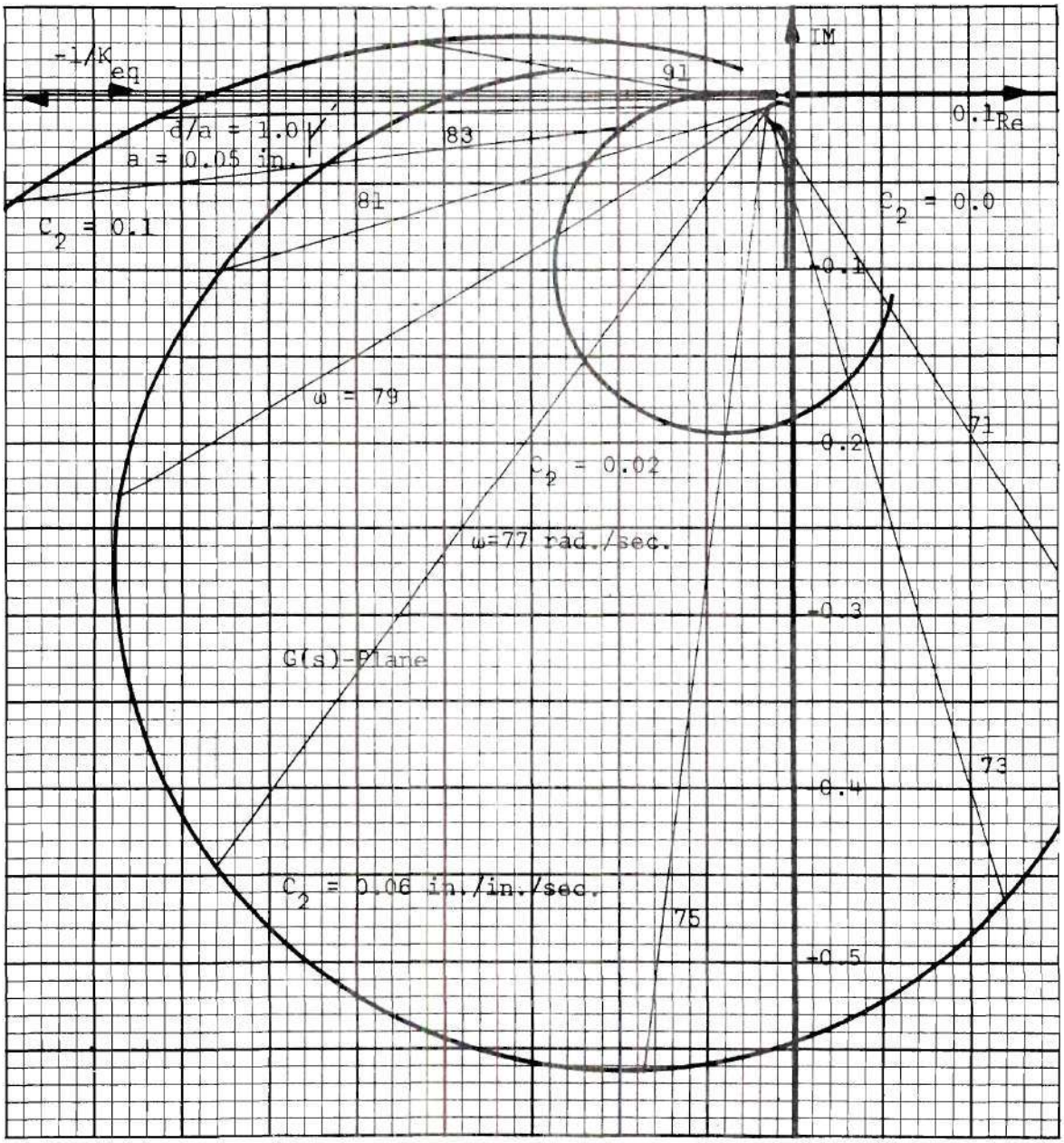

Figure 16. Plot of $G(j\omega)$ and $-1/K_{eq}$ for the Describing Function Analysis of Case II

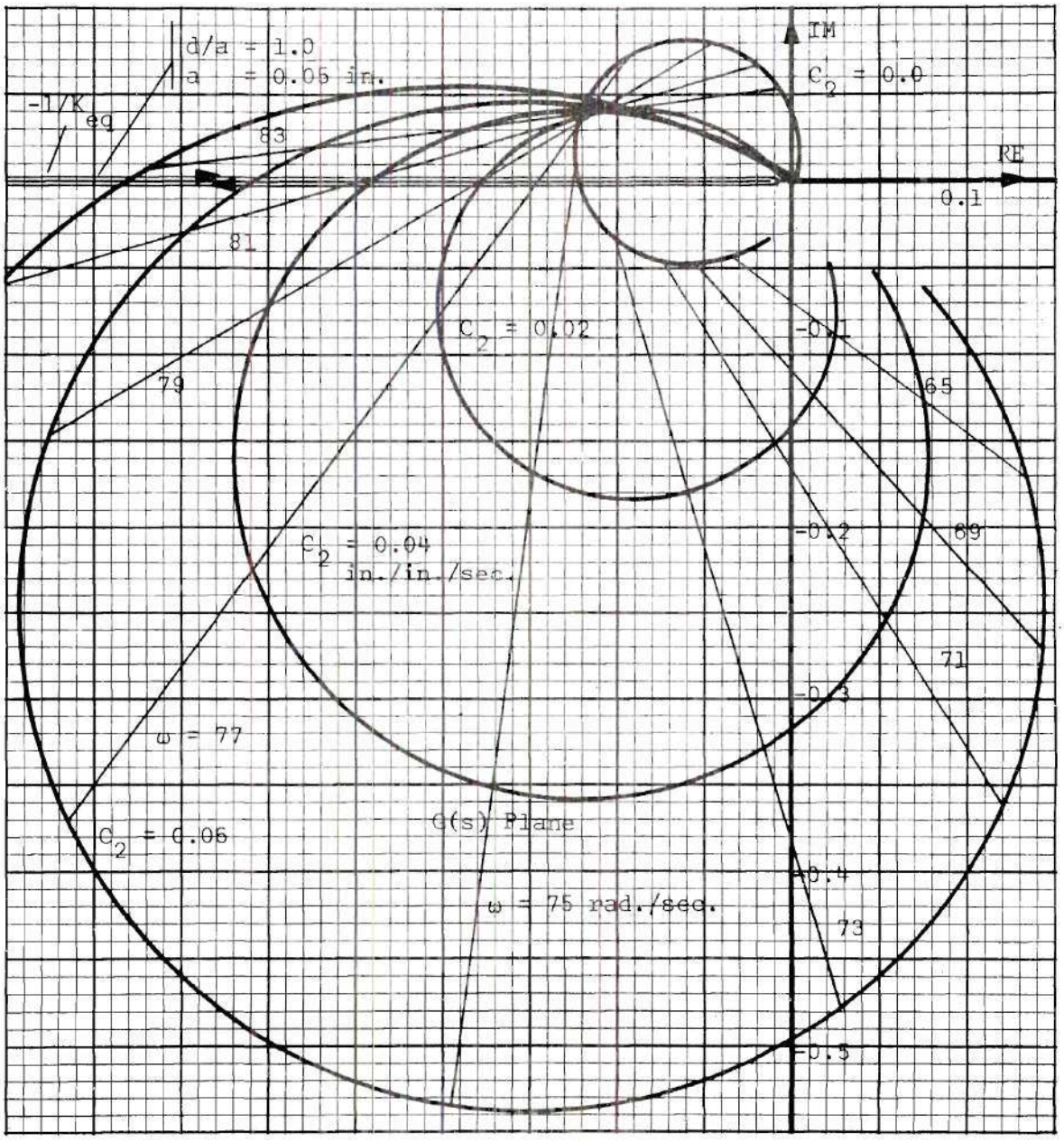

Figure 17. Plot of $G(j\omega)$ and $-1/K_{eq}$ for the Describing Function Analysis of Case III

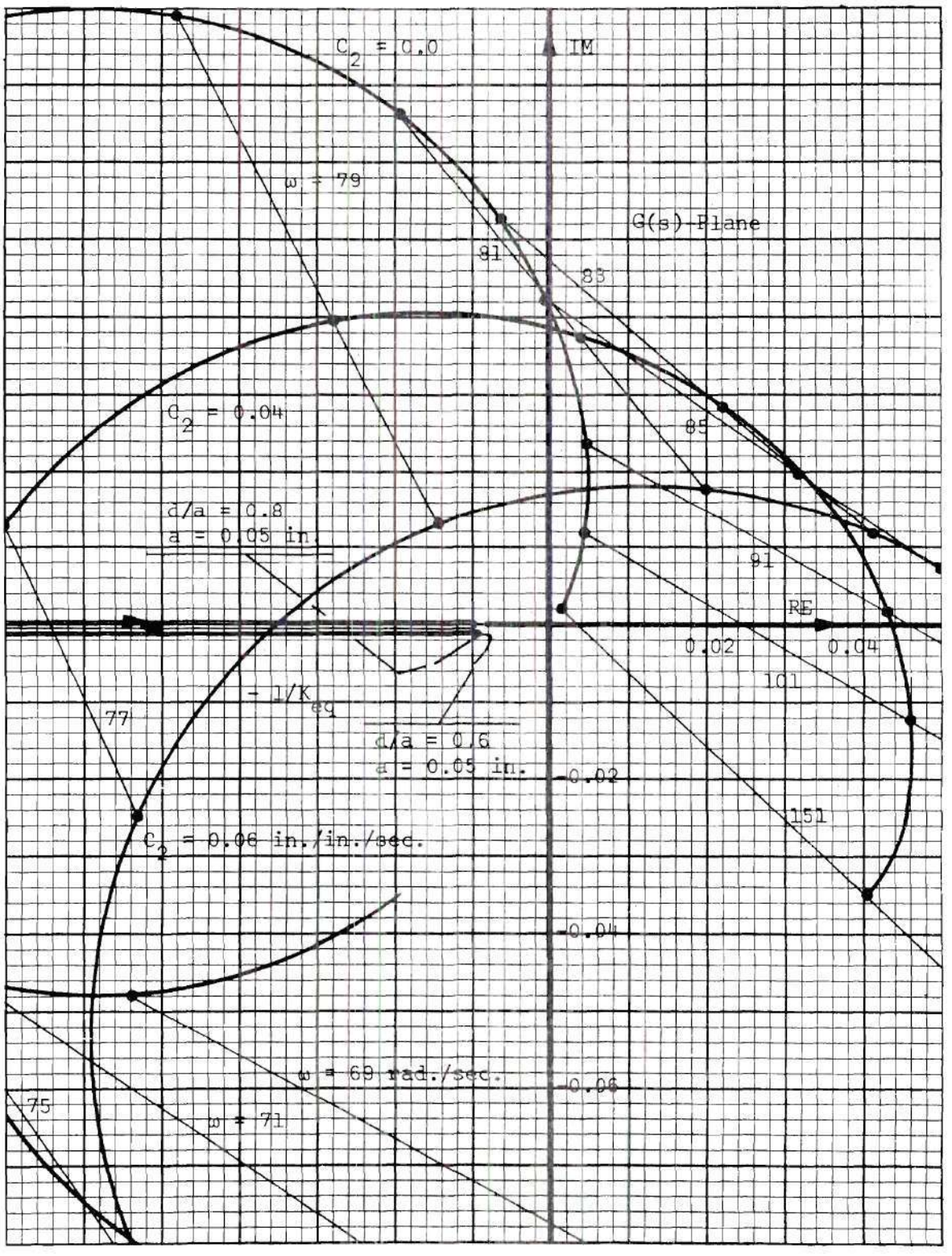

Figure 18. Plot of G(jω) and - $1/K_{eq}$ for the Describing Function Analysis of Case IV

CHAPTER IV

ANALOG COMPUTER STUDY

Introduction

Discussion of clutch qualifications in Chapter II centered on criteria other than dynamic system performance. It is also necessary to investigate system operation under the influence of each of the clutch-types selected in the preliminary analysis before a final decision can be made regarding the recommendation of a clutch type for an electromechanical actuator. Chapter IV presents the details of the dynamic study needed in making that recommendation.

Three clutch types--magnetic-particle, friction-disc, and wrap-spring--were selected prior to any dynamic considerations. In the present chapter each of these clutch-types was "installed" in a mathematical model for an engine gimbal control system. Computer-predicted system performance was recorded in each case for eventual comparison.

The analog computer was chosen to solve the system equations of motion because of the ease of adjusting system parameters and convenience in data presentation.

Equations of Motion

Gimbal System

The equations of motion involved are those introduced in Chapter III, i.e., Equations (3.1) through (3.4). Since the time required for the operation of the clutches is on the order of 10 milliseconds, it was

necessary to time scale the equations before solving them on the analog computer. A time scale factor of 100 was introduced to slow down the computation sufficiently for proper equipment functioning. For magnitude scaling some of the scale factors were based on maximum values which could be calculated quite easily from the data in Tables 5 and 6; others were selected by trial and error after the computer program was set up. The system equations, after time and magnitude scaling, are listed in a form convenient for analog computer solution as Equations (A.29) through (A.32) in Appendix A.

The simulation data used in calculating coefficients for the equations of motion are listed in Tables 5 and 6. Data labelled "Given" in Table 6 is that which was obtained from the NASA Astrionics Laboratory (or derived from given data); other parameter values were assumed as necessary to complete the simulation. After substitution of the data into Equations (A.29) through (A.32), the following final set of equations resulted for a system incorporating an actuator with a rate of 8 in./sec.:

$$10\,\ddot{\beta}_s = -5\,\dot{\beta}_s - 2190\,\beta_s - 154\,\theta + 1930\,\beta_a \tag{4.1}$$

$$10\,\ddot{\theta} = 0.125\left(\frac{TQ}{10}\right) - 0.563\,\dot{\theta} - 12\,\theta - 150\,\beta_s + 150\,\beta_a \tag{4.2}$$

$$40\,\beta_a = 31.6\,\beta_s + 2.53\,\theta + 8.44\,\beta_e \tag{4.3}$$

$$20\,\ddot{\beta}_e = -1.61\,\dot{\beta}_e - 37.7\,\beta_e + 37.7\,\beta_a \tag{4.4}$$

For other actuation rates, it is necessary to recalculate the coefficients in Equations (A.29) through (A.32) involving the factor "N," which was defined earlier as the effective gear ratio between clutch output and power screw.

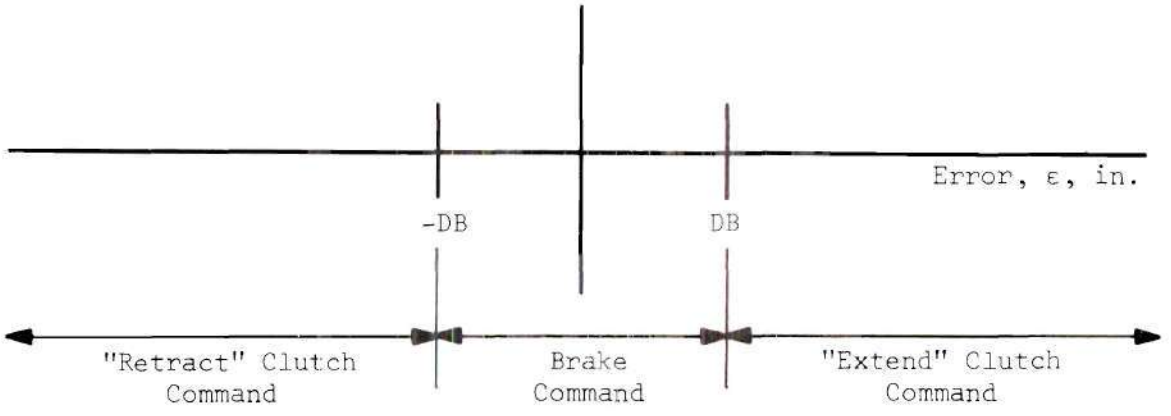

Figure 19. Diagram Showing Proper Phasing of Clutches and Brake

Feedback and Control Logic

Analytical results of Chapter III and experimental results of Chapter V both indicated that the best system performance may be had by closing a loop about the actuator in an engine gimbal actuation system. This is illustrated in the block diagram of Figure 11 (a). Proper phasing of the clutches and brake in a clutch-operated actuator is indicated by the diagram in Figure 19. Thus, when the error is positive and greater in magnitude than the deadband value, extend actuation is commanded; conversely, when the error is negative and greater in magnitude than the deadband value, retract operation is commanded. Any time the error magnitude is less than that of the deadband, a brake command exists. These relations may be stated mathematically by the inequalities

in Table 3, where

ε = control loop error, in.,

or

$$\varepsilon = R\alpha_r - \alpha_r - C_2\dot{\alpha}_r \ , \tag{4.5}$$

$R\alpha_r$ = reference actuator extension, in.,

α_r = actuator extension, in.,

$\dot{\alpha}_r = \frac{d\,\alpha_r}{dt}$ = actuation rate, in./sec., and

C_2 = rate feedback coefficient, in./(in./sec.).

Table 3. Mathematical Relations Governing ON-OFF Clutch-Operated Servoactuator Operation

Actuator Operating Mode	Mathematical Relation
Mode 1 "Extend" Clutch Command	$\begin{bmatrix} [\lvert\varepsilon\rvert - DB] > 0 \\ \varepsilon > 0 \end{bmatrix}$
Mode 2 "Retract" Clutch Command	$\begin{bmatrix} [\lvert\varepsilon\rvert - DB] > 0 \\ \varepsilon < 0 \end{bmatrix}$
Mode 3 Brake Command	$\begin{bmatrix} [\lvert\varepsilon\rvert - DB] < 0 \end{bmatrix}$

In the actual servo hardware, it is necessary to implement these mathematical relations in some manner. A servoamplifier usually serves this function.

Clutch (and Brake) Dynamic Characteristics

At this point the only further information required is a means for determining clutch torque, TQ. This was accomplished in the computer study by introducing typical clutch torque characteristics into the program.

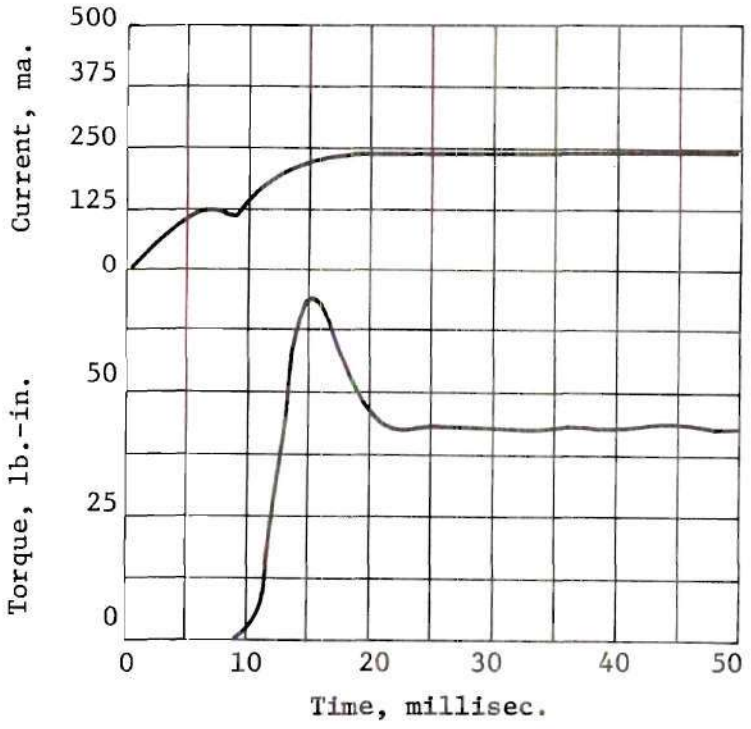

Figure 20. Time Histories for a Wrap-Spring Clutch

Wrap-Spring and Friction-Disc Clutches

References (1) and (2) report the results of tests which were made on each of the three clutch-types being considered in this analog study in order to determine their dynamic torque characteristics. Figures 20 and 21 were reproduced from reference (1) and illustrate typical response data for wrap-spring and friction-disc clutches operated

in an ON-OFF fashion; the test set-up was similar to the arrangement in Figure 22, with the exception that a slip clutch replaced the dashpot. Thus, coulomb friction predominated over viscous damping in that case.

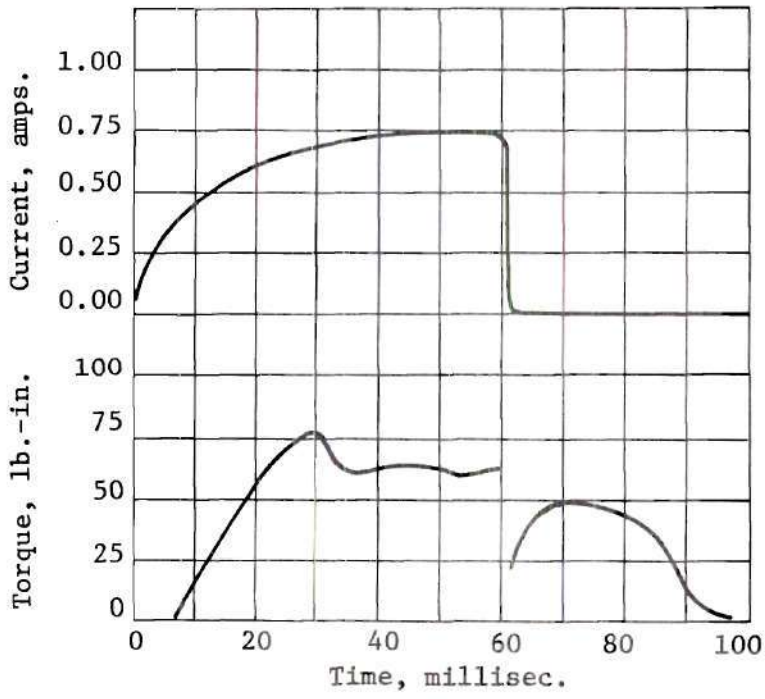

Figure 21. Time Histories for a High Torque-Capacity Precision Disc Clutch

Figures 22 and 23 will aid in explaining the techniques used to simulate clutch torque characteristics in the analog study. For the system of Figure 22, one may write the following equation of motion:

$$J\ddot{\theta} + b\dot{\theta} = TQ \qquad (4.6)$$

Suppose that the clutch is engaged at t=0. As long as slip

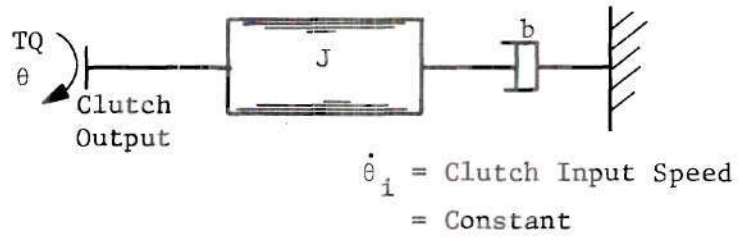

Figure 22. Clutch Load Consisting of Inertia and Damping.

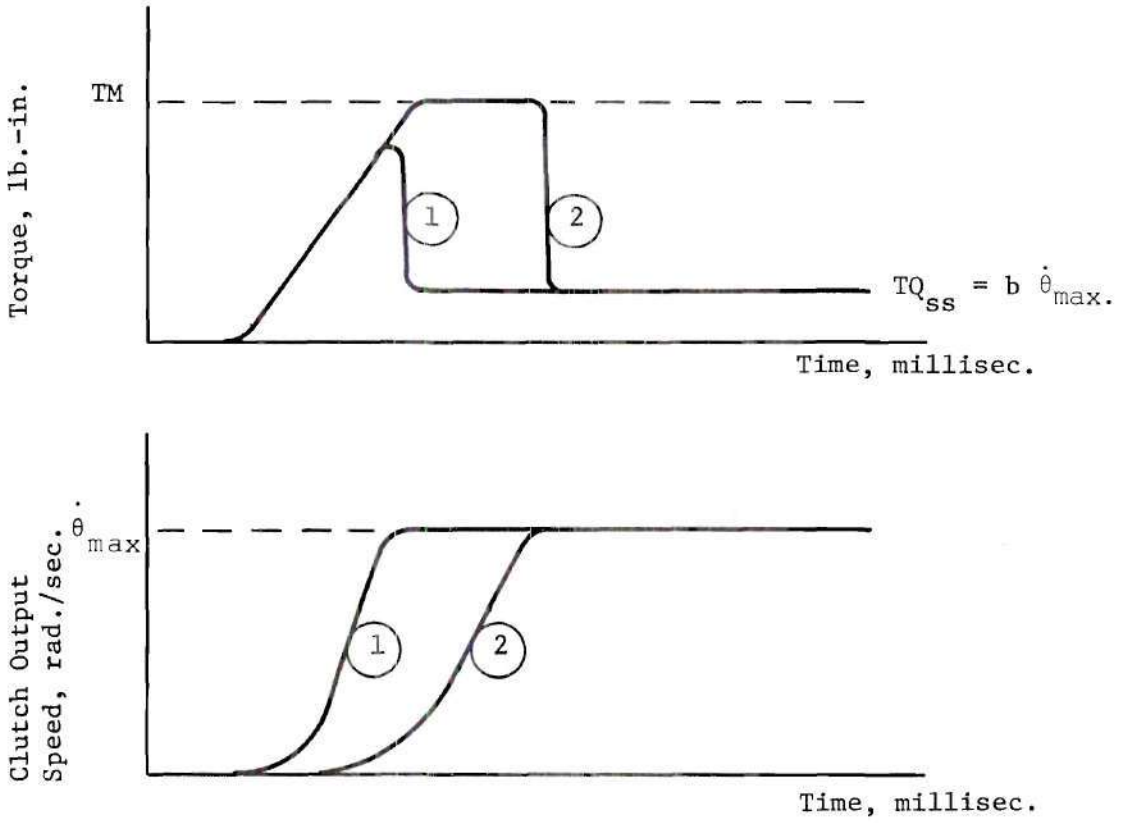

Figure 23. Possible Torque and Speed Histories for the Clutch-Driven Load of Figure 22.

exists,* maximum clutch torque available will be demanded; during engagement the "maximum available" clutch torque is that indicated by the build-up portions of the torque characteristics (Figures 20 and 21). According to Anderson (18) torque build-up is independent of the type of load. Figure 6 of (1), comparing torque build-ups for a frictional load and an inertial load, shows the two to be identical. Examination of the test data in Figures 20 and 21 indicates that the torque build-up characteristics for the wrap-spring and friction-disc clutch-types may be approximated quite well by straight line segments--a pure time delay plus a linear torque build-up.

As the torque build-up phase is passed, operation can be explained by one of the two cases indicated in Figure 23. In the first case, the load is such that it would be accelerated to full clutch input speed before the clutch developed its maximum torque capability. Thus, after full speed is reached, according to Equation (4.6),

$$TQ_{ss} = b\dot{\theta}_{max.} = \dot{b}\theta_i ,$$

i.e., the steady state clutch torque demanded is simply that required to overcome friction, since the load acceleration, $\ddot{\theta}$, becomes zero at clutch input speed.

In the second case, the clutch would reach its maximum torque

---

*Clutch slip exists whenever

$$\dot{\theta}_i - \dot{\theta} \neq 0.$$

capability before the load was accelerated to full speed. If the clutch were a friction-disc clutch, this means that the clutch would slip at maximum torque until the load reached full speed. Considerable power would be dissipated between the clutch plates, with resultant temperature rise. If the clutch were a wrap-spring type, the spring would break or slip would occur, the former being likely. For either clutch-type, the second case is undesirable and would be considered in the actuator design.

In the analog computer simulation of the portion of the torque characteristic after torque build-up, limits were placed on both clutch torque and clutch output speed. Clutch torque was limited at maximum clutch capability, while output speed was limited at clutch input speed. In the first case discussed earlier, relative to Figure 23, the velocity limit would be reached before the torque limit, and the converse would occur in the second case. It should be noted that although in an actual situation the torque demanded of the clutch drops to a steady state value related to the system friction once zero slip is attained, no attempt was made to accomplish this function in the analog simulation. The reason for this is that once speed saturation occurs, system performance is no longer a function of clutch torque. Thus, as will be seen in the next section, the analog program is arranged such that the velocity limit dominates over the torque limit, allowing the torque level to remain constant at T_m as long as a particular clutch remains engaged. This resulted in a simpler program and guaranteed a constant actuation rate as long as a particular clutch was fully engaged.

A remaining factor which must be considered regarding the

torque-characteristic simulation is torque decay. Once a particular clutch or brake is commanded to release, a finite time period is required before complete release is effected. Anderson (19) reports a torque decay time of approximately 50 per cent of torque build-up time for the friction-disc clutch. Reference (20) states that a torque decay equal to engagement time delay is achievable for a wrap-spring clutch. These characteristics were assumed for their respective clutch-types in the present study. The shape of the torque decay curve was assumed to be exponential--decay time being computed on a four time constants basis. Although insufficient data was available to accurately determine the form of the decay characteristic, the exponential decay is considered accurate enough for modeling purposes. The simplicity of the analog programming made it especially attractive. Thus, the torque decay effect was included without undue programming complexity.

Figure 24 displays the torque-characteristic parameters used to generate simulated clutch torque for this investigation.

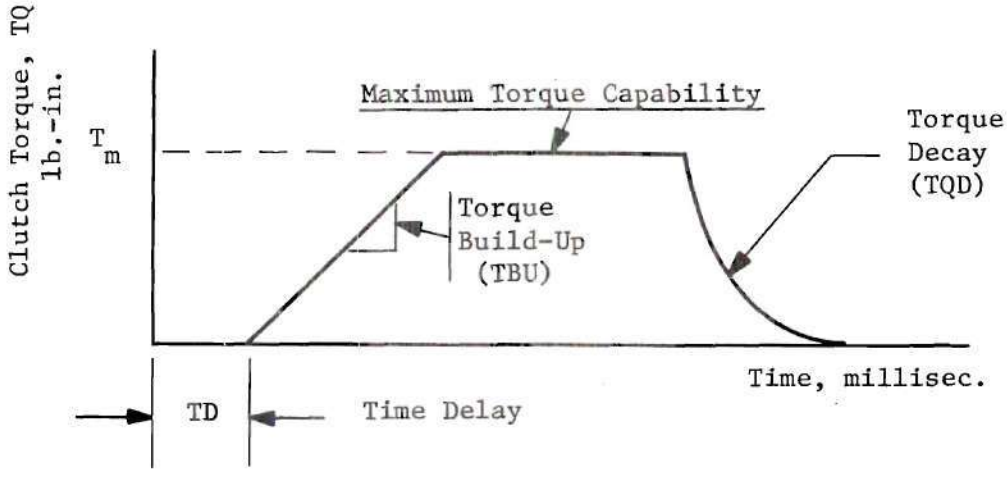

Figure 24. ON-OFF Clutch Torque Characteristic Assumed for Simulation of a Clutch-Operated Actuator

Magnetic-Particle Clutch

All the test data for the magnetic-particle clutch-type covered in reference (2), was for ON-OFF operation. Figure 25, reproduced from reference (2), shows a typical ON-OFF torque characteristic for that clutch-type. One may note that the engagement time is extremely long for ON-OFF operation; however, the magnetic-particle clutch is well-adapted to proportional control. When operated in a continuous-control manner, as discussed in Chapter I, a very good approximation may be had by considering the clutch torque to be proportional to control loop error up to clutch torque-saturation, i.e.,

$$\begin{aligned} TQ &= K\varepsilon \ , \qquad |K\varepsilon| < T_m \\ TQ &= T_m \ \text{sign} \ \varepsilon, \quad |K\varepsilon| \geq T_m \end{aligned} \tag{4.7}$$

where

T_m = clutch saturation torque, lb.-in.,

ε = system error, in., and

K = forward-loop gain.

Thus, this technique will be used to simulate the magnetic-particle clutch-actuator in the analog computer study.

Analog Computer Simulation

Circuit Diagram

The analog computer circuit employed to simulate an engine gimbal actuation system employing clutch-operated actuators is shown in

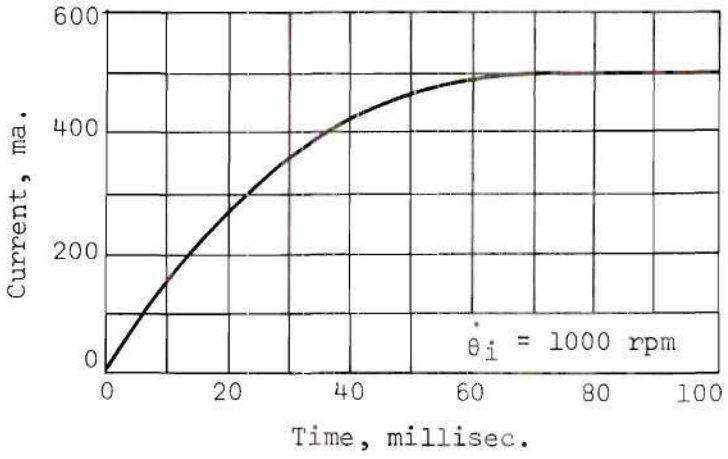

Figure 25(a). Current Time History for a Magnetic-Particle Clutch

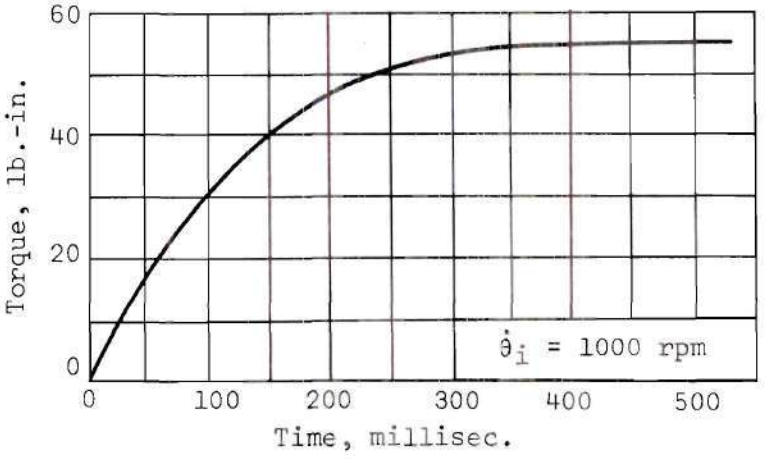

Figure 25(b). Torque Time History for a Magnetic-Particle Clutch

Figure 50 of Appendix B. The diagram as shown was used to simulate the operation of the gimbal system with ON-OFF clutches, wrap-spring and friction-disc. Circuit simplifications, which will be discussed subsequently, were made to accommodate the magnetic-particle clutch-type.

Four main circuit divisions may be noted: Reference Input, Feedback and Control Logic Implementation, Clutch and Brake Torque Simulation, and System Equations Implementations. The *Reference Input* division simply generates command signals to which the gimbal system must respond. The *Feedback* and *Control Logic Implementation* division includes the control signal summing point, feedback signals, and clutch control logic as discussed earlier in the "Feedback and Control Logic" section of this chapter. A torque signal is provided by the *Clutch* and *Brake Torque Simulation* division. The diagram shows *Extend* and *Retract* clutch and brake simulators, which accomplish the torque build-up and decay functions. In addition, one may note the use of a digital clock and *And* gates to provide a clutch (and brake) engagement time delay. The remaining division, *System Equations Implementation* (as the name implies), is the analog implementation of Equations (4.1) through (4.4), which describe the motion of the gimbal actuation system.

Brake "HOLD" Simulator. One other part of the analog circuit which must be explained is the Brake "HOLD" Simulator, which is a subdivision of the Clutch and Brake Torque Simulation division. In the equations of motion listed previously, the term TQ represents the sum of the torques developed by the clutches and brake. This sum is generated at the output of amplifier 20 in the analog simulation and is then fed into the computer implementation of the equations. Since the

analog circuit reacts to a voltage representing TQ, it cannot distinguish between brake torque and clutch torque. Normally the function of a brake is to reduce the velocity of its rotating member to zero and to hold it in that condition until released. In the computer version, the build-up of brake torque properly reduces the clutch (brake) velocity, $\dot{\theta}$, to zero; on the other hand, maintaining the maximum brake torque, T_m, to simulate a fully-engaged brake (as discussed earlier in the "Clutch (and Brake) Dynamic Characteristics" section of this chapter) would cause $\dot{\theta}$ to change sign and increase in magnitude as if a clutch torque were applied. Therefore, some technique is needed to sense when the brake velocity reaches zero and then to force it to remain at that value until brake release is commanded. A simple, drift-free technique for achieving the desired operation was carried out using the Brake "HOLD" Simulator and other associated components.

A detailed description of all parts of the analog computer circuit is included in Appendix B.

Magnetic-Particle Clutch Simulation

According to Equation (4.7) magnetic-particle clutch torque can be calculated by

$$\begin{aligned} TQ &= K\varepsilon, \ |K\varepsilon| < T_m \\ TQ &= T_m, \ |K\varepsilon| \geq T_m \ . \end{aligned} \tag{4.7}$$

Since the error (actually -40ε) is available at the output of amplifier 4 in the analog circuit of Figure 50, it is a simple matter to generate

TQ. A diagram of the circuit used for the simulation is shown in Figure 26. One may note that

$$-0.0125\ TQ = -(0.125\ K'')(K')(40\varepsilon)\ , \tag{4.8}$$

so that

$$TQ = [400\ K'K'']\ \varepsilon\ , \tag{4.9}$$

where

$$K' = \frac{R_f}{R_i} = \text{amplifier 4 gain}$$

$$K'' = \frac{\text{Potentiometer 5 setting}}{0.125}$$

Comparison of Equations (4.7) and (4.9) shows that

$$K = 400\ K'K''$$

Thus, by proper selection of K' and K'' any desired value of gain, K, within limits, may be achieved.

Results of Analog Tests

Structural Damping of Actuator Mass

A simple test was made to determine the amount of damping required to reduce vibration of actuator mass, m_a, (see Figure 7) to a

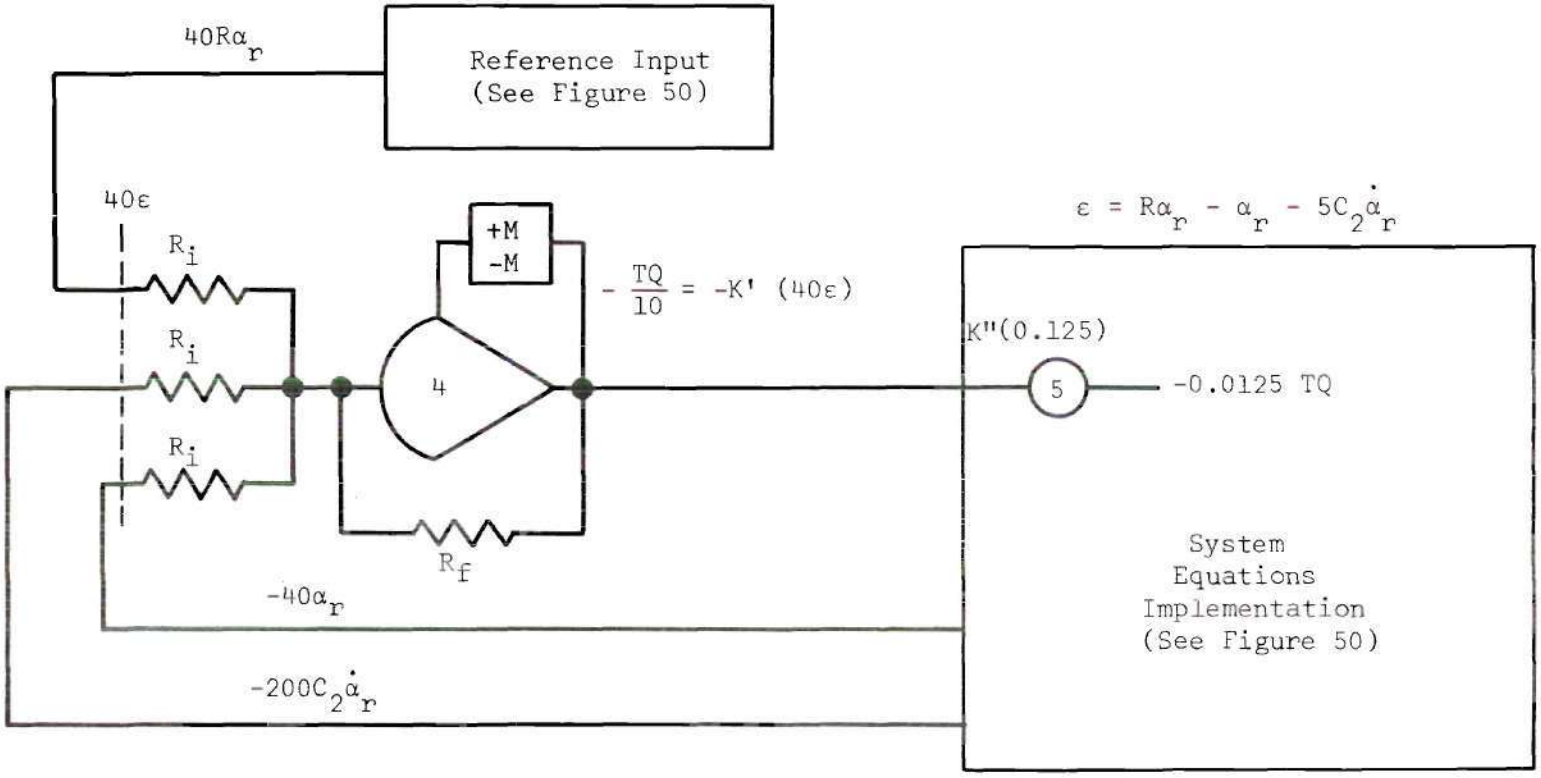

Figure 26. Analog Computer Circuit Diagram for Simulation of an Engine Gimbal Actuation System Employing Magnetic-Particle Clutch-Actuators

level such that it would not affect the rate feedback signal.

Consider the model in Figure 27, which may be derived from Figure 7 by assuming that vibration of the actuator mass is approximately the same when engine mass, m_e, is fixed.

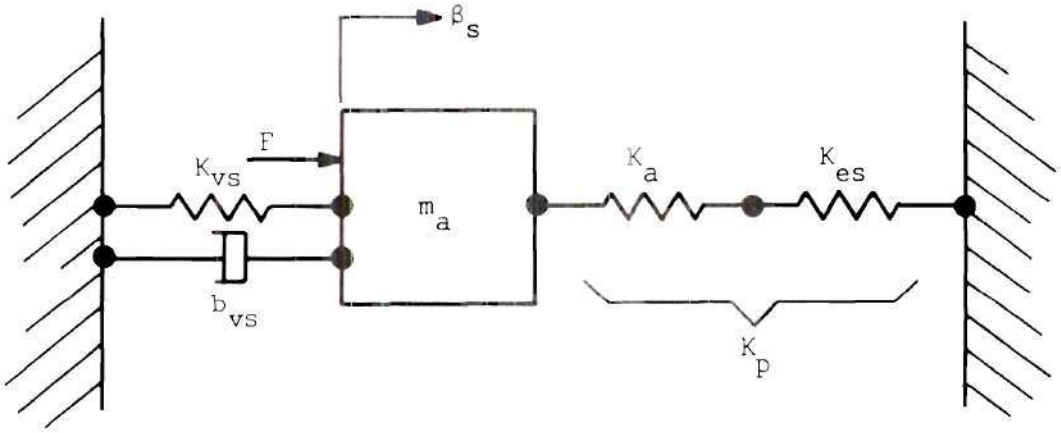

Figure 27. Model for Structural Damping Investigation

This is a good approximation, since $m_e >> m_a$. The actuator is also assumed to be locked, i.e., brake applied.

Equations of Motion. One may write the following dynamic equation for the system of Figure 27:

$$(m_a s^2 + b_{vs} s + K_{vs} + K_p)\beta_s = F \qquad (4.10)$$

where

F = disturbance force, lb.

The system characteristic equation is

$$s^2 + \left(\frac{b_{vs}}{m_a}\right)s + \frac{(K_{vs} + K_p)}{m_a} = 0$$

or

$$s^2 + 2\zeta_a \omega_{na} s + \omega_{na}^2 = 0 \ . \qquad (4.11)$$

This yields

$$\omega_{na}^2 = \frac{K_{vs} + K_p}{m_a} \ , \qquad (4.12)$$

and

$$\zeta_a = \frac{(b_{vs}/m_a)}{2\ \omega_{na}} \ . \qquad (4.13)$$

Figure 28, which displays analog data for β_s from a step response test where m_a was included, shows the effect of b_{vs} in damping actuator vibration. The vibration occurring for $b_{vs}/m_a = 0$ is shown in Figure 28 (a); the frequency of vibration may be seen to be 130 cycles per second. The oscillations are well-damped for $b_{vs}/m_a = 50$.

Substituting data from Table 6 into Equation (4.12), one may calculate

$$\omega_{na} = 815 \text{ rad./sec.}$$

or

$$\omega_{na} = 130 \text{ cycles/sec.}$$

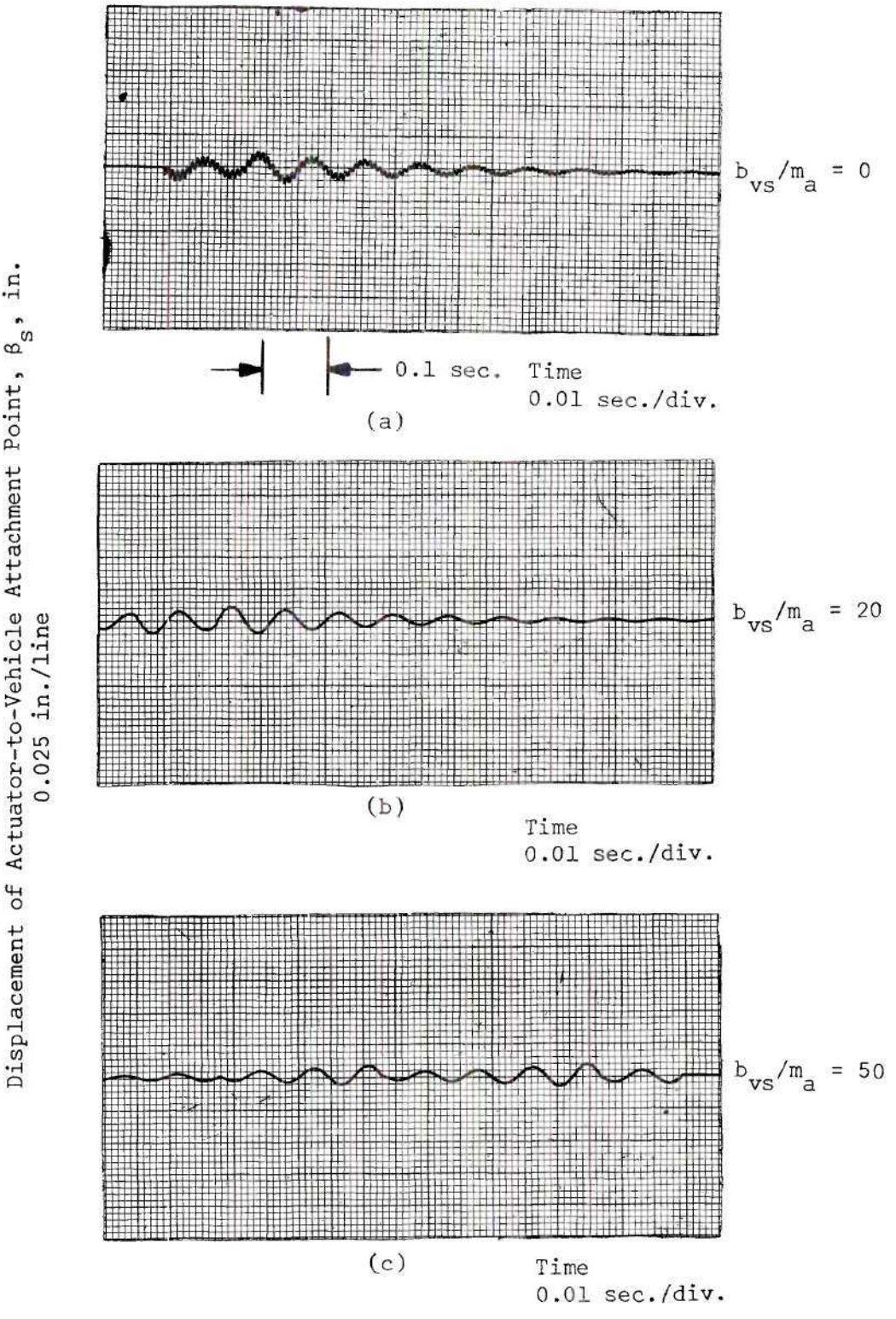

Figure 28. Effect of b_{vs} in Damping Actuator Vibrations

For $\frac{b_{vs}}{m_a} = 50$,

$$\zeta_a = \frac{50}{2\,\omega_{na}} = \frac{50}{2(815)}$$

$$\zeta_a = 0.0307$$

This damping should be easily provided by the structure, so that actuator vibrations of a magnitude sufficient for detrimental feedback effects should not be encountered. Therefore, in succeeding analog investigations, actuator mass, m_a, will be neglected. Damping, b_{vs}, will also be neglected, since its effect other than in damping the actuator's natural vibration is not significant.

Step Response Results

Appendix C contains data from step response tests which were conducted for each of the three clutch-types under consideration. The actuation rate in each case was 8 in./sec., and position and rate feedback were picked off of the "real" actuator output. Torque-characteristic parameters which were assumed are noted as necessary with the data.

General Results. Inspection of the data reveals that the magnetic-particle clutch-actuator dynamics for the torque levels assumed are the best of the three types considered. Best time response, least static error, and smoothest engine response are three characteristics which may be claimed by the magnetic-particle clutch-actuator. With selected values of rate feedback, operation was quite acceptable, but the system response was highly oscillatory for zero rate feedback.

Even though good system response was indicated, it is questionable whether magnetic-particle clutches of the power capability assumed in the study can even be obtained. Alternatives will be discussed shortly.

The friction-disc clutch is considered the second-ranking type dynamically. Even though a longer time delay is involved during engagement than for the wrap-spring clutch, smoother response compensates for the delay. No tendency to limit cycle was indicated as rate feedback was increased for the deadbands investigated.

Wrap-spring clutch operation resulted in the greatest degree of system oscillation because of the rapid engagement involved and accompanying energy storage in the structural compliances. Of the three clutch-types, however, the wrap-spring clutch-actuator was the only one that exhibited reasonable stability for zero rate feedback. The amount of compensation with increased rate feedback was limited, on the other hand, by limit cycle operation. Further discussion of the data for each clutch-type ensues.

Magnetic-Particle Clutch. Figures (55) through (61) are representative of the data recorded during simulation of a magnetic-particle clutch-actuator. For the assumed system, a maximum torque level, T_m, of 800 lb.-in. and a gain K of 1600 (lb.-in.)/in. resulted in good performance. One may note from Figure 55 that system performance improves greatly with an increase in rate feedback up to the point where the amount of lag becomes prohibitive. Figures 56 through 58 display results for a rate feedback coefficient, C_2, of 0.035 in./in./sec. and T_m = 800 lb.-in.

The effect of using a clutch that torque-saturates at a lower torque level is demonstrated in Figure 59, where T_m = 400 lb.-in. and K = 800 (lb.-in.)/in. The system becomes more sluggish with a decrease in T_m, but quite acceptable performance is possible by increasing C_2. However, a penalty in the form of increased response time is paid for the use of lower saturation torque and increased rate feedback, as may be seen by comparing the data for C_2 = 0.03 in Figure 55 to that for C_2 = 0.04 in Figure 59.

Very good system operation was achieved for K = 2000 (lb.-in.)/in. and T_m = 1000 lb.-in. The data is shown in Figure 60. However, a look at Figure 61, which compares clutch output velocities for the three combinations of T_m and K previously mentioned, shows that little is gained by increasing T_m from 800 to 1000 and K from 1600 to 2000. The lower-torque case (T_m = 400, K = 800) on the other hand requires more time for no-slip clutch engagement, with an accompanying increase in clutch heating. Therefore, this illustrates the tradeoff which must be made between clutch torque capability and heating due to slip.

The base clutch output speed assumed for this analog study was 100 rad./sec. (1000 RPM). The torque levels noted in the previous discussion were based on that speed. However, speeds of at least 3000 RPM are feasible with magnetic-particle clutches, so that the required torque levels could be reduced by a factor of 3. For example, for the 800 lb.-in. case,

$$TQ_{3000} = 800/3 = 267 \text{ lb.in.}$$

Maximum power dissipation would remain constant at

$$P_{d_{max.}} = T\dot{\theta}_s = (800)(100)$$

$$= 80{,}000 \text{ (lb.-in.)/sec.}$$

or

$$P_{d_{max.}} \simeq 12 \text{ hp.}$$

This value, of course, represents a maximum heat dissipation and would occur for only an instant, but it illustrates the demands made of a clutch in such a system. Since magnetic-particle clutches are presently available only in a range of power capabilities up to a few hundred watts, their use for the engine gimbal system assumed for this study is impractical. However, as noted earlier their dynamic performance is decidedly superior to that of the other two clutch types and should be seriously considered for the design of smaller systems.

Friction-Disc Clutch. Samples of data recorded during simulation of a friction-disc clutch-actuator are also included in Appendix C. This clutch-type was approximated as discussed earlier in this chapter under the heading "Clutch (and Brake) Dynamic Characteristics." Three primary levels of maximum clutch torque were investigated--200, 400, and 800 lb.-in. This was assumed to be the torque at which the disc clutch slipped, i.e., its maximum torque capability. An engagement time delay of 10 ms. and a torque build-up time of 20 ms. to maximum torque were assumed. Several values of system deadband were checked; the lowest value for which reasonable performance was obtained was 0.050 in.

Figures 62 through 65 show the system response to a 1/2-inch step for several values of rate compensation and the three torque levels previously mentioned. The system was unstable for zero rate feedback, but good results occurred for a rate coefficient of 0.03 to 0.04. Even with T_m = 200 lb.-in. quite acceptable step response was obtained, although a longer time was required to reach the command position as T_m was reduced. The important difference as a function of T_m is shown by Figure 66, where clutch torque and speed time histories were plotted for comparison. For T_m = 200 lb.-in. clutch speed never reaches prime-mover speed. The clutch slips continuously and would wear rapidly. For T_m = 800 lb.-in., in contrast, full speed is reached about the same time that full clutch torque develops. Increasing T_m from 800 to 1200 lb.-in. has little added effect, which indicates that an optimum regarding clutch heating and wear is reached somewhere between 400 lb.-in. and 800 lb.-in. The larger torque levels result in increased system oscillation compared to the T_m = 200 lb.-in. condition. At the sacrifice of clutch life the designer may gain a slight measure of increased smoothness of operation by using the smaller clutch. Figures 67 through 69 display data for 1/8-in. steps and other conditions listed. The first two figures show the increased instability brought about by narrowing the deadband. Figure 69 illustrates the effect of a decreased clutch engagement time, i.e., increased stability.

A serious shortcoming of the ON-OFF system may be noted in the data for the disc clutch--static error due to deadband. This is particularly serious for low amplitude input signals, as is shown in Figures 67 through 69.

Wrap-Spring Clutch. Simulation data for the remaining clutch-type is shown in Figures 70 through 75 of Appendix C. Chapter V reports the results of actuator tests which were made to check the mathematical model assumed for a wrap-spring clutch. That study assumed an actuation rate of 4 in./sec. and resulted in the selection of a maximum torque level, T_m, of 2000 lb.-in. in order to match analog data to actual test data. Additional analog tests showed that in changing from an actuation rate of 4 inches per second to 8 inches per second, increases in T_m above 2000 lb.-in. had little effect on the overall dynamics. The conclusion reached was that the wrap-spring actuator initially compresses the flexible structural members and ensuing motion results from the release of that stored energy. The torque level of 2000 lb.-in. was sufficient to provide the required initial structural deformation. Hence, the 8 in./sec. actuator was simulated using the same clutch model, since the same load and structural compliances were used in both cases. The data in Figure 70 displays engine and actuator response to step inputs of different magnitudes for zero rate feedback. The system operation may be seen to be highly oscillatory because of the impact-like engagement of the wrap-spring clutch, and the amplitude of oscillation may be observed to vary with command position. This latter characteristic may be attributed to the amount of stored energy in the system at the instant that the brake engaged. The effect of the engine load on the actuator appears as alternate compression and elongation of spring, K_a, which was included in the model to simulate actuator stiffness.

Figures 71 through 73 present data for simulated wrap-spring clutch-actuator operation for various amounts of rate feedback, and step magnitudes of 1/8-, 1/2-, and 1-in. For each step size general improvement in the form of decreased engine oscillation was achieved as C_2 was increased, but limit cycle operation occurred in each instance, placing a restriction on the amount of rate compensation which could be applied. The rate coefficient, C_2, at which limit cycle operation occurred appears to be a function of step-command magnitude (decreased rate feedback capability for an increase in step size) for the data shown. This should be discounted, as more complete data should show that no such trend exists as long as full actuation rate is achieved prior to entering the deadband.

A comparison may be made between the actuator and engine rates occurring for a 1-in. step command by referring to Figures 74 (a) and (b). Actuator rate may be observed to oscillate about a value of 8 in./sec. while the command position is being acquired, with engine velocity making greater excursions about the same average rate. Figure 74 (b) shows a reduced engine rate as the command position is approached and illustrates the stepping action of the actuator effected by the rate feedback.

Wrap-spring data displayed to this point was for an assumed clutch time delay of 5 ms. and a deadband of 0.05 in. The effect of a longer time delay was investigated by setting TD to 7 ms. The results (shown in Figure 75) were a more oscillatory engine response and a greater limit cycle amplitude, but more important, an unstable region was located for $C_2 = 0.015$, followed by stable operation and

eventually the expected unstable region for $C_2 > 0.035$. This type of operation is highly undesirable.

In general, the wrap-spring clutch-actuator simulation indicates inability of that device to perform acceptably at high actuation rates.

Digital Check of Analog Solution

In order to verify the analog computer solutions obtained in this study, a digital computer check was undertaken. A computer-library program employing the Runge-Kutta-Gill integration technique was used to solve simultaneously Equations (3.1) through (3.4) for the magnetic-particle clutch-actuator simulation. "Ideal" actuator rate was limited to 8 in./sec.

Figures 29 (a) and (b) present the results of the digital solution for a 1/2-in. step command with a rate feedback coefficient, C_2, of 0.00 and 0.02, respectively. Comparison of the equivalent analog data in Figure 55 shows the analog and digital solutions to be identical.

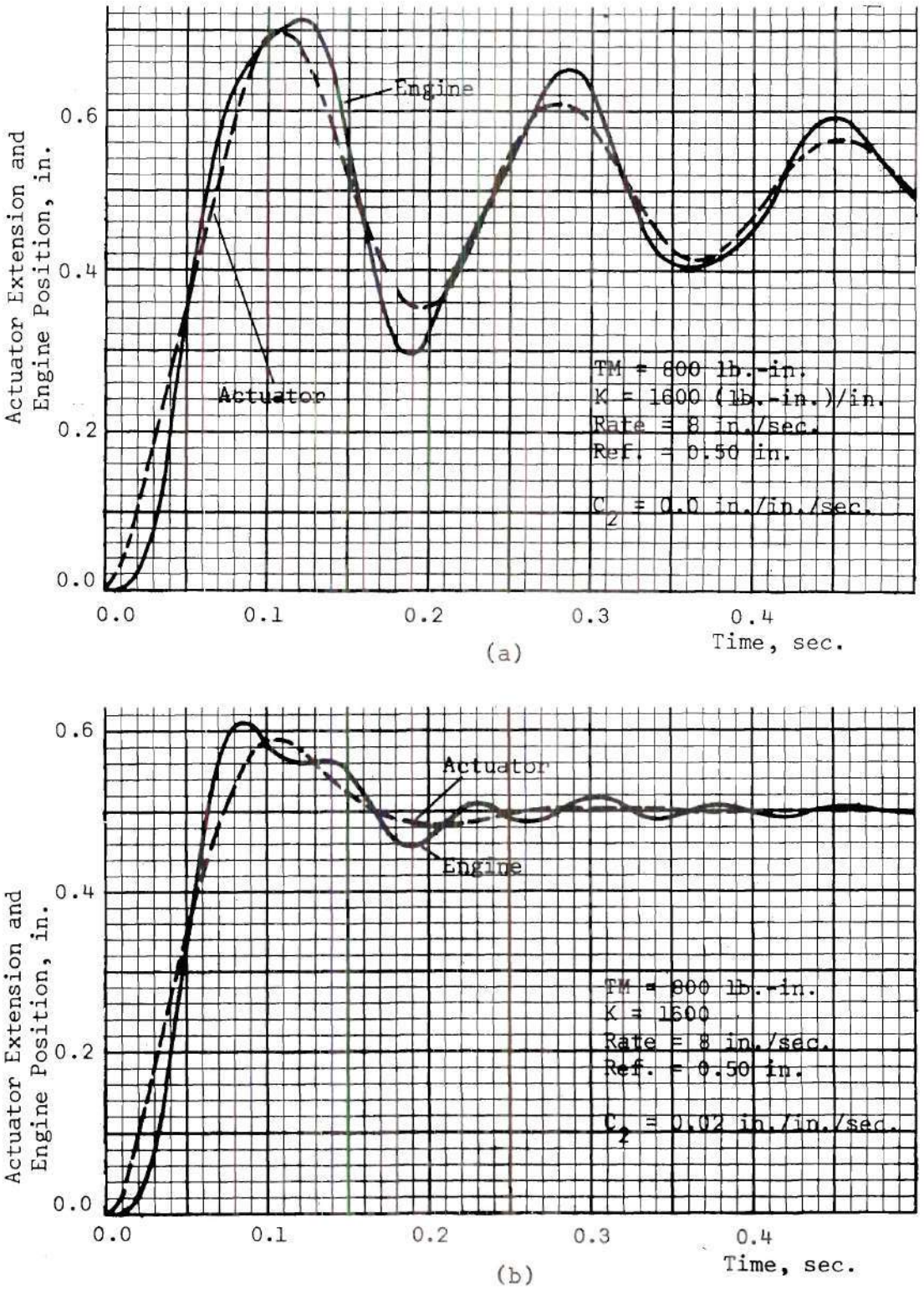

Figure 29. Data for Digital Check of Analog Computer Results

CHAPTER V

ACTUATOR TESTS

Introduction

The accuracy of the results of the analog computer study described in Chapter IV depends upon the degree to which the mathematical model assumed for the clutches represents actual hardware operation. The present chapter reports the results of hardware tests which were made to check the validity of the mathematical model assumed for a wrap-spring clutch. The wrap-spring clutch is especially difficult to model because of the highly non-linear nature of its operation; another factor is that wrap-spring clutches of the quality required for space applications are not readily available for testing to accurately determine their characteristics. Reference (1) reports tests of several industrial-type wrap-spring clutches; those clutches, however, were completely unsuited to the needs of a high speed actuator for space operation.

The above-mentioned tests were conducted on an existing clutch-operated power screw actuator employing high quality wrap-spring clutches. The device was the Curtiss 173300 Small Missile Servo System, manufactured by the Curtiss-Wright Corporation, Curtiss Division, Caldwell, New Jersey. Figure 30 is a schematic representation of the servo system, which includes an actuator equipped with position sensor and a servoamplifier.

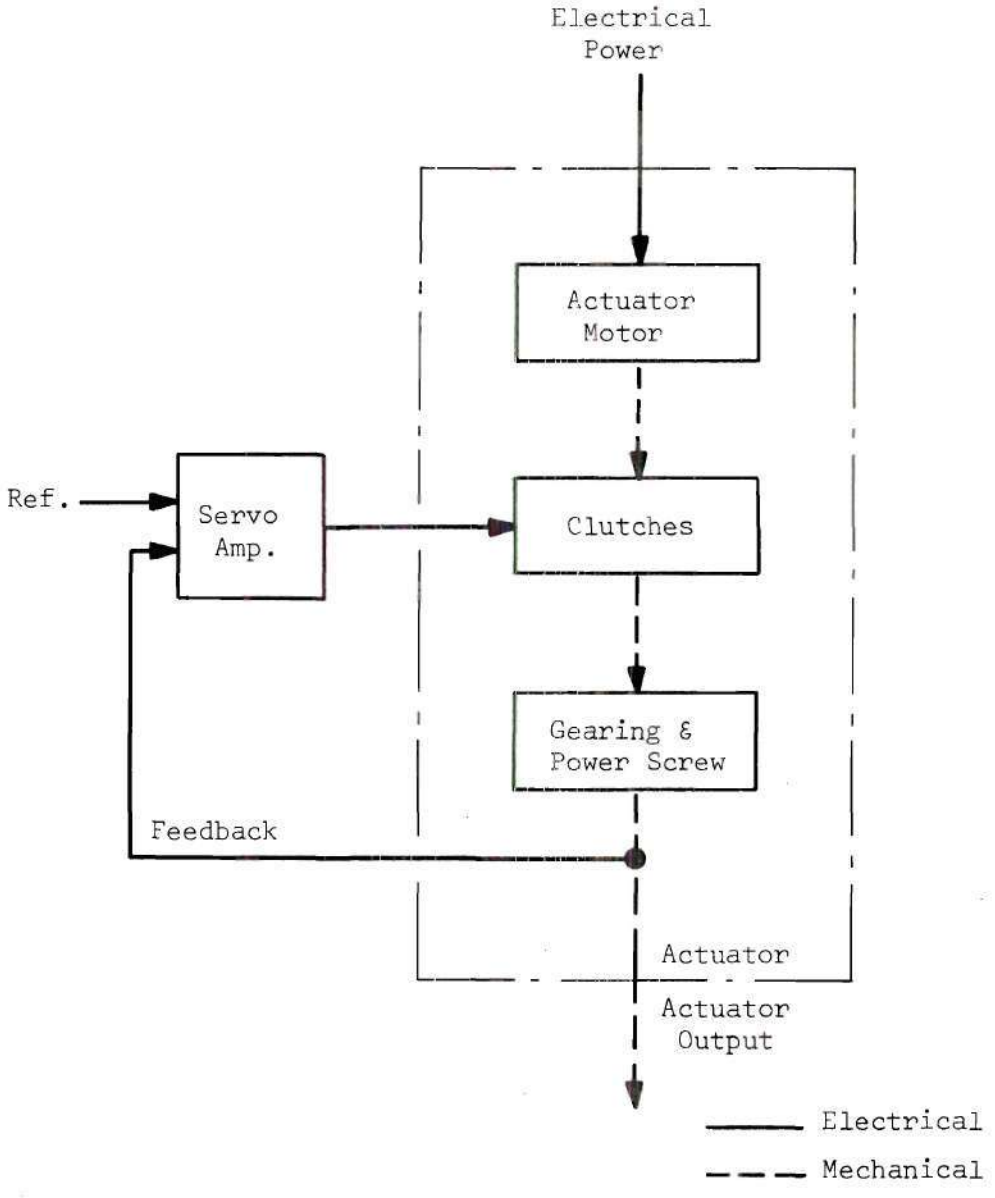

Figure 30. Wrap-Spring Clutch-Actuator Servo System Block Diagram

The actuator has a force capability of 750 lb., weighs 5 lb., and has an actuation rate of approximately 4 in./sec. A detailed discussion of this actuator and its characteristics may be found in reference (15).

The tests, which were conducted at the Astrionics Laboratory, Marshall Space Flight Center, Huntsville, Alabama, were designed to determine the actuator's response to various step and sinusoidal command inputs. The effect of rate feedback in damping the oscillations of a lightly damped gimballed rocket engine load was investigated. The work is discussed in more detail in the following sections of this chapter.

Test Concept

The hardware tests were conducted in such a fashion that the Curtiss actuator provided the wrap-spring clutch dynamics, while rocket engine and structural dynamics were simulated on an analog computer. The manner in which this was accomplished and the assumptions involved will be discussed briefly.

"Ideal" and "Real" Actuator

Before proceeding further it is necessary to establish a definition for the terms "ideal actuator" and "real actuator." As used in the present work the only difference between the two is that the ideal actuator may be considered perfectly stiff; the real actuator, on the other hand, deforms elastically under load--the total deformation being the sum of that experienced by each member of the power train and housing. The extensions of the two actuator types would be identical under no-load conditions. In Figure 31, which shows a system identical

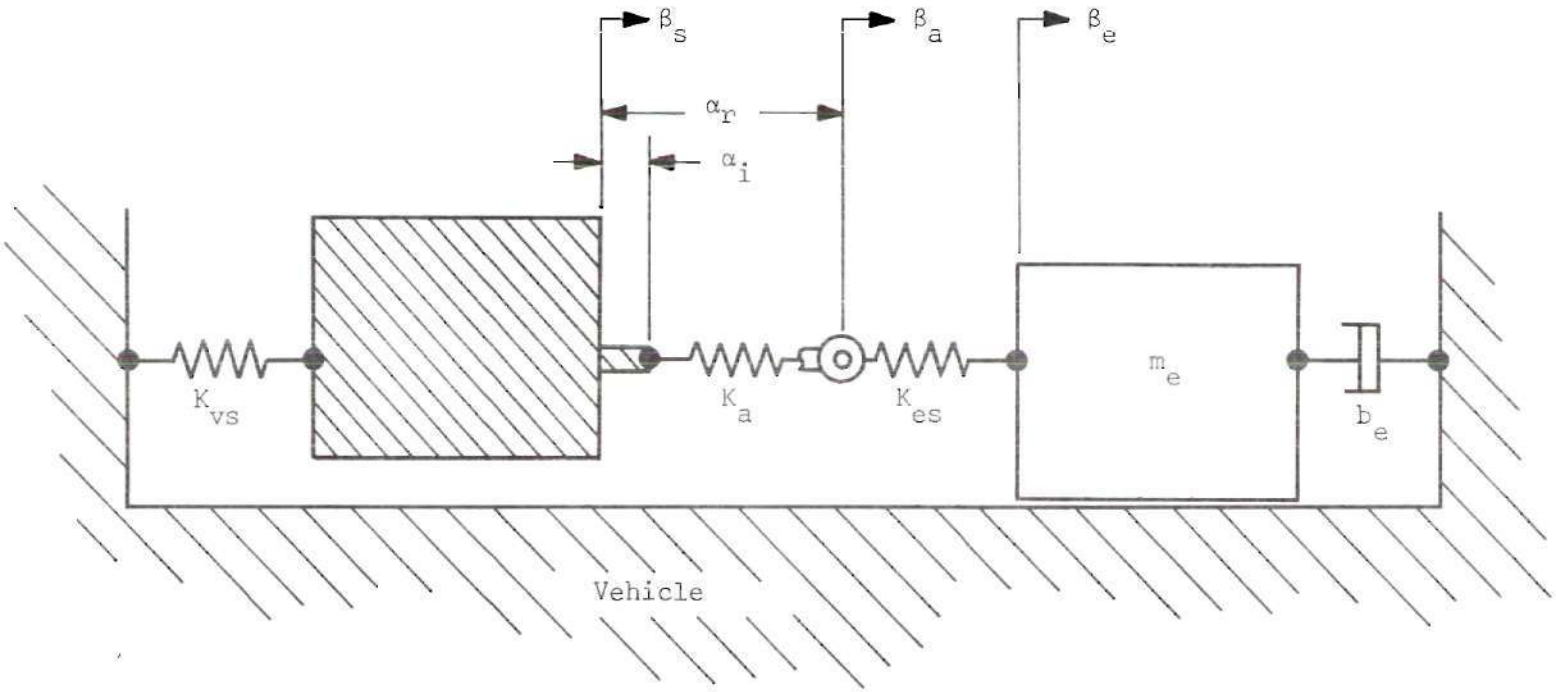

Figure 31. Model for Defining the Terms "Ideal Actuator" and "Real Actuator"

to the mathematical model used in the analog study of Chapter IV, ideal actuator extension is indicated by α_i, while real actuator output is represented by α_r. The real actuator may be considered as the ideal actuator with a lumped spring rate, K_a, included to account for overall deformation due to load.

Equations of Motion

For the ideal actuator,

$$\alpha_i = N\,\theta \tag{3.9}$$

where α_i = "ideal" actuator extension, in.,

N = effective gear reduction between clutch output and actuator ball-screw, in./rad., and

θ = clutch output displacement, rad.

The remaining equations of motion, which are identical to those used in the analog study of Chapter IV, are as follows:

$$m_a\ddot{\beta}_s + b_{vs}\dot{\beta}_s + (K_{vs} + K_a)\,\beta_s + K_a N\,\theta - K_a\beta_a = 0 \tag{3.1}$$

$$(K_a + K_{es})\,\beta_a - K_a\beta_s - K_a N\,\theta - K_{es}\beta_e = 0 \tag{3.3}$$

$$m_e\ddot{\beta}_e + b_e\dot{\beta}_e + K_{es}\beta_e - K_{es}\beta_a = 0 \tag{3.4}$$

The various parameters involved were defined in Chapter III. Neglecting m_a and b_{vs}, and substituting from Equation (3.9), one may obtain:

$$\beta_s = -\left(\frac{K_a}{K_a + K_{vs}}\right)(\alpha_i - \beta_a) \tag{5.1}$$

$$\beta_a = \left(\frac{K_a}{K_a + K_{es}}\right)(\beta_s + \alpha_i) + \left(\frac{K_{es}}{K_a + K_{es}}\right)\beta_e \tag{5.2}$$

$$\ddot{\beta}_e = -\frac{b_e}{m_e}\dot{\beta}_e - \frac{K_{es}}{m_e}\beta_e + \frac{K_{es}}{m_e}\beta_a \tag{5.3}$$

After substituting data from Table 6 for the system parameters, the following equations result:

$$\beta_s = -0.883\ \alpha_i + 0.883\ \beta_a \tag{5.4}$$

$$\beta_a = 0.789\ \alpha_i + 0.789\ \beta_s + 0.211\ \beta_a \tag{5.5}$$

$$\ddot{\beta}_e = -8.04\ \dot{\beta}_e - 18{,}850\ \beta_e + 18{,}850\ \beta_a \tag{5.6}$$

The only additional required information is an expression for α_i. One may note that if it were possible to measure α_i, i.e., to determine

$$\alpha_i = \alpha_i(t)\ ,$$

Equations (5.4) through (5.6) could be solved using an analog computer. In addition, according to Equation (3.9), information concerning clutch operation would be gained.

Realizing the Ideal Actuator

A good approximation to the "ideal" actuator may be attained by operating an actuator under a no-load condition; "ideal" actuator position may be measured using a transducer. Since there is no load to cause deformation, the device appears perfectly stiff. There is, of course, a problem, in that the actuator may not perform the same loaded as when unloaded. This would be true of both magnetic-particle clutch and friction-disc clutch actuators because both types slip during engagement to an extent determined by load.

The nature of clutching action of the wrap-spring, however, will allow an actuator employing that clutch-type to be tested with a reasonable degree of accuracy with no load. During engagement, once the spring wrap-up is complete, no additional slip occurs, and the load is connected rigidly to the actuator motor as long as no overrunning by the load occurs. Hence, unless the wrap-spring clutch is loaded to failure, its engagement is independent of load. The assumption is made here that a high speed actuator motor operating through high-reduction gearing would experience negligible speed variation, resulting in a constant clutch input speed over the normal load range.

The assumption of the wrap-spring clutch-actuator's load independence is supported by reference (15).

The hardware tests, as was previously stated, were conducted so that the Curtiss actuator served as a model for wrap-spring clutch operation. Although under the no-load condition the actuator was considered "ideal" as defined earlier, such factors as clutch and brake engagement and release time delays, inertia and friction of the power

train, and maximum actuation rate remained as characteristics of the device. A linear feedback potentiometer was available on the actuator for measuring extension, α_i; this signal was fed directly into an analog computer as a model for the actuator dynamics.

As noted earlier, the implementation on the computer of Equations (5.4) through (5.6) provided the rocket engine and structural dynamics.

There are a number of advantages to making a test of this type:

1. There is no hardware to construct, so that a minimum of time is required;

2. The testing is independent of the actuator's force capability; the only analog computer input is the actuator position signal. Thus, it is possible to get an estimate of system performance using an existing piece of hardware. It is necessary, however, that the clutch operating time, which will generally increase as power capability increases, be not greatly different from that for the final hardware.

Test Procedure

The actuator tests were of two basic types--step response and frequency response. In both types the effect of providing rate feedback to damp out the oscillations of a lightly-damped, gimballed rocket engine load was investigated. The step tests were made first, what appeared to be optimum values of rate feedback were then selected for a number of frequency response runs. The servoamplifier used with the actuator was equipped for varying the system deadband; the effect of this variable on system performance was also examined.

The manner in which the test equipment was connected is shown

in block diagram form in Figure 32. During the step response tests, the command, or reference, signal was generated by a function switch in the analog computer; a frequency response analyzer supplied a sinusoidal reference input to the servoamplifier for frequency response tests. A function generator was used for miscellaneous testing during the equipment setup phase. All equipment used in the testing is listed in Table 4.

Table 4. List of Test Equipment

Item	Description	Model No.	Manufacturer
1	Frequency Response Analyzer	101	Industrial Measurements Corp., Pomona, California
2	X-Y Recorder	300	Electro Instruments Inc., San Diego, California
3	Strip Chart Recorder	RF1783-70	Brush Instruments Cleveland, Ohio
4	Analog Computer	10/20	Systron Donner
5	Function Generator		Wavetek San Diego, California
6	Rate Sensor (D.C. Motor)		Globe Industries Dayton, Ohio

Servoamplifier

The servoamplifier employed in the work herein described was supplied by Curtiss-Wright and was designed specifically for the actuator. The unit, shown in block diagram form in Figure 33, consists of a

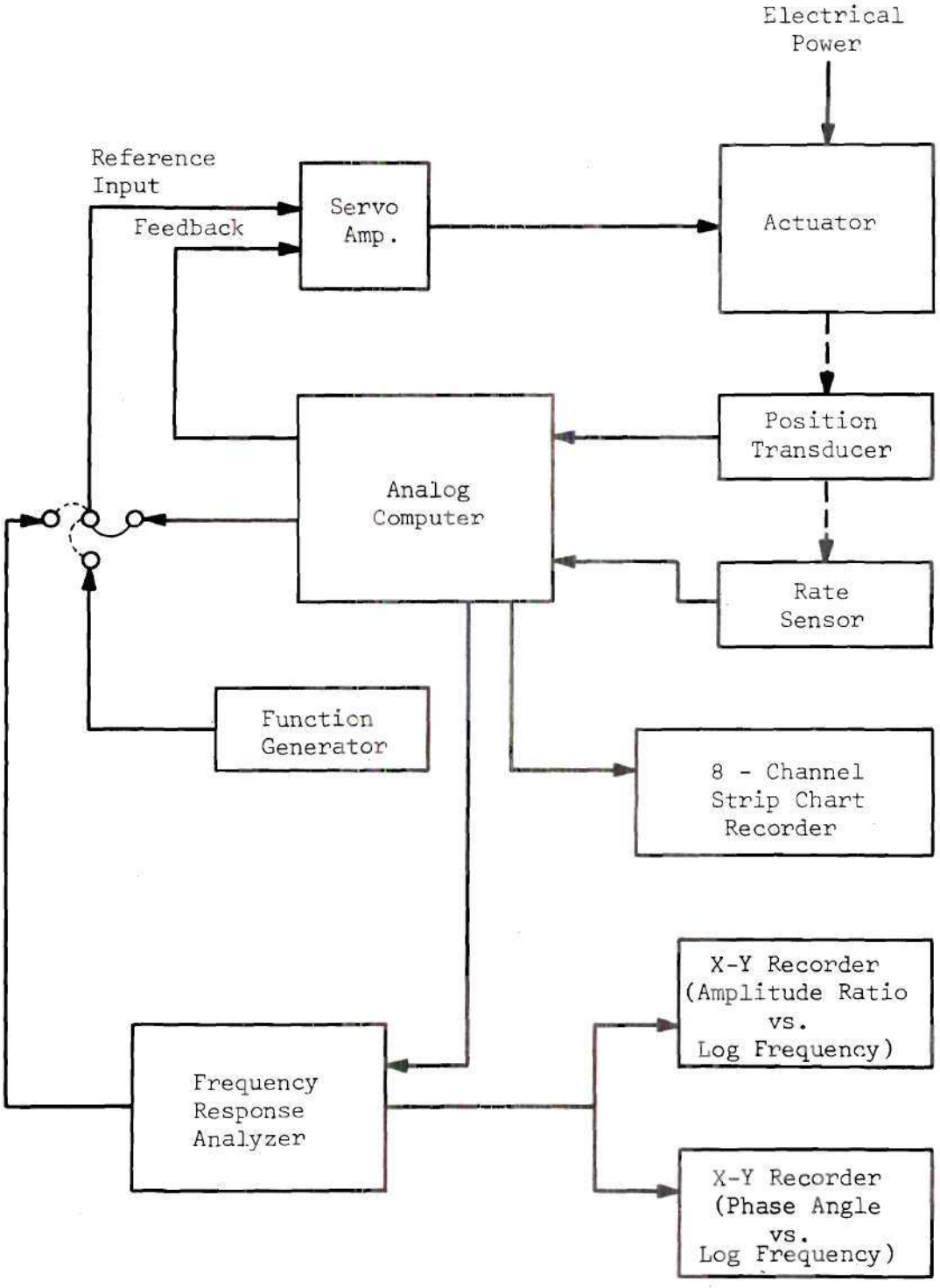

Figure 32. Block Diagram of Test Equipment

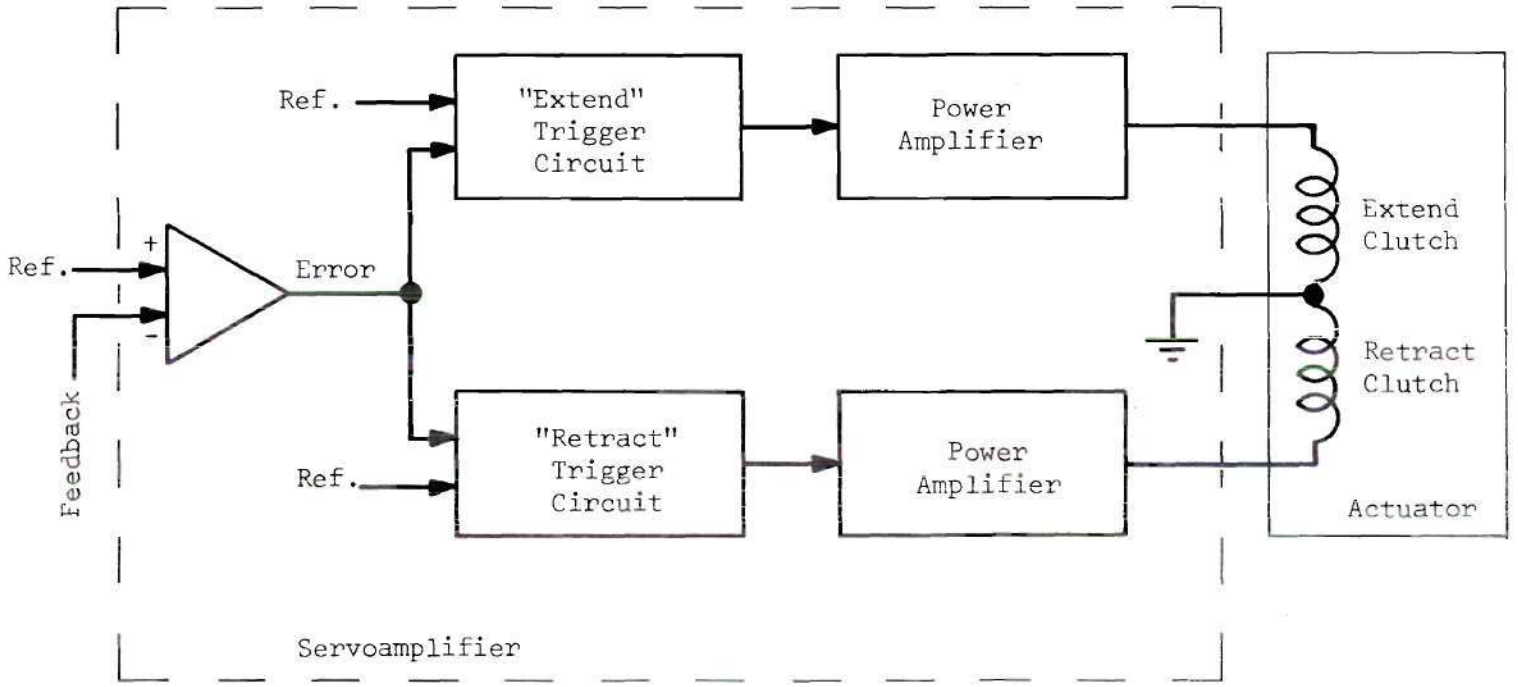

Figure 33. Block Diagram of Servoamplifier

summing amplifier, two trigger circuits, and two power stages. In operation, an error signal is generated by the summing amplifier which sums the reference input and feedback signals. If the magnitude of the error is greater than the system deadband, one of the trigger circuits fires (depending on the sign of the error signal) and turns on its cascaded power stage, thus energizing the proper clutch coil. By adjusting a reference signal which determines the voltage at which the trigger amplifier fires, the system deadband may be varied, as noted previously.

Analog Computer Circuit Used in Test

A block diagram of the test setup is shown in Figure 34; the complete circuit involved is shown in Figure 35.

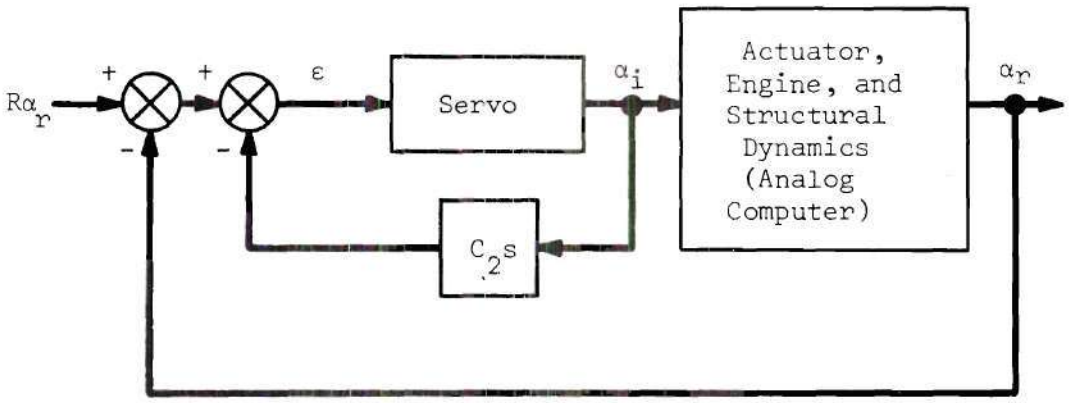

Figure 34. Block Diagram of Simulation Showing Feedback Signals

The latter diagram includes the interconnection of the servoamplifier, actuator, position transducer, rate sensor, and analog computer circuitry.

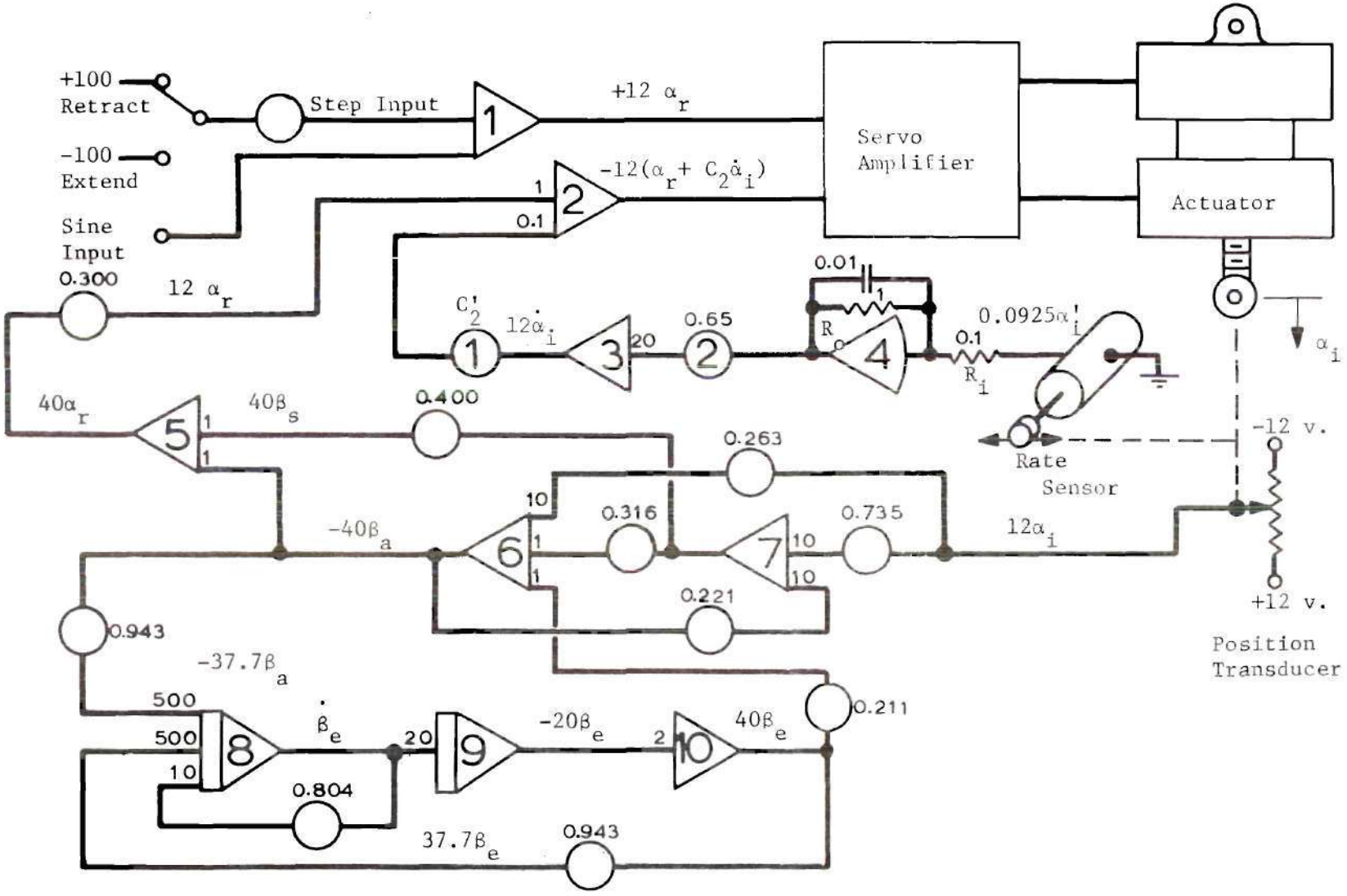

Figure 35. Analog Computer Circuit Diagram for Actuator Test

The portion of the diagram including amplifiers 5 through 10 is the analog computer implementation of the actuator, rocket engine, and structural dynamics as defined by Equations (5-4), (5-5) and (5-6). Amplifiers 2 through 4 were used to generate or condition the feedback signals for the servo system.

Both position and rate feedback should be taken from the actuator output (opposed to engine output) for best system performance. The measurable data from the actual hardware is, of course, that which is represented by the "real" actuator output in Figure 31, i.e., α_r and $\dot{\alpha}_r$ for actuator extension and rate, respectively. From Figure 31, one may note that

$$\alpha_r = \beta_a - \beta_s \ .$$

Thus, amplifier 5 in the circuit diagram of Figure 35 is the implementation of this equation for real actuator extension.

Two techniques were attempted in order to generate a rate feedback signal. One was to differentiate actuator extension, using an analog approximate differentiation circuit. Differentiation, however, is an inherently noisy process, so that as the feedback coefficient was increased, the noise component of the error signal becomes large enough to cause momentary transitions out of the system deadband, giving rise to false clutch signals. Hence, the differentiation technique was abandoned in search of a more favorable one.

The technique actually employed was to attach a rate transducer to the actuator output. As no linear rate sensor was readily available,

one was contrived using a small, permanent-magnet, direct current motor, which was driven by friction from a flat metal strip attached to the actuator output. It is important to note that although $\dot{\alpha}_r$ would be the rate feedback signal in an actual hardware case, according to Figure 35 the rate-sensor technique yielded "ideal" actuator rate, $\dot{\alpha}_i$. The generation of $\dot{\alpha}_i$ was a necessity since, as was discussed earlier in this chapter, the actuator output was "ideal" actuator extension, α_i. The purpose in making the actuator tests, however, was to provide a check on the mathematical model assumed in Chapter IV. Hence, it was possible to compare the Chapter IV analog results for "ideal" actuator rate feedback to the results from the Huntsville tests, and thus achieve the same end.

Amplifiers 3 and 4 in Figure 35 were used to filter and amplify the rate sensor output. It was desired that the input to potentiometer 1 be 12 $\dot{\alpha}_i$. Calibration of the rate sensor showed that its output was 0.0925 $\dot{\alpha}_i'$; hence, it was necessary that

$$12\ \dot{\alpha}_i = 0.0925\ G\ \dot{\alpha}_i'$$

or

$$G = \frac{12}{0.0925} = 130$$

where G = overall steady-state gain of the analog circuit between the rate sensor and potentiometer 1.

This may be seen to be the case by referring to the analog circuit diagram.

The filtering mentioned in the previous paragraph was achieved at amplifier 4, where

$$\frac{e_o}{e_i} = \frac{R_o}{R_i}\left[\frac{1}{\tau s + 1}\right]$$

with

$$\tau = \frac{1}{\omega} = R_o C = 0.01 \text{ sec.}$$

The total feedback signal was generated at the output of amplifier 2:

$$O_2 = -12\ (\alpha_r + 0.1\ C_2'\ \dot{\alpha}_i)\ ^*$$

or

$$O_2 = -12\ (\alpha_r + C_2\dot{\alpha}_i)$$

where O_2 = amplifier 2 output

$C_2 = 0.1\ C_2'$

C_2' = potentiometer 1 setting $(0 \leq C_2' \leq 1)$

---

*The position transducer (feedback potentiometer) on the actuator had ± 12 v. applied. Since the maximum actuator stroke is 1 inch, the output of the transducer must be 12 α_i for a scale factor of 1 v./in. Hence the factor of 12.

Summing this feedback signal with the reference input in the servoamplifier (see Figure 35), the result is error signal:

$$12\ \varepsilon = 12\ (R\alpha_r - \alpha_r - C_2\dot{\alpha}_i)$$

or

$$\varepsilon = R\alpha_r - \alpha_r - C_2\dot{\alpha}_i\ .$$

Compare this to the error signal in the block diagram of Figure 34.

Test Results

Appendix D contains data from the actuator tests described in the foregoing sections of this chapter. The results of both step response and frequency response tests are included, with all data being taken for either of two values of system deadband (DB)— 0.0312 in. or 0.0416 in. The particular values of DB evolved from having chosen

$$12\ DB = 0.375\ v.$$

and

$$12\ DB = 0.500\ v.$$

in the process of making the tests. Allowing

$$1\ v. = 1\ in.$$

in scaling the problem, one may calculate the deadbands above.

Figures 76 through 82 show general operating conditions for step commands of 1/8, 1/4, 1/2, and 1 in. for the case when there is no rate feedback. For example, Figure 72 displays engine position and rate, "ideal" actuator position (actuator feedback potentiometer output), actuation rate (from rate sensor), and combined feedback signal (Amplifier 2 output). One may note that for $C_2 = 0$ (zero rate feedback), the data labelled "Feedback," is "real" actuator position since

$$12\ (\alpha_r + C_2\dot{\alpha}_i) = 12\ \alpha_r$$

Hence, the effect of actuator stiffness, K_a, may be seen by comparing $12\ \alpha_i$ and $12\ \alpha_r$. From Figure 79 actuation rate may be seen to be slightly more than 4 in./sec., and engine rate has an average value which is the same.

Rate feedback coefficient, C_2, was varied to observe its effect on system performance. Figures 83 through 94 show alternately engine position and the corresponding actuator position resulting from that investigation. In each case C_2 was increased in even increments from a value of 0.02 until limit cycle operation was achieved. The zero rate feedback case was shown for reference each time. From the data taken in those tests, the optimum value for C_2 appears to be roughly 0.02. For that coefficient, the engine ringing was reduced significantly (by more than 50 per cent in the case of a 1/8-in. step) compared to the zero-rate case. Increasing C_2 beyond 0.02 results in unnecessary delay in achieving the command position. Figures 83 through 94 also illustrate

the effect of deadband on system performance in that a larger value for C_2 was required to initiate limit cycle operation for the wider deadband. An undesirable increase in static error also results with increased deadband.

Figures 95 and 96 depict the effect of the rate feedback coefficient on engine rate and actuator rate. The latter figure shows the increased stepping action for increases in C_2 as the actuator attempts to reduce system oscillations.

General operating conditions for optimum rate feedback, i.e., for $C_2 \approx 0.02$, are shown in Figures 97 through 101. Finally, general operating conditions are shown for a limit cycle case in Figure 102.

Frequency response data for $\beta_e/R\alpha_r$ is included in Figures 103 and 104 for amplitudes of 1/8, 1/2, and 1 in. and $C_2 = 0.0$ and 0.02 in./in./sec.

Comparison of Analog and Actuator-Test Results

A previously cited goal of the actuator tests was to provide a check on the mathematical model assumed for the wrap-spring clutch-type. This section compares analog simulation data to that obtained from the actuator tests.

The analog data of interest, which is also contained in Appendix D, was generated for an actuation rate of 4 in./sec. to match that of the test actuator. The wrap-spring clutch simulation techniques discussed in Chapter 4 and the analog computer circuitry displayed in Figure 50 of Appendix B were used in conducting the analog tests.

A trial-and-error approach was used to adjust the torque-

characteristic parameters noted on Figure 24. The values given below resulted in a computer simulated system with outputs closely matching those obtained from the actuator tests:

TD = 5 ms.

TBU = 2000 lb.-in./sec.

TM = 2000 lb.-in.

TQD = 10 ms.

A selected set of superimposed step response time histories confirming the matching of actuator test results by the analog computer simulation for rate feedback coefficients of 0.00 and 0.02 in./in./sec. and reference positions of 1/8 and 1/2 in. are shown in Figure 36.

Figure 105 displays additional analog data for various step magnitudes for zero rate feedback and may be compared to actuator test data in Figure 76. Good correlation was achieved.

Figures 106 through 113 show general operating conditions in the system for a rate feedback coefficient, C_2, of 0.0 and 0.02 and for deadbands of 0.031 and 0.042 in. The comparable actuator test data may be found in Figures 77 through 82 and 97 through 101. A limit cycle case is shown in Figure 114 and compares favorably with the actuator test results in Figure 102.

Further analog and actuator-test data for comparison may be found in Figures 115 through 119 and 83 through 94, respectively. These figures show actuator and engine step response data for variations in rate feedback coefficient, C_2. In each case the actuator test data shows more correction achieved than was predicted by the analog simulation for a given increment of rate feedback coefficient, C_2.

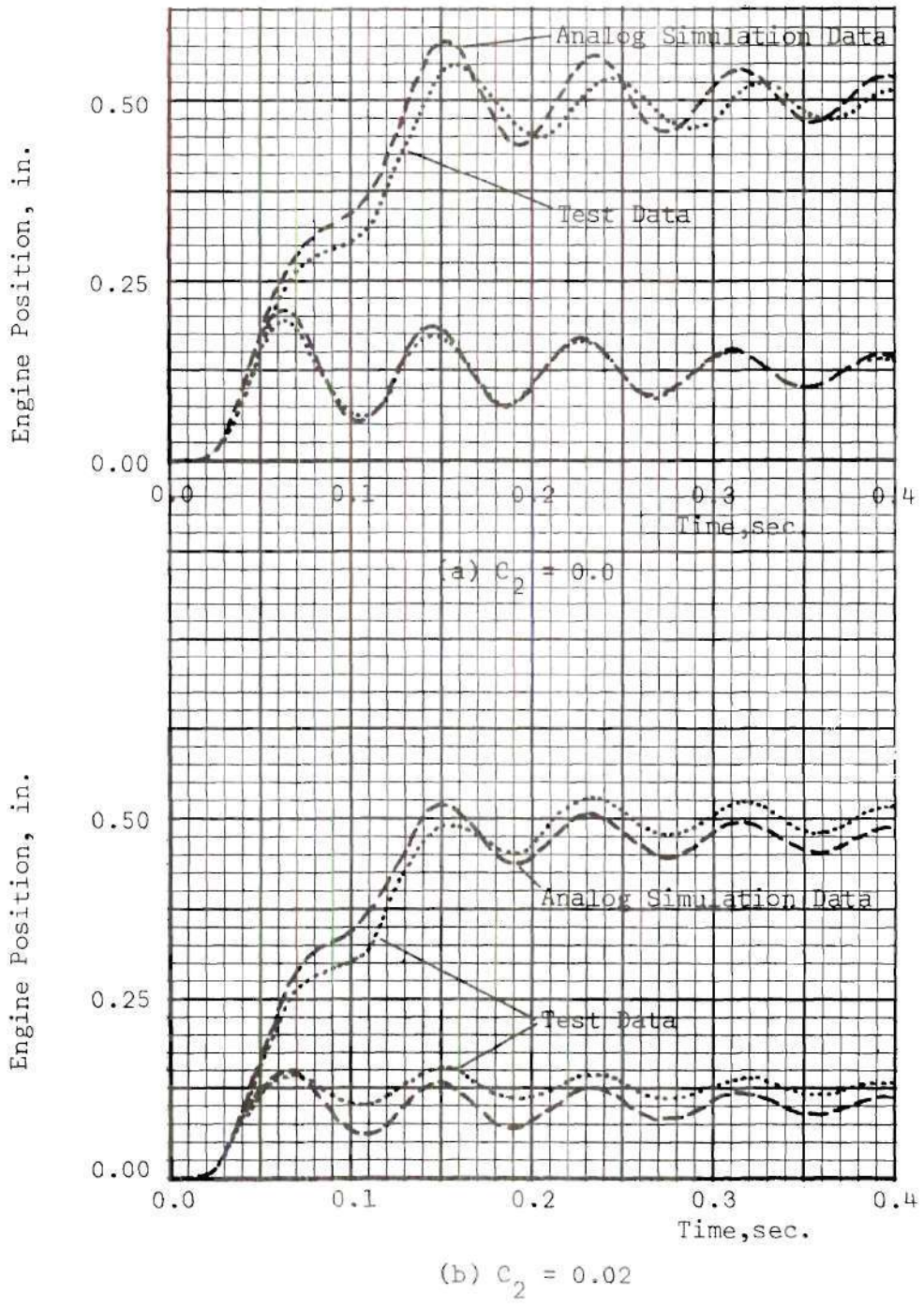

Figure 36. Comparison of Wrap-Spring Clutch-Actuator Test Data and Analog Computer Simulation Data for 1/8- and 1/2-in. Step Response Tests

However, the values of C_2 at which limit cycle operation first occurred showed close agreement in all cases.

In general, very good correlation was obtained between the analog simulation data and actuator test results.

CHAPTER VI

EXTENSION TO OTHER SYSTEMS

Introduction

An attempt was made to extend the results of the preceding work to systems with the same general form as those assumed in this study, but different parameter values. This was possible to a limited extent for a greatly simplified system. Two cases were considered: one, a system having a linear torque-to-error relationship, and two, an ON-OFF system. In both cases the feedback arrangement of Figure 11 (a) was assumed.

System With a Linear Torque-to-Error Relationship

In Chapter IV a linear torque-to-error characteristic with saturation was assumed to simulate a magnetic-particle clutch-actuator in an engine gimbal system. Useful results may also be obtained by assuming simply a linear relationship without saturation. This is true if small error signals are assumed, so that operation is always on the linear portion of the characteristic. Under this assumption the system becomes linear, and all the techniques available for linear analysis are applicable. Furthermore, a third-order system results, so that techniques for the design of such systems may be applied as outlined in reference 21.

One shortcoming of the use of a linear system as discussed above is that no actuation rate limit is imposed. Hence, it is necessary to

check the resulting rate to determine if it greatly exceeds the assumed maximum actuation rate for the design in question. If it departs radically from the maximum value, a more complicated simulation technique, where limiting is imposed may be required, or new parameter values may be selected. For example, a lower torque-to-error gain (resulting in lower velocities) could be allowed, assuming other requirements could still be met.

Mathematical Model and Equations of Motion

Consider the model shown in Figure 37, where α represents actuator motion, K_e is a lumped spring rate which includes spring rates K_a, K_{vs} and K_{es} of the model shown in Figure 7. Parameters m_e and b_e are the same as in the model of Chapter III.

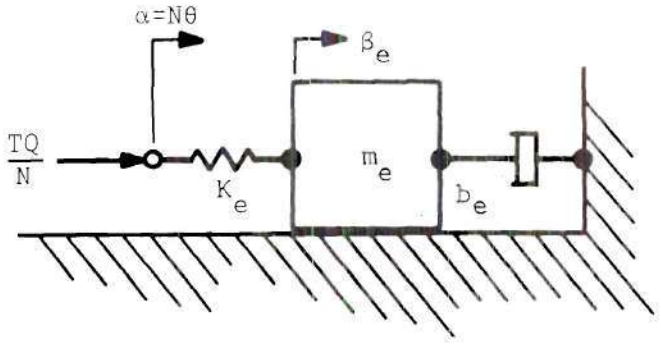

Figure 37. Simplified Model for an Engine Gimbal System

The following relations may be derived for the model:

$$\frac{\alpha}{TQ/N} = G_4(s) = \frac{s^2 + 2\zeta_e\omega_{ne}s + \omega_{ne}^2}{\omega_{ne}^2 s(m_e s + b_e)} \qquad (6.1)$$

$$\frac{\beta_e}{\alpha} = G_5(s) = \frac{\omega_{ne}^2}{s^2 + 2\zeta_e\omega_{ne}s + \omega_{ne}^2} \tag{6.2}$$

where

ω_{ne}^2 = K_e/m_e, 1/sec.^{2},

$2\zeta_e\omega_{ne}$ = b_e/m_e, 1/sec.,

TQ = total clutch output torque, lb.-in.,

TQ/N = actuator force output, lb., and

Other factors as defined earlier.

The entire engine gimbal system may be represented by the block diagram of Figure 38 from which the following equation can be derived:

$$\frac{\beta_e}{R\alpha} = \frac{b_o}{b_3s^3 + b_2s^2 + b_1s + b_o} \tag{6.3}$$

where

$$b_3 = C_2$$

$$b_2 = \frac{K_e N}{K} + \frac{b_e C_2}{m_e} + 1$$

$$b_1 = \frac{b_e}{m_e}\left[\frac{K_e N}{K} + 1\right] + \frac{C_2 K_e}{m_e} \tag{6.4}$$

$$b_0 = \frac{K_e}{m_e} .$$

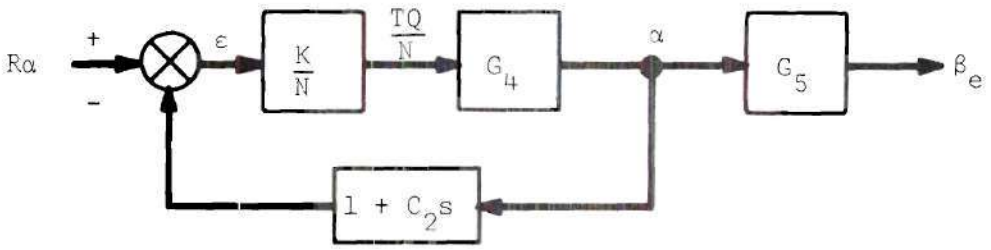

Figure 38. Block Diagram for Assumed Linear Engine Gimbal System

For the parameters in Table 6 and

$$K = 1600 \text{ lb.-in./in.},$$

$$C_2 = 0.02 \text{ in./in./sec.},$$

and

$$K_e = \frac{K_a K_{vs} K_{es}}{K_a K_{vs} + K_{vs} K_{es} + K_{es} K_a}$$

$$= 12{,}250 \text{ lb./in.},$$

Equation (6.3) becomes

$$\frac{\beta_e}{R\alpha} = \frac{5780}{0.02\, s^3 + 1.773\, s^2 + 128.7\, s + 5780} \qquad (6.5)$$

This equation may now be solved by conventional Laplace Transform methods. An alternate approach which will be discussed briefly is to apply a technique outlined in reference (21) in which Gowdy presents a method for predicting transient characteristics for a third-order system of the form shown in Figure 39.

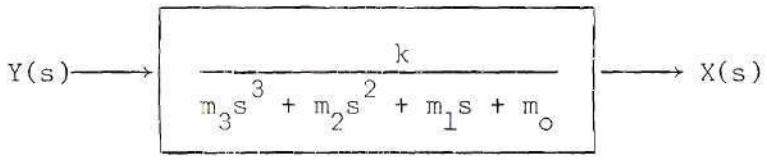

Figure 39. Block Diagram of a Third-Order Linear System

Three important characteristics--overshoot, rise time, and settling time--are rapidly predicted (in about 5 minutes) by the technique outlined by Gowdy if the coefficients m_0, m_1, m_2 and m_3 are known.

Applying Gowdy's analysis procedure to Equation (6.5), the following results are obtained:

Overshoot = 30%

Rise Time = 25 ms.

Settling Time (5%) = 205 ms.

A comparison is shown in Figure 40 of a digital solution of the complete system equations (Equations (3.1) through (3.4)) for a linear torque-to-error relationship with no actuation rate limiting and a digital solution of the simple third-order system equation (Equation 6.5). The simplified equation constitutes a suitable approximation to

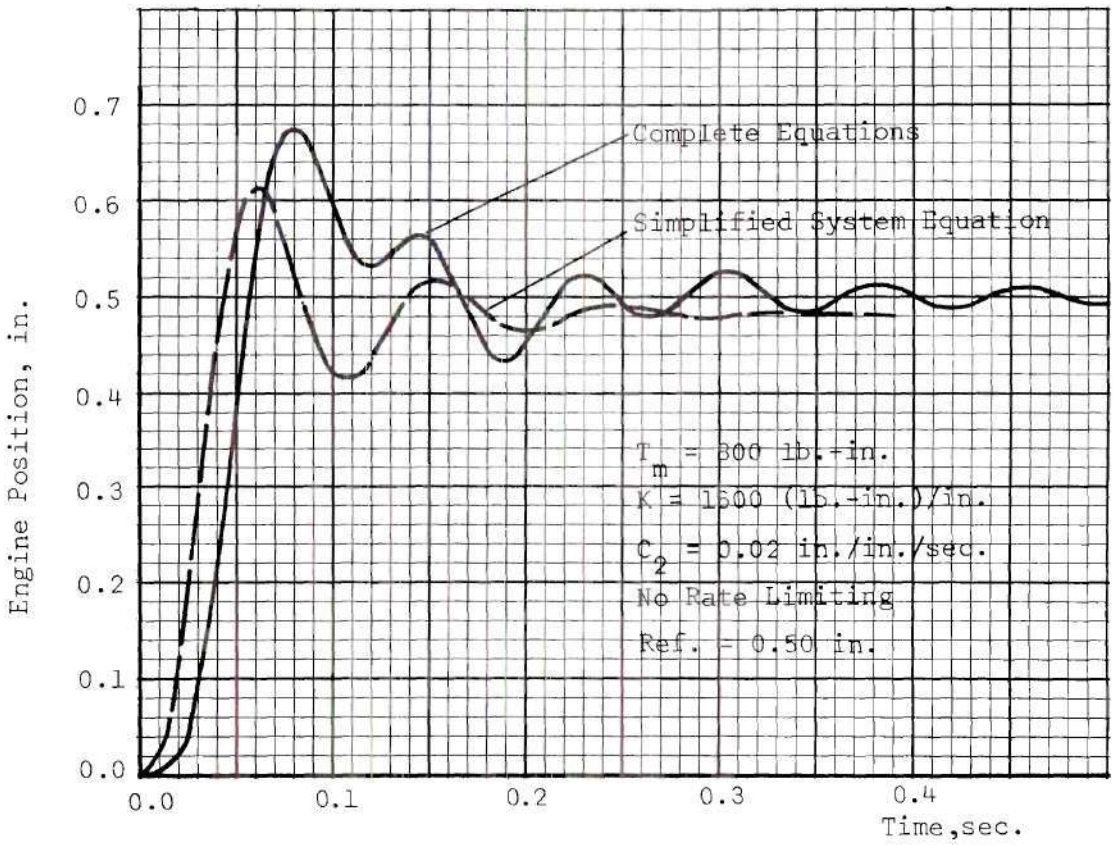

Figure 40. Comparison of Digital Solutions of the Complete Equations of Motion and the Simplified Equation

the more complicated system.

From the complete solution plot in Figure 40 for parameter values identical to those assumed in the simplified analysis by Gowdy, the following characteristics may be obtained:

Overshoot = 35%

Rise Time = 28 ms.

Settling Time (5%) = 208 ms.

The results may be seen to agree quite well for the two approaches.

The results of the linear analysis may be compared to the corresponding case where both torque saturation and rate limiting occur by reference to Figure 55 for $C_2 = 0.02$. There the following data may be computed:

Overshoot = 22%

Rise Time = 32 ms.

Settling Time (5%) = 204 ms.

Again the results are in good agreement.

Checking the maximum actuation rate occurring for the data of Figure 40 (i.e., the linear case without rate limiting, it was found to exceed the assumed 8 in./sec. rate for a period of 30 ms., with a maximum of 10 in./sec. occurring for only 5 ms. Hence, the results are considered acceptable.

ON-OFF System

The nonlinearity characterizing ON-OFF systems makes prediction of performance for different sets of parameters very difficult. However, usable results may be deduced by relatively simple considerations. Discussed below are brake time delay, inertial load deceleration, and peak engine oscillation--factors which influence deadband requirements. In addition, consideration is given to a factor related to brake heating--energy dissipation during load deceleration.

Deadband Requirements Due to Time Delay

Knowledge of engagement time delay for ON-OFF systems incorporating a brake will permit estimation of minimum requirements for deadband. Assuming negligible friction in the gear train, the actuator output position, α (also position feedback pickoff), enters the system deadband and coasts at the full actuation rate (worst case) during the brake engagement time delay. Once the brake engages, the load is brought to rest. Neglecting for the moment deceleration time after brake engagement (i.e., assuming the time required to stop the load once the brake engages is negligible compared to the coasting time), the deadband required for the load to coast to the desired position for a step command and zero rate feedback may be calculated by

$$DB_{TD} = R\,(TD) \tag{6.6}$$

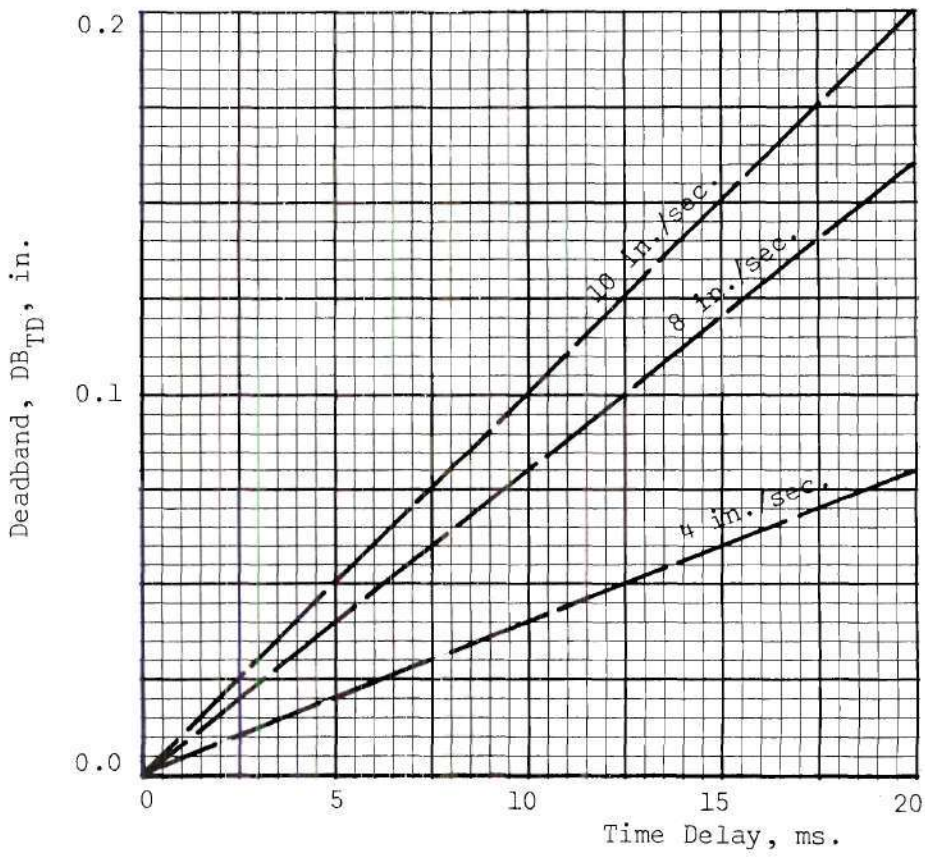

Figure 41. Deadband Requirements Due to Brake Engagement Time Delay for Zero Rate Feedback

where

DB_{TD} = one-half of deadband required because of engagement time delay, in.,

R = full actuation rate, in./sec., and

TD = brake engagement time delay.

Figure 41 depicts this relationship for several actuation rates. The importance of minimizing engagement time delay may be seen. The assumption is made in this analysis that the load is brought to rest on the first entry into the deadband. Otherwise, the response time would be excessive.

Deadband Required for Load Deceleration

As mentioned in the preceding section, after brake engagement occurs a period of time is required for bringing the load to rest. An estimate of the associated deadband increment may be obtained from the following considerations.

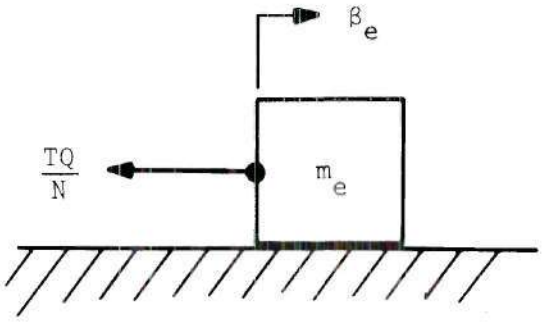

Figure 42. Simple Model for Load Deceleration Calculations

Referring to the simple model of Figure 42, the following relation can be derived:

$$\ddot{\beta}_e = - \frac{TQ/N}{m_e} , \tag{6.7}$$

where all terms are as defined previously, and gimbal friction is neglected. For a braking condition the applied torque opposes the motion, hence a minus sign is included so that TQ may be considered positive throughout this discussion.

Taking the Laplace Transform of Equation (6.7),

$$s \dot{\beta}_e(s) - \dot{\beta}_e(t=0) = - \frac{TQ(s)}{N m_e} \tag{6.8}$$

where

$\dot{\beta}_e(t=0)$ = engine rate at the beginning of brake torque build-up, in./sec.

Solving for $\dot{\beta}_e(s)$,

$$\dot{\beta}_e(s) = \frac{\dot{\beta}_e(t=0)}{s} - \frac{1}{s} \frac{TQ(s)}{N m_e} . \tag{6.9}$$

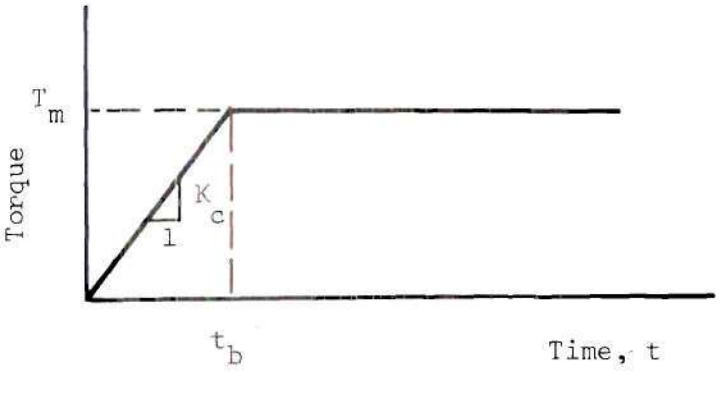

Figure 43. Assumed Torque Characteristic

The assumed torque characteristic is shown in Figure 43 and is composed of a build-up phase and a saturation phase. The torque may be defined mathematically as

$$TQ(t) = K_c t - K_c(t-t_b)\, U(t-t_b) , \qquad (6.10)$$

where

K_c = slope of torque build-up curve, (lb.-in.)/sec.,

t_b = end of build-up phase, sec., and

$U(t-t_b)$ = unit step function

$= 0 , \quad t \leq t_b$

$= 1 , \quad t > t_b .$

The Laplace Transform is

$$TQ(s) = \frac{K_c}{s^2}\left(1-e^{-t_b s}\right) . \qquad (6.11)$$

Substituting for TQ(s) in Equation (6.9),

$$\dot{\beta}_e(s) = \frac{\dot{\beta}_e(t=0)}{s} - \frac{K_c}{N m_e}\,\frac{1}{s^3} + \frac{K_c e^{-t_b s}}{N m_e s^3} . \qquad (6.12)$$

Taking the inverse transform,

$$\dot{\beta}_e(t) = \dot{\beta}_e(t=0) - \frac{1}{2}\frac{K_c}{N m_e}\left[t^2 - (t-t_b)^2\, U(t-t_b)\right] \qquad (6.13)$$

or

$$\dot{\beta}_e(t) = \dot{\beta}_e(t=0) - \frac{K_c}{N\, m_e}\ \frac{t^2}{2}\ , \quad 0 \le t \le t_b\ , \tag{6.14}$$

$$\dot{\beta}_e(t) = \dot{\beta}_e(t=0) - \frac{T_m}{N\, m_e}\ (t - \frac{t_b}{2})\ , \quad t > t_b\ . \tag{6.15}$$

Alternately,

$$\dot{\beta}_e(t) = \dot{\beta}_e(t_b) - \frac{T_m}{N\, m_e}\ (t-t_b)\ , \quad t > t_b\ ,$$

where

$\dot{\beta}_e(t_b)$ = engine rate at the beginning of brake torque saturation, in./sec.

From Equation (6.12) $\Delta\beta_{e_d}(s)$ is

$$\Delta\beta_{e_d}(s) = \frac{\dot{\beta}_e(t=0)}{s^2} - \frac{K_c}{N\, m_e}\ \frac{1}{s^4} + \frac{K_c}{N\, m_e}\ \frac{e^{-t_b s}}{s^4} \tag{6.16}$$

from which

$$\Delta\beta_{e_d}(t) = \dot{\beta}_e(t=0)t - \frac{1}{6}\ \frac{K_c}{N\, m_e}\ [t^3 - (t-t_b)^3\, U(t-t_b)] \tag{6.17}$$

or

$$\Delta\beta_{e_d}(t) = \dot{\beta}_e(t=0)t - \frac{1}{6}\ \frac{K_c}{N\, m_e}\ t^3 \qquad 0 < t \le t_b\ . \tag{6.18}$$

$$\Delta\beta_{e_d}(t) = \dot{\beta}_e(t=0)t - \frac{1}{2}\ \frac{T_m}{N\, m_e}\ (t^2 - t_b t + \frac{1}{3}\ t_b^2)\ , \quad t > t_b. \tag{6.19}$$

Alternately,

$$\Delta\beta_{e_d}(t) = \Delta\beta_{e_d}(t_b) + \left[\dot{\beta}_e(t=0) - \frac{1}{2}\frac{T_m}{N\ m_e}t\right](t-t_b),\ t > t_b,$$

where

$\Delta\beta_{e_d}(t)$ = engine displacement occurring after the onset of brake torque build-up while decelerating the load to rest, in., and

$\Delta\beta_{e_d}(t_b)$ = engine displacement at $t = t_b$ as calculated using Equation (6.18).

The value for $\Delta\beta_{e_d}(t)$ may be taken as an estimate for $\Delta\alpha_d$, the actuator output increment occurring during load deceleration.

In order to apply Equations (6.18) and (6.19), it is necessary to determine the time required to bring the load to rest, i.e., to make

$$\dot{\beta}_e(t) = 0\ .$$

Equation (6.14) can be used if $t \leq t_b$, i.e.,

$$t = 1000\ \sqrt{2(N\ m_e/K_c)\dot{\beta}_e(t=0)}\ ,\ \text{ms}\ . \qquad (6.20)$$

For $t > t_b$ Equation (6.15) applies.

$$t = \frac{t_b}{2} + 1000\ \frac{N\ m_e}{T_m}\dot{\beta}_e(t=0),\ \ \text{ms.}\ , \qquad (6.21)$$

or alternately,

$$t = t_b + 1000 \frac{N m_e}{T_m} \dot{\beta}_e(t_b) \ , \quad \text{ms.} \tag{6.22}$$

Equation (6.14) or (6.15) may be used to determine $\dot{\beta}_e(t_b)$ if Equation (6.22) is employed to determine t.

Calculation of $\Delta\beta_{e_d}(t)$ is straightforward once the time, t, is determined using the appropriate one of Equations (6.20) and (6.21).

Example 1

Suppose that the parameters assumed for the wrap-spring clutch simulation of Chapter IV are taken in order to determine deadband requirements by the methods of this chapter, i.e.,

$TM = 2000$ lb.-in.

$TD = 5$ ms.

$t_b = 1$ ms.

$K_c = 2 \times 10^6$ (lb.-in.)/sec.

$N = 0.08$ in./rad.

$m_e = 2.12$ (lb.-sec.^{2})/in.

$\dot{\beta}_e(t=0) = 16.0$ in./sec. *

$C_2 = 0.0$ in./in./sec.

From Figure 41 the deadband (one-half of total) required due to engagement time delay is 0.04 in.; the deadband necessary for load deceleration may be calculated as follows:

Deceleration time: Assume $t < t_b$.

---

*See page 124.

Using Equation (6.20),

$$t = 1.65 \text{ ms.},$$

i.e., $t > t_b$. Hence, Equation (6.21) applies.

$$t = \frac{t_b}{2} + 1000 \frac{N m_e}{T_m} \dot{\beta}_e(t=0)$$

$$t = 1.858 \text{ ms.}$$

Now using Equation (6.19),

$$\Delta\beta_{e_d} = 0.018 \text{ in.}$$

Total required system deadband is given by

$$DB = DB_{TD} + \Delta\beta_{e_d} \tag{6.23}$$

$$DB = 0.058 \doteq 0.06 \text{ in.}$$

Therefore, one-half of the total deadband required is approximately 0.06 in. (by definition of DB as one-half of the total deadband) by this prediction method. That value of DB would theoretically allow the load to stop precisely at the reference position for a step command.

The comparable analog computer data may be found in Figure 70. For a step command of 0.25 in. and DB = 0.05 in., a stopping distance of

about 0.07 in. was required, since the load stopped at a position 0.02 in. past the command.

Example 2

Consider the friction-disc clutch-actuator simulation parameters of Chapter IV in an attempt to predict the deadband necessary for that system with zero rate feedback:

T_m = 800 lb. in.

t_b = 20 ms.

TD = 10 ms.

K_c = 40,000 (lb.-in.)/sec.

N = 0.08 in./rad.

m_e = 2.12 (lb.-sec.^{2})/in.

$\dot{\beta}_e(t=0)$ = 16 in./sec.

C_2 = 0.0 in./in./sec.

DB = 0.05 in.

Proceeding as in Example 1,

$$DB_{TD} = 0.08 \text{ in.}$$

Time for load deceleration:

$$t = 11.65 \text{ ms}, \quad \text{i.e.,} \quad t < t_b .$$

Hence,

$$\Delta\beta_{e_d} = \dot{\beta}_e(t=0)t - \frac{1}{6}\frac{K}{N\, m_e}t^3$$

$$= 0.124 \text{ in.}$$

Thus, a one-half deadband of 0.20 in. is needed to bring the load to a rest condition at the command position on the first braking attempt with zero rate feedback. In other words, for a deadband of 0.05 in., it is impossible to stop the engine with zero rate feedback. Limit cycle operation is the result as is verified by the analog data in Figure 62.

Introducing rate feedback makes suitable operation possible for acceptable deadbands. The amount of rate feedback required for a given maximum deadband may be calculated by the following simple technique.

Consider the error equation

$$\varepsilon = R\alpha - \alpha - C_2\dot{\alpha} \tag{6.24}$$

where the terms are as defined previously.

From Figure 19 for a positive error, braking is initiated when

$$\varepsilon = DB \text{ ,}$$

or

$$R\alpha - \alpha - C_2\dot{\alpha} = DB \tag{6.25}$$

Define

$$\varepsilon' = R\alpha - \alpha \ , \quad \text{and} \tag{6.26}$$

$$DB' = DB + C_2\dot{\alpha} = DB + DB_{\dot{\alpha}} \tag{6.27}$$

so that

$$\varepsilon' = DB' \tag{6.28}$$

is the new requirement for switching, where DB' is an effective deadband. For a constant actuation rate, $\dot{\alpha}$, $DB_{\dot{\alpha}}$ has a fixed value. In Figure 44, the effective deadband is shown for a step command, $R\alpha$.

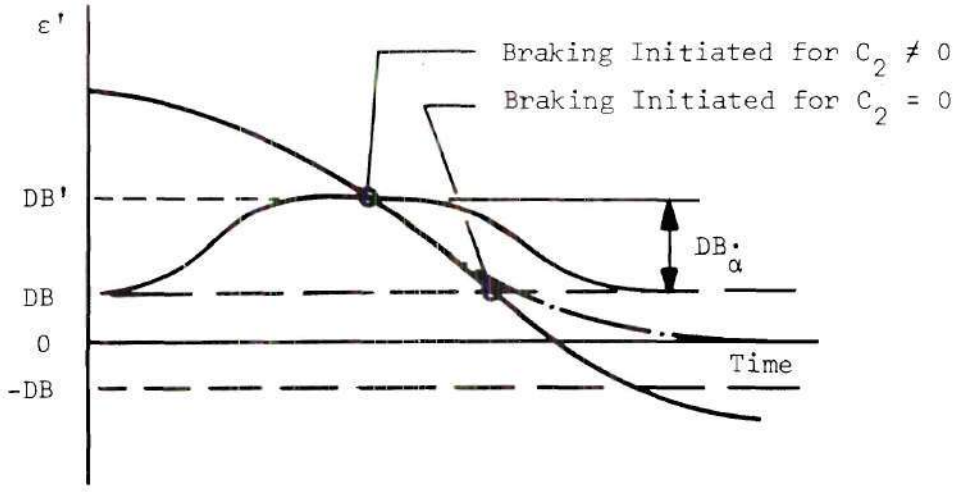

Figure 44. Diagram Illustrating Effective Deadband

For a given required stopping distance, DB_S, where

$$DB_S = DB_{TD} + \Delta\beta_{e_d} , \tag{6.29}$$

and a desired deadband, DB, the value for $DB_\alpha^\cdot$ is given by

$$DB_\alpha^\cdot = DB_S - DB \quad . \tag{6.30}$$

However,

$$DB_\alpha^\cdot = C_2\dot{\alpha} = C_2 R \tag{6.31}$$

or

$$C_2 = \frac{DB_\alpha^\cdot}{R} = \frac{DB_S - DB}{R} \quad .$$

Example 3

Consider the system of Example 2 where

DB_S = 0.20 in., and

DB = 0.05 in.

Calculate C_2 so that the load will come to rest at the command position with one brake engagement when the actuator is extending at a full rate of 8 in./sec.

From Equation (6.31),

$DB_\alpha^\cdot$ = 0.15 in.,

$$C_2 = \frac{DB_{\alpha}^{\cdot}}{R} = \frac{0.15}{8}$$

$$\approx 0.02 \text{ in./in./sec.}$$

Figure 62 presents data for the system in question which shows the trend as C_2 is varied, although data for $C_2 = 0.02$ is not included. This simple approach gives a first-order estimate of rate feedback requirements. Stability must be considered separately.

Amplitude of Engine "Ringing"

It is possible to predict from an energy standpoint the maximum engine "ringing" occurring for the system in Figure 7 due to structural compliances. Once the command position is achieved and the brake is engaged, engine oscillations (ringing) occur (occurs) because of an exchange between potential energy in the structural compliances and kinetic energy of the engine mass. Assuming the brake engages at a time when all the system energy is kinetic, the maximum amplitude of oscillation occurs. This amplitude can be calculated easily by neglecting gimbal point damping and realizing that all of the kinetic energy is converted to potential energy at the peak of oscillation. That is, since energy is conserved,

$$\text{P. E.} = \text{K. E.}, \tag{6.32}$$

but

$$\text{P. E.} = \frac{1}{2} K_e (\Delta\beta_e)^2 , \tag{6.33}$$

and

$$K.\ E. = \frac{1}{2} m_e \dot{\beta}_e^2 \ , \tag{6.34}$$

so that

$$\Delta\beta_e = \sqrt{m_e/K_e}\ \dot{\beta}_e \tag{6.35}$$

or

$$\Delta\beta_e = \frac{1}{\omega_{ne}}\ \dot{\beta}_e \ , \tag{6.36}$$

where

$\Delta\beta_e$ = engine position excursion from the steady-state position in response to a step command, in.

If $\dot{\beta}_e$ is known at the time the brake engages, the overshoot may be determined.

The maximum velocity, $\dot{\beta}_{e_{max.}}$, may be calculated by considering the model in Figure 37 for which

$$\frac{\dot{\beta}_e}{\dot{\alpha}}(s) = \frac{K_e}{m_e s^2 + b_e s + K_e} \ . \tag{6.37}$$

A good approximation to an actual actuator system is to let

$$\dot{\alpha} = R\ U(t) \ , \tag{6.38}$$

where

R = constant = actuation rate, in./sec.

Then

$$\dot{\beta}_e(s) = \frac{(K/m_e)\, R}{s(s^2 + (b_e/m_e)s + K_e/m_e)} \qquad (6.39)$$

$$= \frac{\omega_{ne}^2\, R}{s(s^2 + 2\zeta_e \omega_{ne} s + \omega_{ne}^2)}$$

The inverse transform yields

$$\dot{\beta}_e(t) = R\left[1 + \frac{1}{\sqrt{1 - \zeta_e^2}}\, e^{-\zeta_e \omega_{ne} t}\, \sin(\omega_{ne}\sqrt{1 - \zeta_e^2}\, t - \phi)\right]$$

where

$$\phi = \tan^{-1}\left[\frac{\sqrt{1 - \zeta_e^2}}{-\zeta_e}\right]$$

From Kuo (22) the first maximum occurs for

$$t = \frac{\pi}{\omega_{ne}\sqrt{1 - \zeta_e^2}}$$

so that

$$\dot{\beta}_{e_{max.}}(t) = R\left[1 + \frac{1}{\sqrt{1-\zeta_e^2}}\, e^{-\frac{\pi\zeta_e}{\sqrt{1-\zeta_e^2}}} \sin(\pi - \phi)\right] .$$

For $\zeta_e = 0.05$,

$$\phi \simeq 90^{\circ} .$$

Hence

$$\dot{\beta}_{e_{max.}}(t) = 1.9\ R \simeq 2\ R .$$

Example 4

Find the maximum amplitude of engine oscillation occurring for R = 8 in./sec. and the system of Figure 7.

$$K_e = \frac{K_a K_{vs} K_{es}}{K_a K_{vs} + K_{vs} K_{es} + K_{es} K_a}$$

$$= 12{,}250 \text{ lb./in.}$$

$$\dot{\beta}_{e_{max.}}(t) = 2\ R = 16 \text{ in./sec.}$$

$$\omega_{ne} = 76 \text{ rad./sec.}$$

$$\Delta\beta_{e_{max.}} = (1/76)\ 16 = 0.21 \text{ in.}$$

Figure 70 presents analog simulation data for which the overshoot is 0.175 in. for a 1/4-in. step command.

It should be pointed out that the method outlined here yields worst-case data. It assumes negligible gimbal friction, and brake engagement at the maximum engine velocity. It also assumes that the actuator imparts a rate-step input to the engine and structure. A more realistic approximation would be to assume that

$$\dot{\beta}_{e_{max.}} = 1.5\ R\ ,$$

for example. The maximum overshoot would then be 0.158 in., which more nearly fits all of the data of Figure 70.

Effect of Engine "Ringing" on Deadband Requirements

Since the actuator has been assumed to have a stiffness, K_a, an oscillating engine causes the feedback parameter, α_r, to vary about the locked-brake position by some amount related to the structural stiffness parameters. The amount of deadband required to envelope this variation of α_r is determined in this section.

The structural spring rates assumed and defined in Chapter III of this study are shown in Figure 7. Let $\Delta\beta_s$, $\Delta\beta_a$, and $\Delta\beta_e$ represent excursions from the locked-actuator value of their respective variables β_s, β_a, and β_e which were also defined earlier.

Since $\Delta\alpha_r = \Delta\beta_a - \Delta\beta_s$ the following relationship between $\Delta\beta_e$ and $\Delta\alpha_r$ exists:

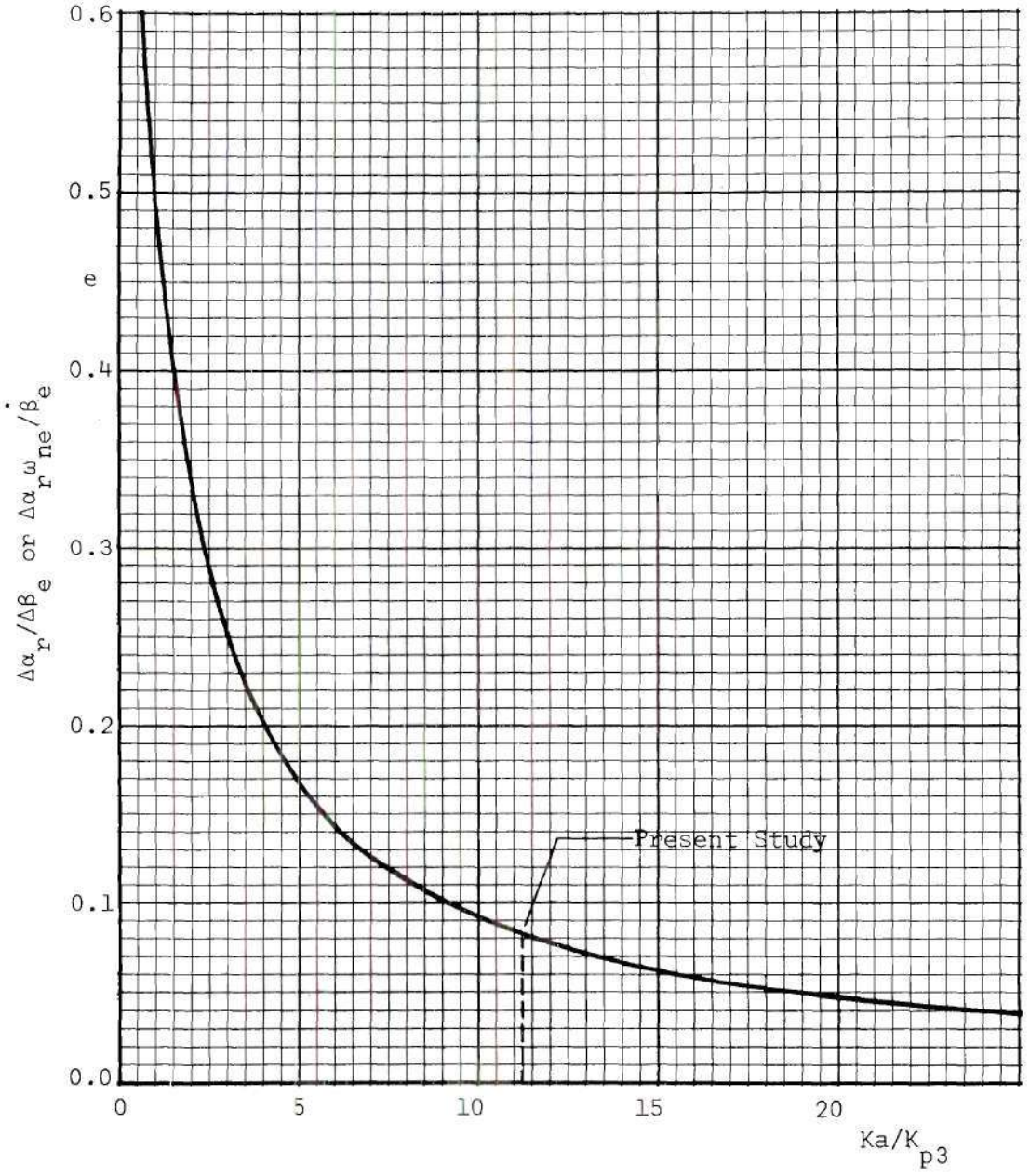

Figure 45. Maximum Oscillation of Locked-Actuator Output as a Function of Load and Structural Parameters

$$\frac{\Delta\alpha_r}{\Delta\beta_e} = \frac{K_{es}\, K_{vs}}{K_a\, K_{vs} + K_{vs}\, K_{es} + K_{es}\, K_a} \tag{6.42}$$

or

$$\Delta\alpha_r = \Delta\beta_e \left[\frac{1}{1 + K_a/K_{p3}}\right] , \tag{6.43}$$

where

$$K_{p3} = \frac{K_{es}\, K_{vs}}{K_{es} + K_{vs}} . \tag{6.44}$$

Since by Equation (6.36)

$$\Delta\beta_e = \frac{1}{\omega_{ne}} \dot{\beta}_e ,$$

$$\frac{\Delta\alpha_r}{(1/\omega_{ne})\dot{\beta}_e} = \frac{1}{1 + (K_a/K_{p3})} . \tag{6.45}$$

Thus, Equation (6.45) relates actuator output oscillation about the locked-actuator position to ω_{ne} and $\dot{\beta}_e$. Figure 45 presents this relationship graphically.

Example 5

For the system assumed in this study determine the maximum value of $\Delta\alpha_r$.

$$K_{p3} = \frac{(4)(2)}{4 + 2} \times 10^4 = \frac{8}{6} \times 10^4 = 13{,}333 \text{ lb.-in.}$$

$$K_a = 150{,}000 \text{ lb.in.}$$

$$\frac{K_a}{K_{p3}} = \frac{150{,}000}{13{,}333} = 11.25 \ .$$

From Figure 45

$$\frac{\Delta\alpha_r}{(1/\omega_{ne})\dot{\beta}_e} = 0.082 \ .$$

For

$$\dot{\beta}_{e_{max.}} = 16 \text{ in./sec.} \ ,$$

and

$$\omega_{ne} = 76 \text{ rad./sec.} \ ,$$

$$\Delta\alpha_{r_{max.}} = 0.013 \text{ in.}$$

For DB = 0.05 in. this amounts to about 1/8 of the total deadband. Thus, α_r oscillation does not become prohibitive for this assumed system. Reference to Figure 70 shows the above technique to be a good approximation to the amount of actuator output excursion in the locked condition.

Figure 45 shows that for K_a/K_{p3} less than 5 the effect on system deadband requirements becomes excessive.

Energy and Power Relations

Consider the system of Figure 42 in an effort to determine the average power required to bring the rocket engine load to rest as a function of actuation rate, engine mass, and assumed torque characteristic parameters.

The load will be assumed to have a rate at the onset of braking equal to the maximum actuation rate, R. It will also be assumed that the load will be brought to rest when the energy dissipated in the brake is equal to the initial kinetic energy of the engine mass, i.e., when

$$K.\ E. = \frac{1}{2} m_e R^2 .$$

Thus

$$P_{d_{avg.}} t = \frac{1}{2} m_e R^2 , \qquad (6.46)$$

where

$P_{d_{avg.}}$ = average power dissipated by brake, in.-lb./sec., and

t = time elapsed since the beginning of brake torque build-up, sec.

Assuming the torque characteristic given by Equation (6.10), the braking time may be calculated by Equation (6.20) or Equation (6.21), depending on whether t is less than or greater than t_b.

For $t < t_b$, Equation (6.20) applies and

$$P_{d_{avg.}} \sqrt{2\ N\ m_e\ R/K_c} = \frac{1}{2} M_e\ R^2 \ . \qquad (6.47)$$

Since

$$R = N\ \dot{\theta}_{max.} \ ,$$

$$N = \frac{R}{\dot{\theta}_{max.}} \ . \qquad (6.48)$$

Equation (6.47) may be re-written

$$P_{d_{avg.}} \sqrt{\frac{8}{m_e\ R^2\ K_c}} = \sqrt{\dot{\theta}_{max.}} \ , \ t < t_b \ . \qquad (6.49)$$

For $t > t_b$, Equation (6.21) should be used.

$$P_{d_{avg.}} \left[\frac{t_b}{2} + \frac{N\ m_e\ \bar{R}}{T_m} \right] = \frac{1}{2}\ m_e\ R^2 \ , \qquad (6.50)$$

or applying Equation (6.48) and rearranging,

$$P_{d_{avg.}} \left[\frac{t_b}{m_e\ R^2} + \frac{2}{\dot{\theta}_{max.}\ T_m} \right] = 1, \ \ t > t_b \ . \qquad (6.51)$$

Equations (6.49) and (6.51) are presented graphically in Figures 46 and 47.

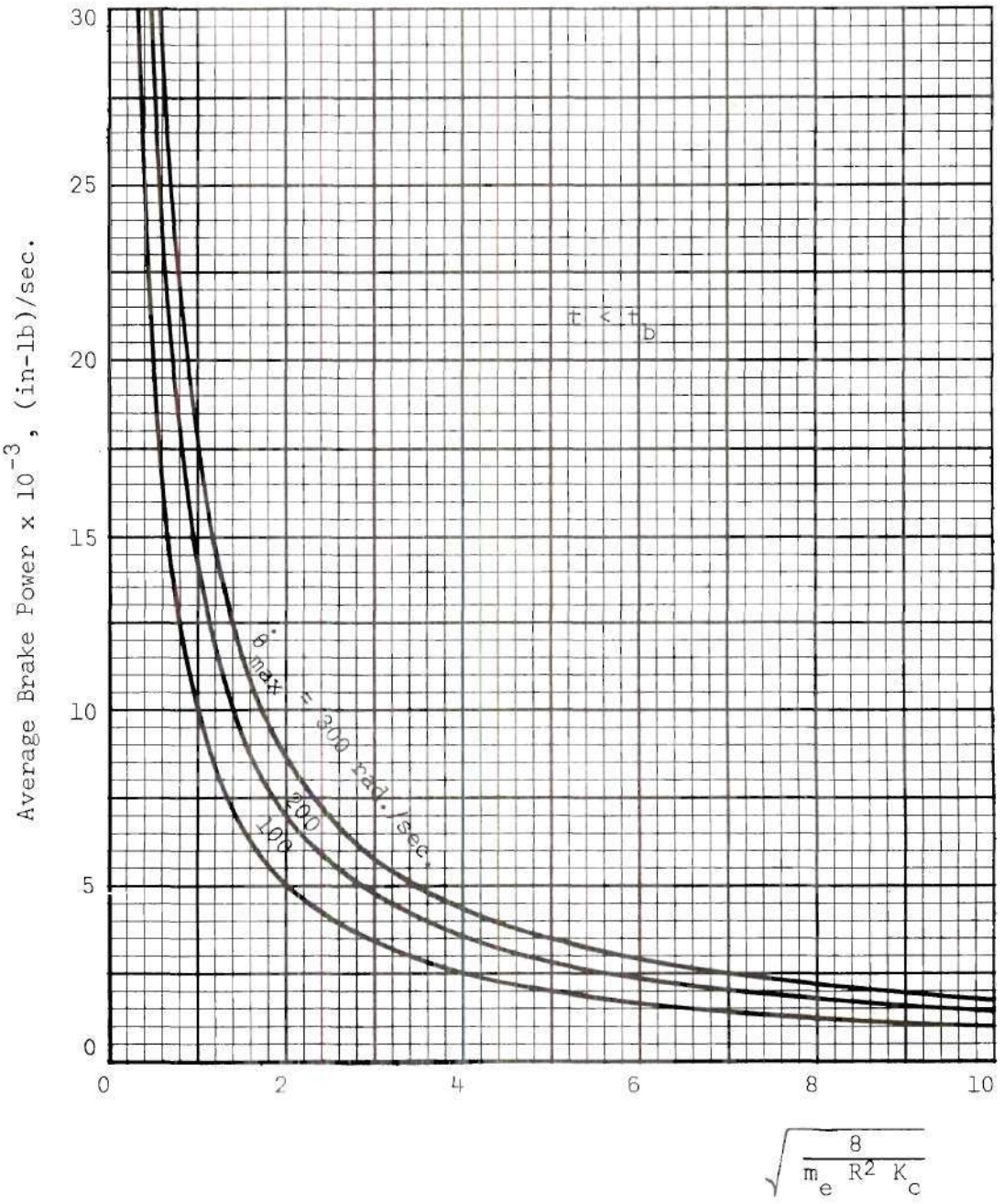

Figure 46. Average Braking Power as a Function of System Parameters for $t < t_b$

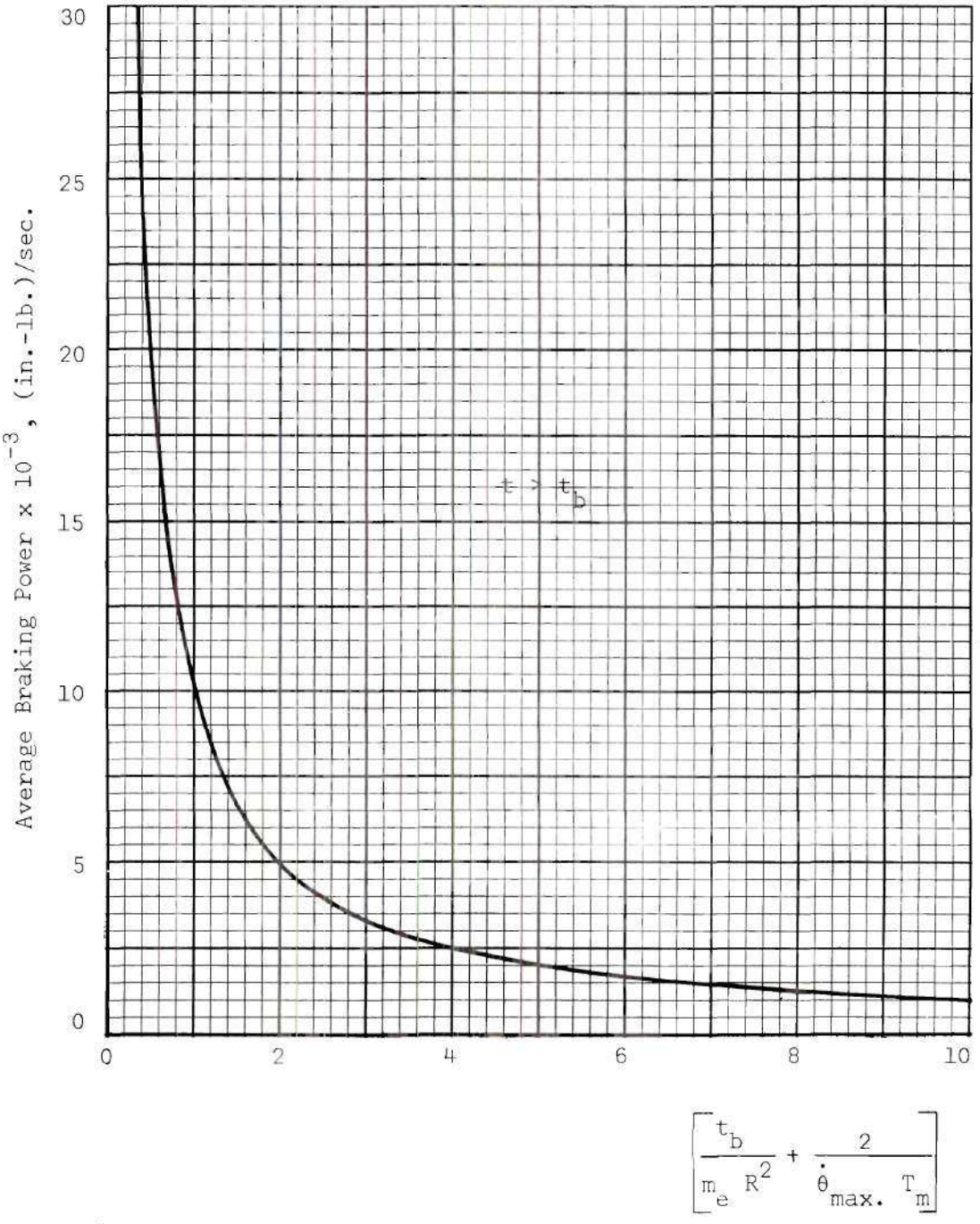

Figure 47. Average Braking Power as a Function of System Parameters for $t > t_b$

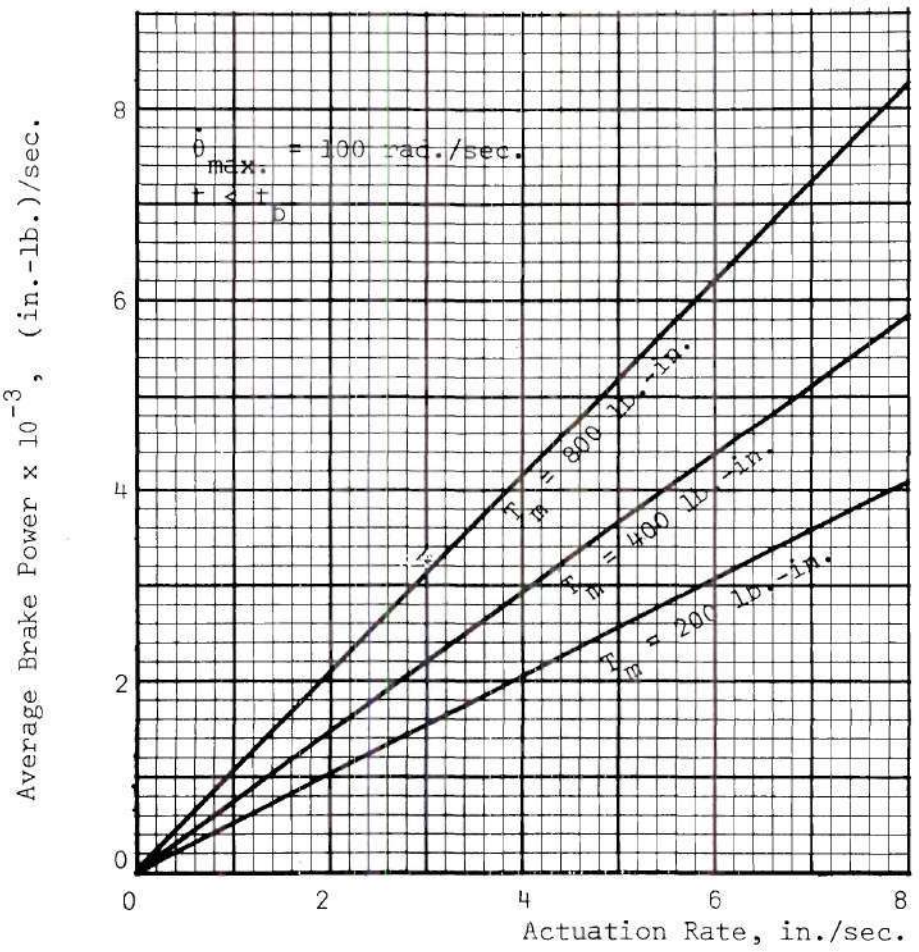

Figure 48. Average Braking Power as a Function of Actuation Rate and Maximum Brake Torque

Figure 48 illustrates the power dissipated in a brake as a function of actuation rate and maximum torque capability, for the case where $t < t_b$.

The results obtained here are also applicable to load acceleration, since the same amount of energy is transmitted for a purely inertial load. In the actual case additional power is required to overcome friction during load acceleration. On the other hand, friction reduces braking power requirements.

Summary

The techniques discussed in this chapter are for the most part simple methods for obtaining first-order predictions of engine gimbal system performance with clutch-actuators for parameters differing from those used in this study. The results discussed for ON-OFF systems are generally most useful for the case where zero rate feedback is used, although some of the results are independent of that factor.

For more satisfactory results where the effects of rate feedback or other parameters are desired, it will be necessary to perform a computer study such as was done in Chapter IV of this work. Appendices A and B present detailed discussions of the equations of motion and their analog computer implementation, so that one familiar with analog computer techniques should be able to easily evaluate systems of a similar form with different parameters.

CHAPTER VII

CONCLUSIONS

Evaluation of Clutch-Types Investigated

The dynamic study undertaken in this work indicates that clutch-operated electromechanical actuators would perform suitably for engine gimbal functions. However, it is recommended that the applications be restricted to low actuation rates (4 in./sec. or less). Analog simulation data was recorded in this study for a RL-10 engine gimbal system with an actuation rate of 8 inches per second. The engine mass for the system was such that clutch power requirements were excessive at the assumed rate. Thus, the magnetic-particle clutch-actuator, which simulation results show to be superior dynamically to the friction-disc and wrap-spring types on an equivalent torque basis, is ruled out because the magnetic-particle clutch is presently manufactured only in a limited power range (to a few hundred watts). For systems with slower actuation rates and/or less mass, the magnetic-particle clutch could be employed and would yield good dynamic performance. On the other hand, more reliability tests must be conducted to ascertain if clutch binding, which was mentioned in Chapter II, is indeed a problem at all. The clutch heating problem, although serious, is apparently being solved by use of higher temperature materials and an artificial environment. If these reliability problems can be solved, the magnetic-particle clutch type will be a first-choice for low power systems. Moreover, the state-of-

the-art for high response magnetic-particle systems is probably more advanced than for any other clutch-type. Hence, for projects demanding little development time the magnetic-particle clutch is again the choice.

Reduction of actuation rate would also improve the performance of friction-disc and wrap-spring ON-OFF clutch-actuators. Chapter V results for a 4-inch per second rate with a wrap-spring clutch-actuator are much better than those for the same clutch-type at 8 inches per second as presented in Chapter IV. ON-OFF clutch systems are not limited to low rates because of power capability to the extent that magnetic-particle systems are restricted. On the other hand, system deadband requirements dictate the maximum possible rates. Figure 41 illustrates the problem, in that for rates above 4 in./sec., the necessary deadband due to clutch time delay (about 10 ms. is a good average) becomes intolerable.

Friction-disc clutch-actuator performance data displayed in Appendix C and discussed in Chapter IV show that quite acceptable operation is possible even at the 8-inch per second rate. The clutch-type is available in a considerable torque range (up to approximately 200 lb.-in. with acceptable engagement times) and is capable of very high speeds. Even though basically a larger and heavier package than the other clutch-types, use of a smaller high-speed disc clutch with wear-resistant clutch surfaces, such as the ceramic material discussed in (11), could lead to a design which would perform very well in deep space. Moreover, the friction-disc clutch is the simplest and potentially the most reliable of the clutches investigated. However, wear

characteristics of the friction material in space must be determined.

The wrap-spring clutch-actuator, based on simulation data and actuator tests, is not as recommendable at present as the other clutch types. However, for space applications the device has potentially much to offer as discussed in Chapter II. The main question raised is one of reliability, in that the actuator tested showed a tendency to bind, even though the test was conducted only under NO-LOAD conditions. The device is simple, rugged, and potentially reliable, but further development work is considered advisable.

Derived Mathematical Model and Computer Program

The mathematical model for an engine gimbal system developed in Chapter III and the clutch characteristics assumed in Chapter IV yielded very good results. Correlation of analog computer simulation data and analog test data was quite satisfactory as may be noted from Figure 36 and the data in Appendix D. The analog computer circuit employed may be easily changed to simulate other systems of a similar form.

Analytical Techniques

The techniques discussed in Chapter VI may be used for quick estimates of system performance and in initial selection of parameter values. Use of these techniques along with the analog computer simulation offered will allow a quick analysis of other clutch-operated systems.

APPENDIX A

DERIVATION OF EQUATIONS OF MOTION FOR AN ENGINE GIMBAL SYSTEM

Mathematical Model

The mathematical model used in deriving equations of motion for an engine gimbal system employing clutch-operated electro-mechanical actuators is shown in Figure 7. Although the motion involved is translational, this model is mathematically equivalent to the system shown in Figure 1. The manner in which the equivalent parameter values were calculated is discussed later in this Appendix.

Since an actuator is a fairly complicated piece of equipment, it was necessary to provide a model which was considerably simplified in order that the simulation could be performed with the analog equipment available. The system shown in Figure 7 retains enough of the conceptual actuator of Figure 2 for meaningful results without undue complexity. Since the primary objective of this study is to consider the effects of various clutch types on overall system operation, a constant prime-mover speed was assumed. A high speed motor driving through a gear reduction ahead of the clutches approximates this condition fairly accurately and allows the examination of the effect of the clutches alone on the system. Another simplification was made by using only one clutch in the model; clutch output torque, TQ, shown in Figure 7, represents the sum of the torque outputs of both clutches and that

of the brake (if included). Finally, J_a and b_a represent the lumped moment of inertia and friction of the drive train, respectively, with the gears and power screw shown in the figure assumed perfect.

Deformation of system components with the accompanying storage of energy is an ever present cause of instability. Springs with rates K_{vs}, K_a, and K_{es} were included in the model to simulate the vehicle structure, lumped actuator, and engine structure deformations, respectively, in order to predict any inherent instabilities. Equivalent engine inertia and gimbal point friction are represented by mass, m_e, and dashpot with damping coefficient, b_e, respectively.

Since this simulation is concerned with only the engine gimbal system, the vehicle was assumed to be the frame and all other motion relative to this base.

Derivation of Equations

Since the only force applied to the actuator is that arising as a reaction to the force produced to gimbal the engine, one may write:

$$m_a \ddot{\beta}_s + b_{vs} \dot{\beta}_s + K_{vs} \beta_s + K_a (\beta_i - \beta_a) = 0 \qquad (A.1)$$

and

$$\beta_i = \beta_s + \alpha_i \ , \qquad (A.2)$$

where

m_a = lumped actuator mass (lb.-sec.^{2})/in.,

b_{vs}^{*} = lumped viscous damping of the vehicle structure (lb.-sec.)/in.,

K_{vs} = vehicle structural spring rate, lb./in.,

K_a = lumped actuator spring rate, lb./in.,

$\ddot{\beta}_s$ = $d^2\beta_s/dt^2$ = acceleration of the point of attachment of the actuator to the vehicle, in./sec.^{2},

$\dot{\beta}_s$ = $d\beta_s/dt$ = velocity of the point of attachment of the actuator to the vehicle, in./sec.,

β_s = displacement of the point of attachment of the actuator to the vehicle, in.,

β_i = displacement of the "ideal" actuator output, i.e., neglecting any deflections between the clutch and actuator output, in.,

β_a = displacement of the real actuator output, in., and

α_i = "real" actuator extension, in. When the actuator is centered, $\alpha_i = 0$, so that $\beta_i = \beta_s$.

Displacement, β_i, was introduced to aid in the derivation of the system's equations of motion and will subsequently be eliminated.

Substituting Equation (A.2) for β_i in Equation (A.1), the following result is obtained:

$$m_a\ddot{\beta}_s + b_{vs}\dot{\beta}_s + (K_{vs} + K_a)\beta_s + K_a(\alpha_i - \beta_a) = 0 \qquad (A.3)$$

Considering the actuator gear train and power screw, one may

---

*No data was available for b_{vs}, so a reasonable value was selected by trial and error in order to prevent excessive vibration of the actuator mass. See Chapter IV, p. 70.

write:

$$\alpha_i = N\,\theta\ , \tag{A.4}$$

where

N = effective gear ratio between clutch output and power screw, in./rad., and

θ = displacement of clutch output shaft, rad., measured from the clutch position when the actuator output is centered.

When Equation (A.4) is introduced into Equation (A.3), α_i can be eliminated with the following result:

$$m_a\ddot{\beta}_s + b_{vs}\dot{\beta}_s + (K_{vs} + K_a)\,\beta_s + K_a(N\theta - \beta_a) = 0\ . \tag{A.5}$$

Summing forces at the feedback pick-off point,

$$K_a(\beta_a - \beta_i) + K_{es}(\beta_a - \beta_e) = 0\ , \tag{A.6}$$

where

K_{es} = engine structural spring rate, lb./in., and

β_e = equivalent linear displacement of gimballed engine, in.

One may eliminate β_i by substituting Equation (A.2), so that

$$(K_a + K_{es})\,\beta_a - K_a\,(\beta_s + \alpha_i) - K_{es}\beta_e = 0\ . \tag{A.7}$$

Making use once again of Equation (A.4), the above equation becomes:

$$(K_a + K_{es})\,\beta_a - K_a\,(\beta_s + N\theta) - K_{es}\beta_e = 0\ . \qquad (A.8)$$

The following equation may be derived by summing forces applied to the equivalent engine mass, m_e:

$$m_e\ddot{\beta}_e + b_e\dot{\beta}_e + K_{es}\beta_e - K_{es}\beta_a = F_d \qquad (A.9)$$

where

m_e = equivalent engine mass, (lb.-sec.^{2})/in.,

b_e = equivalent gimbal point friction, (lb.-sec.)/in.,

$\ddot{\beta}_e = d^2\beta_e/dt^2$ = equivalent linear acceleration of gimballed engine, in./sec.^{2},

$\dot{\beta}_e = d\beta_e/dt$ = equivalent linear velocity of gimballed engine, in./sec., and

F_d = thrust-vector offset, lb.

The equation needed to complete the description of the system is obtained by a summation of torques applied to the lumped actuator moment of inertia, J_a. A preliminary result is as follows:

$$J_a\ddot{\theta} + b_a\dot{\theta} = TQ - N\,F_a\ , \qquad (A.10)$$

where

J_a = lumped moment of inertia of actuator gear train and screw, lb.-in.-sec.^{2},

b_a = lumped actuator friction, lb.-in.-sec.,

$\ddot{\theta} = d^2\theta/dt^2$ = angular acceleration of clutch output shaft, rad./sec.^{2},

$\dot{\theta} = d\theta/dt$ = angular velocity of clutch output shaft, rad./sec.,

TQ = summation of clutch and brake torques applied to the system, lb.-in., and

F_a = actuator force output, lb.

However,

$$F_a = K_a(\beta_i - \beta_a) = K_a(\beta_s + \alpha_i - \beta_a) ,$$

and going one step further

$$F_a = K_a(\beta_s + N\theta - \beta_a) ,$$

with Equations (A.2) and (A.4) being used to eliminate β_i and α_i. Finally, the resulting equation is:

$$J_a\ddot{\theta} + b_a\dot{\theta} + N^2 K_a\theta + N K_a(\beta_s - \beta_a) = TQ \qquad (A.11)$$

Equations (A.5), (A.8), (A.9), and (A.11) make up the desired system of equations of motion for an engine gimbal system.

Calculation of Numerical Coefficients

The task of calculating numerical coefficients for the previously derived equations still remains. Part of the data required for this

purpose was obtained from the Astrionics Laboratory, Marshall Space Flight Center, Huntsville, Alabama, and is contained in Table 5.

Table 5. RL-10 Actuation Requirements and System Characteristics

Item	Parameter	Value
1	Actuation force capability	1800 lb., maximum 1200 lb., rated
2	Actuation rate	10.83 in./sec., no load 6.67 in./sec., rated load
3	Actuator stroke	±1.375 in., maximum
4	Factor for conversion from actuator motion to engine motion	2.78 deg./in.
5	Maximum gimbal angle	±3.875 deg.
6	Moment arm, r, of the actuator force about the gimbal point	20.6 in.
7	Engine moment of inertia with respect to the gimbal point	75 slug-ft.^{2}
8	Thrust vector offset	20% of actuator force capability, lb.
9	Vehicle structure spring rate	20,000 lb./in.
10	Engine structure spring rate	40,000 lb./in.

This data comprises characteristics of and actuation requirements for the RL-10 engine, which was used on the Saturn IV vehicle; the remainder was assumed as necessary to complete the study.

Based on the data in Table 5, the following actuation requirements were adopted for the computer study:

Actuation rate - 8.0 in./sec.

Actuator stroke - ±1.0 in.

Since a constant clutch input speed was assumed, there is no difference between the maximum and rated actuation rates. Therefore, the 8 in./sec. rate was chosen as a compromise.

Table 6 presents the data used in calculating the above-mentioned numerical coefficients. Parameter values listed as "Given" were used as obtained or calculated from the data contributed by the NASA Astrionics Laboratory. A discussion of the calculations and assumptions made in gathering the data in Table 6 follows.

Calculation of Given Data

Three parameters--m_e, b_e, and F_d--listed as "Given" in Table 6 were calculated as discussed in the following:

m_e: The gimballed engine moment of inertia with respect to the gimbal point was given as

$$J_{ge} = 75 \text{ slug-ft.}^2 .$$

The mathematical model in Figure 7 requires that engine inertia be referred to the actuator output; the equivalent mass may be calculated by the equation:

$$m_e = (1/r)^2 J_{ge} \qquad (A.12)$$

where

1/r = equivalent gear ratio between actuator output and gimballed engine, rad./in.,

Hence,

$$m_e = 2.12 \frac{\text{lb.-sec.}^2}{\text{in.}}$$

b_e: This parameter was determined from a transfer function derived by NASA Astrionics for a gimballed RL-10 engine in a system employing hydraulic actuators. NASA's evaluation of the parameter is valid for the case at hand.

F_d: NASA Astrionics Laboratory advised the allotment of 20 per cent of the rated actuator force capability to counteract forces due to thrust vector offset. For a rated force capability of 1200 lb.

$$F_d = 240 \text{ lb.}$$

In the present study, however, thrust vector offset will be neglected.

Calculation of Assumed Data

The manner of acquiring the data labelled "Assumed" in Table 6 will be discussed briefly. Each of these parameters will be considered in the order in which it appears in the table.

K_a: Discussion of effective actuator stiffness with individuals in the NASA Astrionics Laboratory revealed that actuators (hydraulic) presently used in engine gimbal systems are much stiffer than other parts of the structure--approximately five times as stiff. The assumed value of 150,000 lb./in. is only slightly less than four times that given for K_{es}. Neglecting backlash, simple calculations indicate that this assumption is reasonable.

m_a: This data was calculated from an assumed actuator weight of 30 pounds.

N: This factor is an effective gear reduction between the output of the clutch and the actuator power screw; it must be taken into account in order to achieve the desired actuator output rate consistent with the choice of operating speed for the clutch, i.e.,

$$N = \frac{\dot{\alpha}_i}{\dot{\theta}}$$

For the study at hand, a clutch speed of 100 rad./sec. (approximately 1000 RPM) was chosen. Hence, for an actuation rate of 8 in./sec.,

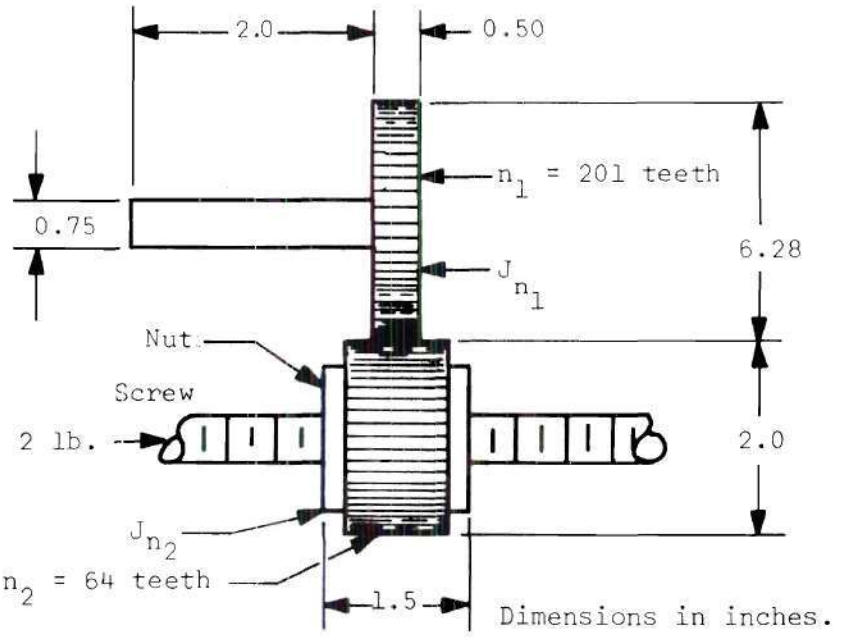

Figure 49. System Assumed for Calculating Lumped Actuator Drive Train Inertia, Ja

$$N = \frac{8}{100} \frac{\text{in./sec.}}{\text{rad./sec.}} = 0.08 \text{ in./rad.}$$

J_a: * Lumped actuator inertia comprises shafting inertia, gearing inertia, and ball screw inertia all referred to the output of the clutch, Figure 49 shows the system assumed in calculating a value for J_a. The following further assumptions were made in arriving at this model:

1. Power screw lead of 0.200 in./rev. (23). This yields a value of 3.14 for n_1/n_2 when $N = (n_1) P/n_2 = 0.1$, where

   P = pitch of power screw, in./rev.,

   n_1 = number of teeth on input gear, and

   n_2 = number of teeth on gear attached to power screw nut.

2. Gears with a diametral pitch of 32 (4). This assumption allows one to calculate the gearing pitch circle diameters by the following equation:

$$p_d = \frac{\text{Number of Teeth}}{32} \qquad \text{(A.13)}$$

Assuming

$$\frac{n_1}{n_2} = \frac{200}{64} = 3.14 \ ,$$

---

*J_a and b_a were initially calculated for an actuation rate of 10 in./sec. Since the values chosen were just rough estimates, the same values were also used later for an 8 in./sec. rate. Hence, the reference to N = 0.1 in the sample calculations.

$$p_{d1} = 6.25 \text{ inches, and}$$

$$p_{d2} = 2.00 \text{ inches.}$$

3. Other dimensions and parameters as shown in Figure 49.

The lumped inertia may be determined using the equation which follows:

$$J_a = J_{shaft} + (n_1/n_2)^2 J_{n_2} + N^2 m_s \qquad (A.14)$$

where

J_{shaft} = shafting inertia, lb.-in.-sec.^{2},

J_{n_1} = input gear inertia,

J_{n_2} = output gear inertia, and

m_s = mass of power screw, (lb.-sec.^{2})/in.

Considering the model in Figure 49 to be composed of a number of steel cylinders of different diameters, the value for J_a shown in Table 6 may be determined.

b_a: The assumed value for lumped actuator damping was determined from power considerations. For an actuator extension rate of 10 in./sec. and force output of 1800 lb., the power output, P_o, is

$$P_o = (1800)(10) = 18{,}000(\text{in.-lb.})/\text{sec.}$$

Table 6. Data for Calculation of Coefficients in Equations of Motion

Item	PARAMETER Symbol	PARAMETER Description	Numerical Value	Units	How Obtained
1	K_{vs}	Vehicle structure spring rate	20,000	lb./in.	Given
2	K_{es}	Engine structure spring rate	40,000	lb./in.	Given
3	K_a	Overall actuator spring rate	150,000	lb./in.	Assumed
4	m_a	Actuator mass	0.0777	$(lb.-sec.^2)/in.$	Assumed
5	N	Effective gear ratio between clutch output shaft and power screw	0.08	in./rad.	Assumed
6	m_e	Equivalent mass of engine	2.12	$(lb.-sec.^2)/in.$	Given
7	b_e	Equivalent gimbal-point friction	17.05	(lb.-sec.)/in.	Given
8	F_d	Equivalent force due to thrust vector off-set	240	lb.	Given
9	J_a	Lumped actuator inertia	8.0×10^{-2}	$lb.-in.-sec.^2$	Assumed
10	b_a	Lumped actuator damping	0.45	lb.-in.-sec.	Assumed

Assuming power screw and gearing efficiencies of 90 per cent gives an overall efficiency of approximately 80 per cent. From the power output and this overall efficiency, one can calculate a power loss of 4500 (in.-lb.)/sec. If this loss is assumed to be due to viscous friction, it may be expressed as

$$P_l = T_v \dot{\theta} = 4500 \ , \qquad (A.15)$$

where

P_l = power loss, (in.-lb.)/sec.,

T_v = drag torque due to viscous friction = $b_a \dot{\theta}$, lb.-in., and

$\dot{\theta}$ = clutch output shaft velocity, rad./sec., since the lumped damping is being referred to that member of the drive train.

Substituting for T_v in the above equation, one obtains

$$P_l = b_a \dot{\theta}^2 \ , \qquad (A.16)$$

from which

$$b_a = P_l/\dot{\theta}^2 = 4500/10{,}000 = 0.45 \text{ lb.-in.-sec.}$$

Calculation of Coefficients

Equations (A.5), (A.11), (A.8), and (A.9) may be re-written to facilitate computer solution:

$$\ddot{\beta}_s = -(b_{vs}/m_a)\,\dot{\beta}_s - ((K_a + K_{vs})/m_a)\,\beta_s - (K_a/m_a)\,N\,\theta + (K_a/m_a)\,\beta_a \qquad (A.17)$$

$$\ddot{\theta} = -(b_a/J_a)\,\dot{\theta} - (K_a/J_a)\,N^2\,\theta - (K_a/J_a)\,N\,\beta_s \qquad (A.18)$$

$$+ (K_a/J_a)\,N\,\beta_a + (1/J_a)\,TQ$$

$$\beta_a = (K_a/(K_a + K_{es}))\,\beta_s + (K_a/(K_a + K_{es}))\,N\,\theta + (K_{es}/(K_a + K_{es}))\,\beta_e \qquad (A.19)$$

$$\ddot{\beta}_e = -(b_e/m_e)\,\dot{\beta}_e - (K_{es}/m_e)\,\beta_e + (K_{es}/m_e)\,\beta_a \qquad (A.20)$$

$$+ (1/m_e)\,F_d$$

Table 7 presents the coefficients calculated from the data in Table 6. After substitution of those coefficients into the above equations, the following set of equations results:

$$\ddot{\beta}_s = -(b_{vs}/m_a)\,\dot{\beta}_s - (2.19 \times 10^6)\,\beta_s \qquad (A.21)$$

$$-(1.93 \times 10^6)\,N\,\theta + (1.93 \times 10^6)\,\beta_a$$

$$\ddot{\theta} = -5.63\,\dot{\theta} - (1.875 \times 10^6)\,N^2\,\theta \qquad (A.22)$$

$$-(1.875 \times 10^6)\,N\,\beta_s + (1.875 \times 10^6)\,N\,\beta_a$$

$$+ 12.5\,TQ$$

Table 7. Numerical Coefficients for Equations (A.17) through (A.20)

Item	Algebraic Coefficient	Numerical Coefficient	Units
1	b_{vs}/ma	*	1/sec.
2	$(K_a + K_{vs})/m_a$	2.19×10^6	$1/sec.^2$
3	K_a/m_a	1.93×10^6	$1/sec.^2$
4	b_a/J_a	5.63	1/sec.
5	K_a/J_a	1.875×10^6	$1/(in.^2 - sec.^2)$
6	$1/J_a$	12.5	$1/(lb.-in.-sec.^2)$
7	$K_a/(K_a + K_{es})$	0.789	-
8	$K_{es}/(K_a + K_{es})$	0.211	-
9	b_e/m_e	8.04	1/sec.
10	K_{es}/m_e	1.885×10^4	$1/sec.^2$
11	$1/m_e$	0.472	$in./(lb.-sec.^2)$

*See page 70.

$$\beta_a = 0.789\ \beta_s + 0.789\ N\ \theta + 0.211\ \beta_e \qquad (A.23)$$

$$\ddot{\beta}_e = -8.04\ \dot{\beta}_e - (1.885 \times 10^4)\ \beta_e \qquad (A.24)$$

$$+(1.885 \times 10^4)\ \beta_a + 0.472\ F_d$$

Time-Scaled Equations. Since the operating time of the clutches under consideration is of the order of 10 ms., it is necessary to time scale the problem for proper analog solution. A time scale of 100 will slow down the computation sufficiently, i.e., let

$$\tau_c = 100\ t$$

where

t = real time, and

t_c = computer time.

Introduction of the time scale factor into Equations (A.17) through (A.20) results in Equations (A.25) through (A.28).

$$\ddot{\beta}_{s_{tc}} = -10^{-2}(b_{vs}/m_a)\ \dot{\beta}_s - 10^{-4}((K_a + K_{vs})/m_a)\ \beta_s \qquad (A.25)$$

$$-10^{-4}(K_a/m_a)\ N\ \theta + 10^{-4}(K_a/M_a)\ \beta_a$$

$$\ddot{\theta}_{tc} = -10^{-2}(b_a/J_a)\ \dot{\theta} - 10^{-4}(K_a/J_a)\ N^2\ \theta \qquad (A.26)$$

$$-10^{-4}(K_a/J_a)\ N\ \beta_s + 10^{-4}\ (K_a/J_a)\ N\ \beta_a$$

$$+\ 10^{-4}(1/J_a)\ TQ$$

$$\beta_{a_{tc}} = (K_a/(K_a + K_{es}))\ \beta_s + (K_a/(K_a + K_{es}))\ N\ \theta + (K_{es}/(K_a + K_{es}))\ \beta_e \qquad (A.27)$$

$$\ddot{\beta}_{e_{tc}} = -10^{-2}(b_e/m_e)\,\dot{\beta}_e - 10^{-4}(K_{es}/m_e)\,\beta_e \qquad (A.28)$$

$$+ 10^{-4}(K_{es}/m_e)\,\beta_a + 10^{-4}(1/m_e)\,F_d$$

Amplitude- and Time-Scaled Equations. Amplitude scaling is required to insure that the output voltages on the amplifiers generating the problem variables are in the proper range for accurate solution. Initial scaling was done by considering the maximum values (where known) of the variables; the final scale factors were chosen after the problem was programmed on the computer and trial runs were made. The equations of motion including both time and amplitude scale factors are given below:

$$10\,\ddot{\beta}_{s_{tc}} = -(10^{-1})(b_{vs}/m_a)\,\dot{\beta}_s - (10^{-3})((K_a + K_{vs}/m_a)\,\beta_s \qquad (A.29)$$

$$-(10^{-3})(K_a/m_a)\,N\,\theta + (10^{-3})(K_a/m_a)\,\beta_a$$

$$10\,\ddot{\theta}_{tc} = -(10^{-1})(b_a/J_a)\,\dot{\theta} - (10^{-3})(K_a/J_a)N^2\,\theta \qquad (A.30)$$

$$-(10^{-3})(K_a/J_a)\,N\,\beta_s + (10^{-3})(K_a/J_a)\,N\,\beta_a$$

$$+ (10^{-3})(1/J_a)\,TQ$$

$$40\,\beta_{a_{tc}} = 40(K_a/(K_a + K_{es}))\,\beta_s + 40(K_a/(K_a + K_{es}))\,N\,\theta \qquad (A.31)$$

$$+ 40(K_{es}/(K_a + K_{es}))\,\beta_e$$

$$20\ \ddot{\beta}_{e_{tc}} = -2(10^{-1})(b_e/m_e)\ \dot{\beta}_e - 2(10^{-3})(K_{es}/m_e)\ \beta_e \qquad (A.32)$$

$$+ 2(10^{-3})(K_{es}/m_e)\ \beta_a + 2(10^{-3})(1/m_e)\ F_d$$

Table 8 contains the numerical coefficients resulting from substituion of data from Table 6 into the coefficients of Equations (A.29) through (A.32).

Table 8. Numerical Coefficients for Equations (A.29) through (A.32)

Item	Algebraic Coefficient	Numerical Coefficient	Units
1	$(10^{-1})(b_{vs}/m_a)$	*	1/sec.
2	$(10^{-3})((K_a + K_{vs})/m_a)$	2190	$1/sec.^2$
3	$(10^{-3})(K_a/m_a)$	1930	$1/sec.^2$
4	$(10^{-1})(b_a/J_a)$	0.563	1/sec.
5	$(10^{-3})(K_a/J_a)$	1875	$1/(in.^2\text{-}sec.^2)$
6	$(10^{-3})(1/J_a)$	0.0125	$1/(lb.\text{-}in.\text{-}sec.^2)$
7	$40\ (K_a/(K_a + K_{es}))$	31.58	-
8	$40\ (K_{es}/(K_a + K_{es}))$	8.42	-
9	$2\ (10^{-1})(b_e/m_e)$	1.608	1/sec.
10	$2\ (10^{-3})(K_{es}/m_e)$	37.7	$1/sec.^2$
11	$2\ (10^{-3})(1/m_e)$	0.000944	$in./(lb.\text{-}sec.^2)$

*See page 70.

The final equations are, therefore,

$$10 \ddot{\beta}_s = -5 \dot{\beta}_s - 2190 \beta_s - 1930 N \theta + 1930 \beta_a \quad \text{(A.33)}$$

$$10 \ddot{\theta} = -0.563 \dot{\theta} - 1875 N^2 \theta - 1875 N \beta_s + 1875 N \beta_a + 0.0125 TQ \quad \text{(A.34)}$$

$$40 \beta_a = 31.58 \beta_s + 31.58 N \theta + 8.42 \beta_e \quad \text{(A.35)}$$

$$20 \ddot{\beta}_e = -1.608 \dot{\beta}_e - 37.7 \beta_e + 37.7 \beta_a + 0.000944 F_d \quad \text{(A.36)}$$

These latter equations are ready for analog computer solution once the actuation rate has been chosen, i.e., once "N" has been fixed.

APPENDIX B

ANALOG COMPUTER IMPLEMENTATION OF ENGINE GIMBAL ACTUATION SYSTEM EQUATIONS OF MOTION

Introduction

The following discussion presents the analog computer implementation of techniques employed in this work to simulate an engine gimbal actuation system incorporating clutch-operated power screw actuators. Details of the simulation techniques were discussed in Chapter IV; Appendix B is concerned with an explanation of the computer circuitry involved. The circuit diagram is shown in Figure 50 and for ease of description may be broken down into four main divisions: Reference Input, Feedback and Control Logic, Clutch and Brake Torque Simulator, and System Equations Implementation. Each of these divisions is labelled as such on the circuit diagram and will subsequently be discussed in detail.

Digital Logic Elements

Several digital logic elements were used in this simulation; hence, a brief discussion of their operation is necessary.

In all of the digital elements used, the logic implementation is as follows:

Logical 0 - False - 28 volts

Logical 1 - True - 0 volts (System ground) .

Some of the elements are level sensitive, i.e., they require that either a 0- or 28-volt signal be maintained for operation, while others respond

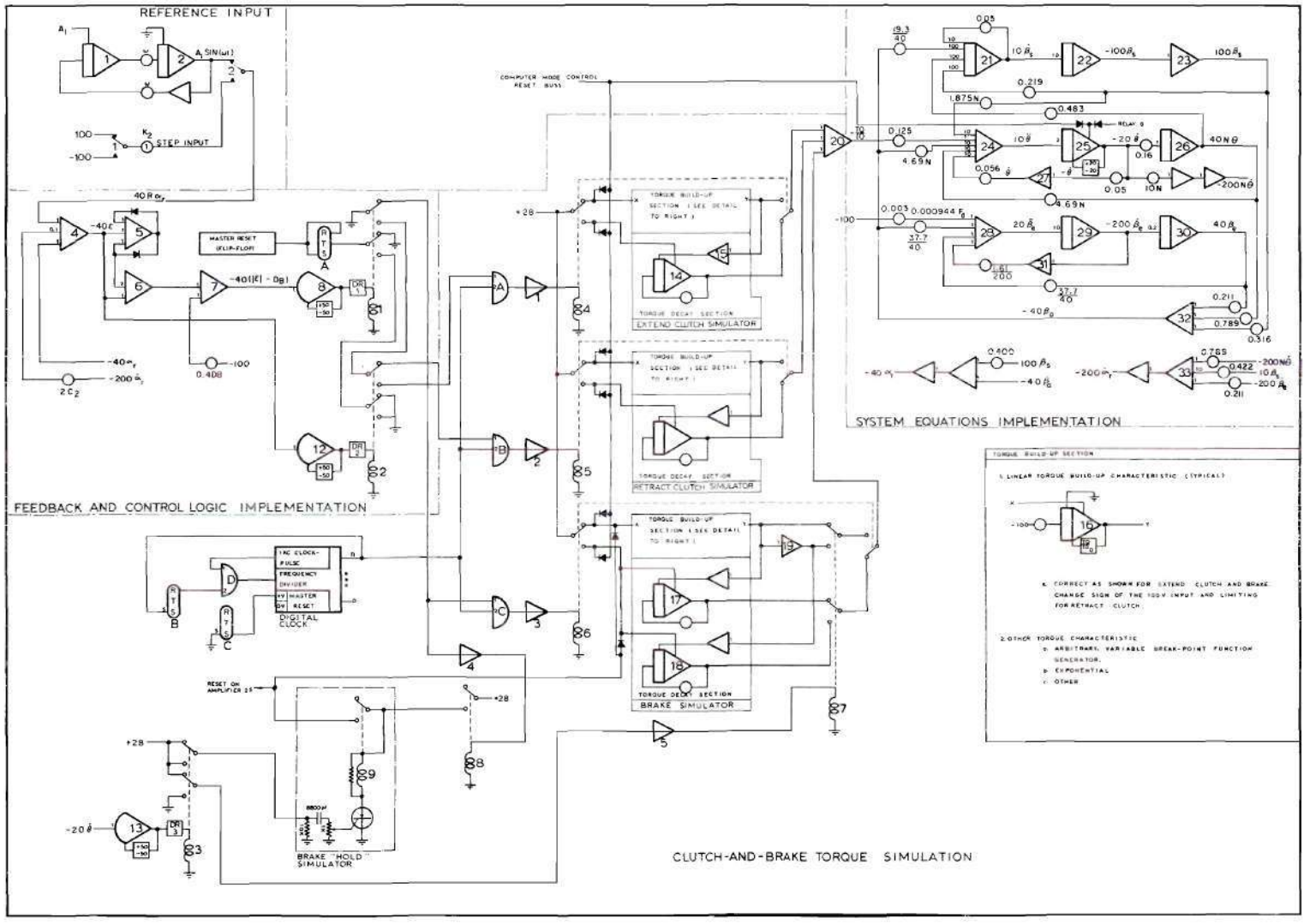

Figure 50. Analog Computer Circuit Diagram for Simulation of a Clutch-Operated Power Screw Actuator

to a transition from logical 0 to logical 1, or vice versa. A change from logical 0 to logical 1 is a negatively-going voltage pulse, while a positively-going pulse is involved in a change from logical 1 to logical 0.

AND Gate. One of the digital elements employed in this simulation is the *AND Gate*. The program symbol for this device is shown in Figure 51.

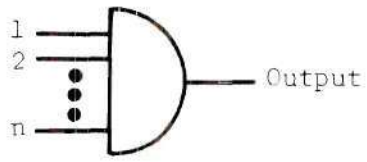

Figure 51. Program Symbol for the AND Gate

It may have any number of inputs but only one output; this output will be in the logical 1 state only if all of the inputs have a logical 1 applied.

FLIP-FLOP. Another device commonly used is the *Flip-Flop*--a one-bit binary memory element. The program symbol is given by Figure 52.

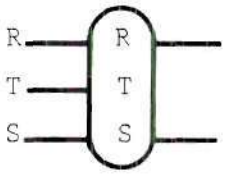

Figure 52. Program Symbol for the Flip-Flop

A flip-flop has two outputs, but only one of these can exhibit a logical 1 at any given time; the other output will be in a logical 0 state. The flip-flops used in this program have three inputs--R, S, and T. The R and S inputs are level sensitive, so that the application of a logical 1 to either of these causes its corresponding output to assume a logical 1 state. The T input, on the other hand, is responsive to a change of state from logical 0 to logical 1--a negatively-going pulse--which causes the outputs to undergo a reversal of state.

A flip-flop with its S output applied to the R input and input pulses applied at the T input (see flip-flop A on the circuit diagram) acts like another special digital element, the *One-Shot Multivibrator*. Either change of state introduced at the T input will cause a 5-microsecond transition (with these particular flip-flops) of the S output from the logical 0 state to the logical 1 state and back again, as illustrated in Figure 53.

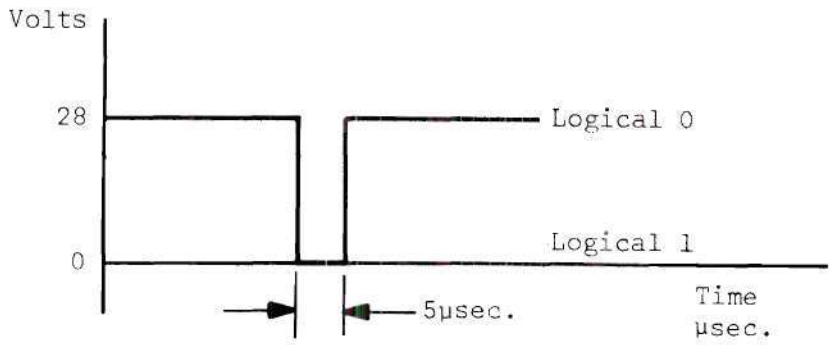

Figure 53. S-Output Waveform for a Flip-Flop Programmed as a One-Shot Multivibrator

A master reset (MRFF) is available which resets all flip-flops simultaneously to the R state.* Two inputs are available: one resets all flip-flops when a negatively-going pulse is applied; the other is level sensitive, holding all flip-flops in the R state as long as the logical 1 is maintained. The latter was used in this simulation.

DIGITAL CLOCK. One of the most important digital elements used in this program is the *Digital Clock*, some of the features of which are as follows: a 1 KC clock pulse signal, a 6-decade frequency divider, and two master reset inputs--one (0-V input) resets all counters to zero and stops the clock for as long as a logical 1 is applied (not used in this study); the other (+V input) resets all counters to zero with the application of a positively-going pulse, but does not stop the clock. Time increments from 1-millisecond to 999-seconds duration are possible from this clock. A logical 1 appears momentarily at the appropriate counter output when a given time increment has expired. The desired time increment is chosen by patching into the counter outputs.

RELAY DRIVER. The final digital logic device employed in this simulation is the *Relay Driver*, a power buffer which inverts its logical 1 (0-volt) input to a 28-volt output which is required to operate a relay. Five of these drivers were employed in this program; they are represented by the symbol shown in Figure 54.

---

*"R state" means that the R output is in the logical 1 state (S in 0 state); "S state" means that the S output is in the logical 1 state (R in 0 state).

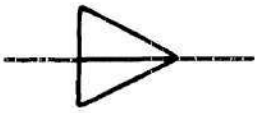

Figure 54. Program Symbol for the Relay Driver

Reference Input Division

The *Reference Input* division is displayed in the upper left corner of the circuit diagram. Either of two command signals may be chosen by proper manipulation of the manual switches in the circuit. When Switch 2 is in the *UP* position, the reference input, $40\ R\alpha_r$*, is given by

$$40\ R\alpha_r = (A_1 \sin\omega t) \tag{B.1}$$

By adjusting A_1, ω, and the gain of amplifiers 1 and 2 any desired sine function may be generated.

When Switch 2 is in the *DOWN* position, the reference input consists of a step function of adjustable magnitude. The polarity is chosen by positioning Switch 1 as indicated on the circuit diagram; magnitude is adjusted by varying potentiometer 1. A step function may be represented mathematically by Equation (B.2), where the step is assumed to occur at t = 0.

---

*A scale factor of 40 was introduced into the computer equations to achieve proper voltage levels for good analog computation.

$$40\ R\alpha_r = \pm A_2 \qquad (B.2)$$

Feedback and Control Logic Division

The *Feedback and Control Logic* division contains the feedback circuitry, summing point for the reference input and feedback signals, and the relays which control the operating mode of the simulated actuator. In Chapter IV operation of an actuator employing ON-OFF clutches was discussed. Table 9 presents the mathematical relations developed there, which have been modified to incorporate the scale factor of 40 mentioned earlier. The feedback and control logic section is basically an implementation of those relations.

Table 9. Mathematical Relations Governing Servoactuator Operation

Actuator Operating Mode	Mathematical Relation
Mode 1 "Extend" Clutch Command	$40(\lvert\varepsilon\rvert - DB) > 0$ $40\ \varepsilon > 0$
Mode 2 "Retract" Clutch Command	$40(\lvert\varepsilon\rvert - DB) > 0$ $40\ \varepsilon < 0$
Mode 3 Brake Command	$40(\lvert\varepsilon\rvert - DB) < 0$

Referring to the circuit diagram in Figure 50, the reference input, and position and rate feedback signals are summed by amplifier

4, whose output is the inverted implementation of 40 ε, before being fed into an absolute value circuit composed of amplifiers 5 and 6. The output of amplifier 6 is then summed with the deadband signal from potentiometer 2 by amplifier 7, and the result is the inverted implementation of $40(|\varepsilon| - DB)$.

Polarized relays 1 and 2 were used to implement the logical relations in Table 9. Relay operation occurred at +28 volts; the normally closed (NC) configuration shown on the circuit diagram is assumed by the relays for voltages more negative than that value. Open loop amplifiers 8 and 12 served as relay drivers, their outputs being limited to ±50 volts to insure positive relay operation. The outputs of these high-gain amplifiers were always at one or the other limit; only a slight change of polarity was required at the input to cause switching to the opposite limit. Thus, a given relay and its corresponding driver may be considered as a relay comparator set to trip at zero volts.

The inputs to amplifiers 8 and 12 are $-40[|\varepsilon| - DB]$ and -40ε, respectively. The polarities of these inputs were sensed by the two comparators, so that the relations in Table 9 were implemented as follows:

$$\text{Condition:} \quad \begin{bmatrix} 40[|\varepsilon| - DB] > 0 \\ 40\ \varepsilon > 0 \end{bmatrix}$$

If this condition is present in the system, negative voltages will exist at the inputs of amplifiers 8 and 12, causing relays 1 and

2 to assume their normally open (NO) configurations. A ground (logical 1) is thus applied to input 1 of gate A. A logical 1 is also applied to gate-input 2 at the proper instant by the time delay simulator. Hence, the EXTEND clutch simulator is engaged as necessary for Mode 1 in Table 9. That the other two modes in Table 9 are accomplished by relays 1 and 2 may be verified in a similar manner.

It may be helpful to note that relay 1 chooses between clutch and brake operation, while relay 2 reacts to select the appropriate clutch, i.e., either EXTEND or RETRACT.

Clutch- and Brake-Torque Simulator Division

Simulation of the torque characteristic of the clutches and brake for introduction into the System Equations Implementation division requires that four phases of operation be considered: clutch and brake engagement time delay, torque build-up, fully engaged clutch (or brake), and torque decay. The "Clutch (and Brake) Dynamic Characteristics" section of Chapter IV may be consulted for a discussion of techniques used to simulate clutch and brake torque characteristics.

Time Delay (TD) Simulation

AND gates A, B, and C, and the digital clock are the basic elements in the time delay simulation. As discussed earlier, relays 1 and 2 determine the mode of actuator operation, using the top set of contracts in each relay. Depending upon the reference input and feedback conditions in the circuit, these relays apply a ground (logical 1) to input 1 of one of the three above-mentioned AND gates. These gates have two inputs, however, each gate sharing a common input (applied at

gate-input 2) from the digital clock, so that until a programmed time increment has expired, none of the gates can have a logical 1 output. Therefore, relays 4, 5 and 6 all remain in their NC condition during this time, and no torque is produced by any of the clutch and brake simulators. When the programmed time increment expires, a logical 1 is applied at the common input to gates A, B, and C, so that the gate whose input 1 has a logical 1 already present then applies a logical 1 to the input of its associated relay driver, operating the corresponding relay.

This gate would be closed only momentarily, however, unless the clock were stopped in precisely the configuration (called N state for future reference) which caused a logical 1 to appear at the previously mentioned common input to the gates. The clock is stopped using AND gate D and flip-flop B. The flip-flop was in the R state at the beginning of the time increment under consideration by virtue of a reset pulse applied to the MRFF at the end of the preceding actuator mode. Therefore, until the clock reached its N state, a logical 1 was present at input 2 of gate D, allowing clock pulses (alternately logical 1 and logical 0) to pass to the frequency divider and allowing the clock to continue running. When the clock's N state was reached, however, a logical 1 appeared at the S input to flip-flop B, ultimately closing gate D and stopping the clock in the required configuration. Thus, the necessary logical 1 is maintained at the common input to gates A, B and C, as long as a given actuator mode is commanded.

It is also necessary to discuss the sequence of events involved in a change of actuator mode as outlined in Table 9. Any mode change

requires that the clock be reset to its 0 state, thus initiating a new clutch (brake) engagement time delay. This is accomplished by flip-flops A and C and the bottom set of contacts in relays 1 and 2. During the mode change a momentary loss of ground (logical 1) at the T input of flip-flop A (one-shot multivibrator) causes a logical 1 to be applied for an instant to the MRFF, placing all flip-flops in their R state. It should be noted that flip-flop C is constrained in its S state by the permanent application of a logical 1 to its S input, so that only a momentary transition to the R state is experienced by this flip-flop. This transition is sufficient to reset the clock, however, since a positively-going pulse is generated and applied at the +V input of the clock's master reset. In addition, the clock starts to run again since flip-flop B was placed in its R state, with the result discussed in the preceding paragraph.

Torque Build-Up (TBU)

Actuation of one of relays 4, 5 or 6, removes the 28-volt reset signal from the torque build-up section of the corresponding clutch or brake simulator. Simultaneously, the output of the same TBU section is connected to one of the inputs of amplifier 20, and the torque decay section is placed in its reset mode. Assume for illustrative purposes that EXTEND actuator operation is commanded. In that event gate A would have a logical 1 output, causing relay 4 to operate. This action places amplifier 16 in the COMPUTE mode, generating a linear torque signal which builds up until the clutch's maximum torque capability is reached. A limiter on amplifier 16 begins to function at that point to simulate the maximum torque level that the clutch can

produce. As long as extend operation is commanded, a positive torque signal is fed into amplifier 20, producing further extension of the simulated actuator.

Fully Engaged Clutch

Once torque build-up commences, the clutch's output member is accelerated until full engagement is accomplished, i.e, until no slip exists between the input and output members. Full engagement is simulated in this study by limiting the output of the amplifier generating clutch input speed.

A different approach was necessary to simulate a fully engaged brake. This will be discussed in a later section entitled "Brake Simulation."

Torque Decay (TQD)

Operation of one of relays 4, 5 or 6 previously discussed in the TBU description, in addition to initiating torque build-up in a clutch or brake simulator, also places the corresponding torque decay section in its RESET mode. The output of the TBU section is fed as an initial condition to the torque decay amplifier. Thus, when TQD is commanded at a later time, the decay will begin at the TBU section torque level existing just prior to the command.

The portion of the diagram in the block labelled "Torque Decay Section" in Figure 50 may be seen to consist of an exponential decay circuit. The fact that the output of the torque decay amplifier (amplifier 14, for example) eventually becomes zero was used to advantage, since different pairs of the torque decay simulators are always in the COMPUTE mode, their outputs being summed by amplifier 20 as part of the

total torque delivered to the system. This causes no error, however, because once the decay is complete, a given torque-decay section maintains a zero output until returned to the RESET mode to track its corresponding torque build-up simulator.

Brake Simulation

The sign of the torque generated by the brake depends on the sign of brake input shaft velocity, $\dot{\theta}$, since a torque is developed to oppose the motion. In the Brake Simulator the outputs of the TBU and the TQD sections are inverted by amplifiers 19 and 18, respectively, so that both positive and negative build-up and decay torques are available. Relay 7 is used to select the proper combination of torques depending on the polarity of $\dot{\theta}$, which is sensed by a relay comparator composed of amplifier 13 and relay 3.

In situations where brake operation is cancelled before the brake becomes fully engaged, i.e., before

$$\dot{\theta} = 0 \ ,$$

the Brake Simulator functions in the same manner as the Clutch Torque Simulator as explained in the preceding sections. However, if conditions are such that brake torque is maintained long enough for $\dot{\theta}$ to be reduced to zero and change polarity,* relay 3 will operate and a voltage pulse will be applied at the gate of the SCR in the Brake "Hold"

---

*The analog simulation of a fully engaged brake was discussed in Chapter IV under "Brake 'Hold' Simulator."

Simulator. If the braking mode is still commanded at that instant, relay 8 will already be closed and the Brake "Hold" Simulator armed (i.e., 28 volts applied). Thus, the SCR fires and closes the contacts of relay 9. The result is the application of a 28-volt reset signal to amplifier 25, placing it in the RESET mode with a zero initial condition. Hence, the brake velocity, $\dot{\theta}$, once reduced to zero by torque build-up in the Brake Simulator, is forced to remain at zero by the Brake "Hold" Simulator until a new actuation command is received.

System Equations Implementation Division

The System Equations Implementation division of the circuit diagram displays the analog program required to solve the gimbal system equations of motion (Equations (A.33), (A.34), (A.35), and (A.36)) which were derived in Appendix A. Since the usual analog computer techniques were employed in this part of the simulation, no explanation is necessary for anyone familiar with analog programming.

Equipment

The analog hardware used consisted of an Ease Model 1000 computer and a Systron-Donner Model 10/20 solid-state computer patched together and operated from a common control unit. Interfacing was no major problem, since both computers are capable of 100-volt output. Each of the S/D integrators has its RESET and HOLD mode control relays terminated on the patch-board, so that it can be patched to a common buss, or individually patched for special mode control. This feature was especially useful in implementing the circuitry described above in the "Clutch and Brake Torque Simulation" section. Another useful feature

of S/D 10/20 was that two modules of digital logic were available, which added flexibility in varying the time delay associated with torque build-up, as was also discussed above. Finally, the Brake "Hold" Simulator was conceived as a simple means of accomplishing drift-free simulation of an engaged brake and was constructed especially for that purpose using electronic parts that were available.

APPENDIX C

CLUTCH-ACTUATOR SIMULATION DATA

This appendix contains data from the analog computer simulation of a clutch-operated power screw actuator employing three different clutch types: magnetic-particle, friction-disc, and wrap-spring. In each case the actuation rate was 8 inches per second, while the rate feedback pickoff was $\dot{\alpha}_r$. Other conditions are noted on the data sheets. A discussion of the data is included in Chapter IV.

Magnetic-Particle Clutch-Actuator Simulation Data

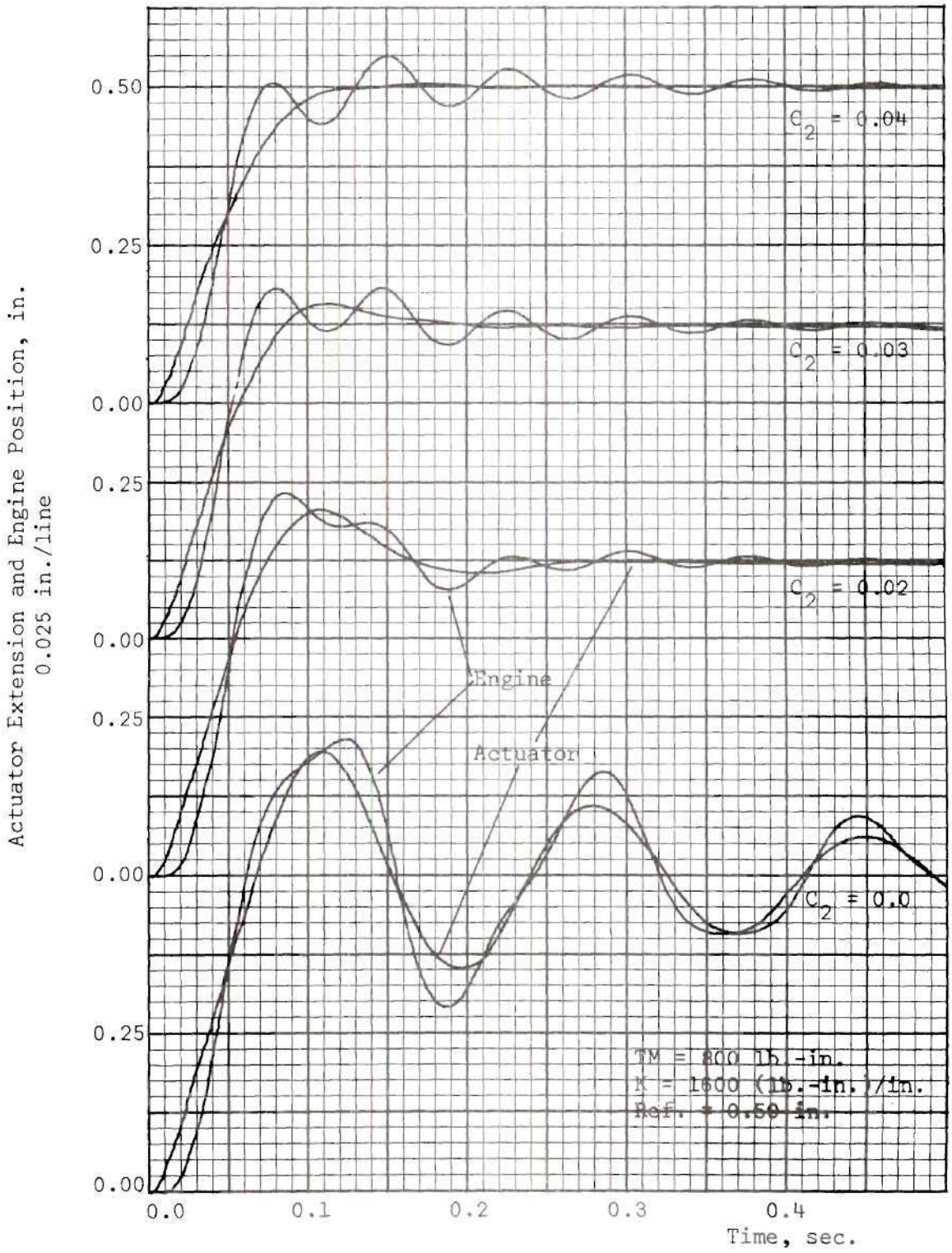

Figure 55. Effect of Variation of Rate Feedback Coefficient, C_2, on Actuator Extension and Engine Position Step Response for T_m = 800 lb.-in.

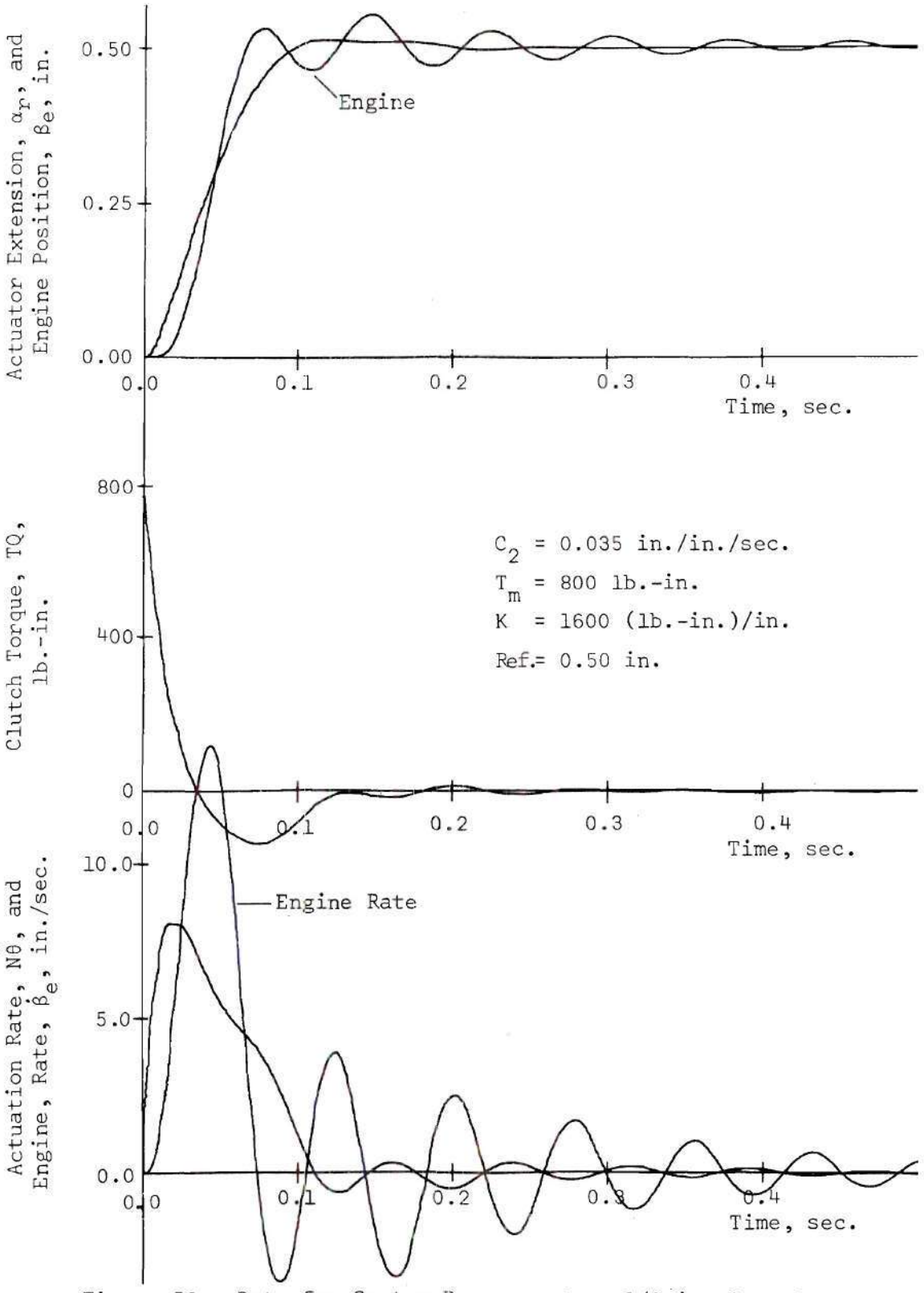

Figure 56. Data for System Response to a 1/2-in. Step Command. Magnetic-Particle Clutch-Actuator Simulation

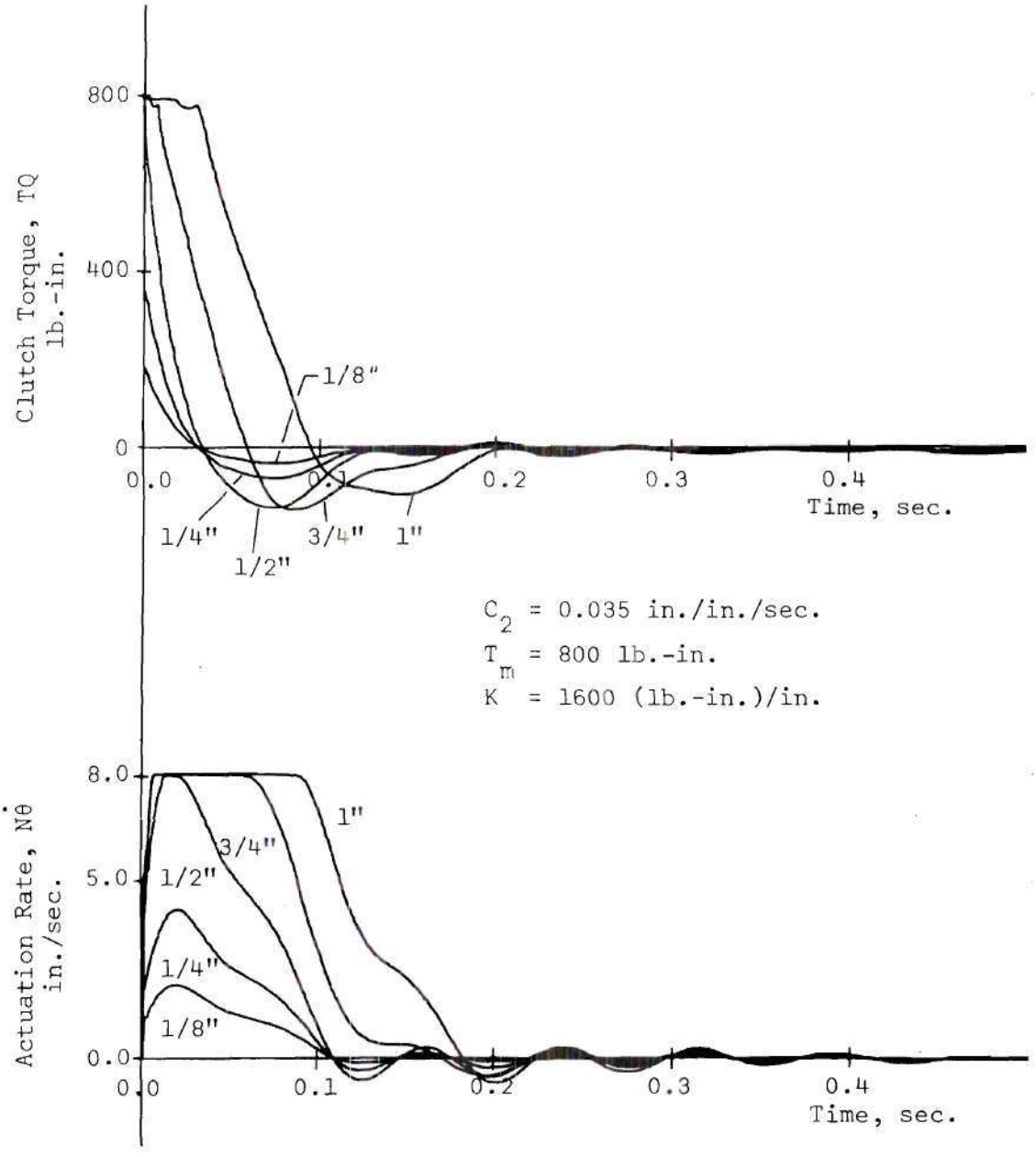

Figure 57. Clutch Torque and Actuation Rate Time Histories in Response to Step Commands of Varying Magnitude

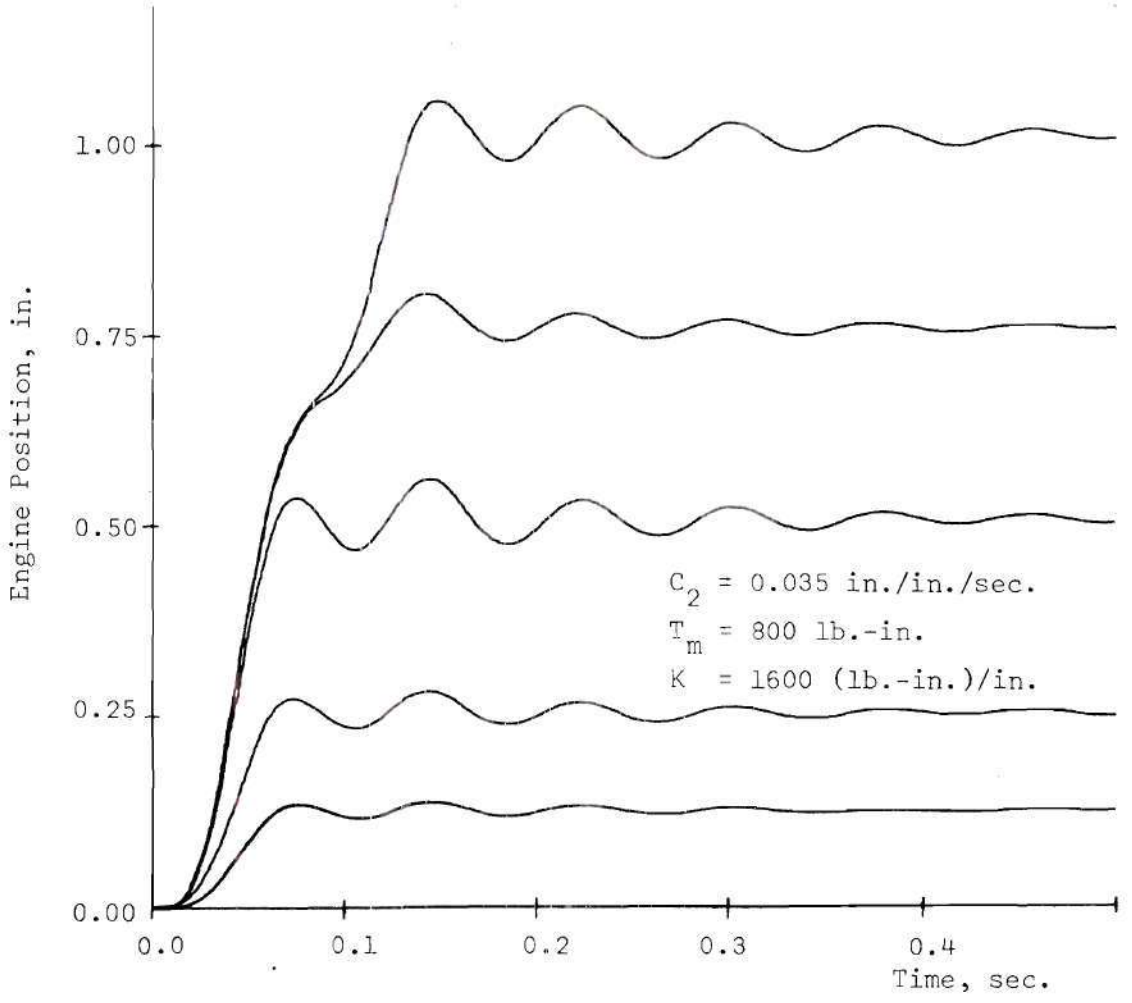

Figure 58. Engine Position Response to Several Step Commands

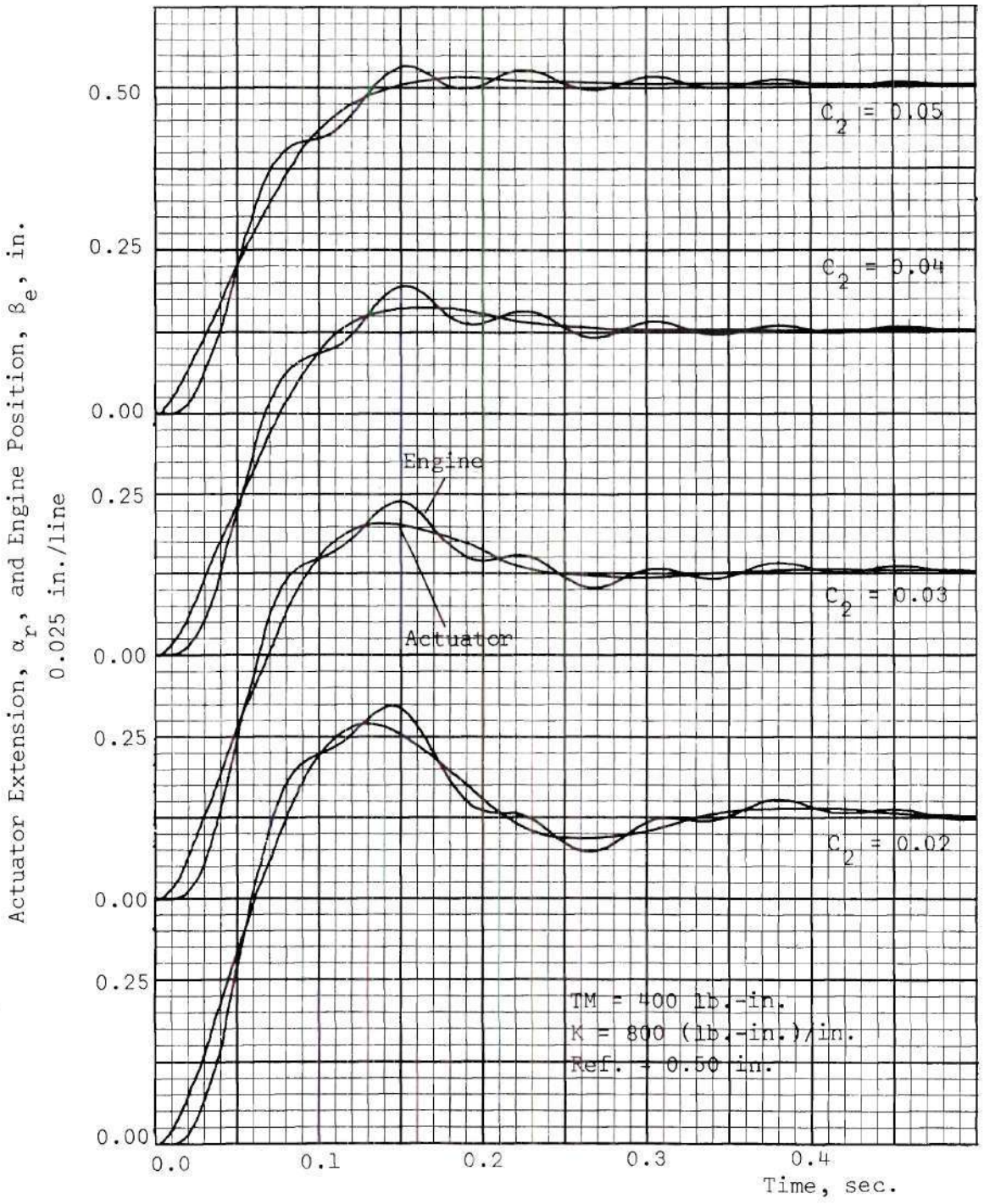

Figure 59. Effect of Variation of Rate Feedback Coefficient, C_2, on Actuator Extension and Engine Position Step Response for T_m = 400 lb.-in.

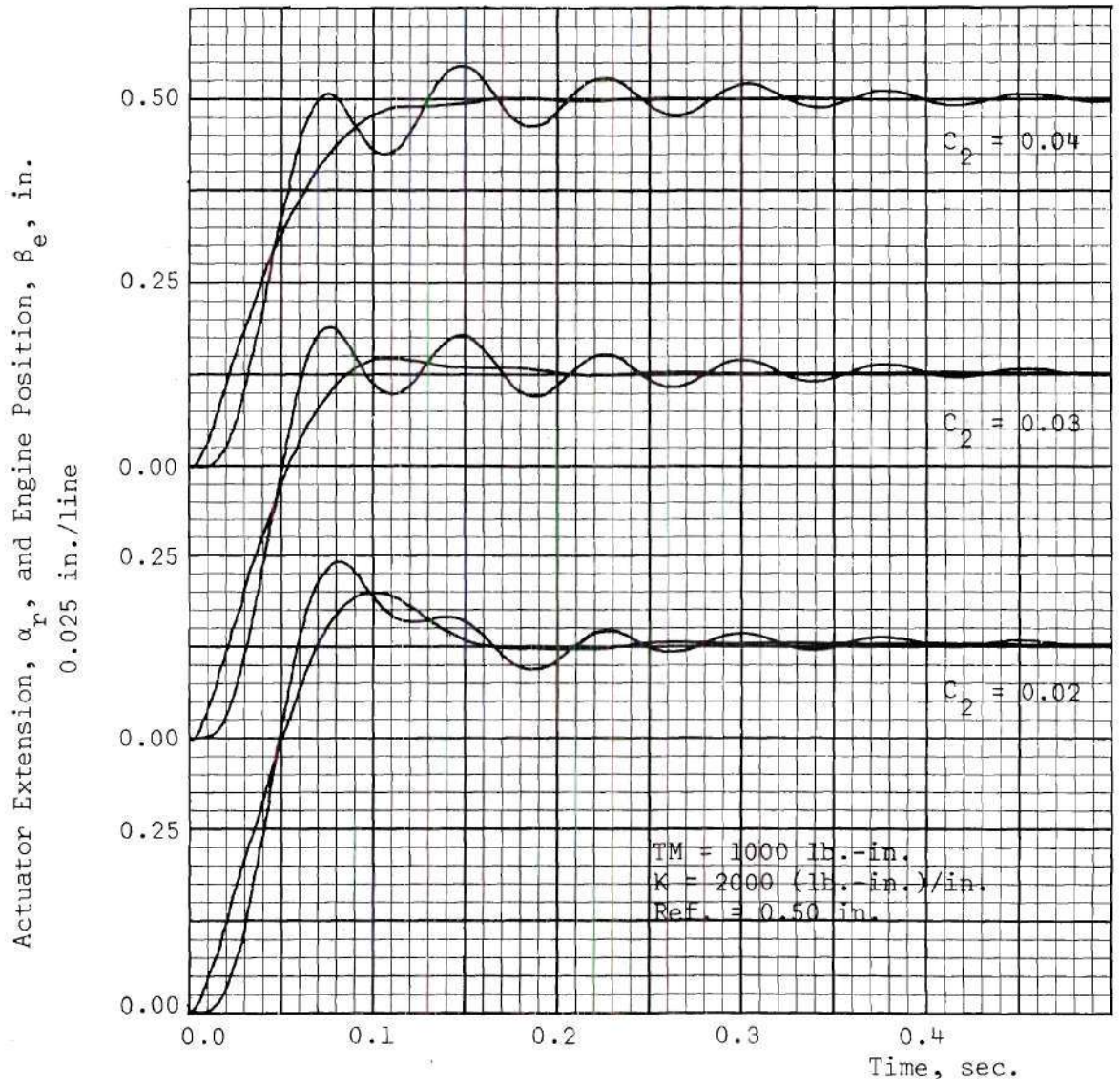

Figure 60. Effect of Variation of Rate Feedback Coefficient, C_2, on Actuator Extension and Engine Position Step Response for T_m = 1000 lb.-in.

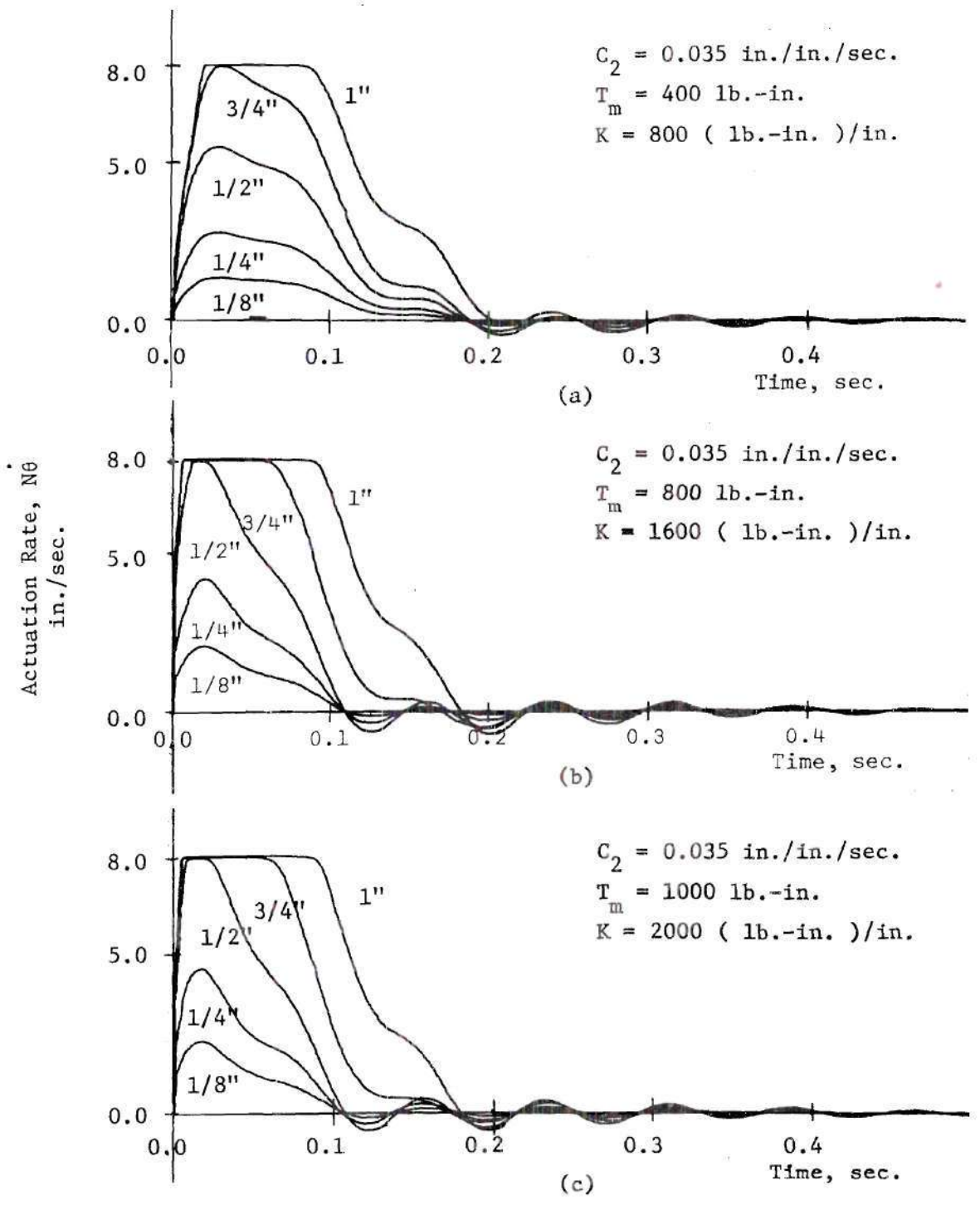

Figure 61. Clutch Output Velocity Time Histories for Variations of Maximum Torque, T_m, and Gain, K

Friction-Disc Clutch-Actuator Simulation Data

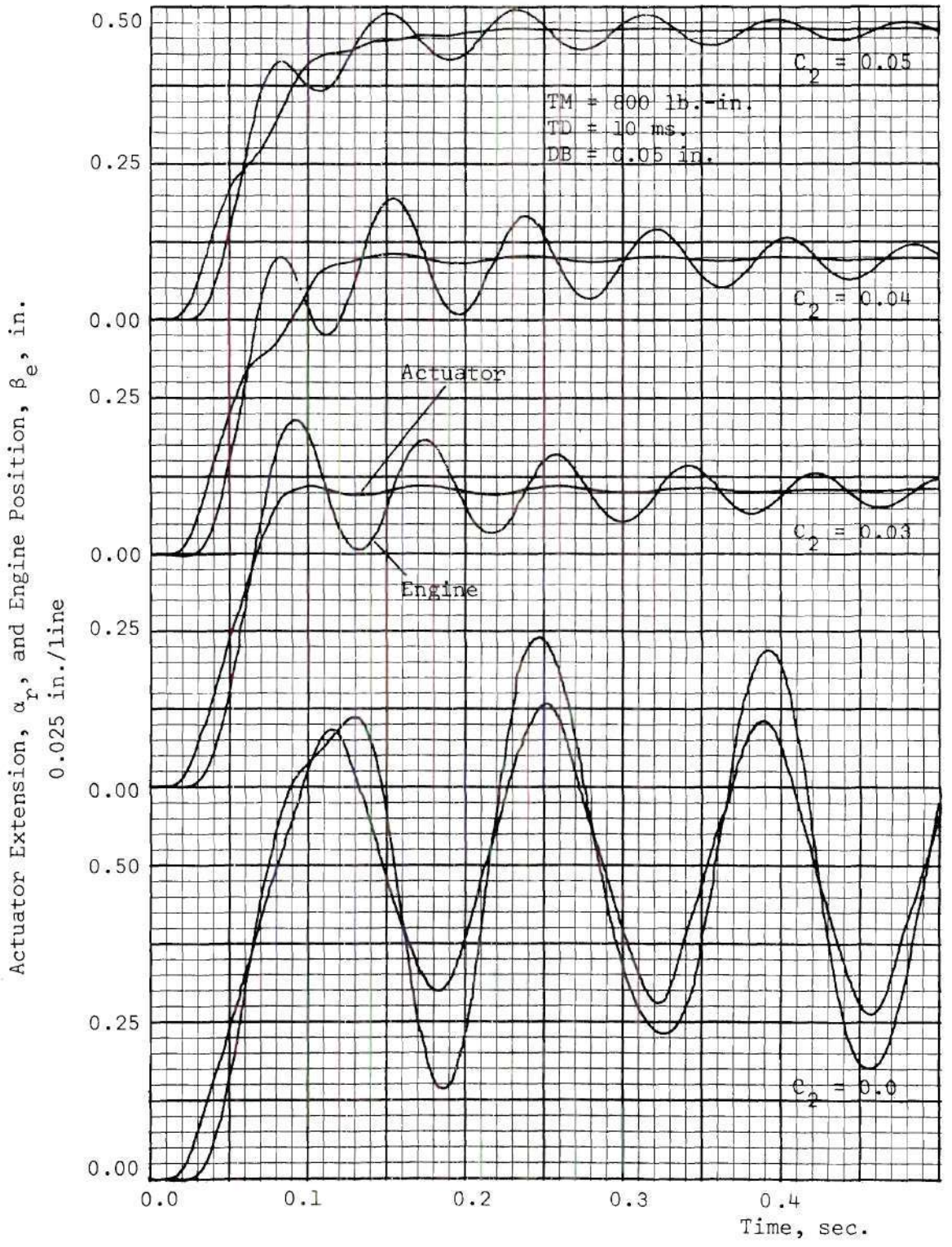

Figure 62. Effect of Variation of Rate Feedback Coefficient, C_2, on Actuator Extension and Engine Position Step Response for T_m = 800 lb.-in., TD = 10 ms., and DB = 0.05 in.

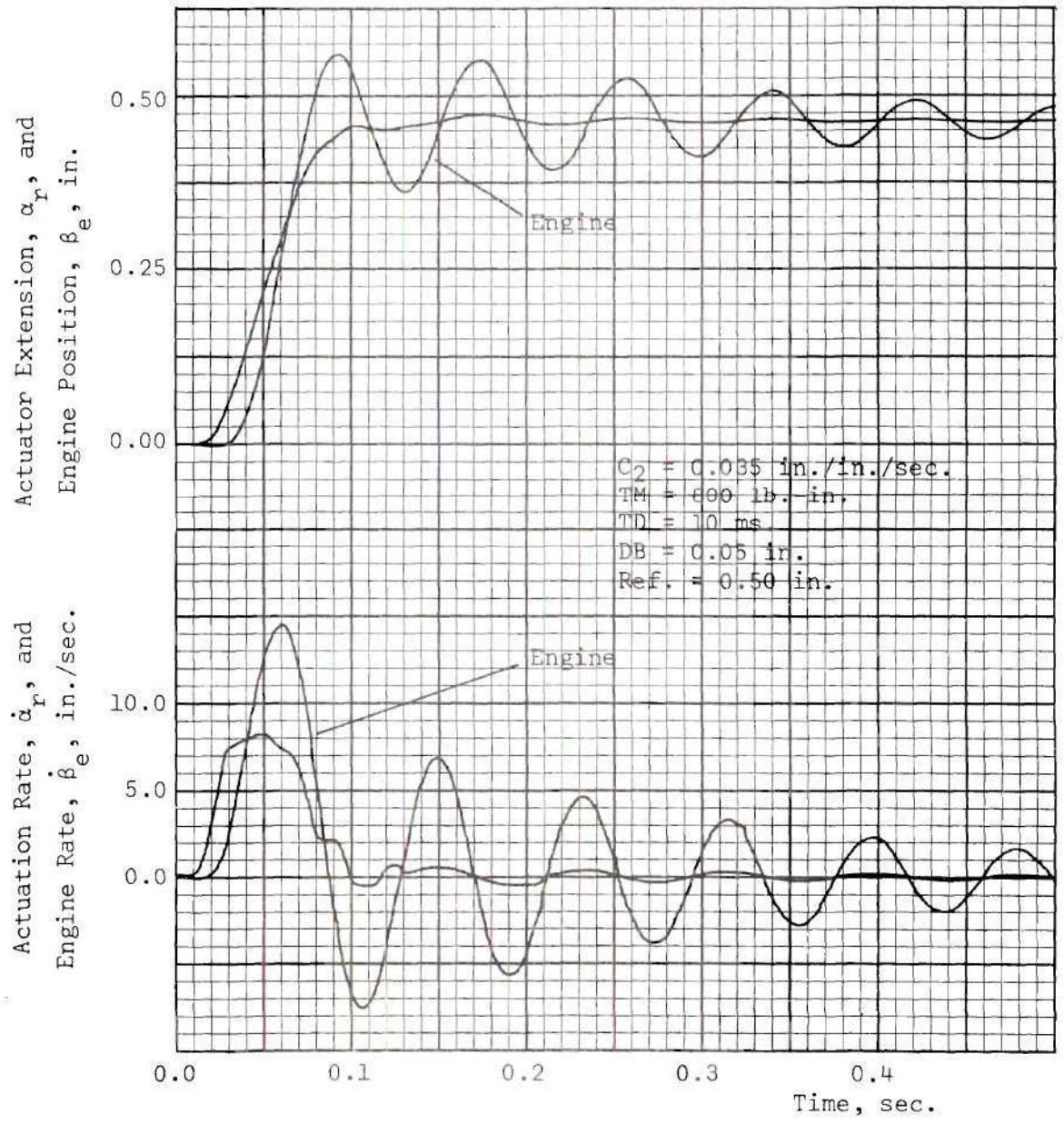

Figure 63. Actuator and Engine Position and Rate Response to a 1/2-in. Step Command for Friction-Disc Clutch-Actuator Simulation

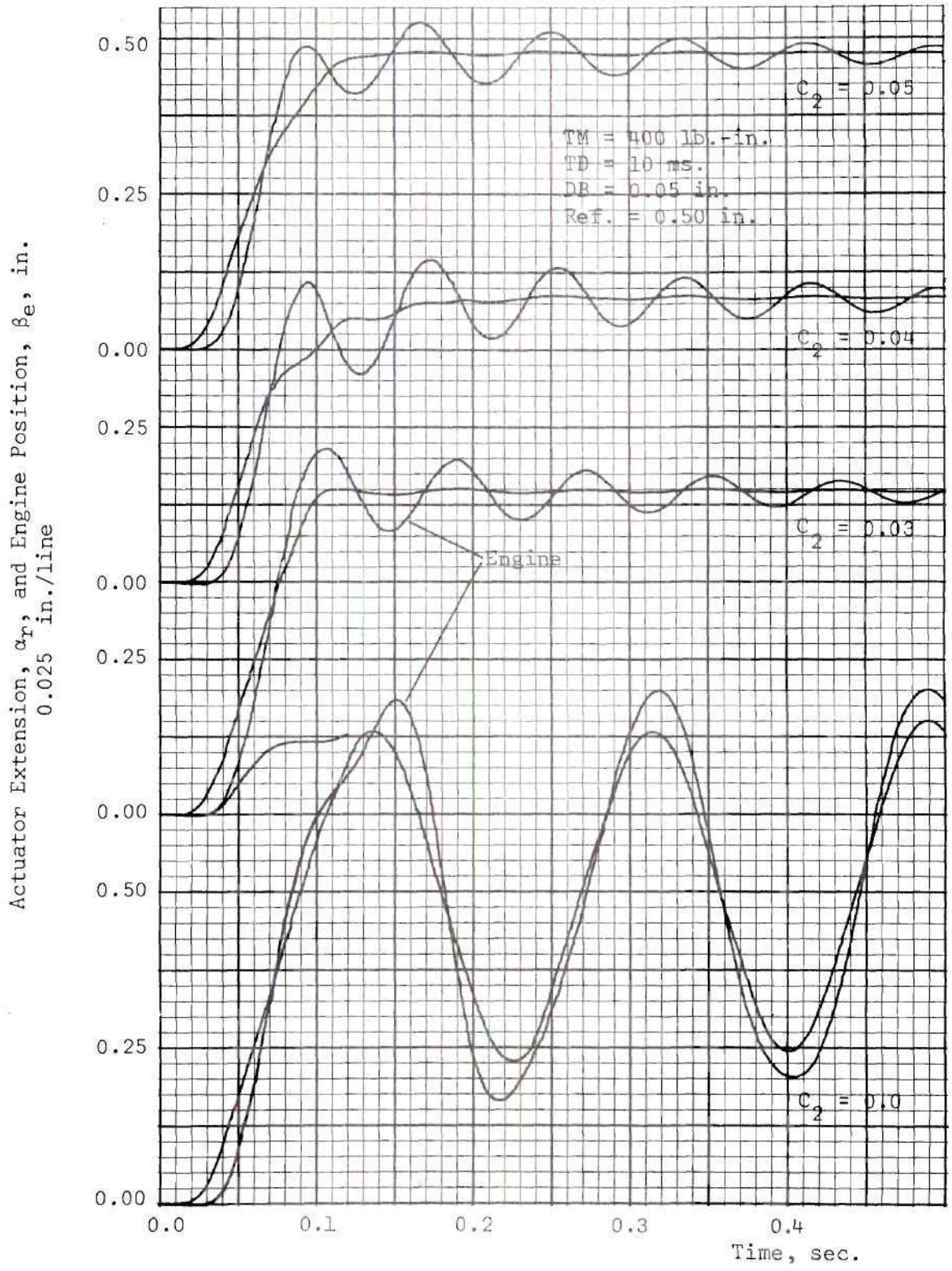

Figure 64. Effect of Variation of Rate Feedback Coefficient, C_2, on Actuator Extension and Engine Position Step Response for T_m = 400 lb.-in., TD = 10 ms., and DB = 0.05 in.

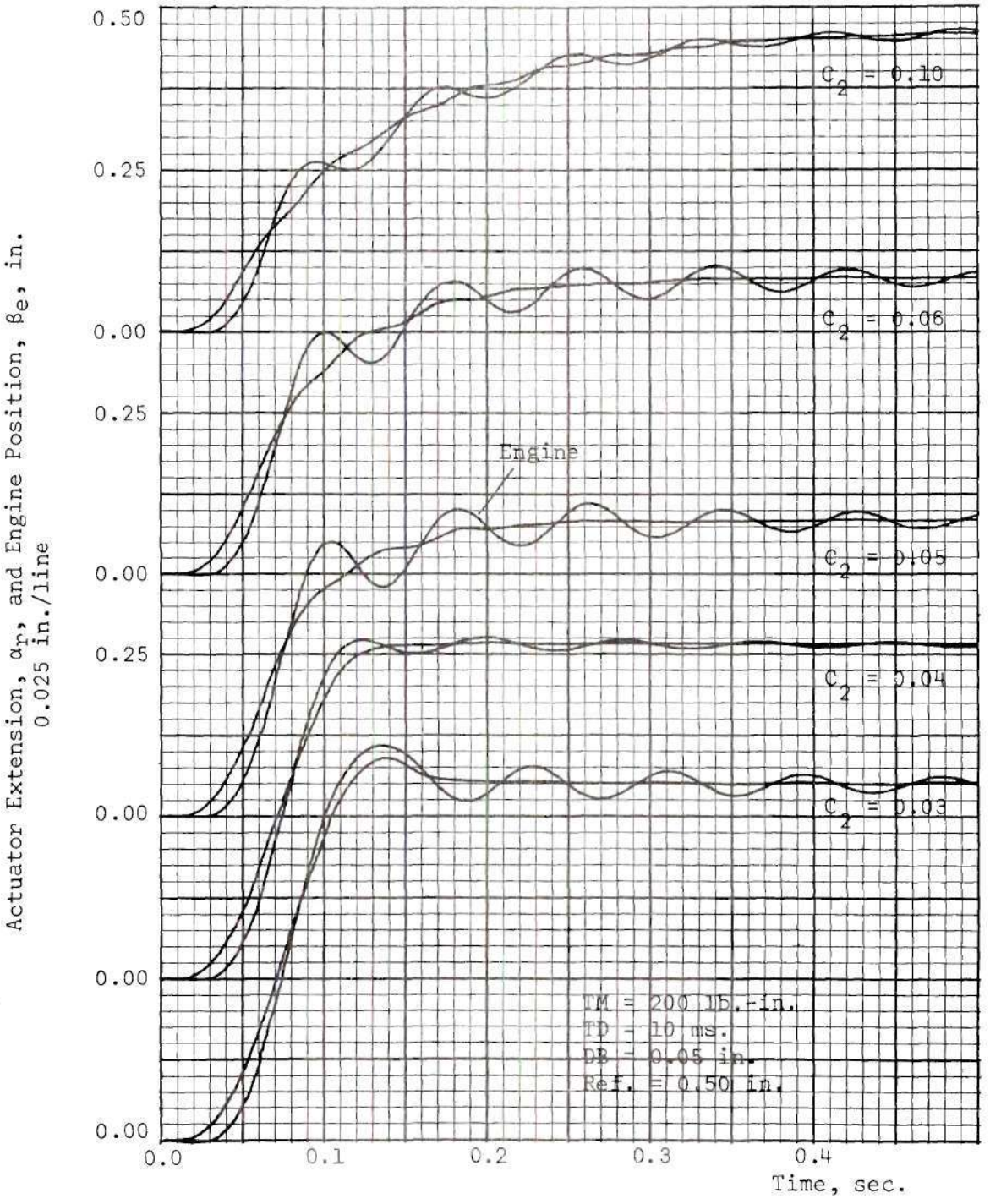

Figure 65. Effect of Variation of Rate Feedback Coefficient, C_2, on Actuator Extension and Engine Position Step Response for T_m = 200 lb.-in., TD = 10 ms., and DB = 0.05 in.

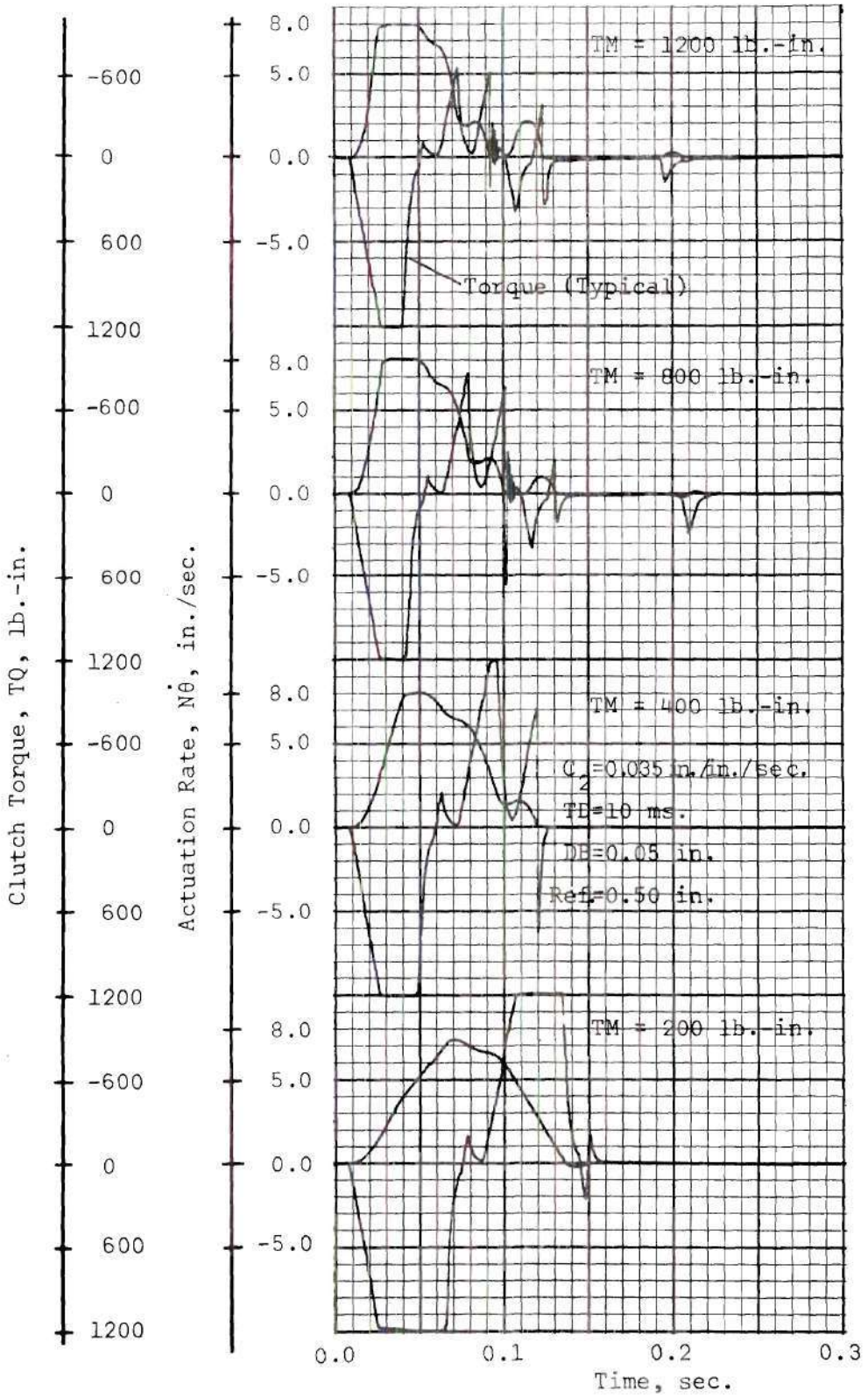

Figure 66. Effect of Maximum Torque Level on Engagement Time

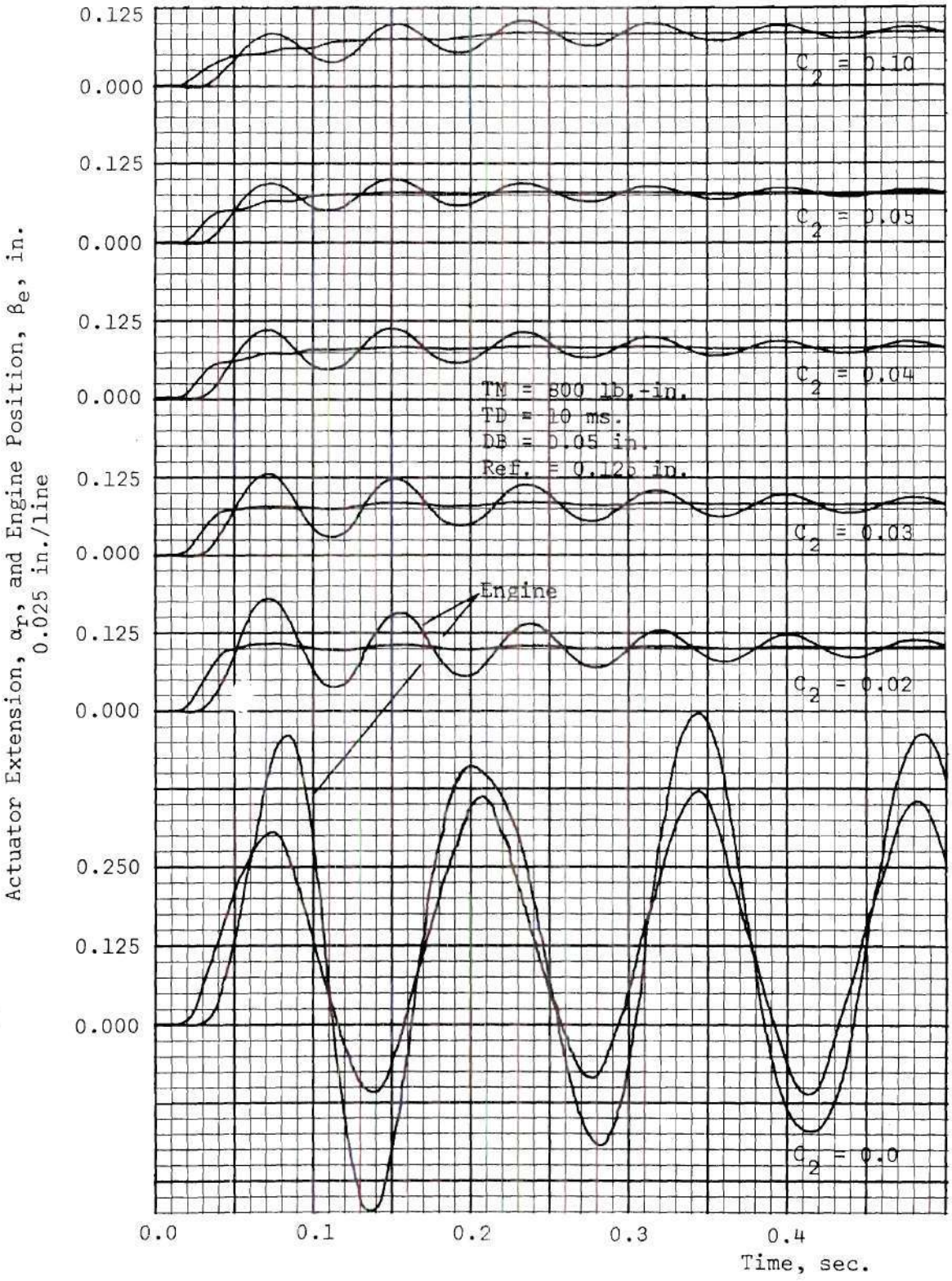

Figure 67. Effect of Variation of Rate Feedback Coefficient, C_2, on Actuator Extension and Engine Position Step Response for Ref. = 0.125 in.

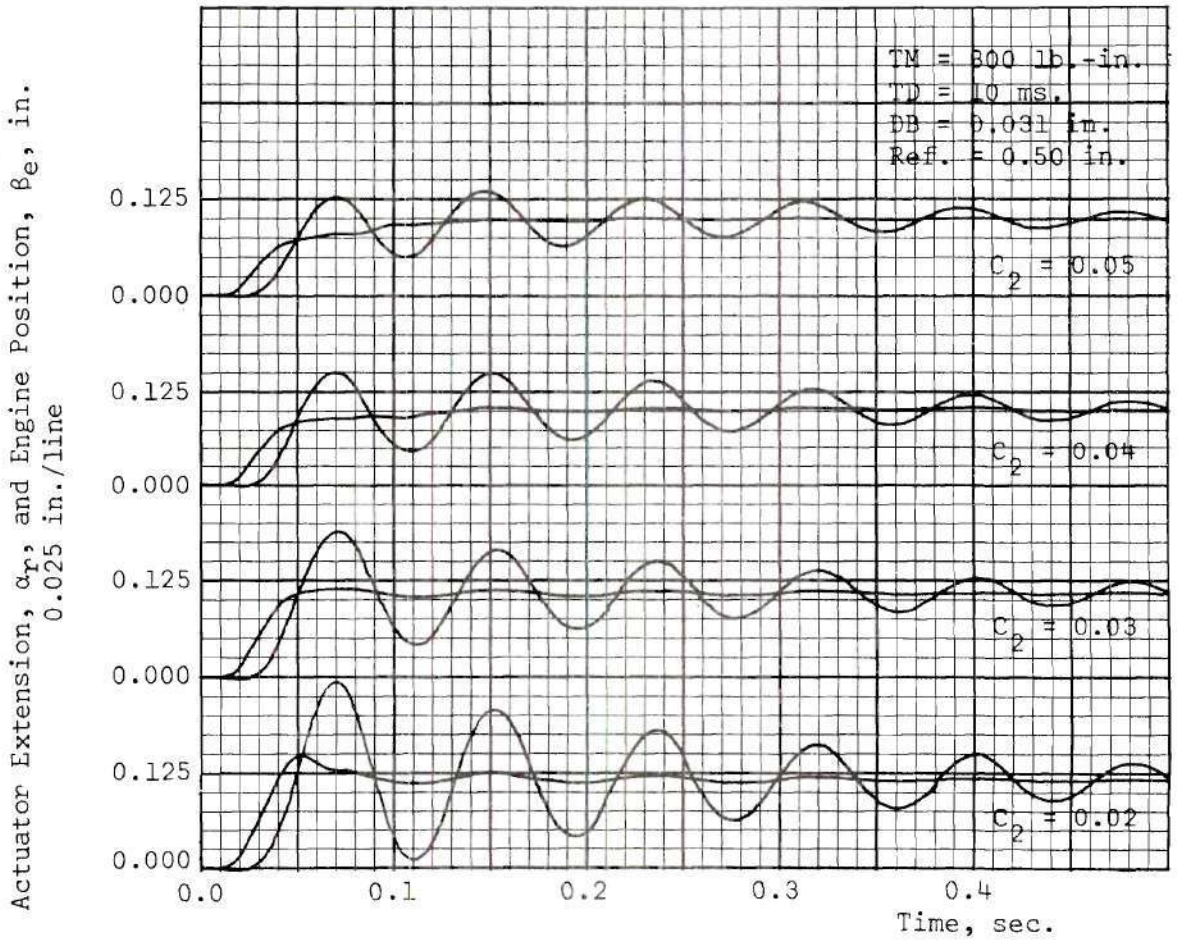

Figure 68. Data for Demonstrating the Effect of a Reduction of System Deadband

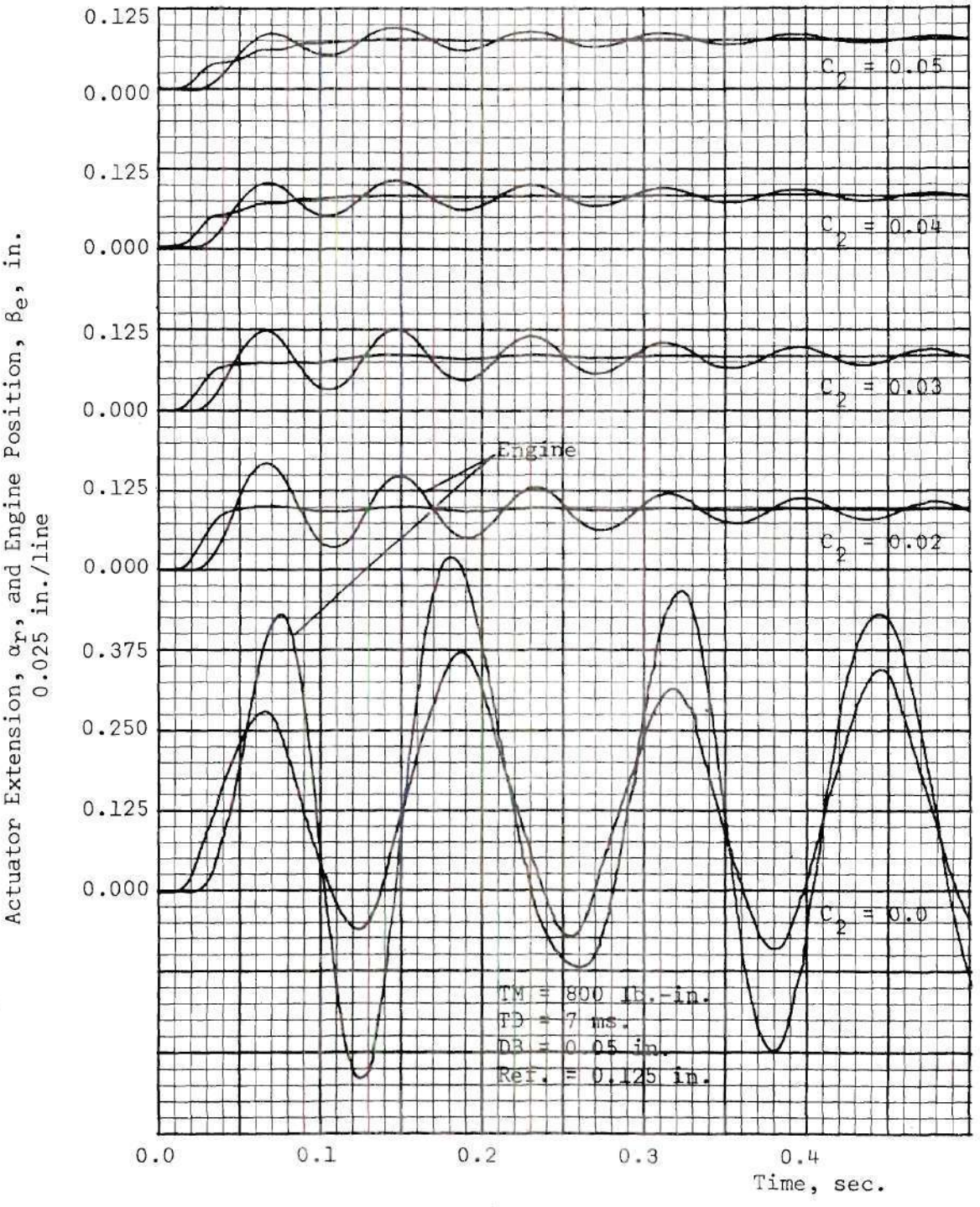

Figure 69. Data Illustrating the Influence of Decreased Clutch Engagement Time Delay on System Stability

Wrap-Spring Clutch-Actuator Simulation Data

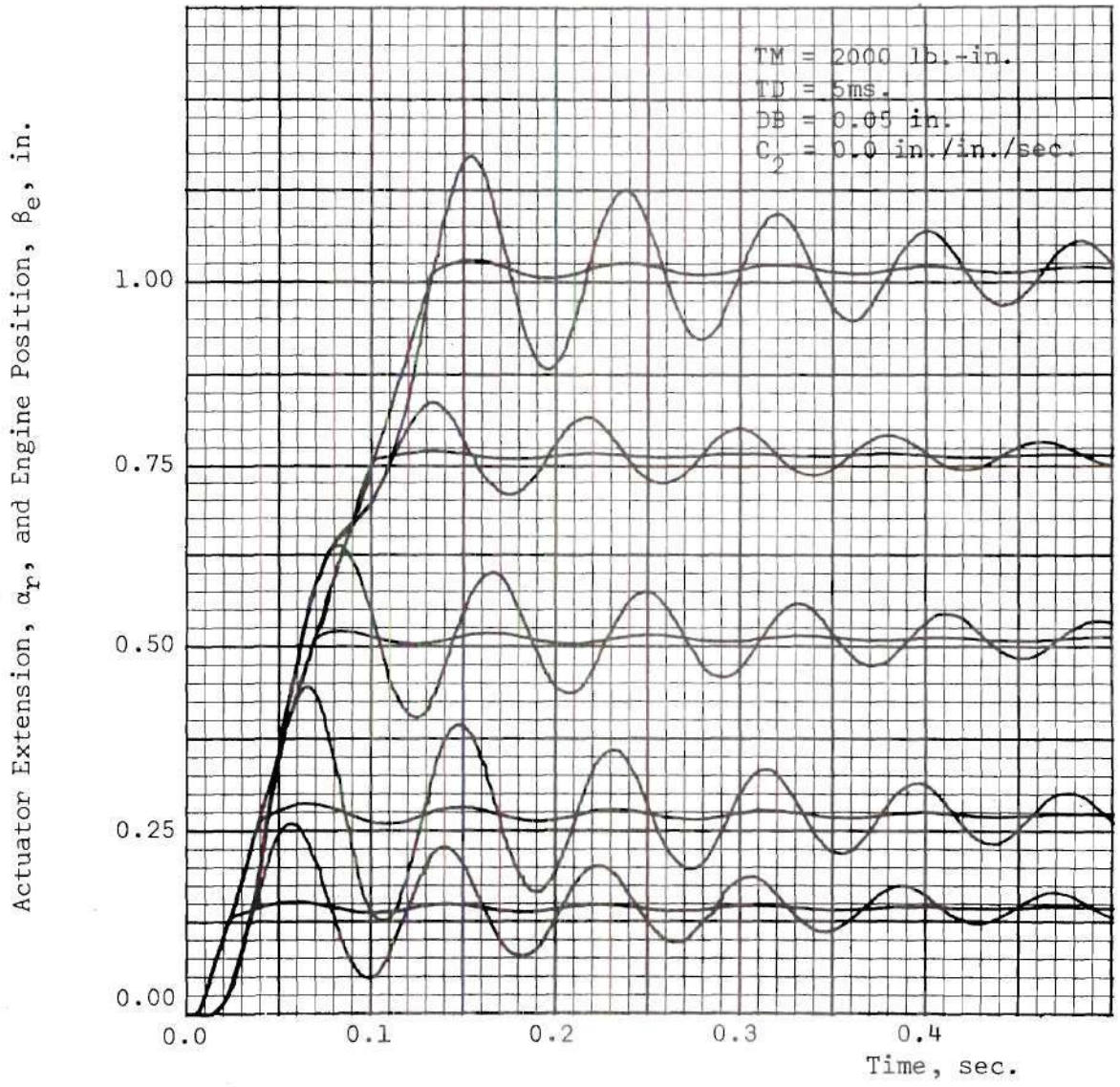

Figure 70. Actuator Extension and Engine Position Response to Various Step Commands. Wrap-Spring Clutch-Actuator Simulation

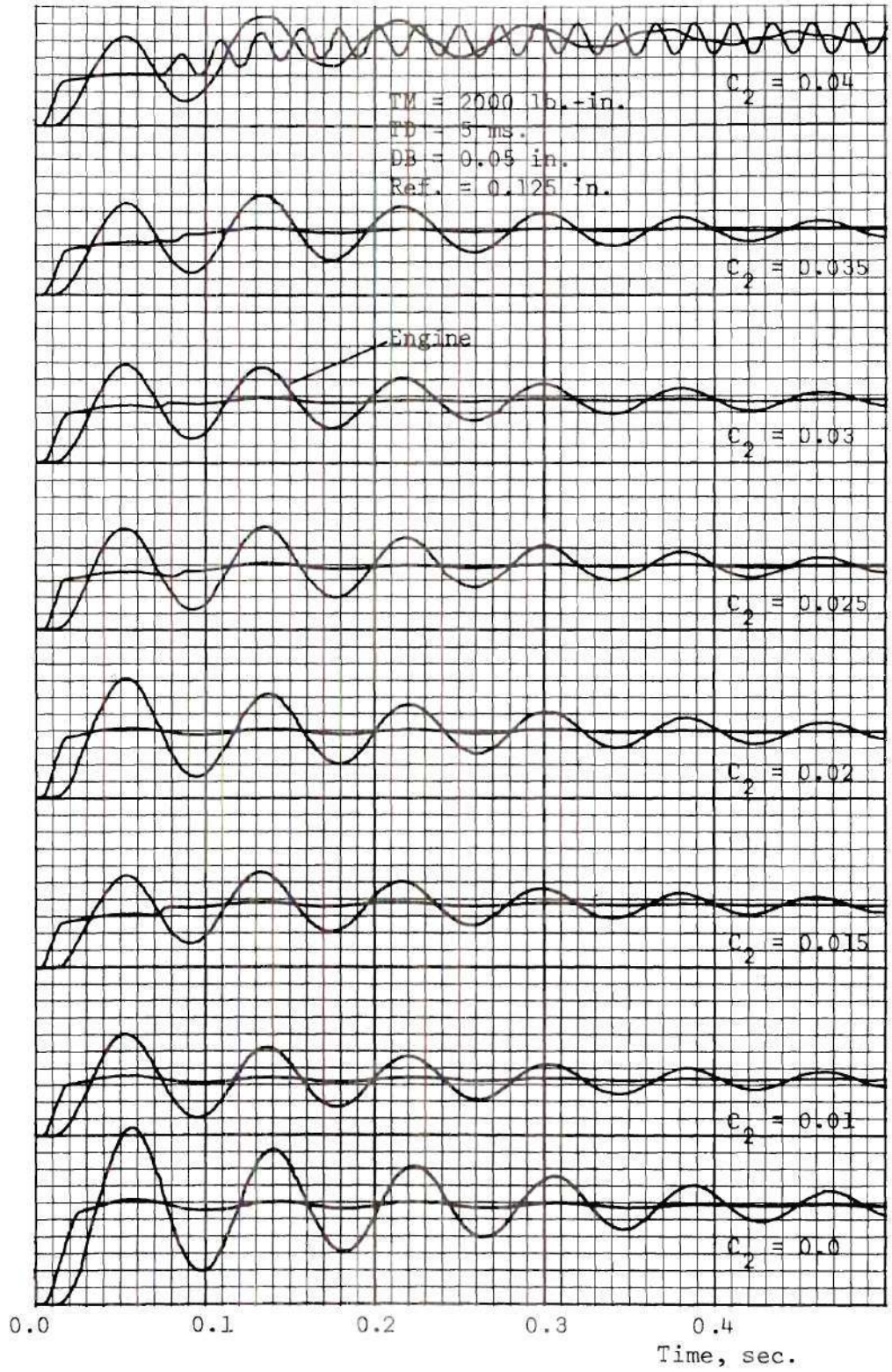

Figure 71. Effect of Variation of Rate Feedback Coefficient, C_2, on Actuator Extension and Engine Position Step Response. Wrap-Spring Clutch-Actuator Simulation. Ref. = 0.125 in.

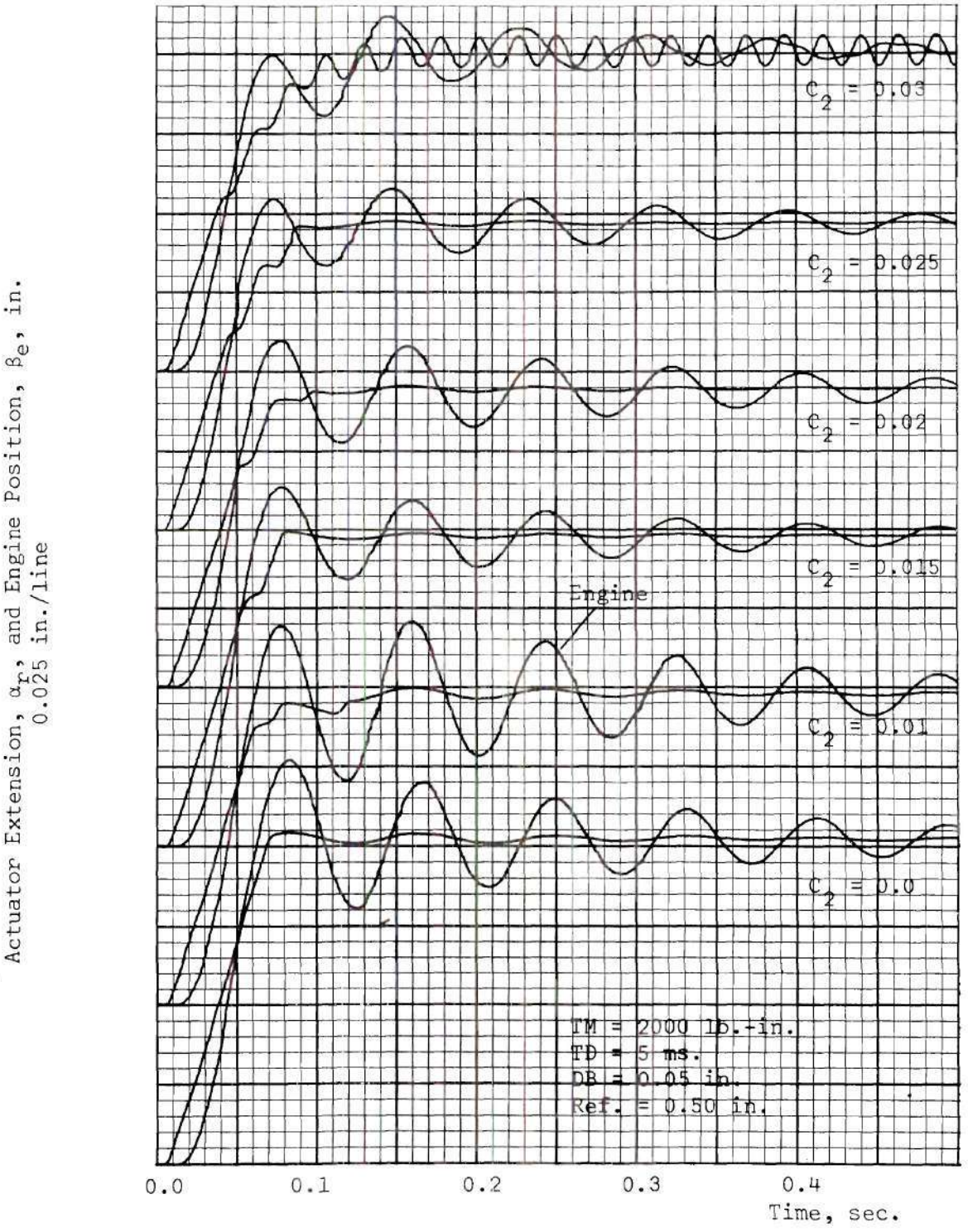

Figure 72. Effect of Variation of Rate Feedback Coefficient, C_2, on Actuator Extension and Engine Position Step Response. Wrap-Spring Clutch-Actuator Simulation, Ref. = 0.50 in.

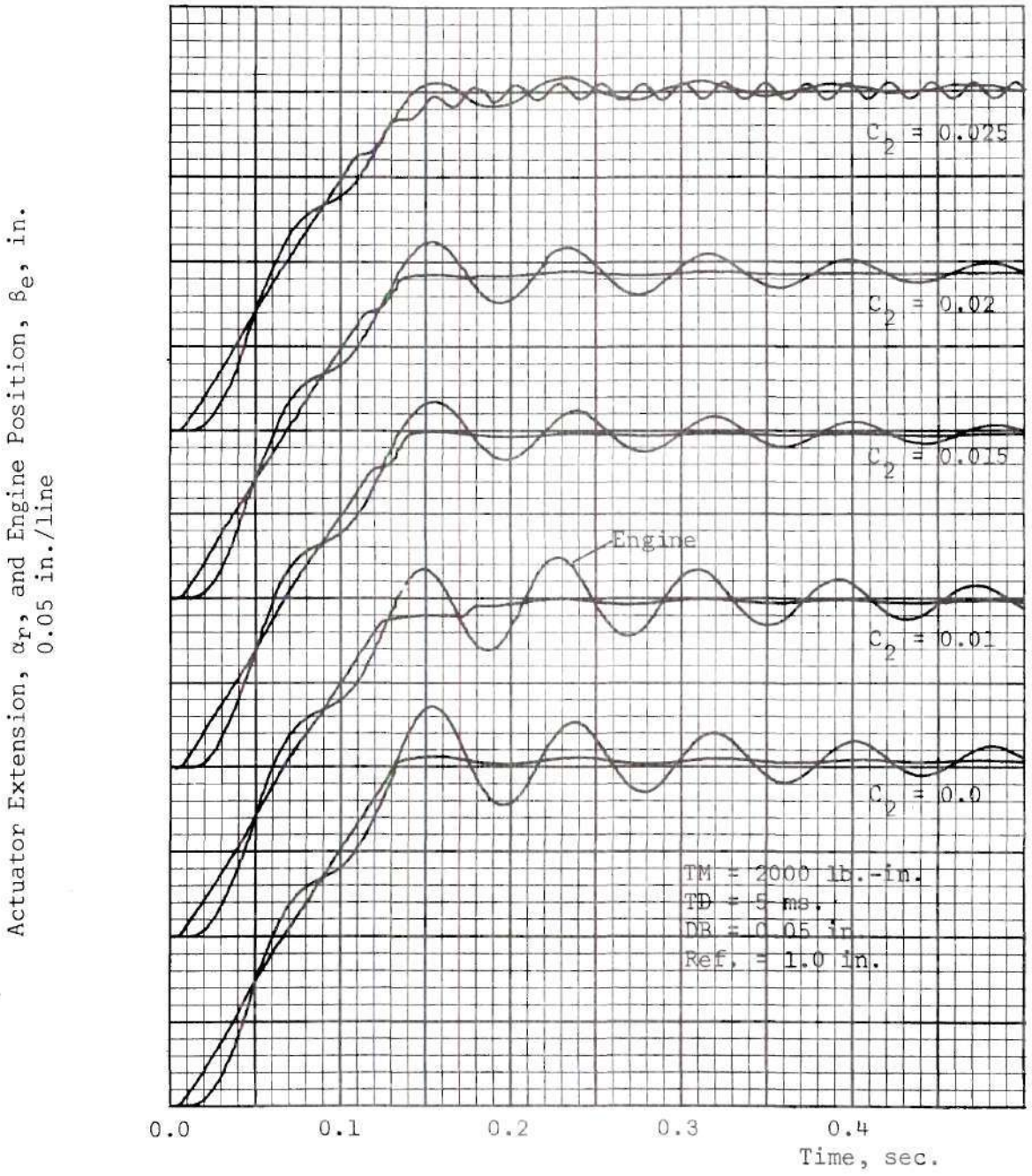

Figure 73. Effect of Variation of Rate Feedback Coefficient, C_2, on Actuator Extension and Engine Position Step Response. Wrap-Spring Clutch-Actuator Simulation. Ref. = 1.0 in.

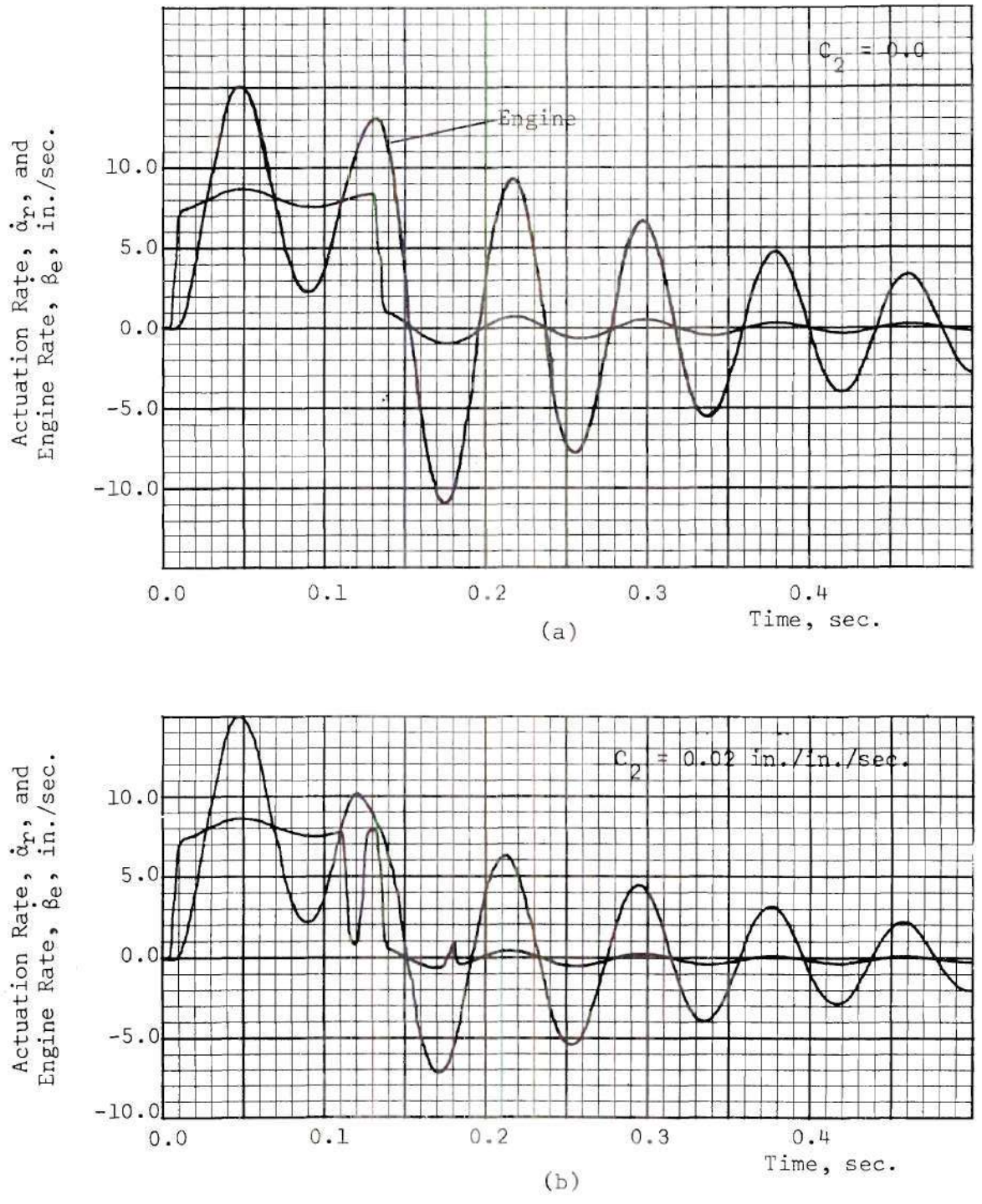

Figure 74. Comparison of Actuation and Engine Rates for a Simulated Wrap-Spring Clutch-Actuator for Two Rate-Feedback Conditions. T_m = 2000 lb.-in., TD = 5 ms., DB = 0.05 in., Ref. = 1.0 in.

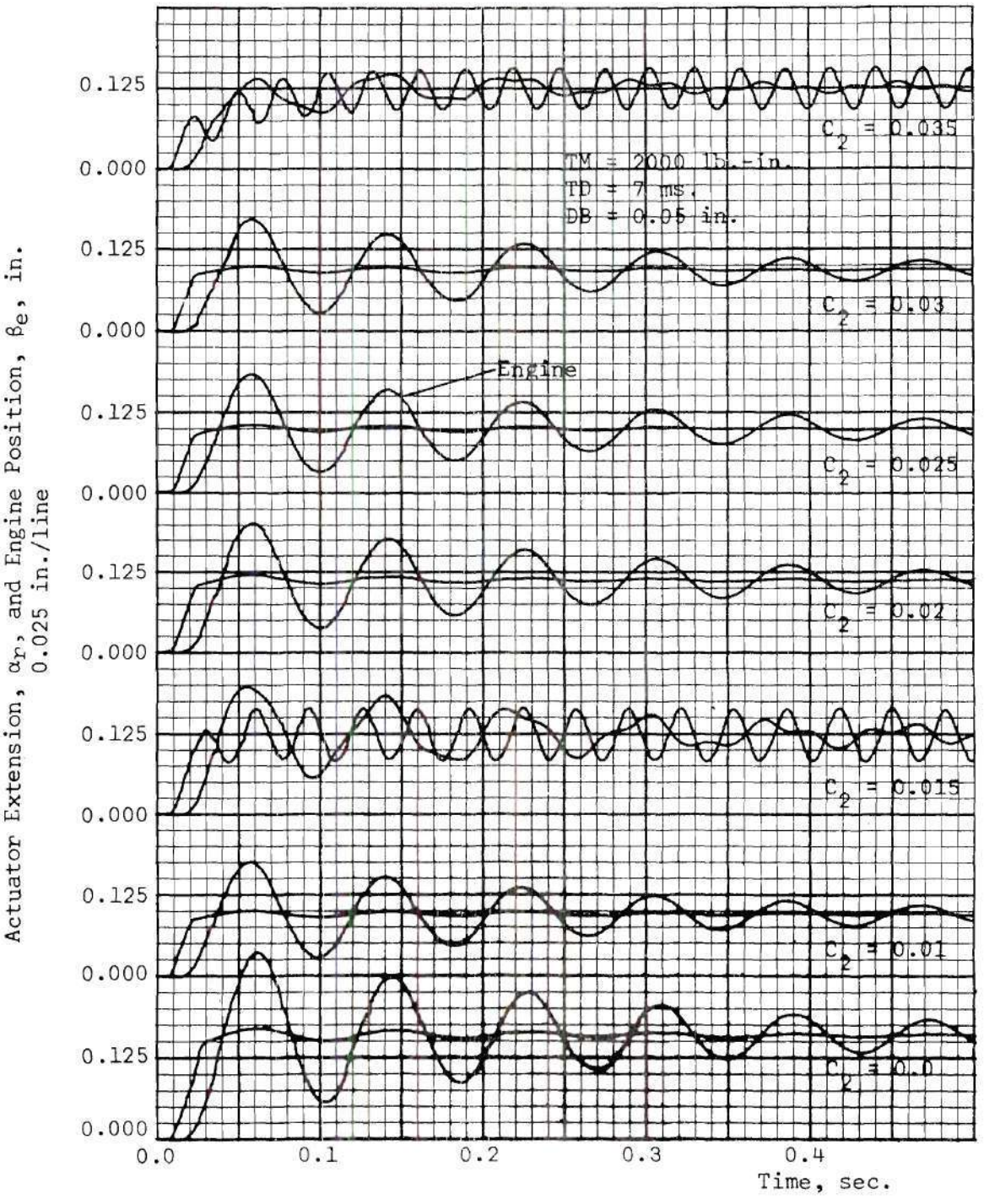

Figure 75. Data Illustrating the Effect of Increased Clutch Engagement Time Delay on System Stability. Wrap-Spring Clutch-Actuator Simulation. Ref. = 0.125 in.

APPENDIX D

WRAP-SPRING CLUTCH-ACTUATOR TEST AND SIMULATION DATA

The data which follows consists of data recorded during wrap-spring clutch-actuator tests performed at the Marshall Space Flight Center, Astrionics Laboratory, Huntsville, Alabama, and of analog computer simulation runs made at the Georgia Institute of Technology, Atlanta, Georgia. The actuation rate was 4 in./sec. in each case, and the rate feedback pickoff was $\dot{\alpha}_i$.

Actuator-Test Data

Scale Factors:

1 volt = 1 inch

and

1 volt = 1 in./sec.

Example: In Figure 76

40 β_e = (1000 mv./line)('X' lines)(1/1000 v/mv.)(1 in./v.)

40 β_e = 'X' in.

β_e = 'X'/40 in.

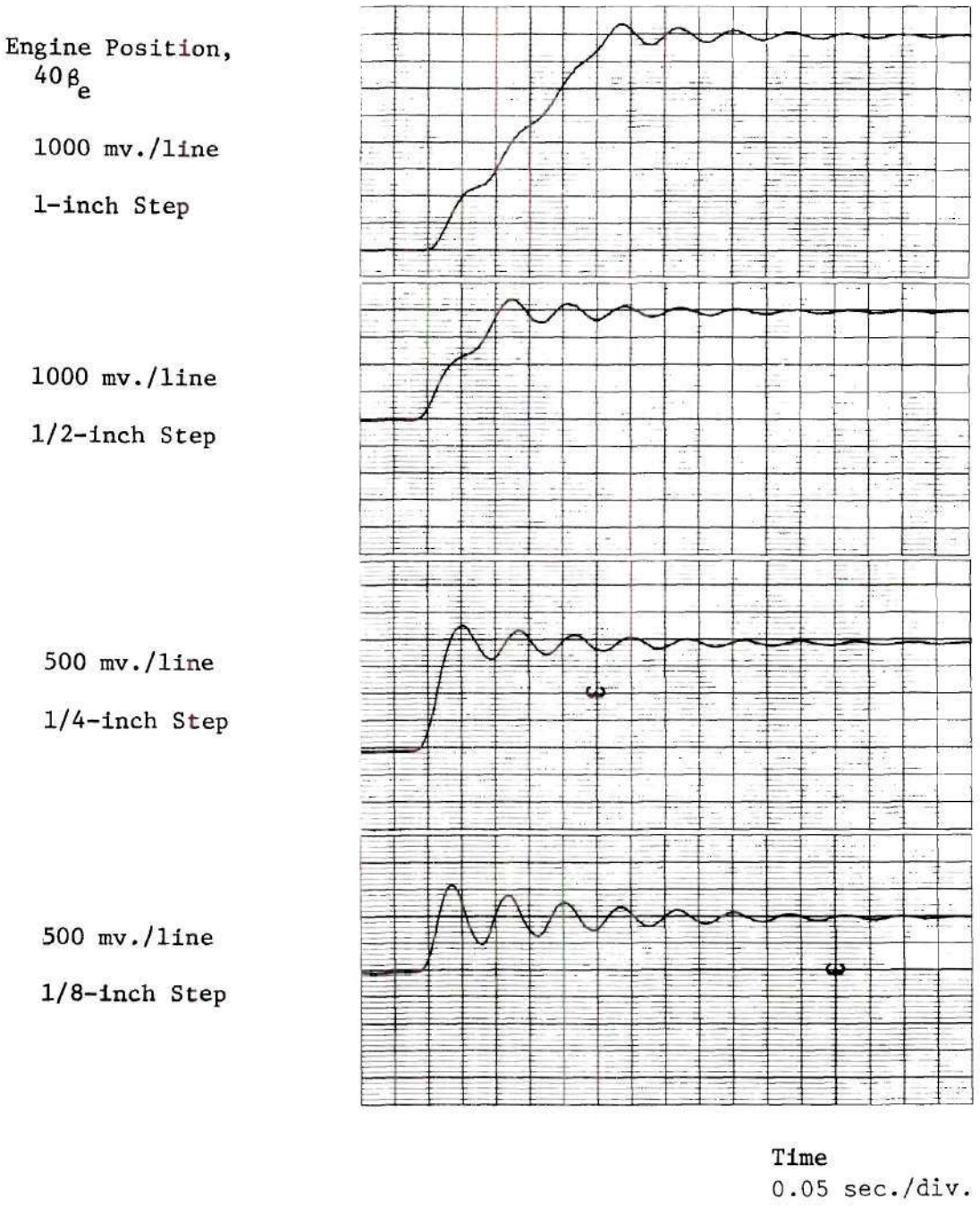

Figure 76. Data Sheet, Actuator Test: Step Inputs of Varying Magnitude; Rate Coefficient, C_2 = 0.00; DB = 0.031 in.

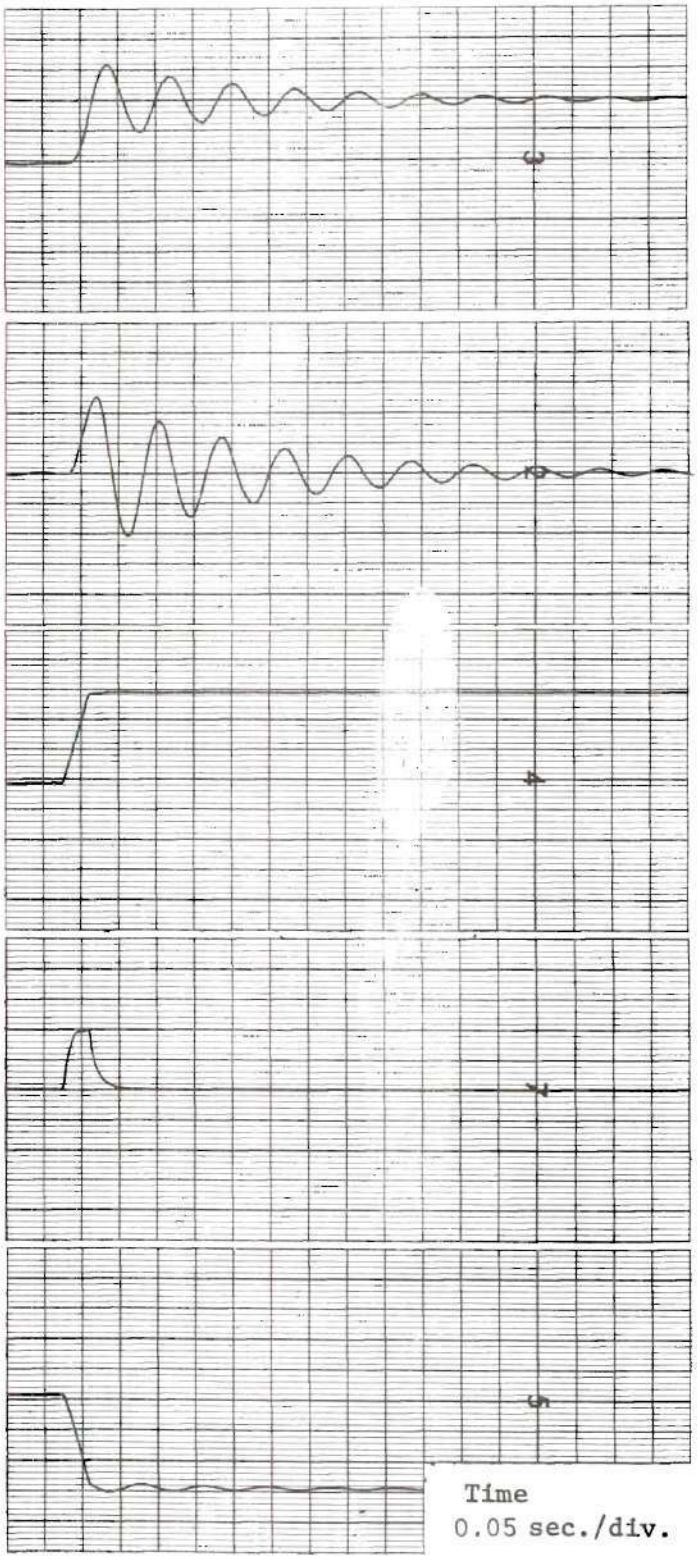

Figure 77. Data Sheet, Actuator Test: 1/8-in. Step; Rate Coefficient, C_2 = 0.00; DB = 0.031 in.

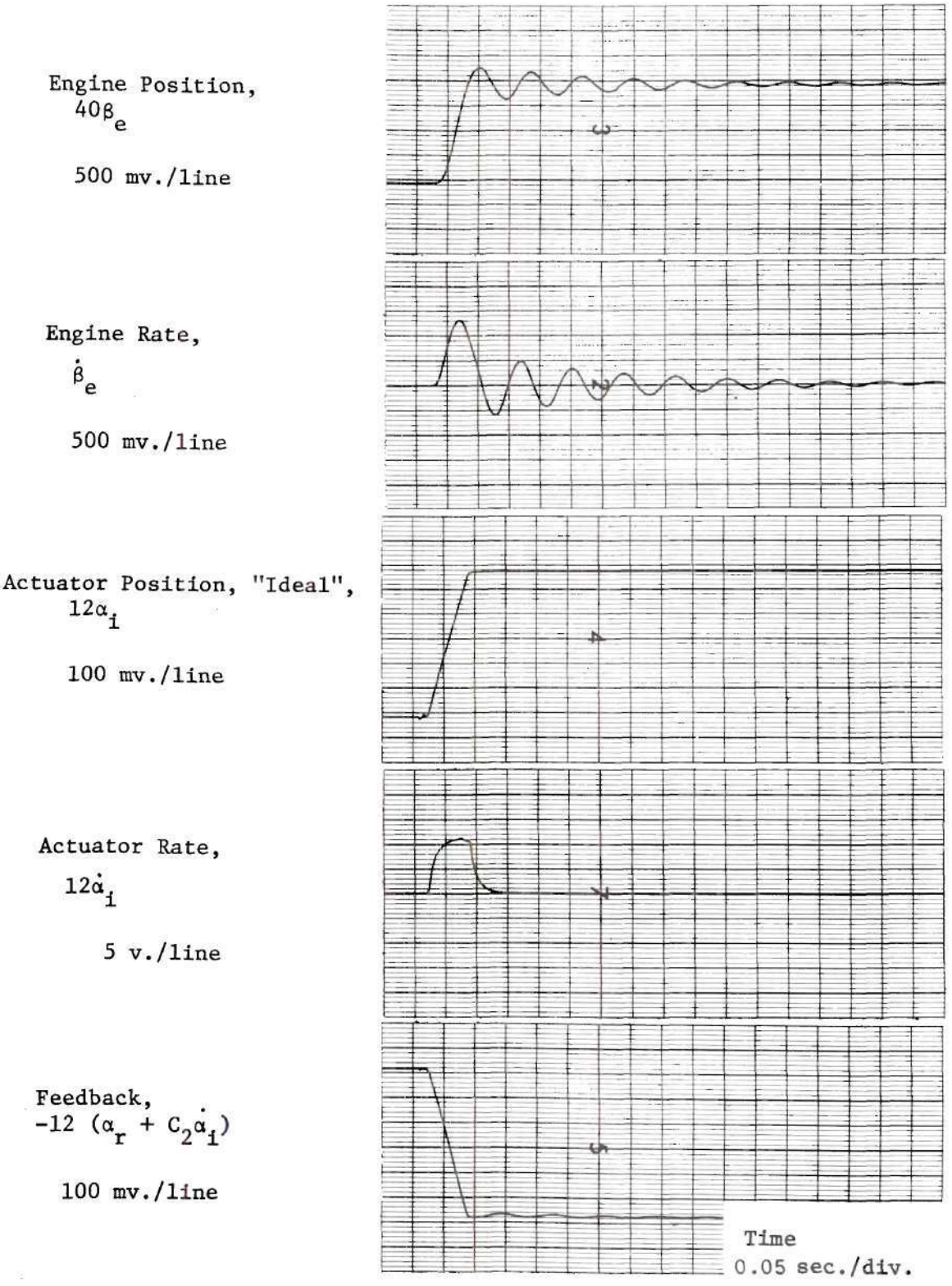

Figure 78. Data Sheet, Actuator Test: 1/4-in. Step; Rate Coefficient, C_2 = 0.00; DB = 0.031 in.

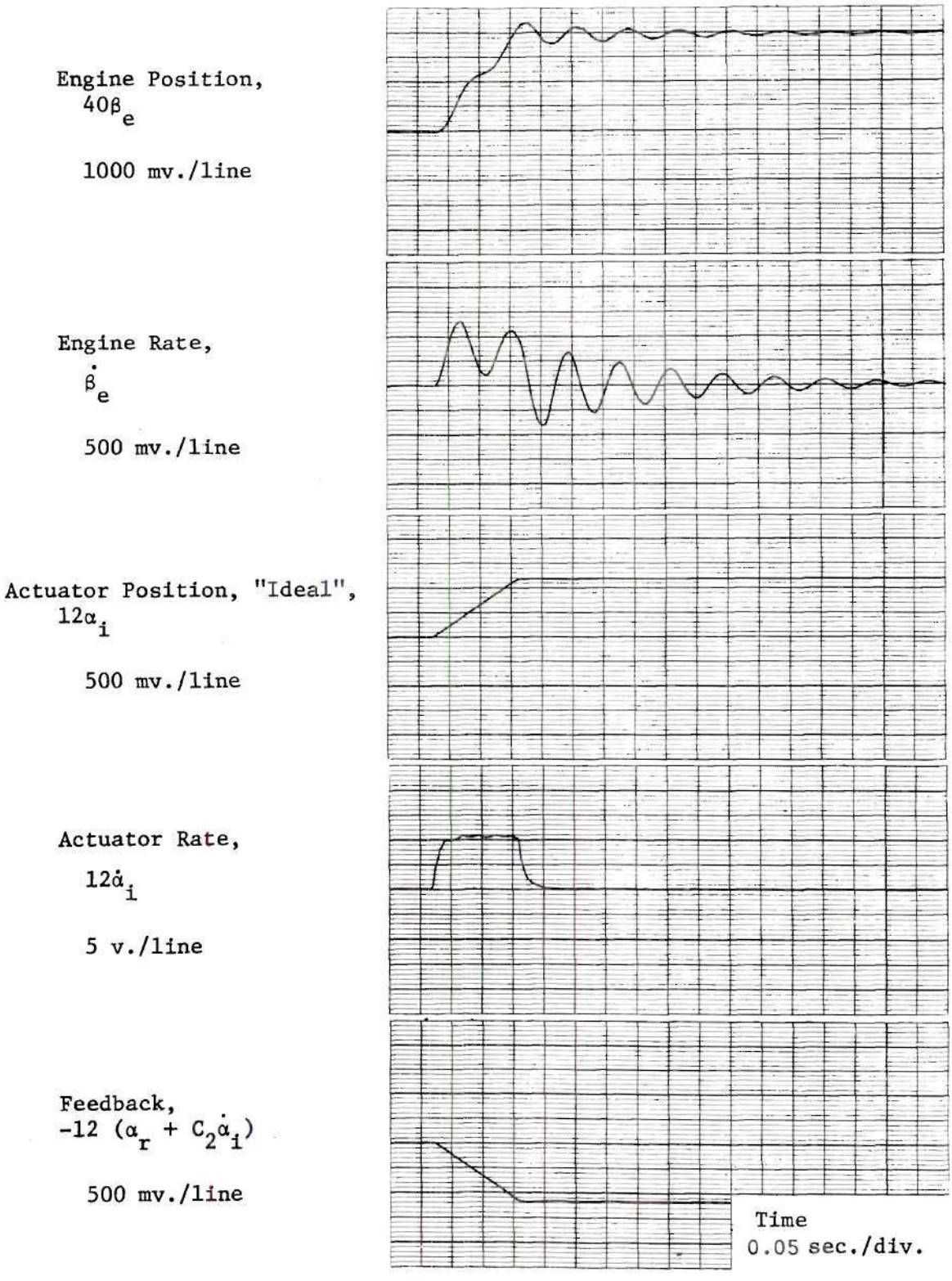

Figure 79. Data Sheet, Actuator Test: 1/2-in. Step; Rate Coefficient, C_2 = 0.00; DB = 0.031 in.

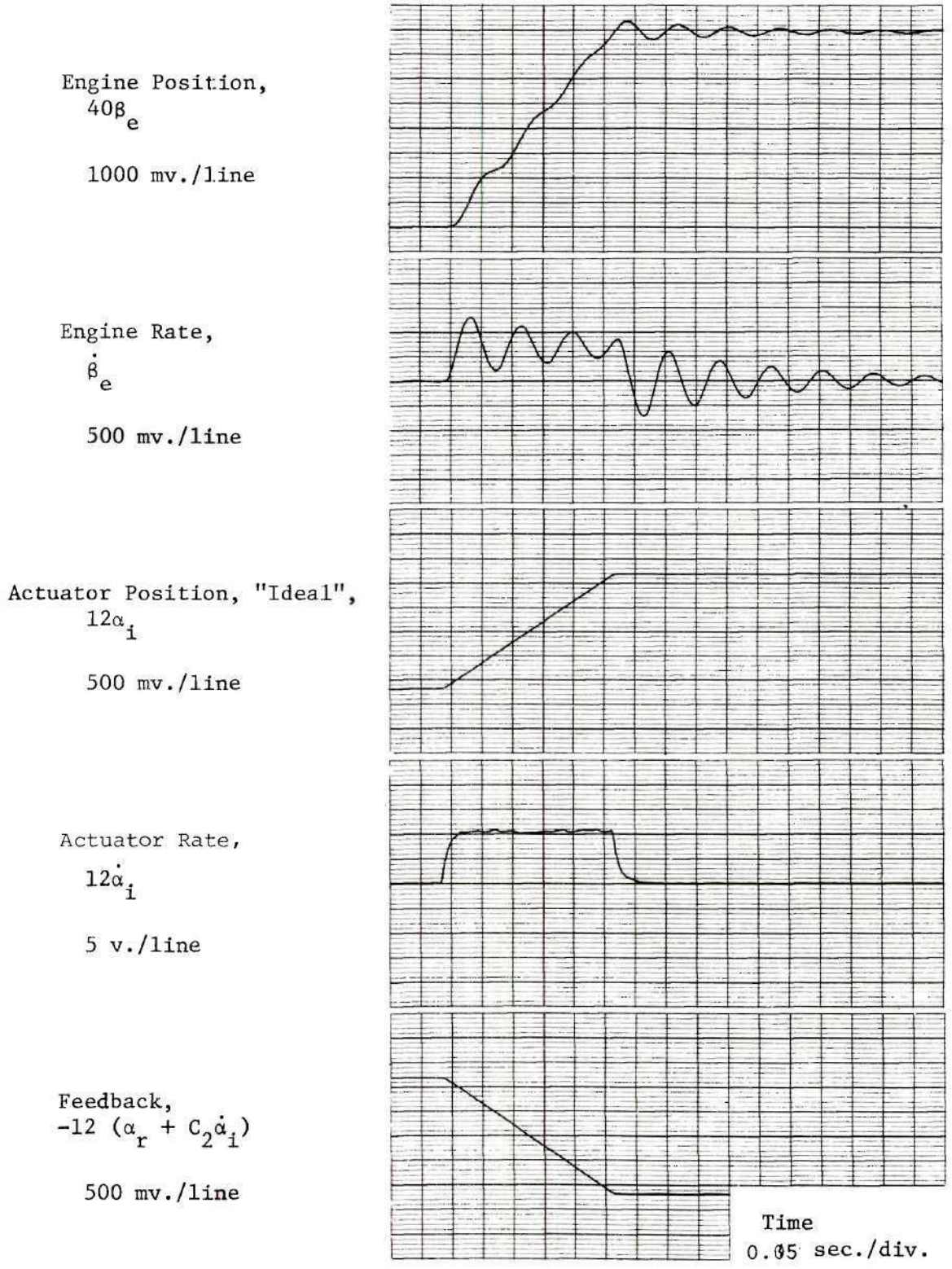

Figure 80. Data Sheet, Actuator Test: 1-in. Step; Rate Coefficient, C_2 = 0.00; DB = 0.031 in.

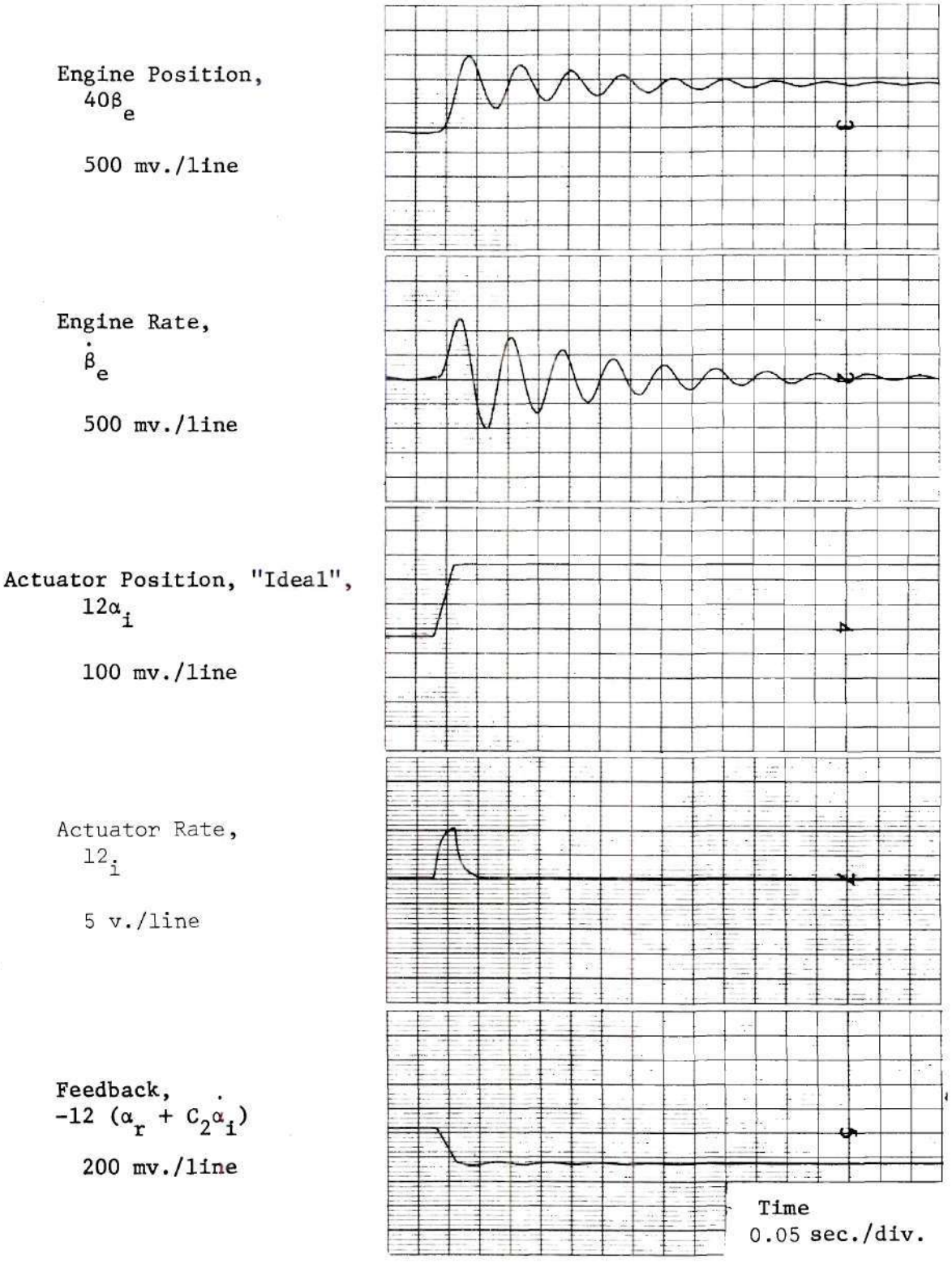

Figure 81. Data Sheet, Actuator Test: 1/8-in. Step; Rate Coefficient, C_2 = 0.00; DB = 0.042 in.

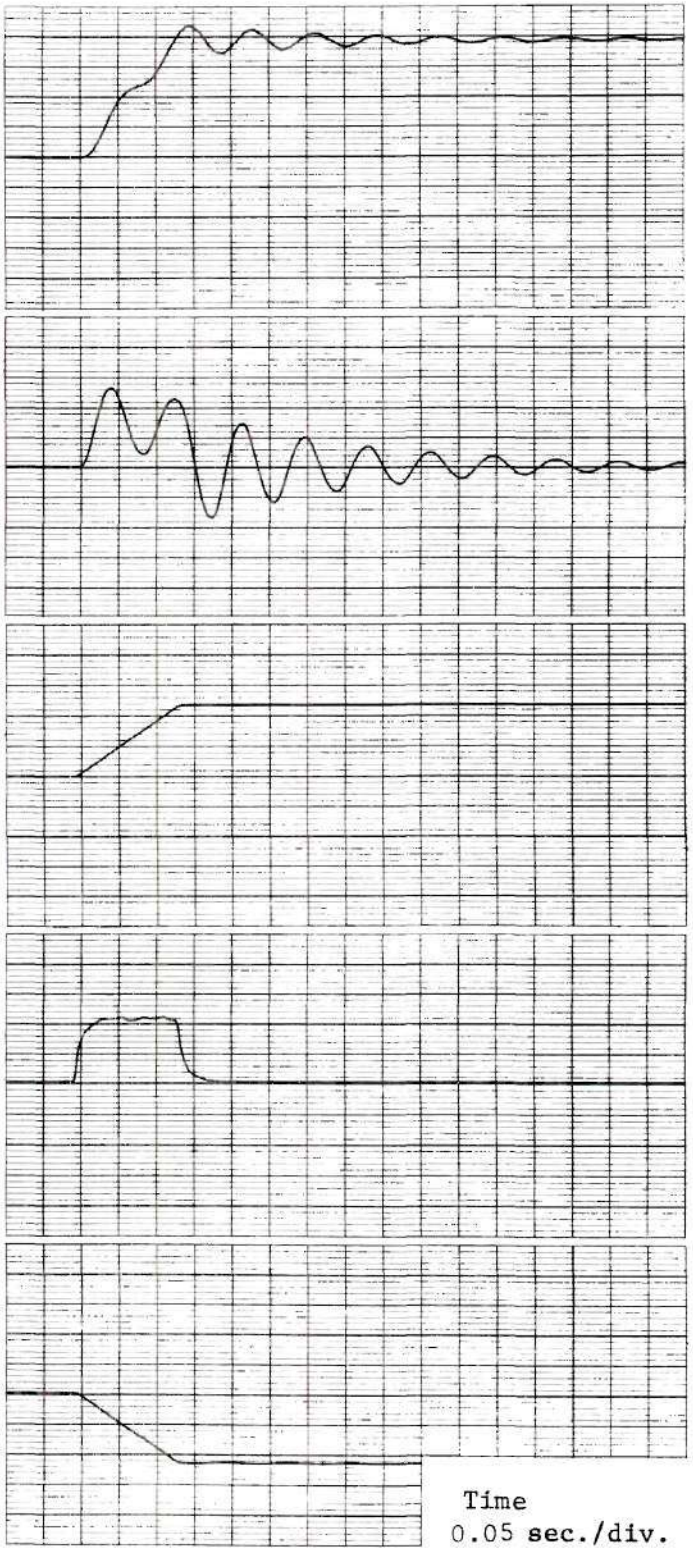

Figure 82. Data Sheet, Actuator Test: 1/2-in. Step; Rate Coefficient, C_2 = 0.00; DB = 0.042 in.

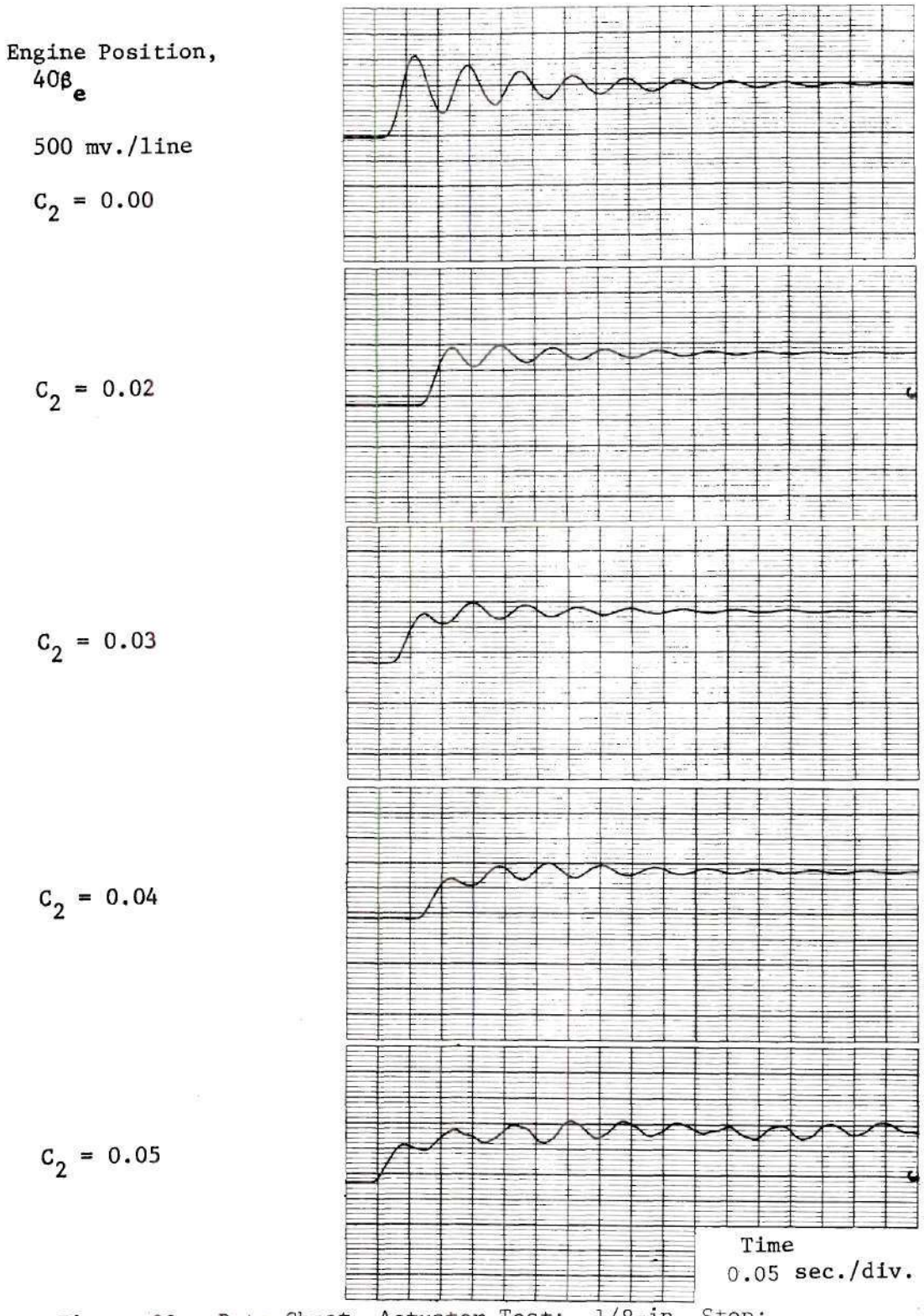

Figure 83. Data Sheet, Actuator Test: 1/8-in. Step; Rate Coefficient, C_2, Variable; DB = 0.031 in.

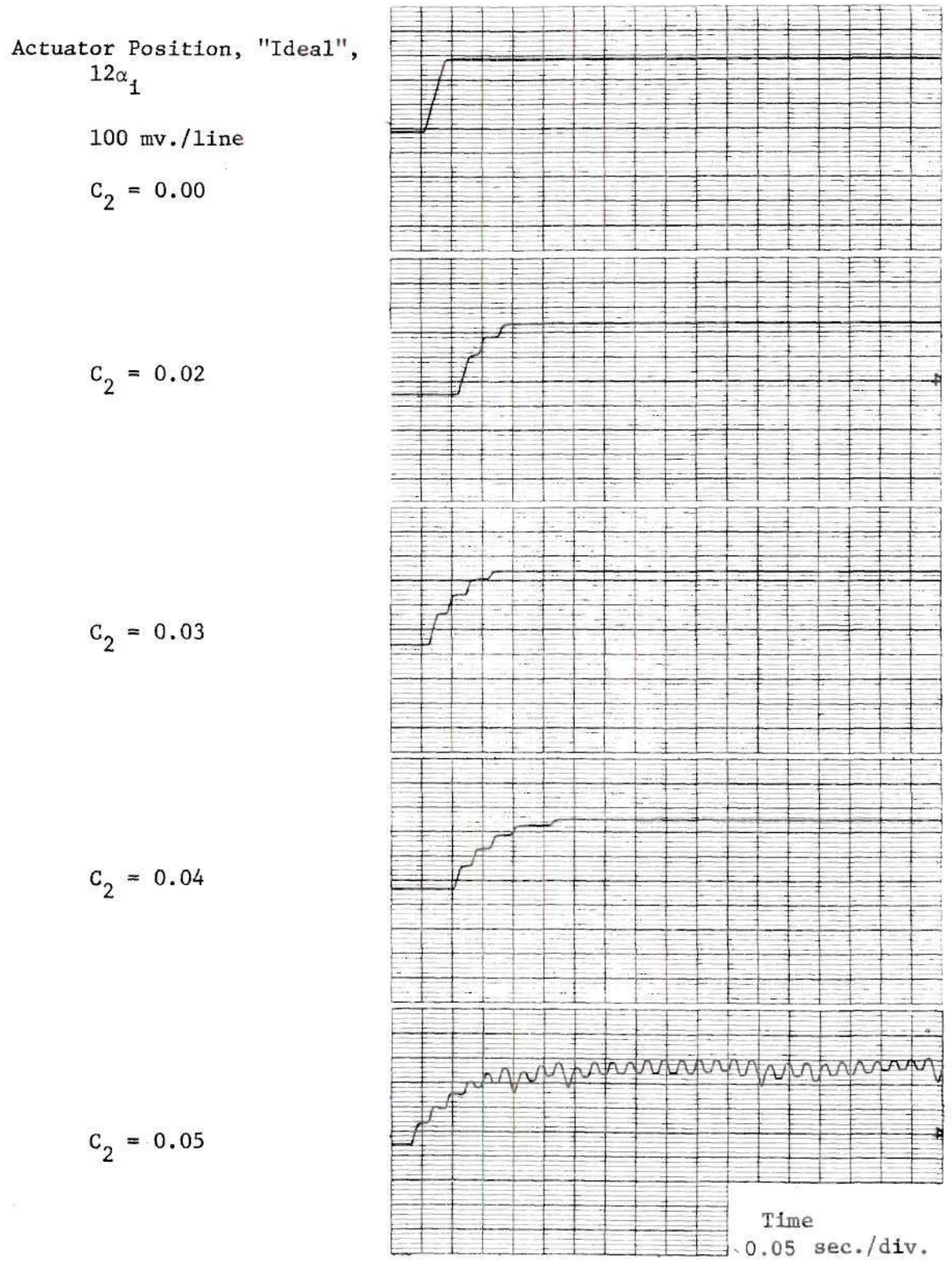

Figure 84. Data Sheet, Actuator Test: 1/8-in. Step; Rate Coefficient, C_2, Variable; DB = 0.031 in.

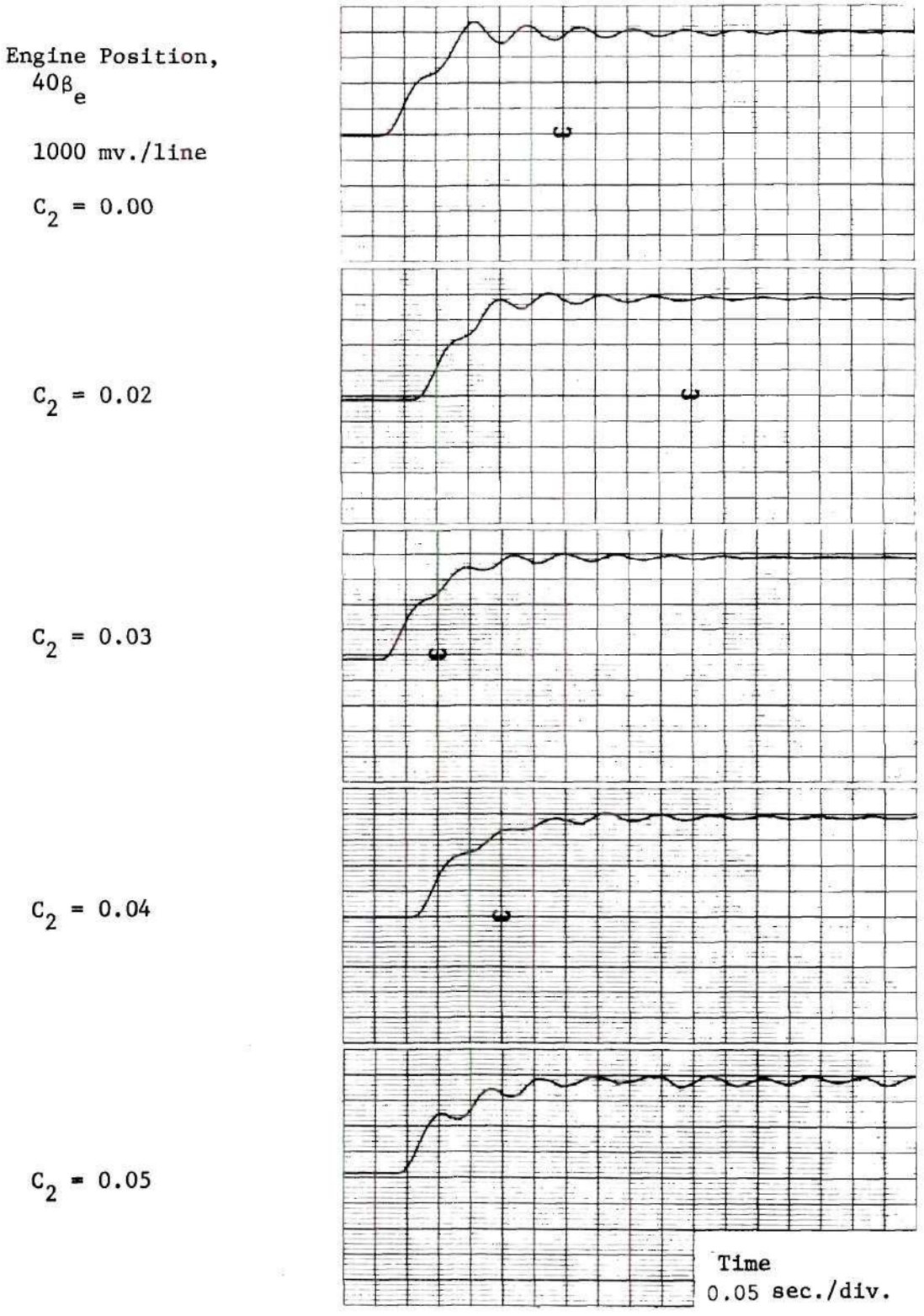

Figure 85. Data Sheet, Actuator Test: 1/2-in. Step; Rate Coefficient, C_2, Variable; DB = 0.031 in.

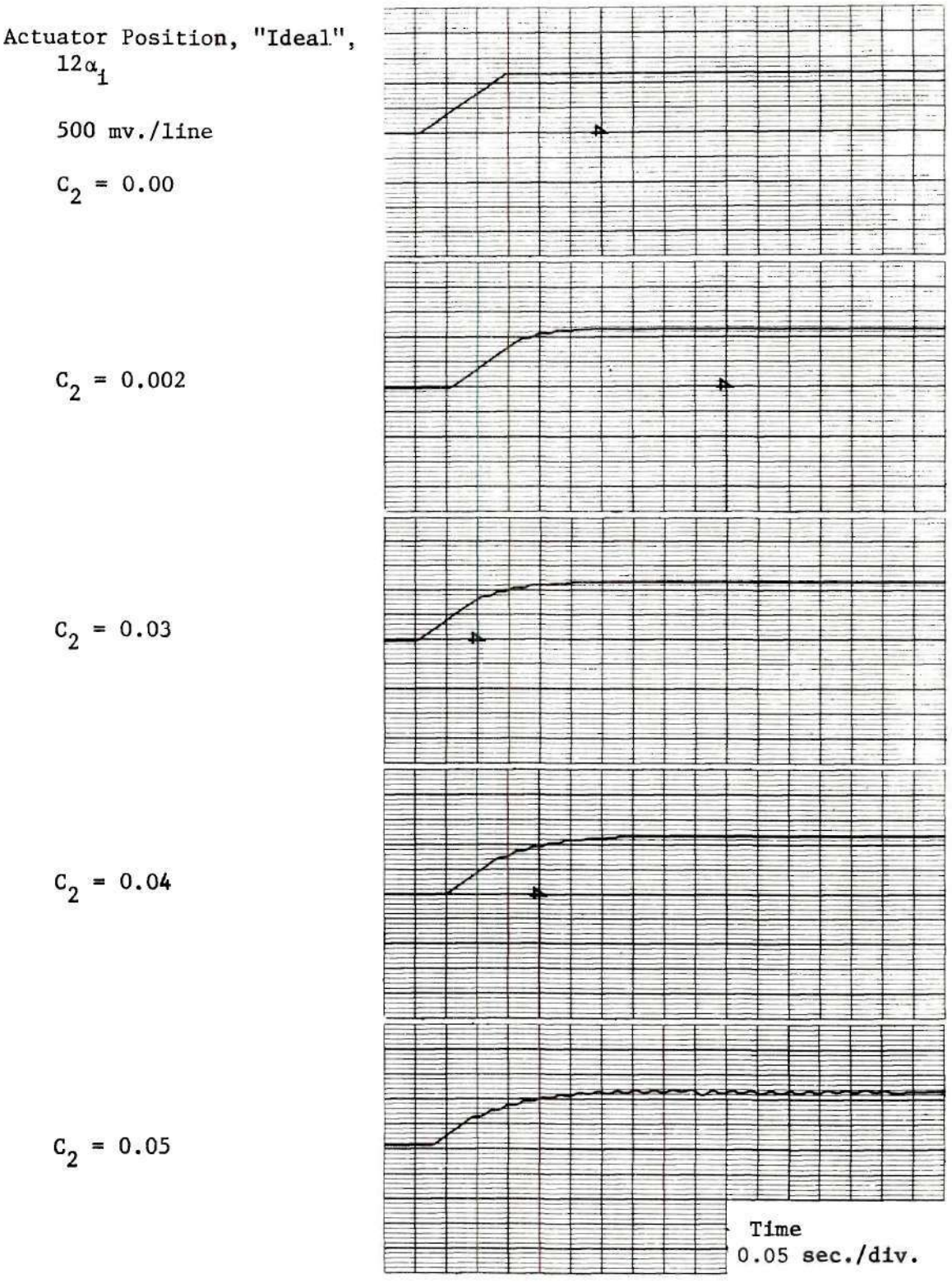

Figure 86. Data Sheet, Actuator Test: 1/2-in. Step; Rate Coefficient, C_2, Variable; DB = 0.031 in.

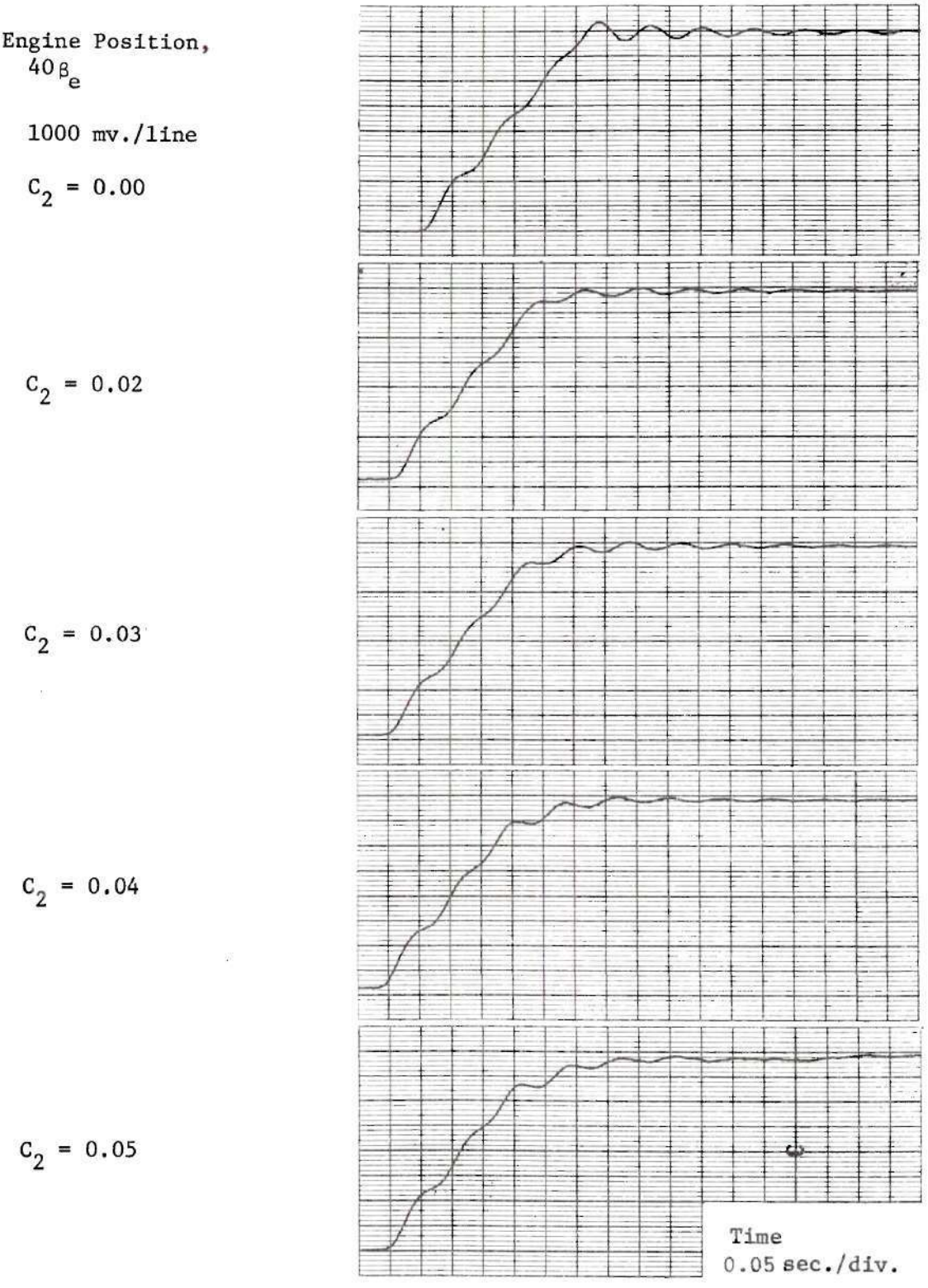

Figure 87. Data Sheet, Actuator Test: 1-in. Step; Rate Coefficient, C_2, Variable; DB = 0.031 in.

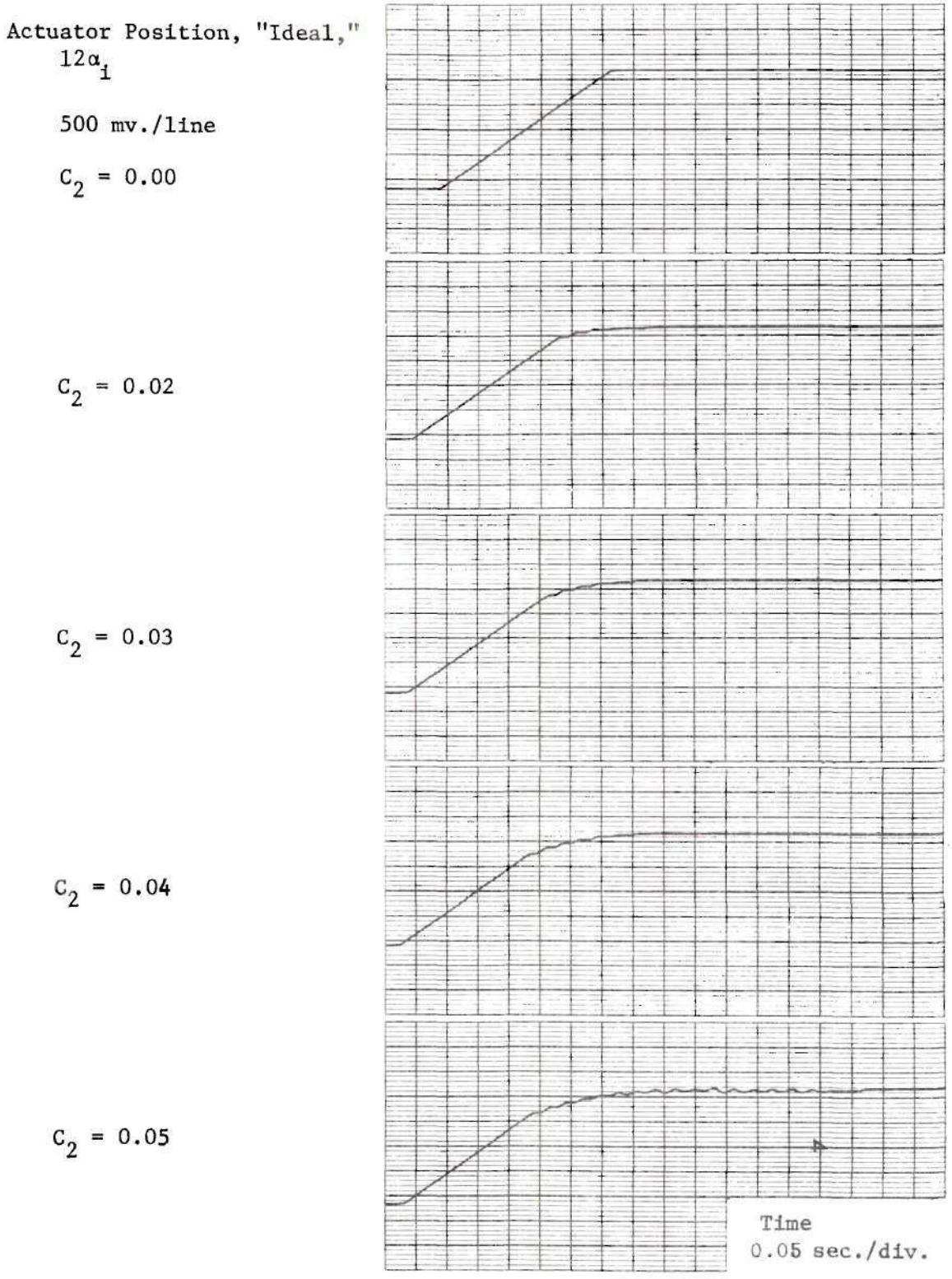

Figure 88. Data Sheet, Actuator Test: 1-in. Step; Rate Coefficient, C_2, Variable; DB = 0.031 in.

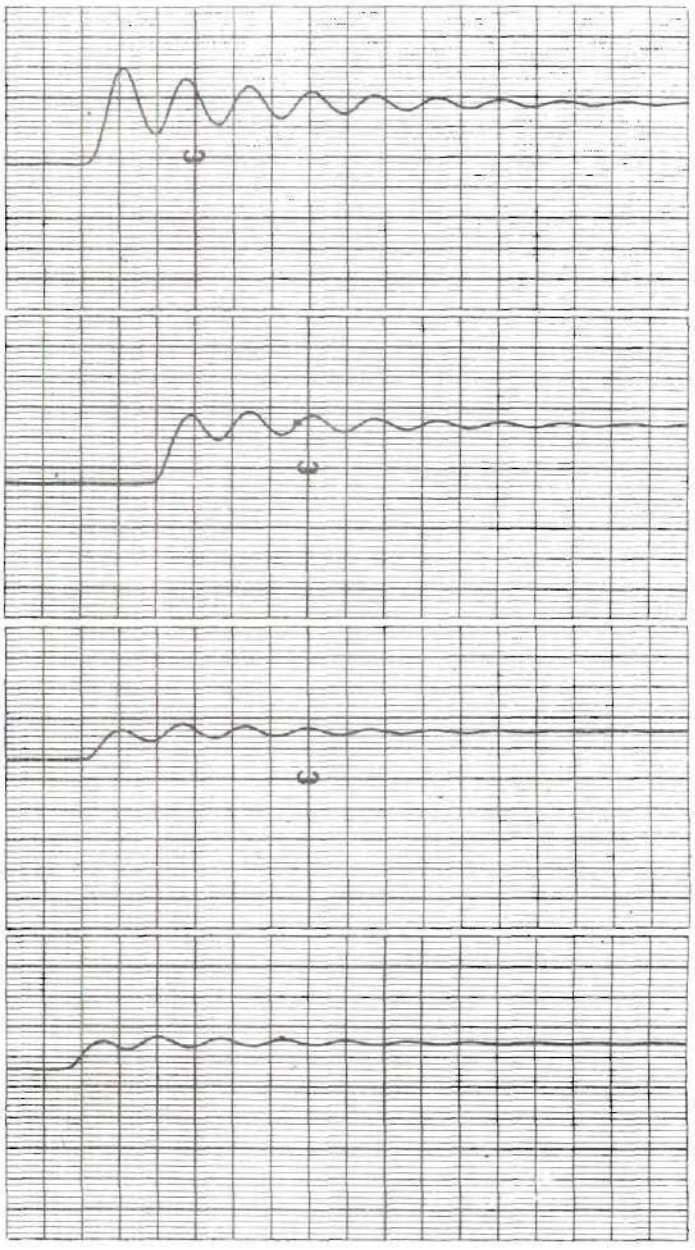

Figure 89. Data Sheet, Actuator Test: 1/8-in. Step; Rate Coefficient, C_2, Variable; DB = 0.042 in.

Engine Position,
$40\beta_e$

500 mv./line

$C_2 = 0.05$

$C_2 = 0.06$

$C_2 = 0.07$

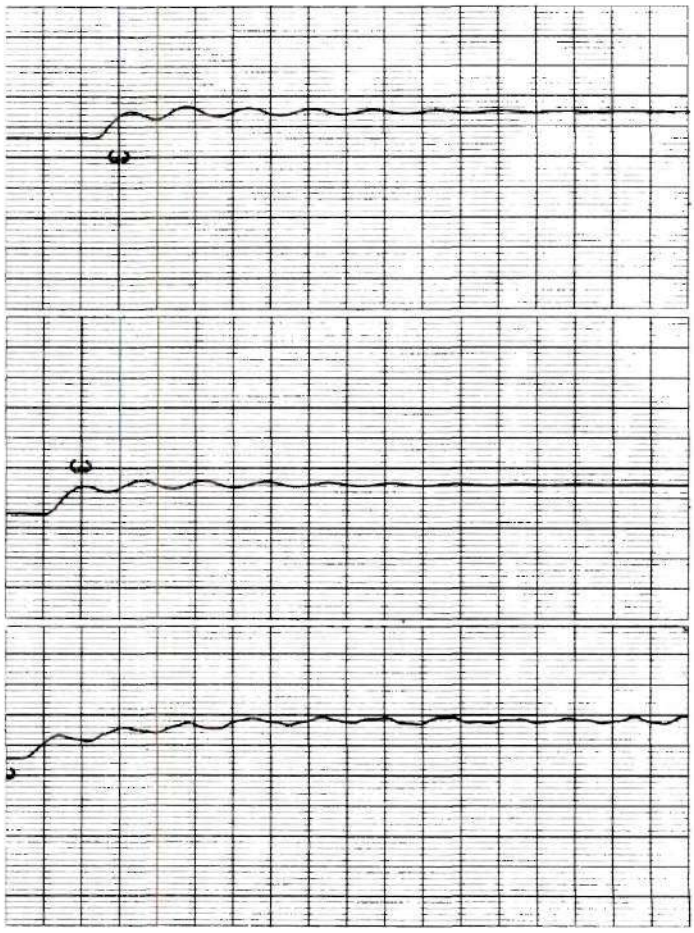

Time
0.05 sec./div.

Figure 89. Continued

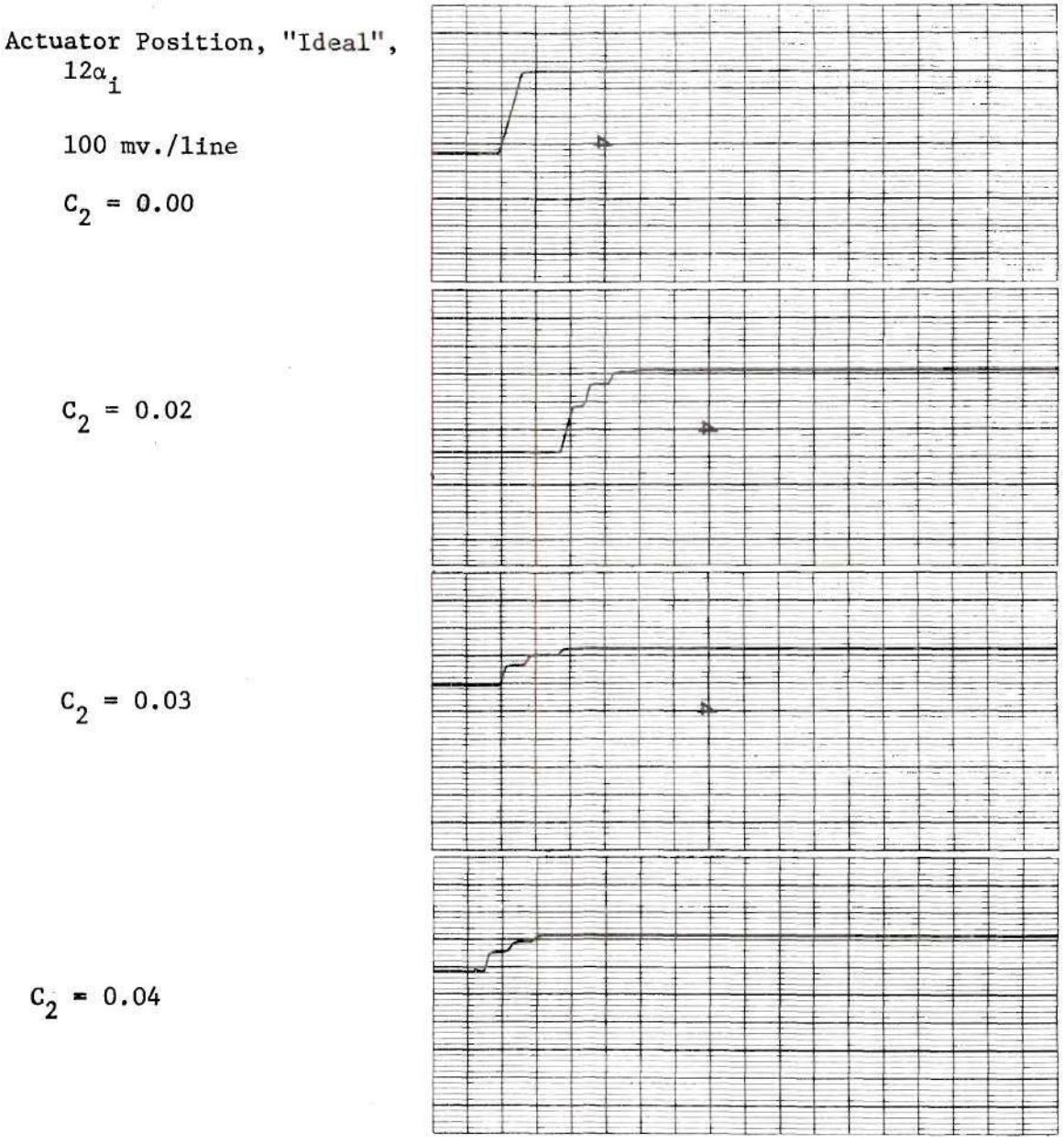

Figure 90. Data Sheet, Actuator Test: 1/8-in. Step; Rate Coefficient, C_2, Variable; DB = 0.042 in.

Actuator Position, "Ideal", $12\alpha_i$

100 mv./line

$C_2 = 0.05$

$C_2 = 0.06$

$C_2 = 0.07$

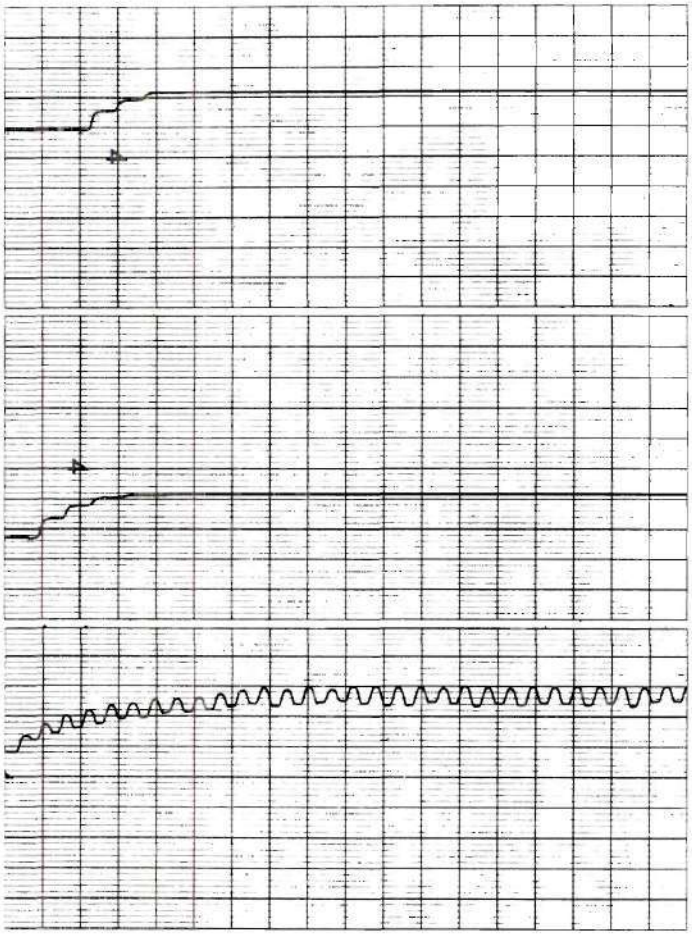

Time
0.05 sec./div.

Figure 90. Continued

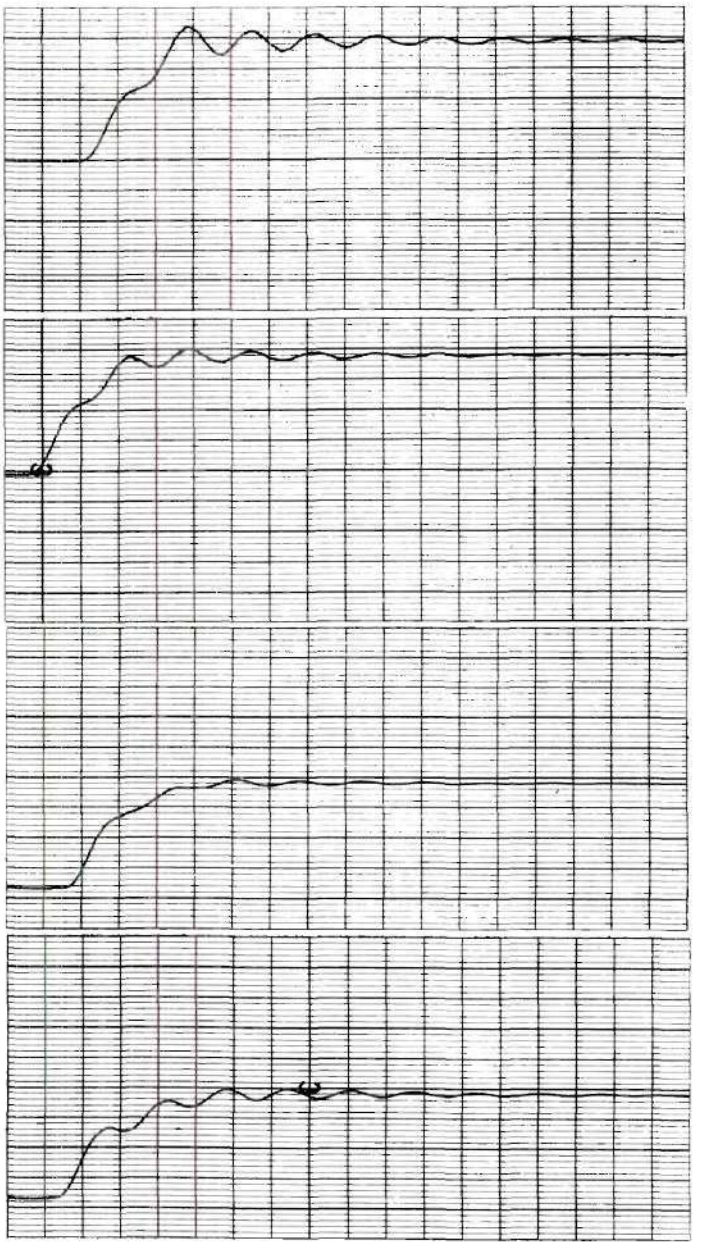

Figure 91. Data Sheet, Actuator Test: 1/2-in. Step; Rate Coefficient, C_2, Variable; DB = 0.042 in.

Engine Position,
$40\beta_e$

1000 mv./line

$C_2 = 0.05$

$C_2 = 0.06$

$C_2 = 0.07$

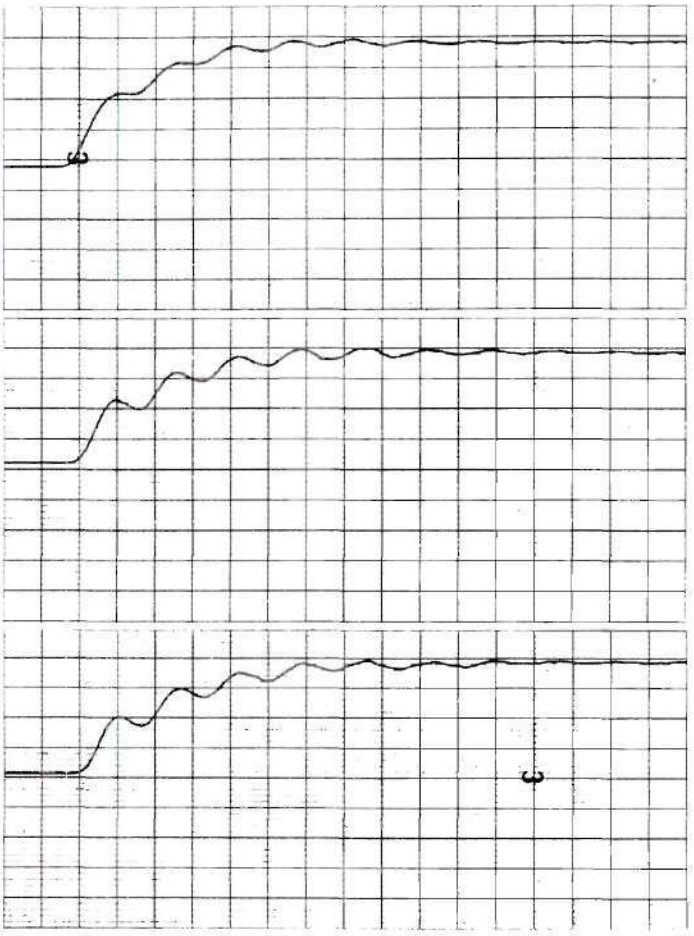

Time
0.05 sec./div.

Figure 91. Continued

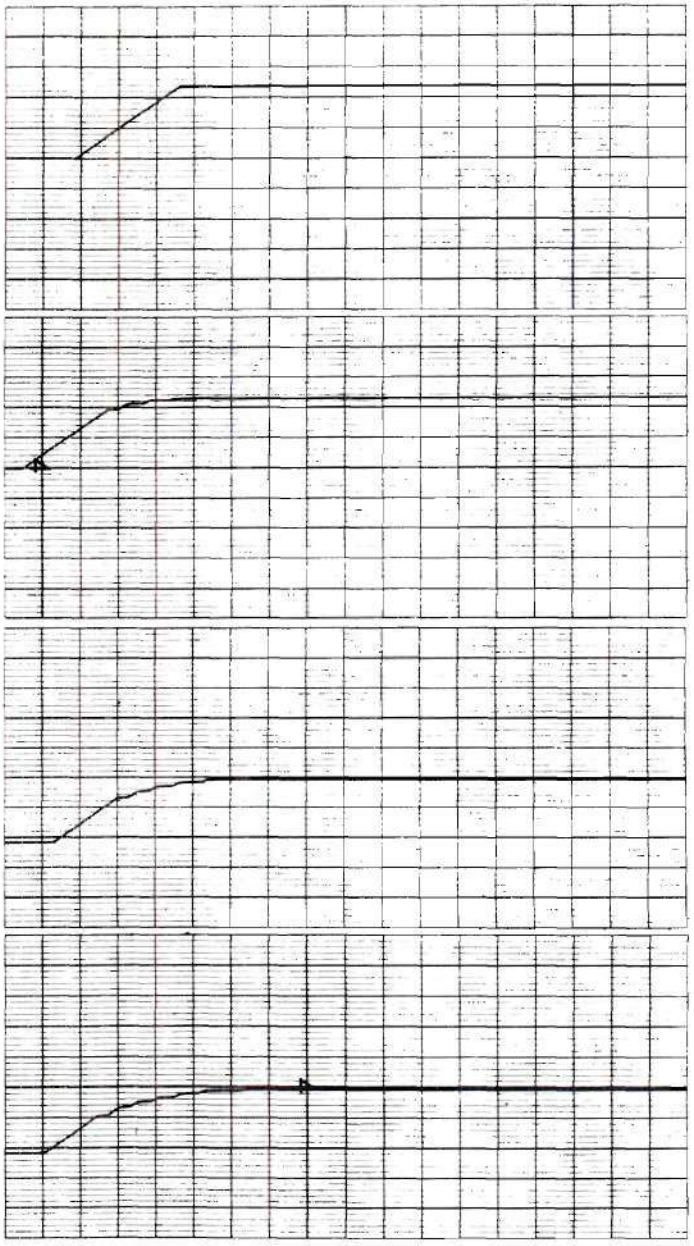

Figure 92. Data Sheet, Actuator Test: 1/2-in. Step; Rate Coefficient, C_2, Variable; DB = 0.042 in.

Actuator Position, "Ideal",

$12\alpha_i$

500 mv./line

$C_2 = 0.05$

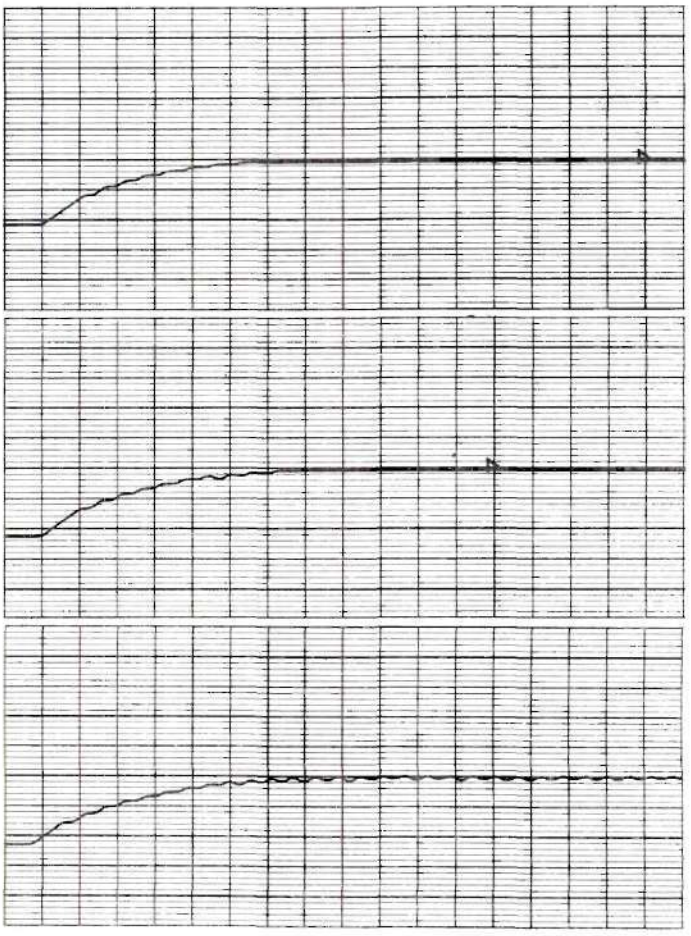

$C_2 = 0.06$

$C_2 = 0.07$

Time

0.05 sec./div.

Figure 92. Continued

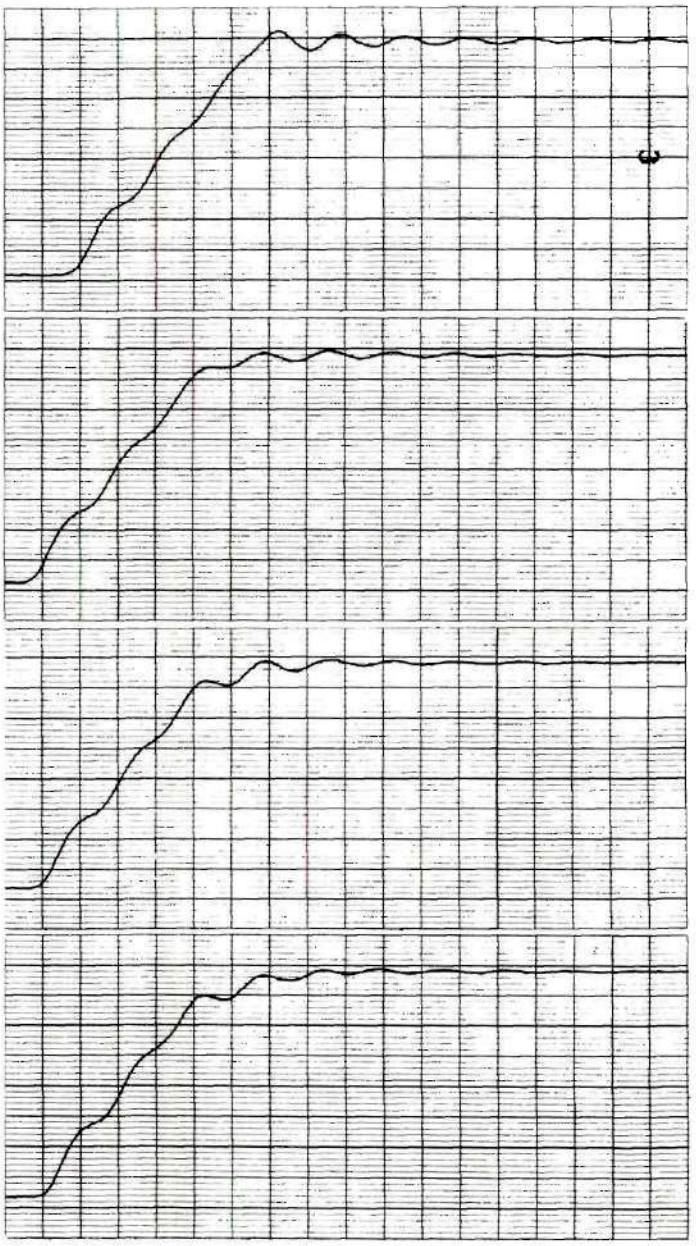

Figure 93. Data Sheet, Actuator Test: 1-in. Step; Rate Coefficient, C_2, Variable; DB = 0.042 in.

Engine Position,
$40\beta_e$

1000 mv./line

$C_2 = 0.05$

$C_2 = 0.06$

$C_2 = 0.07$

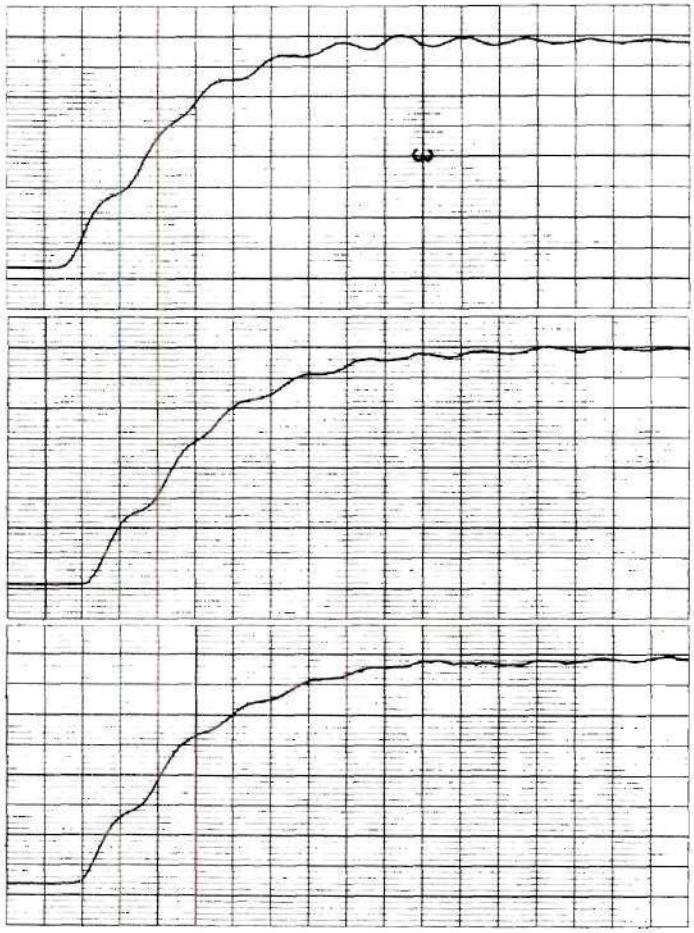

Time
0.05 sec./div.

Figure 93. Continued

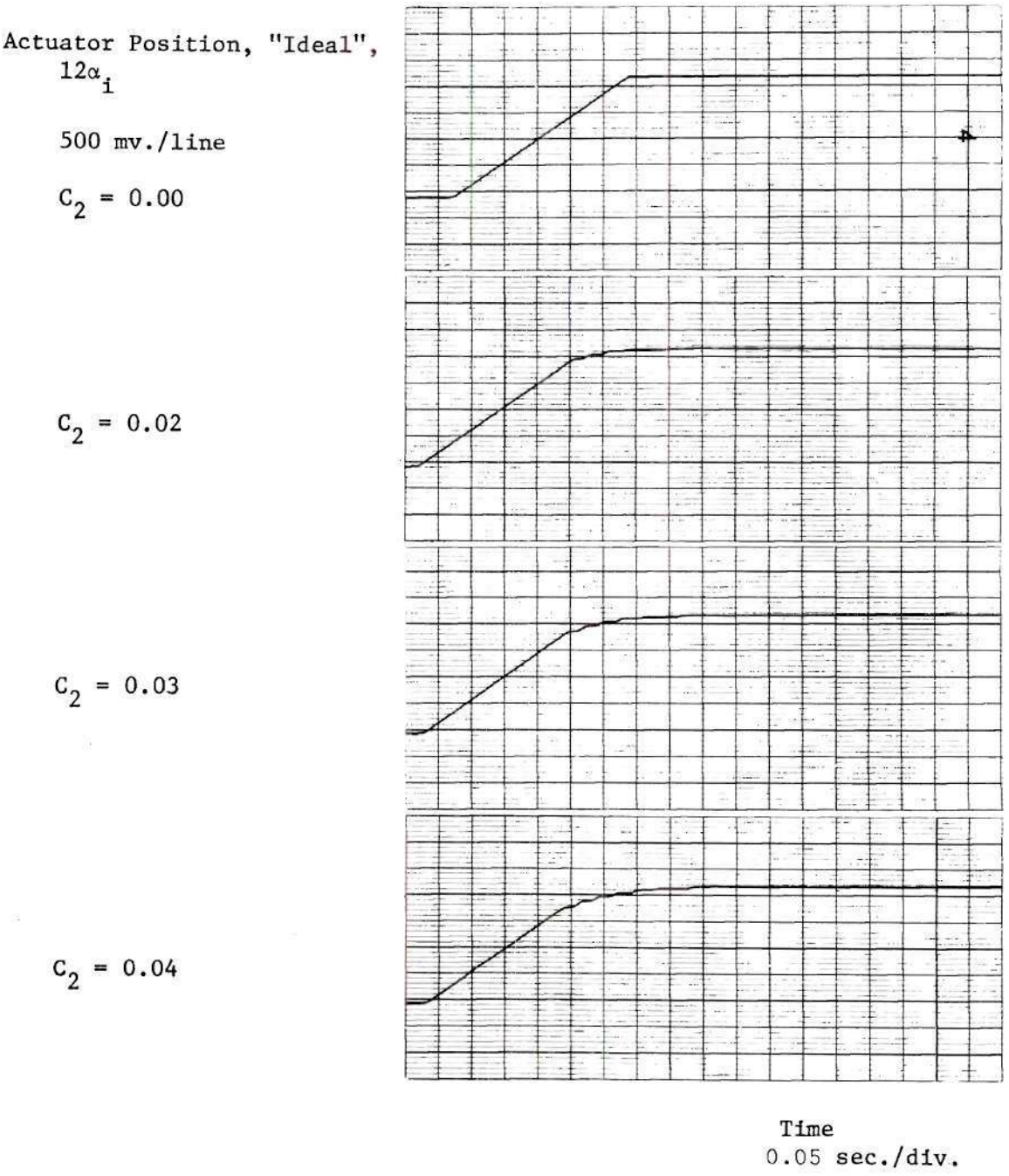

Figure 94. Data Sheet, Actuator Test: 1-in. Step; Rate Coefficient, C_2, Variable; DB = 0.042 in.

Actuator Position, "Ideal", $12\alpha_i$

500 mv./line

$C_2 = 0.05$

$C_2 = 0.06$

$C_2 = 0.07$

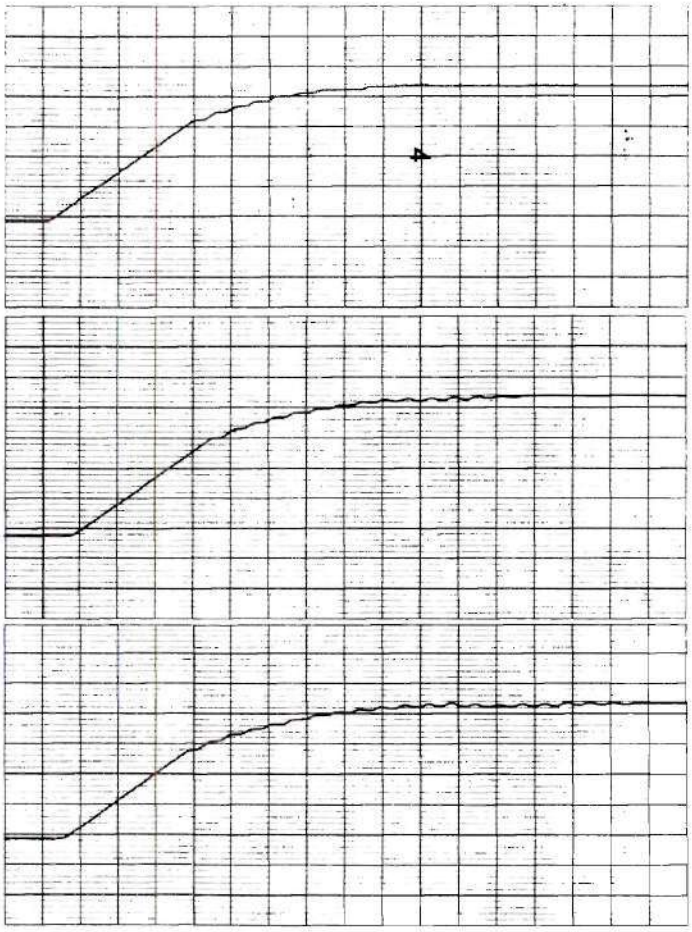

Time
0.05 sec./div.

Figure 94. Continued

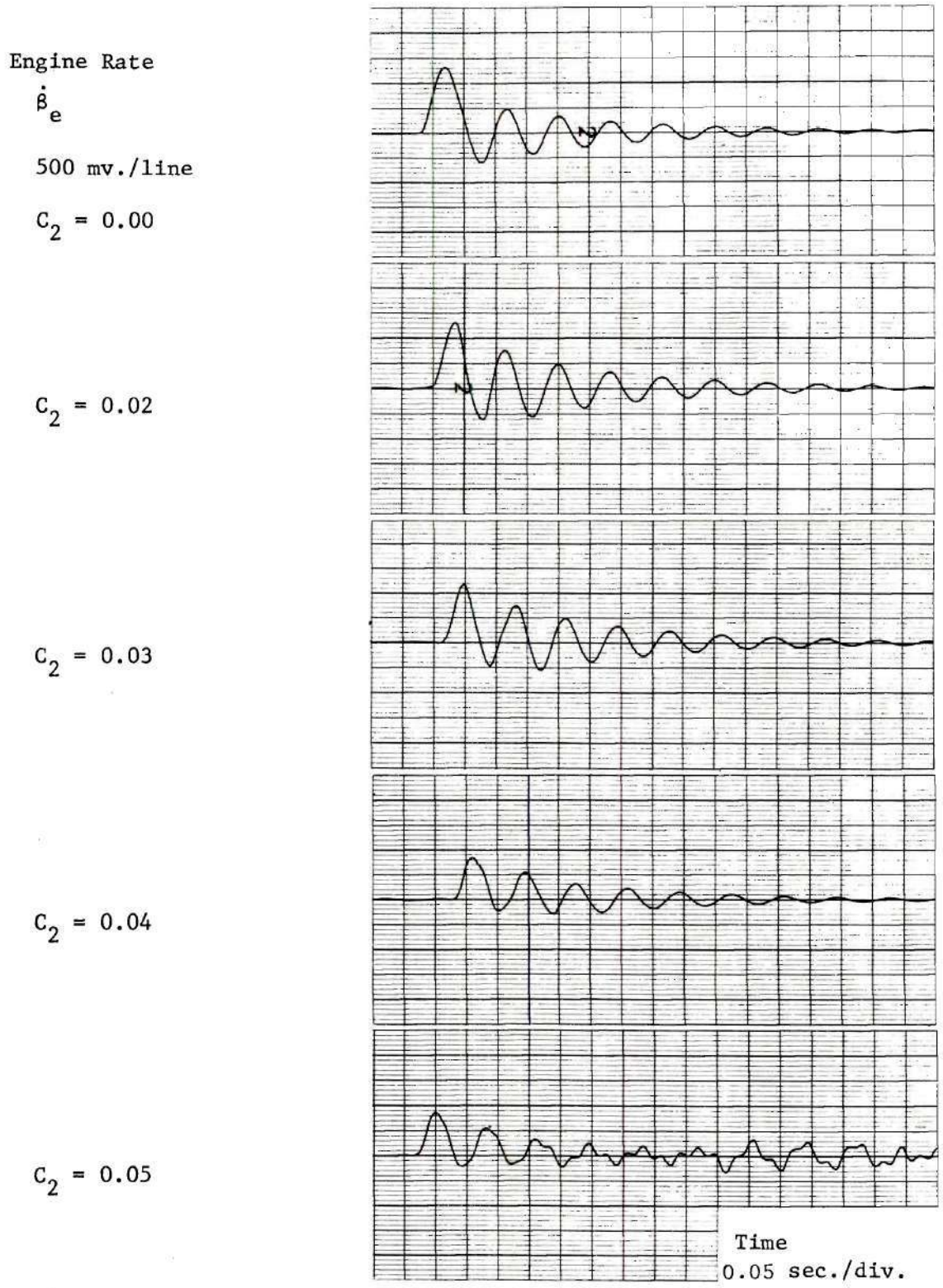

Figure 95. Data Sheet, Actuator Test: 1/4-in. Step; Rate Coefficient, C_2, Variable; DB = 0.031 in.

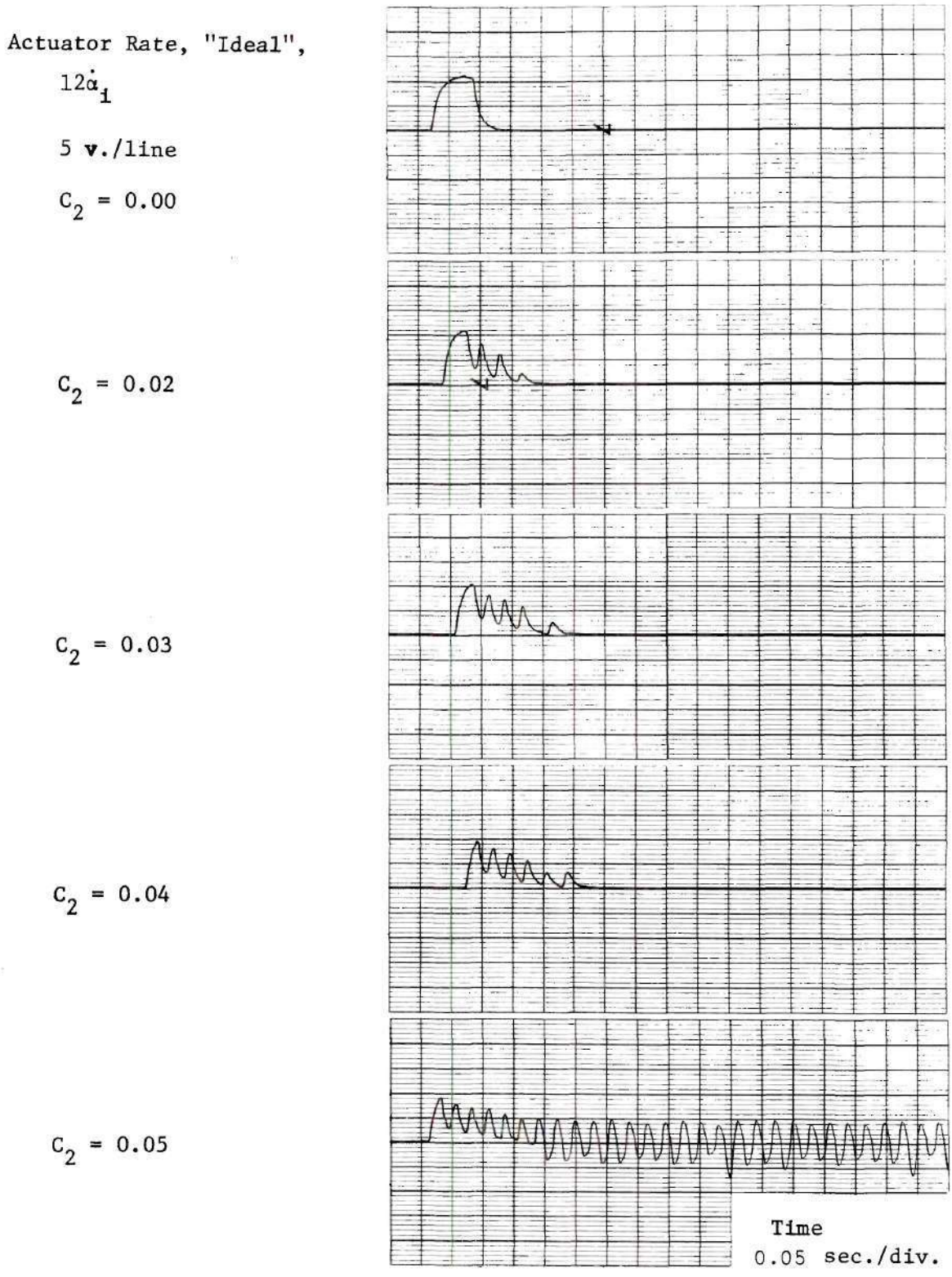

Figure 96. Data Sheet, Actuator Test; 1/4-in. Step; Rate Coefficient, C_2, Variable; DB = 0.031 in.

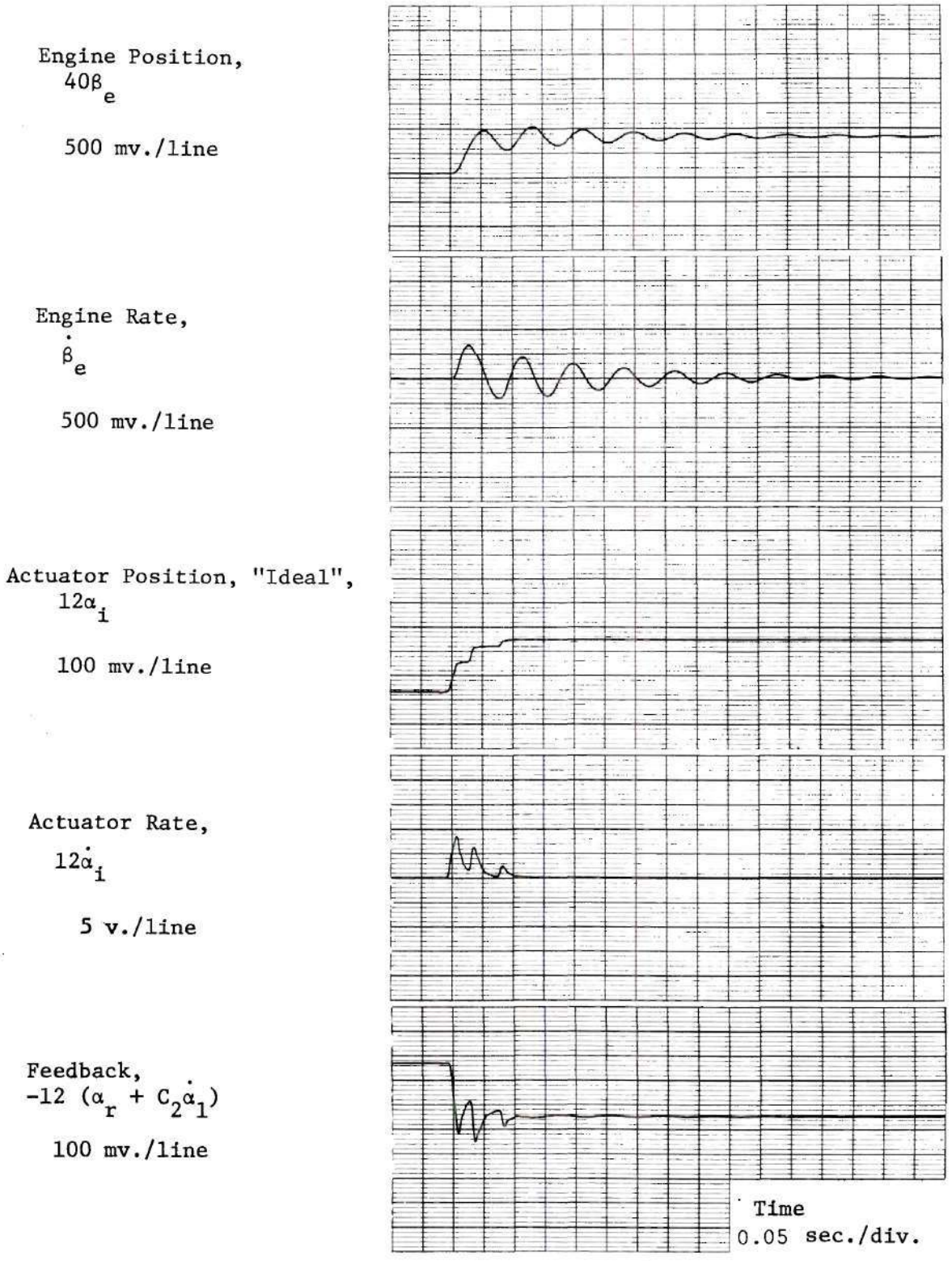

Figure 97. Data Sheet, Actuator Test: 1/8-in. Step. Rate Coefficient, C_2 = 0.02; DB = 0.031 in.

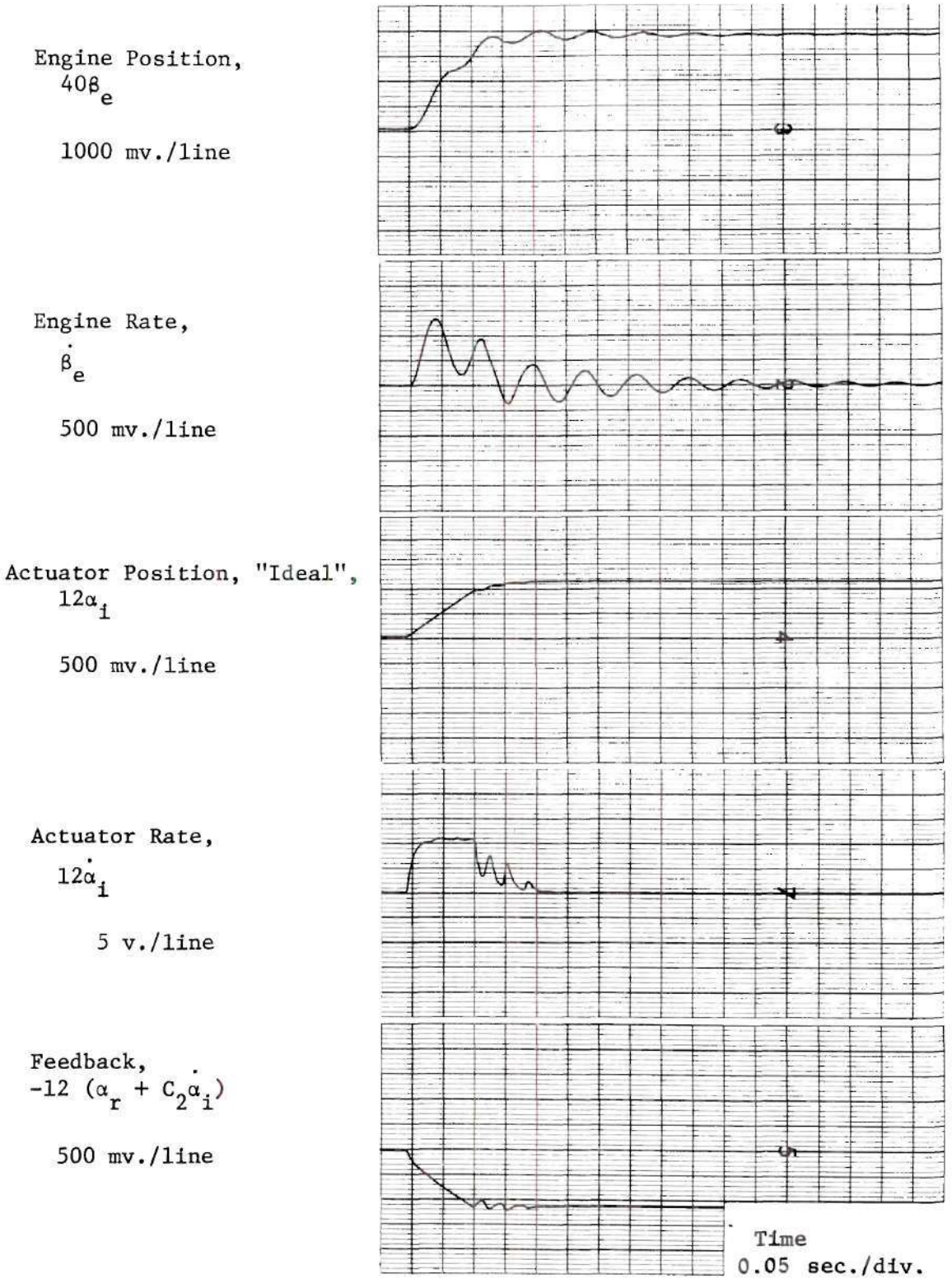

Figure 98. Data Sheet, Actuator Test: 1/2-in. Step; Rate Coefficient, C_2 = 0.02; DB = 0.031 in.

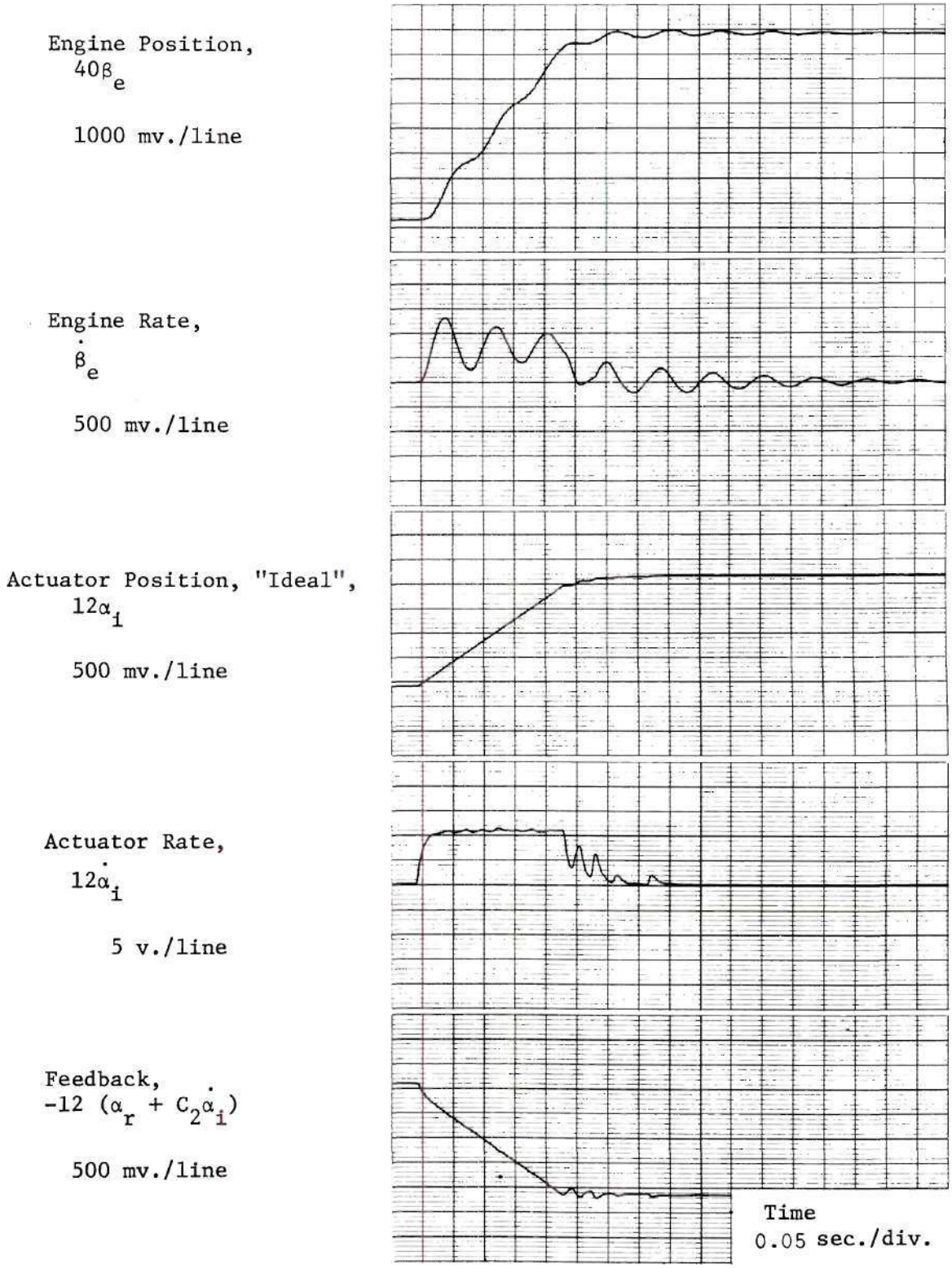

Figure 99. Data Sheet, Actuator Test: 1-in. Step; Rate Coefficient, C_2 = 0.02; DB = 0.031 in.

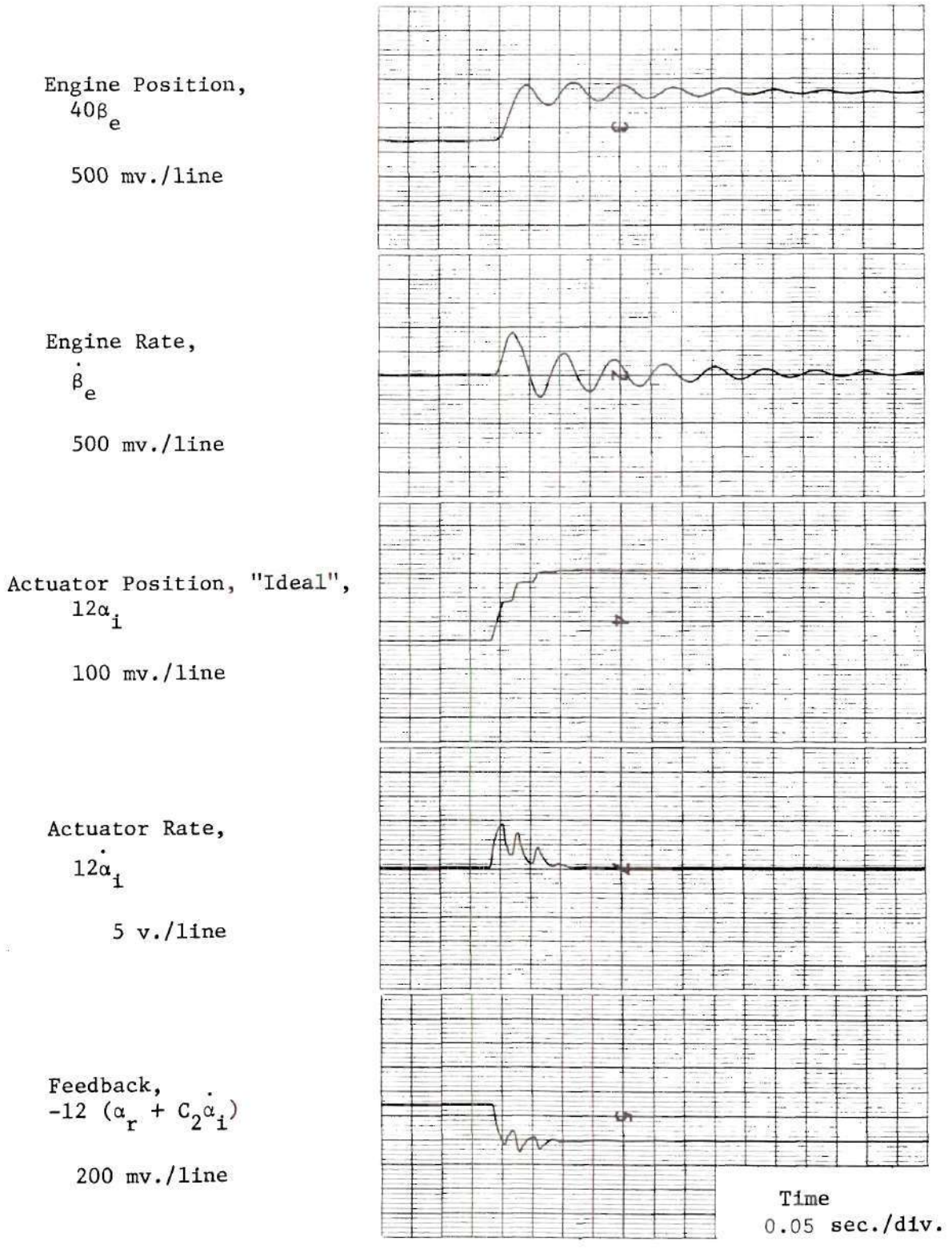

Figure 100. Data Sheet, Actuator Test: 1/8-in. Step; Rate Coefficient, C_2 = 0.02; DB = 0.042 in.

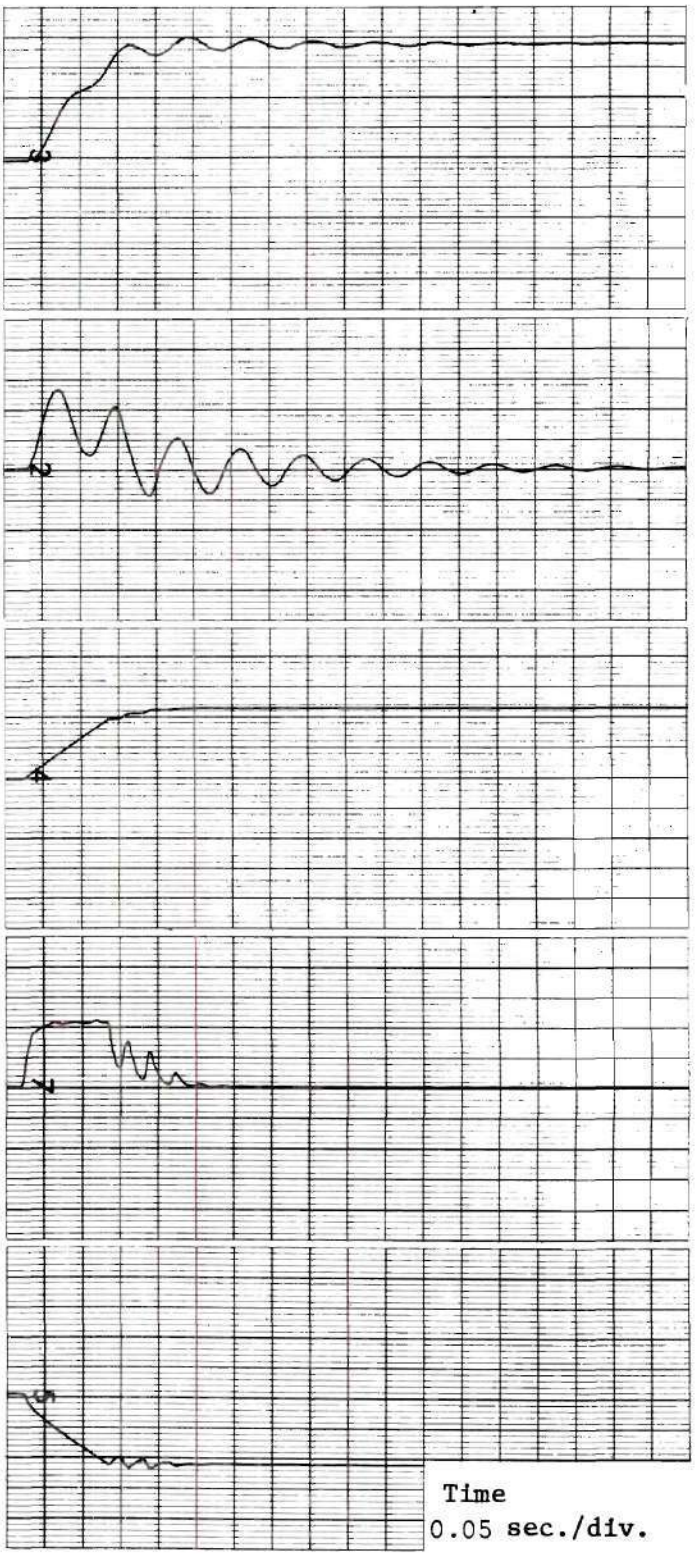

Figure 101. Data Sheet, Actuator Test: 1/2-in. Step; Rate Coefficient, C_2 = 0.02; DB = 0.042 in.

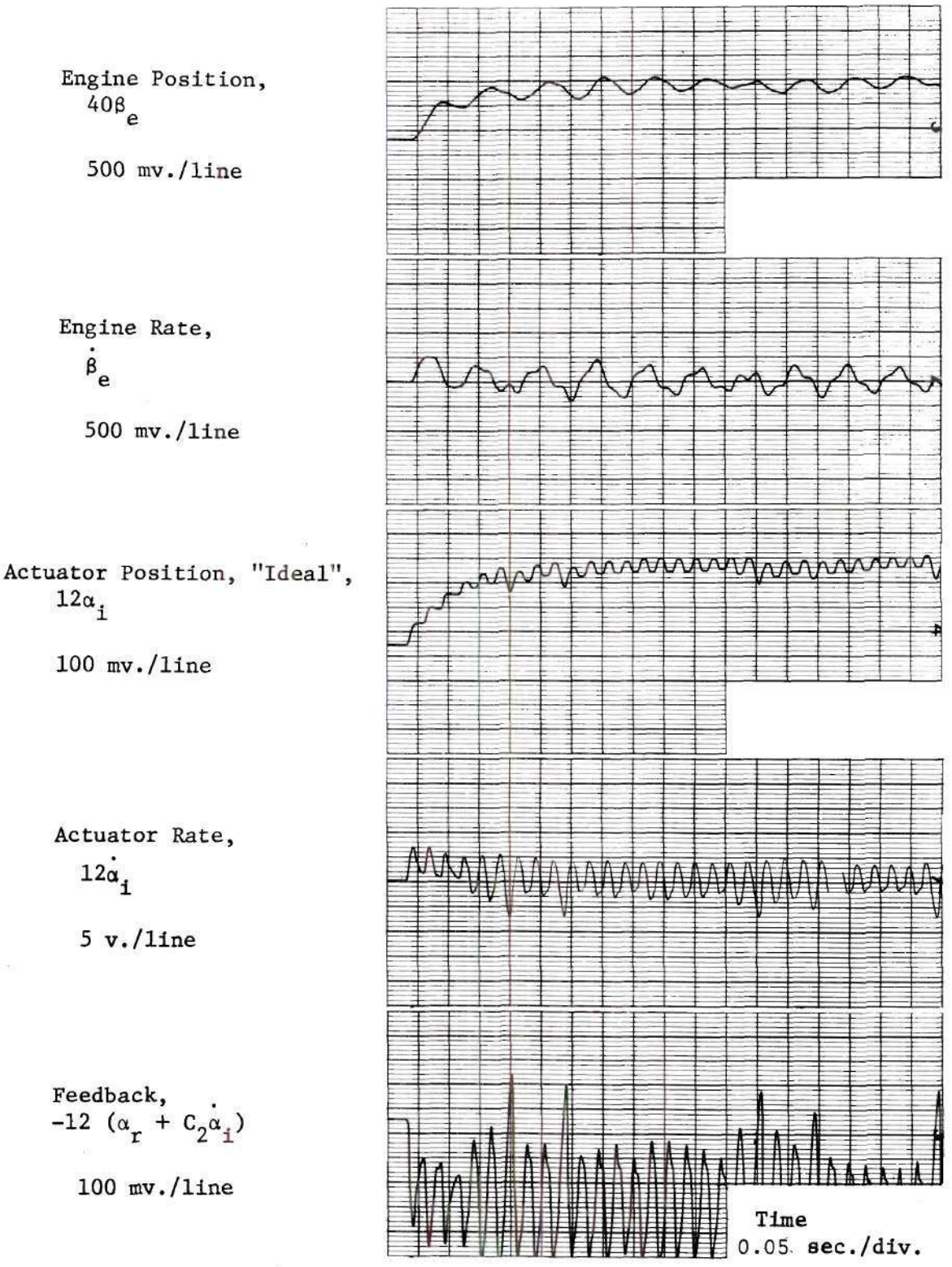

Figure 102. Data Sheet, Actuator Test: 1/8-in. Step; Rate Coefficient, C_2 = 0.05; DB = 0.031 in.

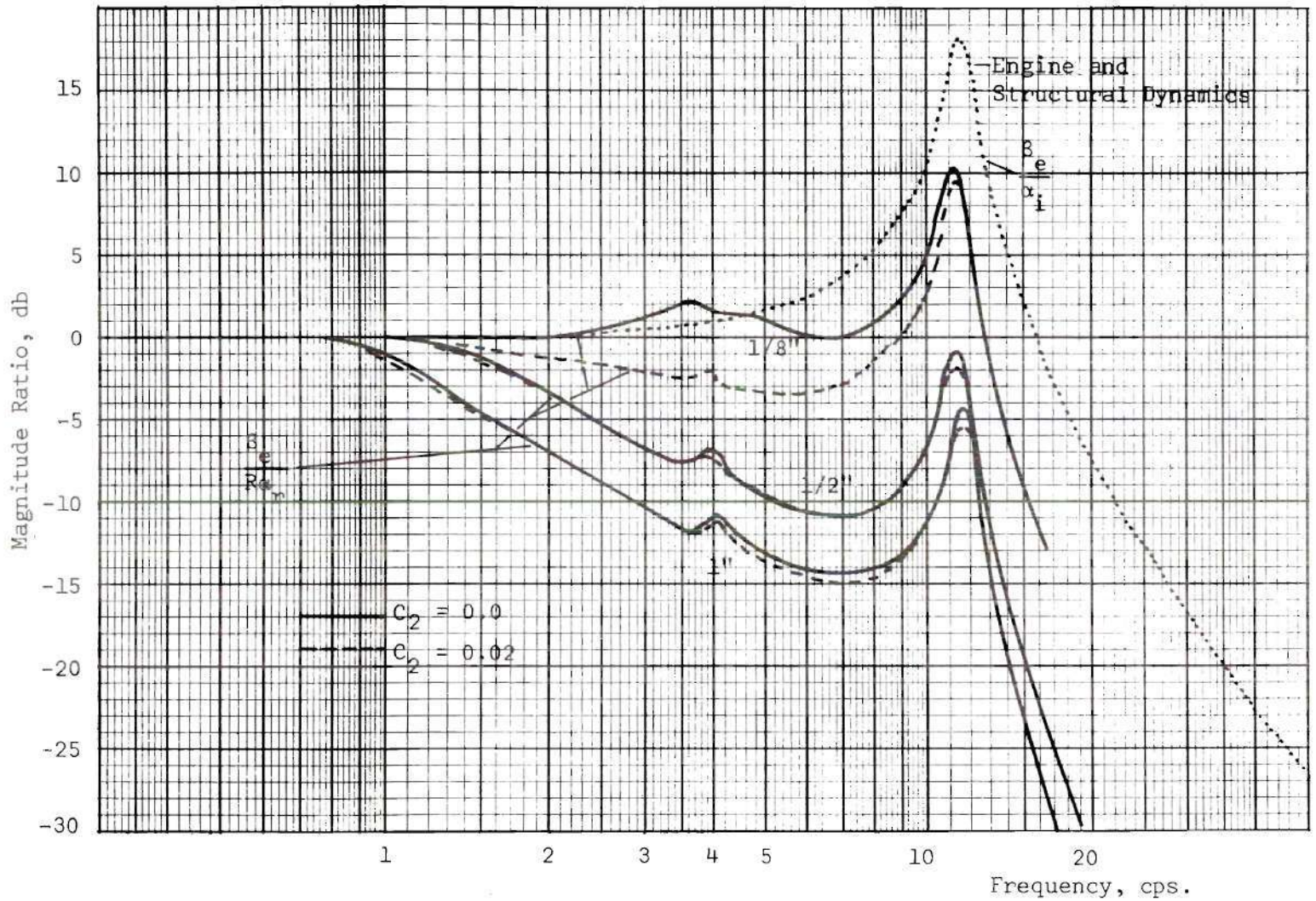

Figure 103. Magnitude versus Frequency Plot for Command Signals of Varying Amplitude

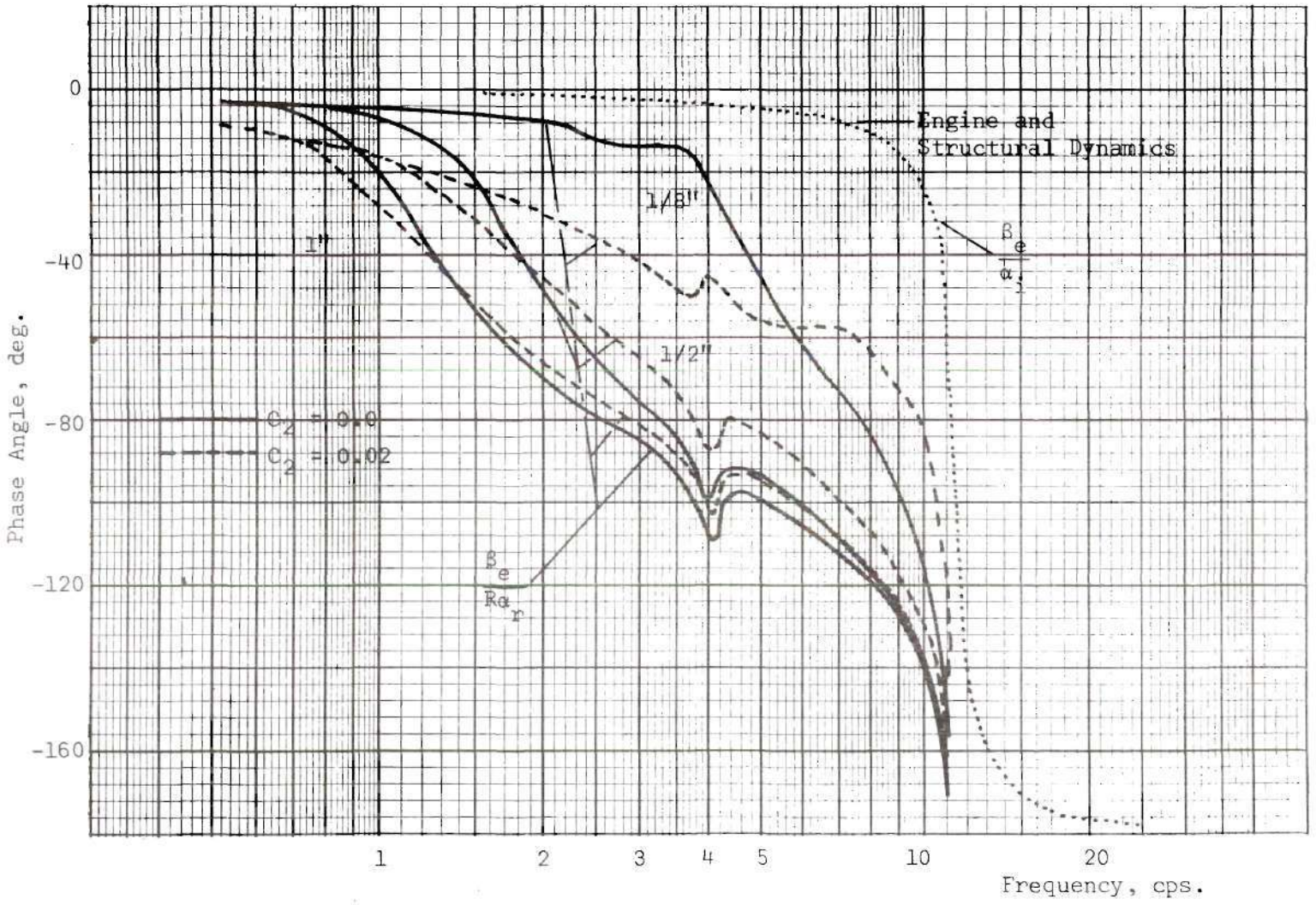

Figure 104. Phase Angle versus Frequency Plot for Command Signals of Varying Amplitude

Simulation Data

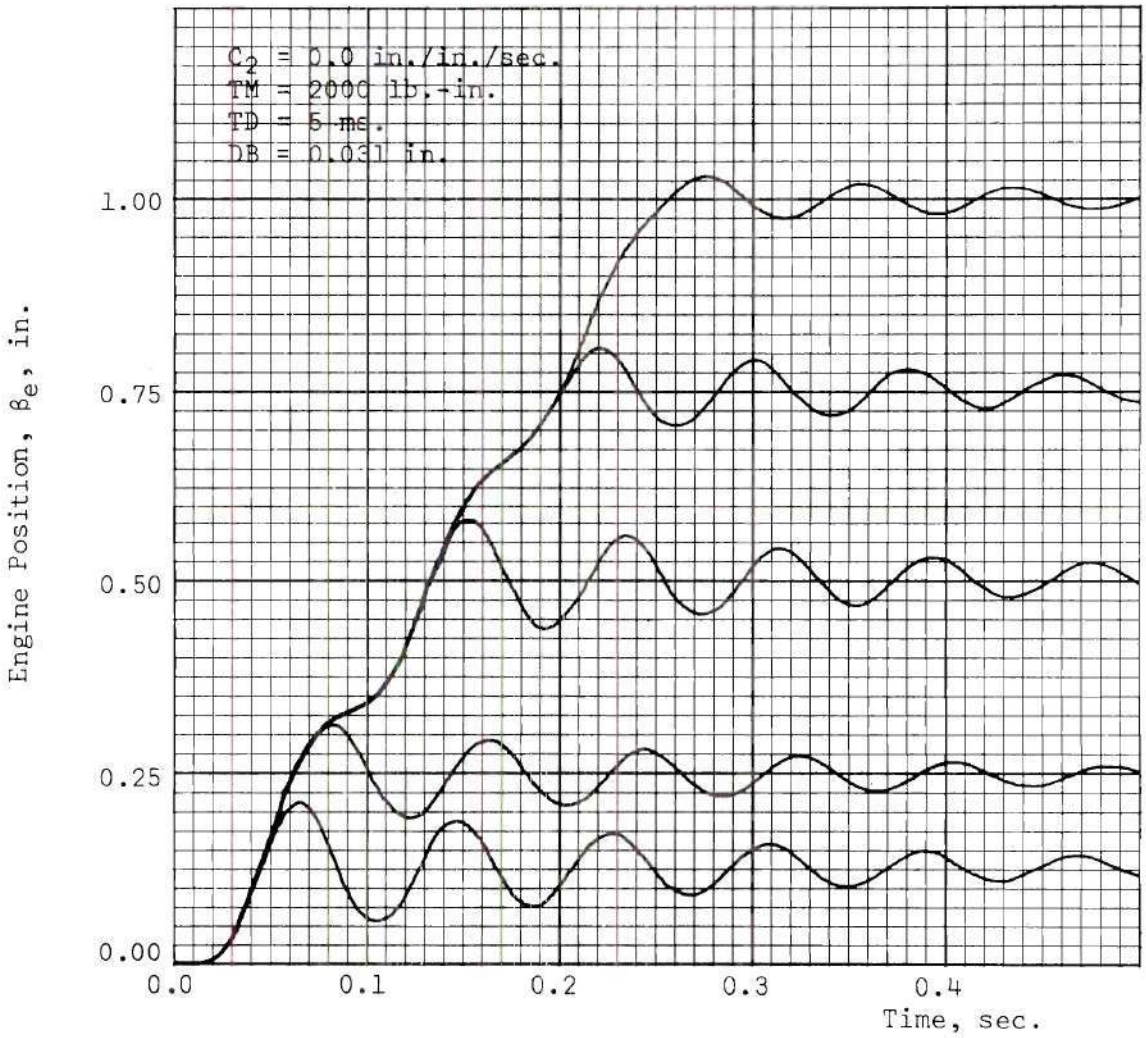

Figure 105. Engine Position Response to Several Step Commands. Wrap-Spring Clutch-Actuator Simulation. Actuation Rate = 4 in./sec.

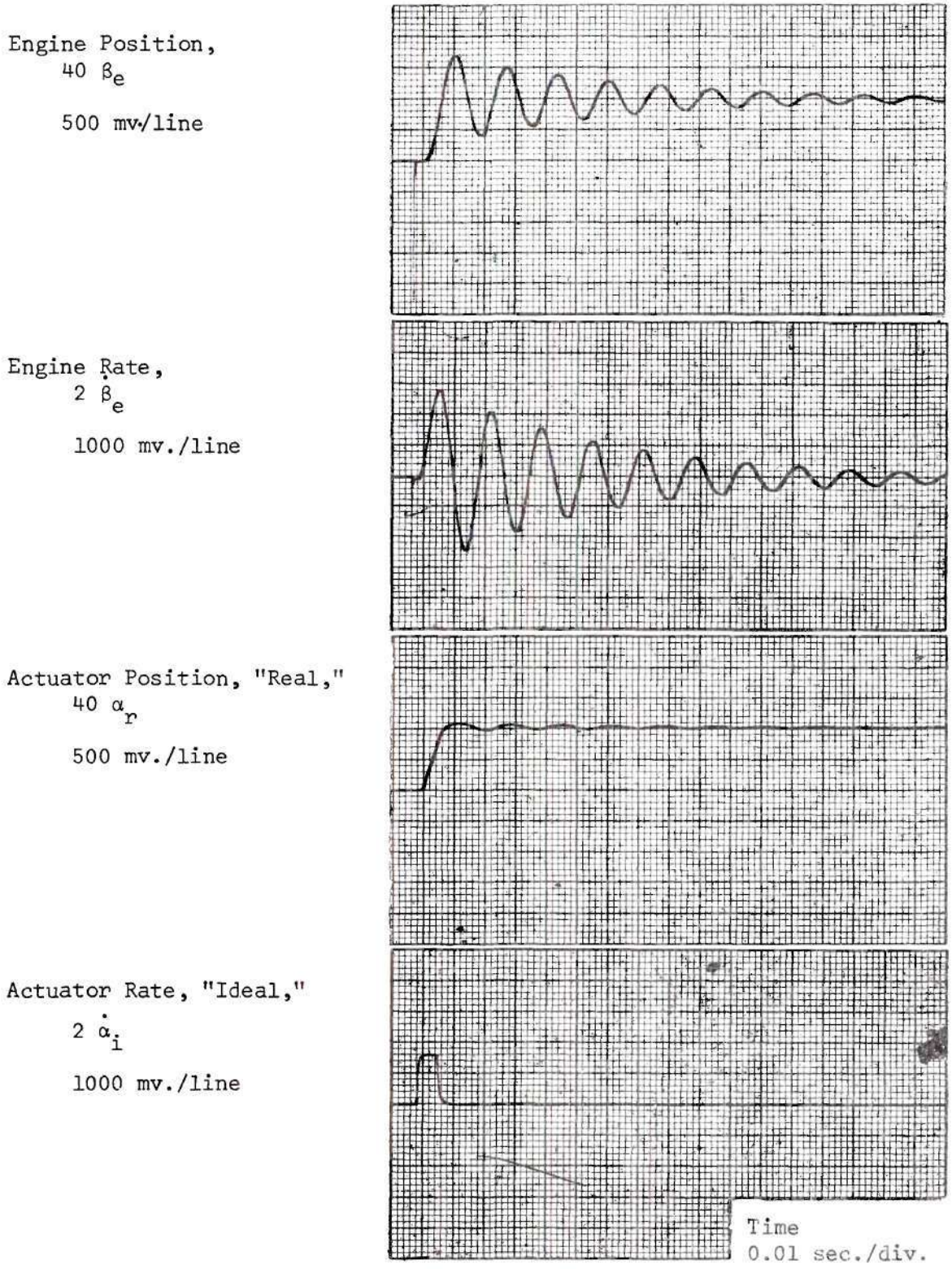

Figure 106. Data Sheet, Analog Simulation: 1/8-in. Step; Rate Coefficient, C_2 = 0.00; DB = 0.031 in.

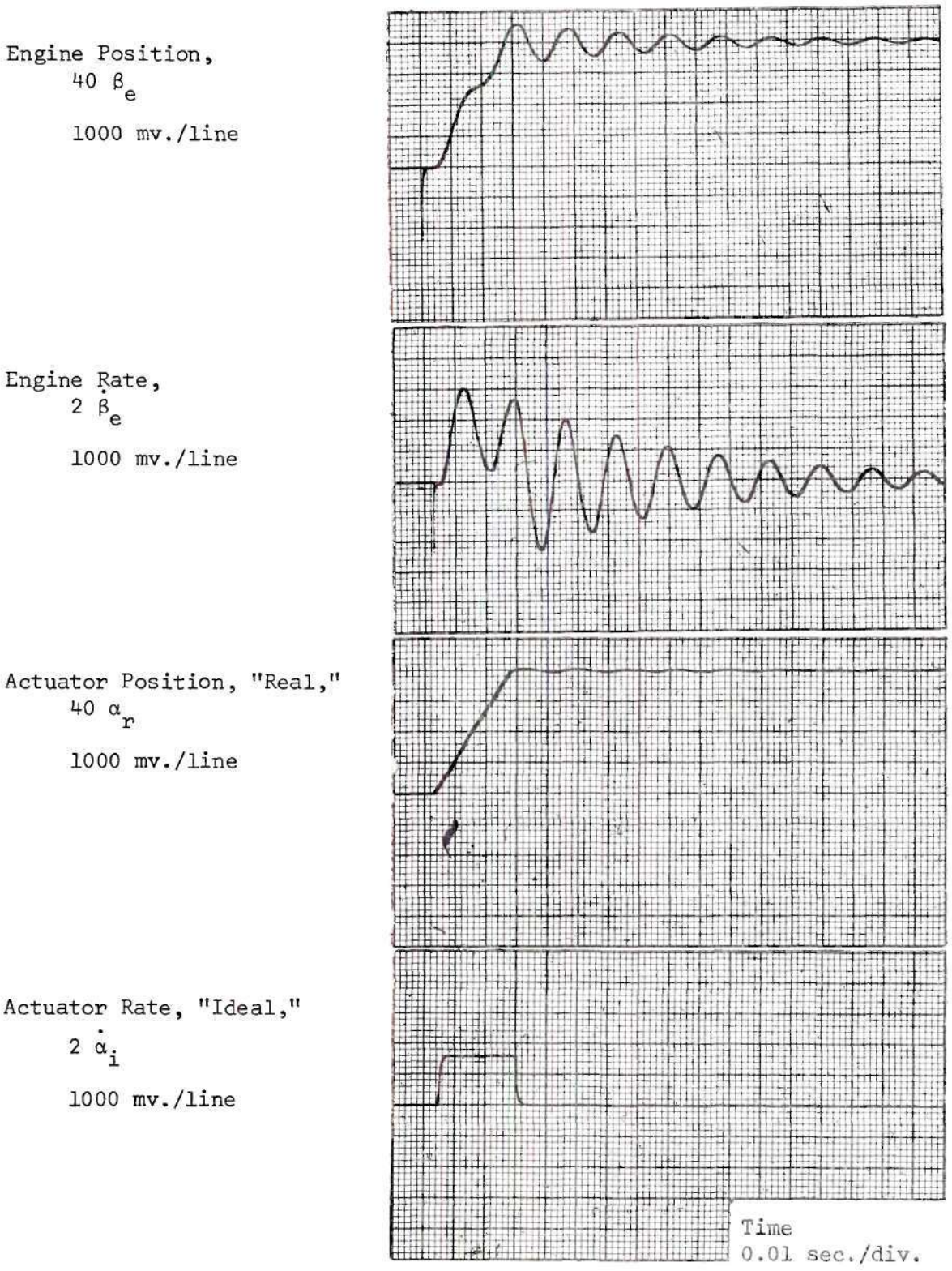

Figure 107. Data Sheet, Analog Simulation: 1/2-in. Step; Rate Coefficient, C_2 = 0.00; DB = 0.031 in.

Engine Position,
40 β_e
500 mv./line

Engine Rate,
2 $\dot{\beta}_e$
1000 mv./line

Actuator Position, "Real,"
40 α_r
500 mv./line

Actuator Rate, "Ideal,"
2 $\dot{\alpha}_i$
1000 mv./line

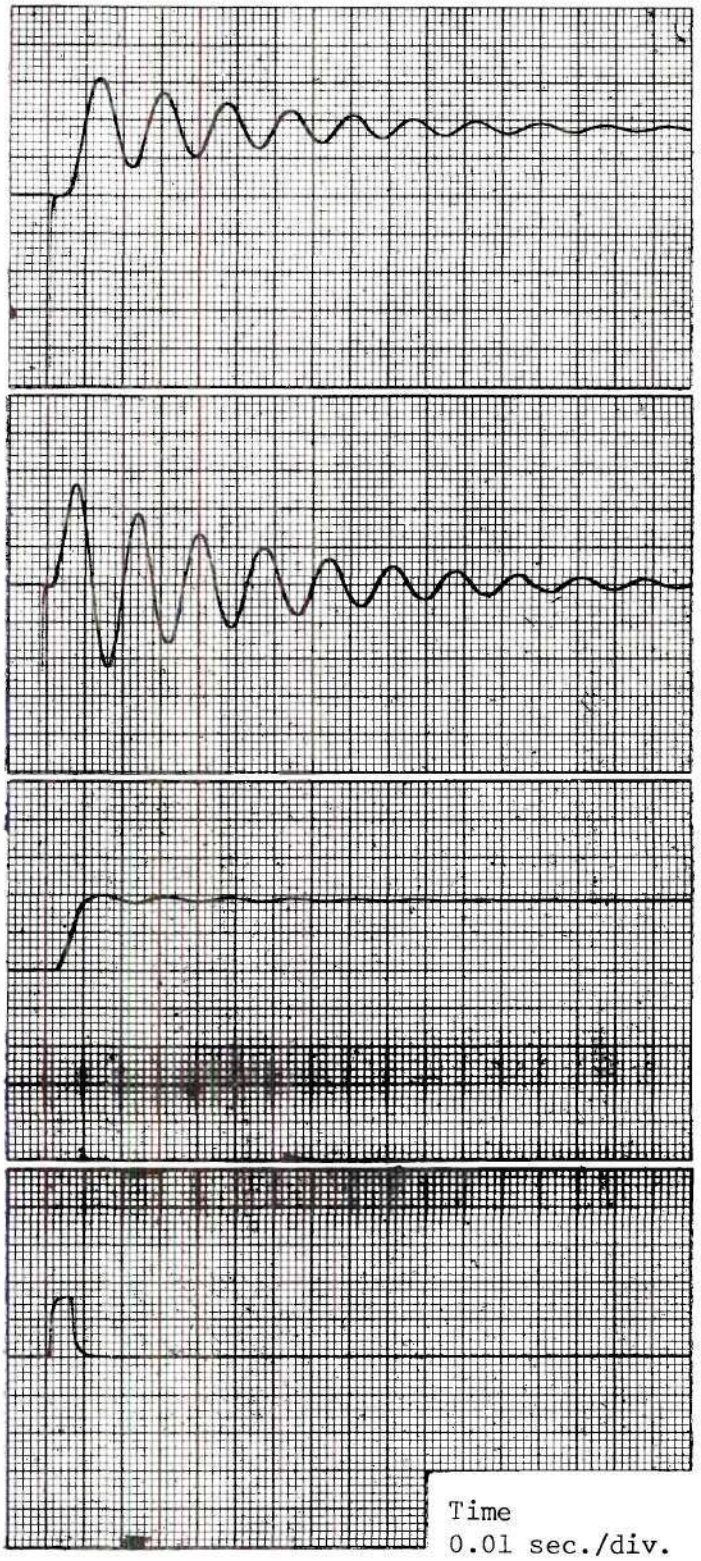

Figure 108. Data Sheet, Analog Simulation: 1/8-in. Step; Rate Coefficient, C_2 = 0.00; DB = 0.042 in.

Engine Position,
40 β_e

1000 mv./line

Engine Rate,
2 $\dot{\beta}_e$

1000 mv./line

Actuator Position, "Real,"
40 α_r

1000 mv./line

Actuator Rate, "Ideal,"
2 $\dot{\alpha}_i$

1000 mv./line

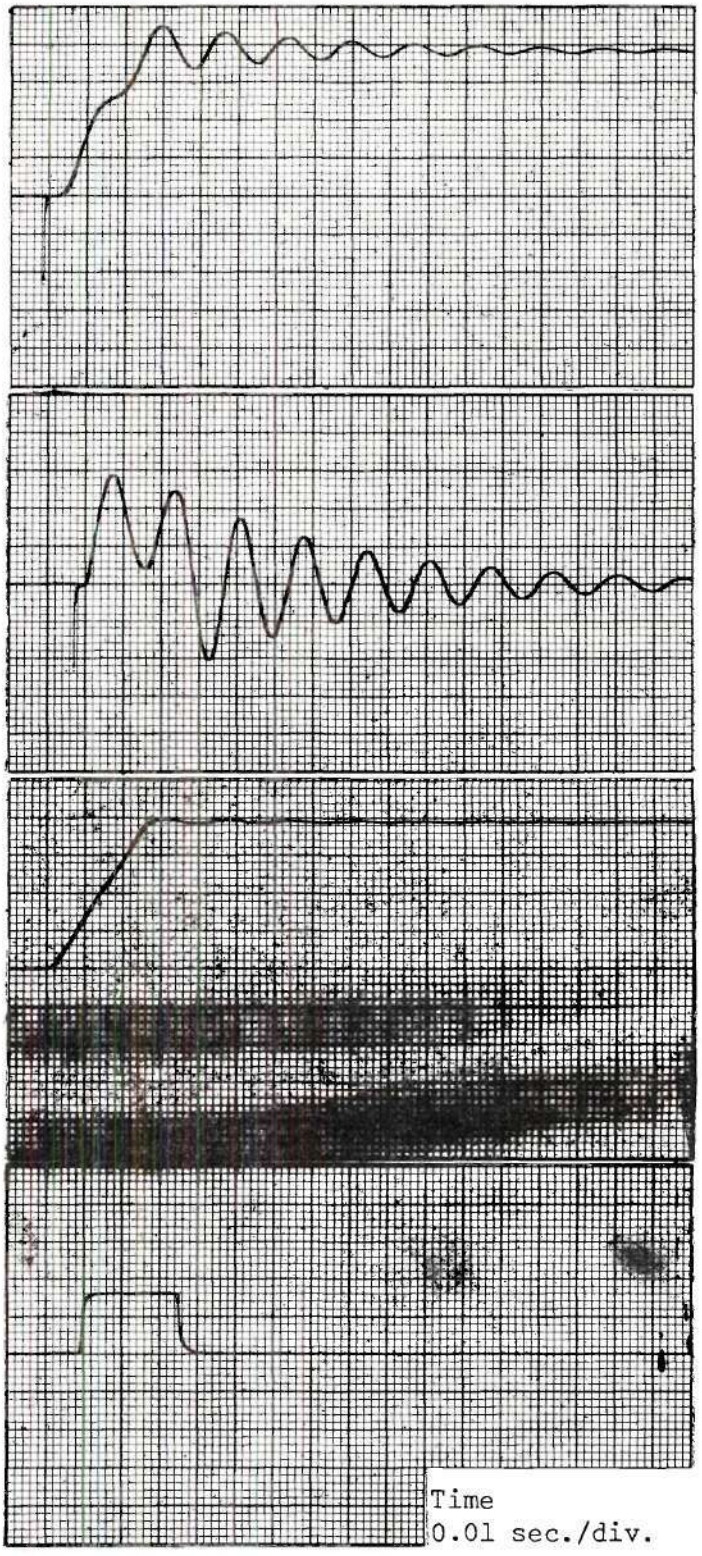

Figure 109. Data Sheet, Analog Simulation: 1/2-in. Step; Rate Coefficient, C_2 = 0.00; DB = 0.042 in.

Engine Position,
40 β_e
500 mv./line

Engine Rate,
2 $\dot{\beta}_e$
1000 mv./line

Actuator Position, "Real,"
40 α_r
500 mv./line

Actuator Rate, "Ideal,"
2 $\dot{\alpha}_i$
1000 mv./line

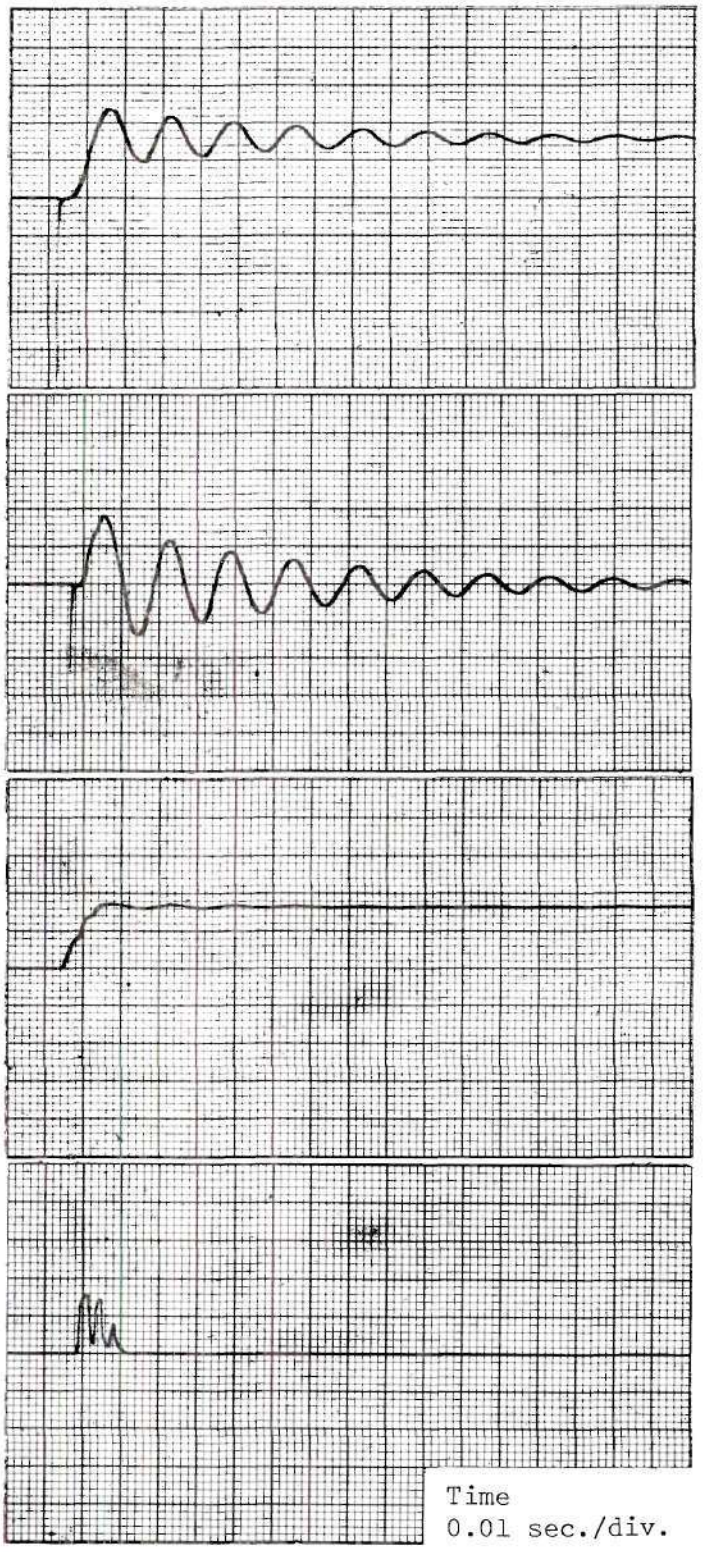

Figure 110. Data Sheet, Analog Simulation: 1/8-in. Step; Rate Coefficient, C_2 = 0.02; DB = 0.031 in.

Engine Position,
$40\ \beta_e$

1000 mv./line

Engine Rate,
$2\ \dot{\beta}_e$

1000 mv./line

Actuator Position, "Real,"
$40\ \alpha_r$

1000 mv./line

Actuator Rate, "Ideal,"
$2\ \dot{\alpha}_i$

1000 mv./line

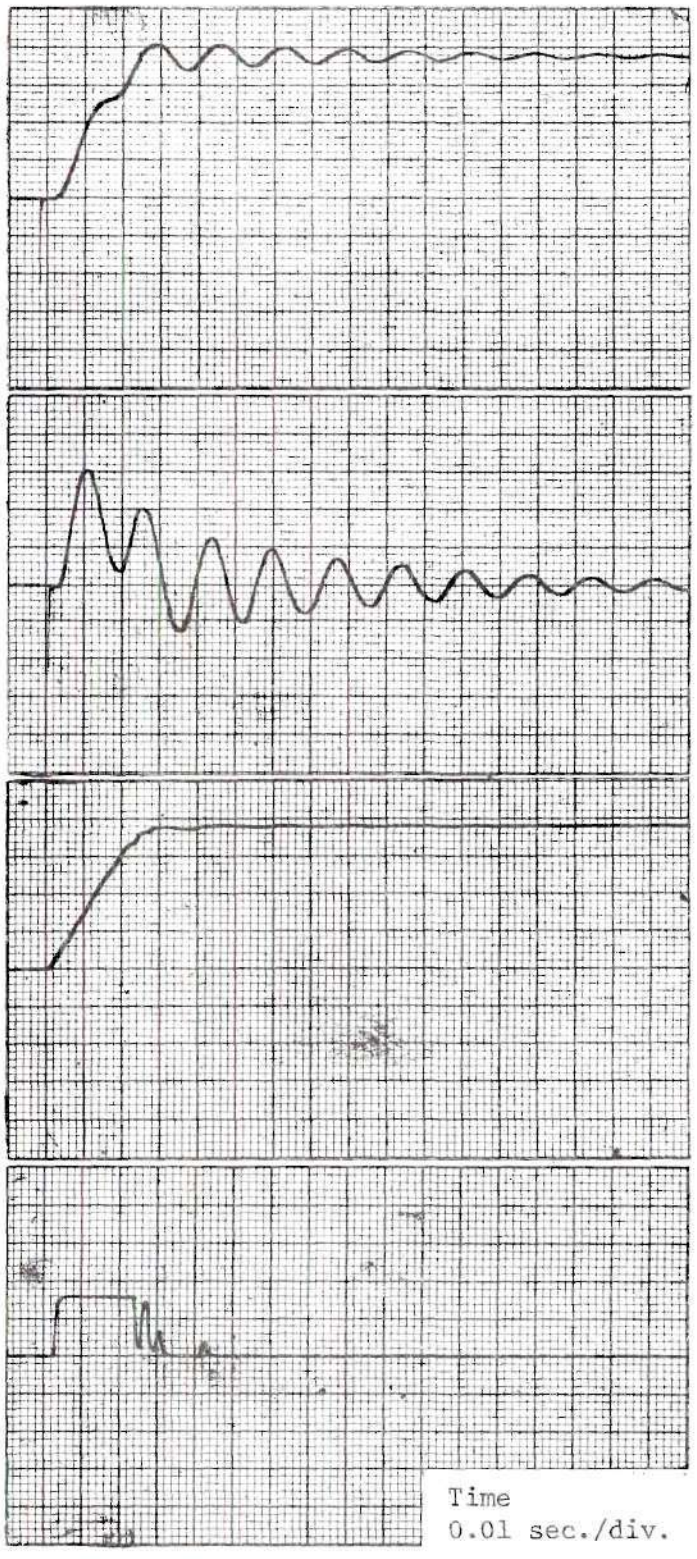

Figure 111. Data Sheet, Analog Simulation: 1/2-in. Step; Rate Coefficient, $C_2 = 0.02$; DB = 0.031 in.

Engine Position,
40 β_e
500 mv./line

Engine Rate,
2 $\dot{\beta}_e$
1000 mv./line

Actuator Position, "Real,"
40 α_r
500 mv./line

Actuator Rate, "Ideal,"
2 $\dot{\alpha}_i$
1000 mv./line

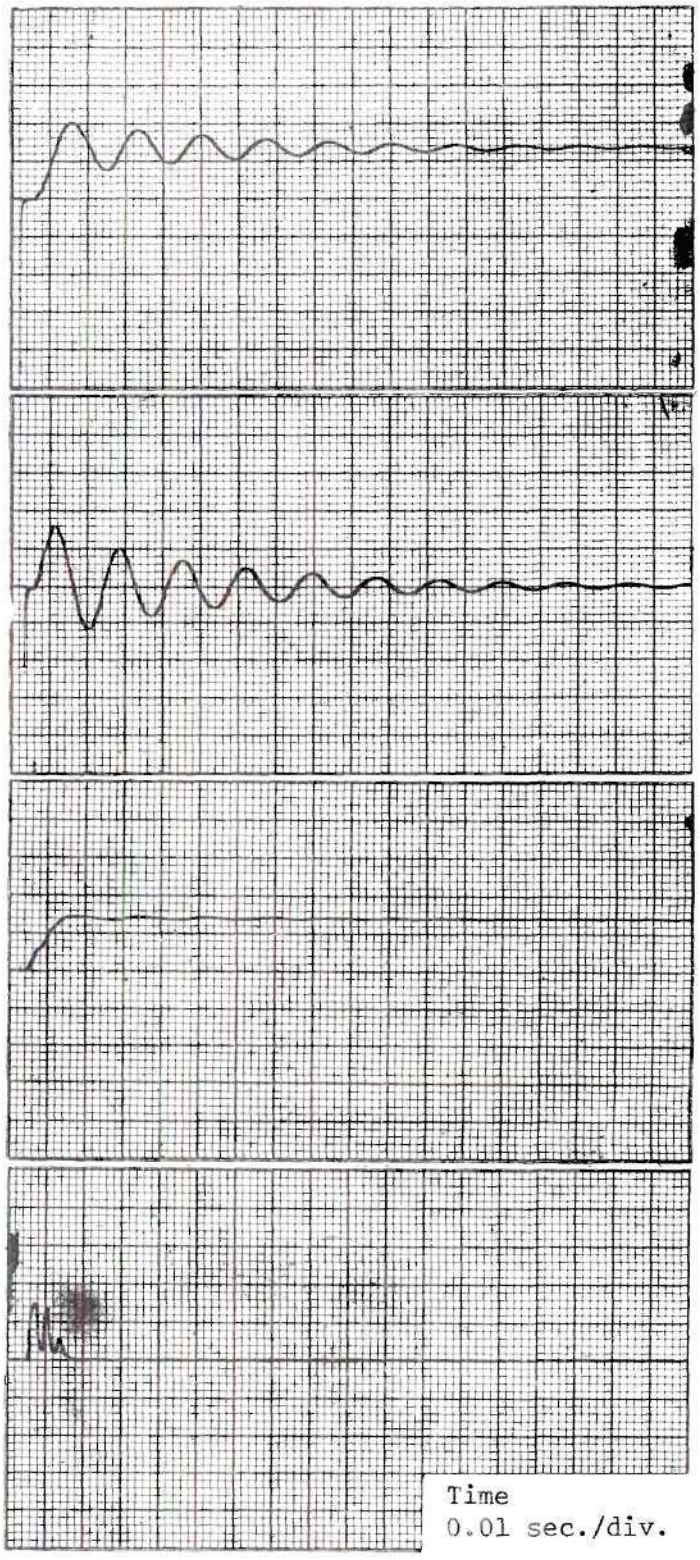

Figure 112. Data Sheet, Analog Simulation: 1/8-in. Step; Rate Coefficient, C_2 = 0.02; DB = 0.042 in.

Engine Position,
40 β_e

1000 mv./line

Engine Rate,
2 $\dot{\beta}_e$

1000 mv./line

Actuator Position, "Real,"
40 α_r

1000 mv./line

Actuator Rate, "Ideal,"
2 $\dot{\alpha}_i$

1000 mv./line

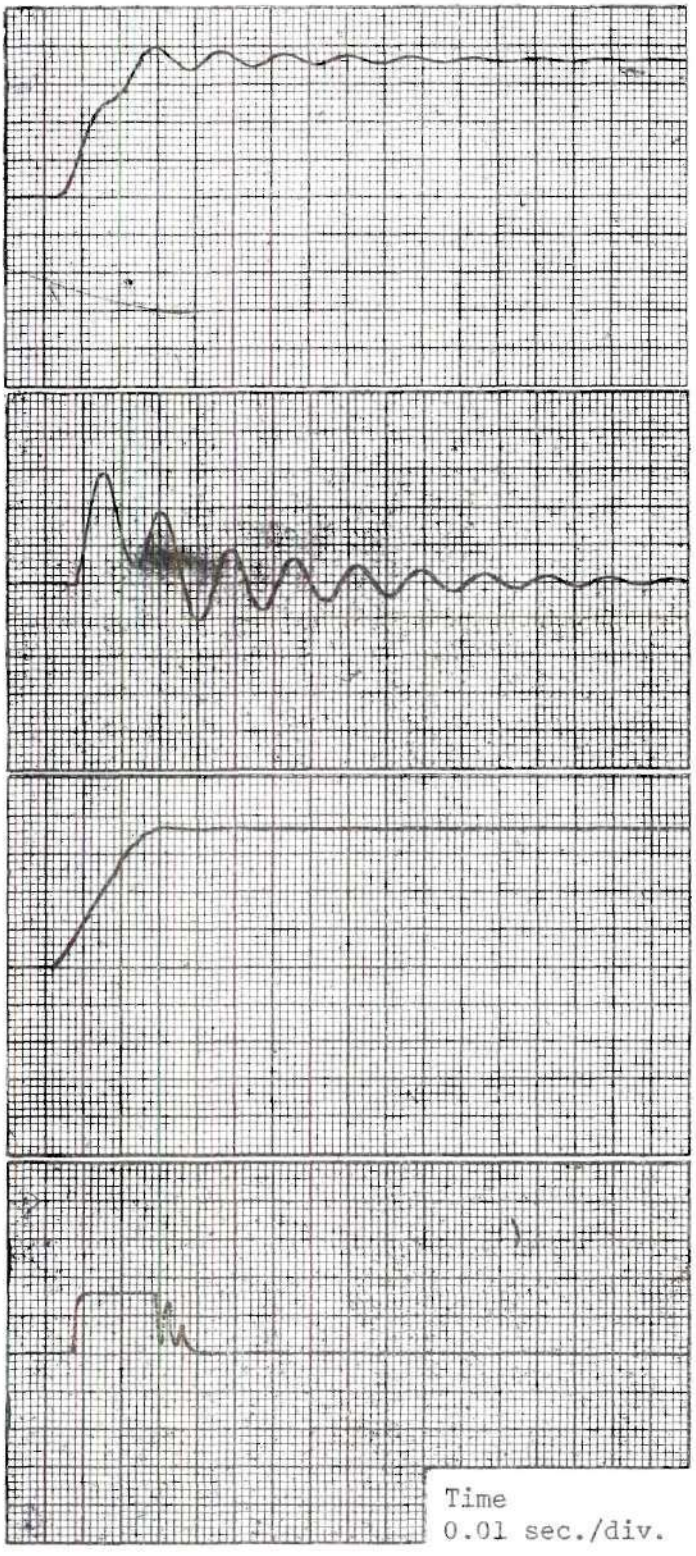

Figure 113. Data Sheet, Analog Simulation: 1/2-in. Step; Rate Coefficient, C_2 = 0.02; DB = 0.042 in.

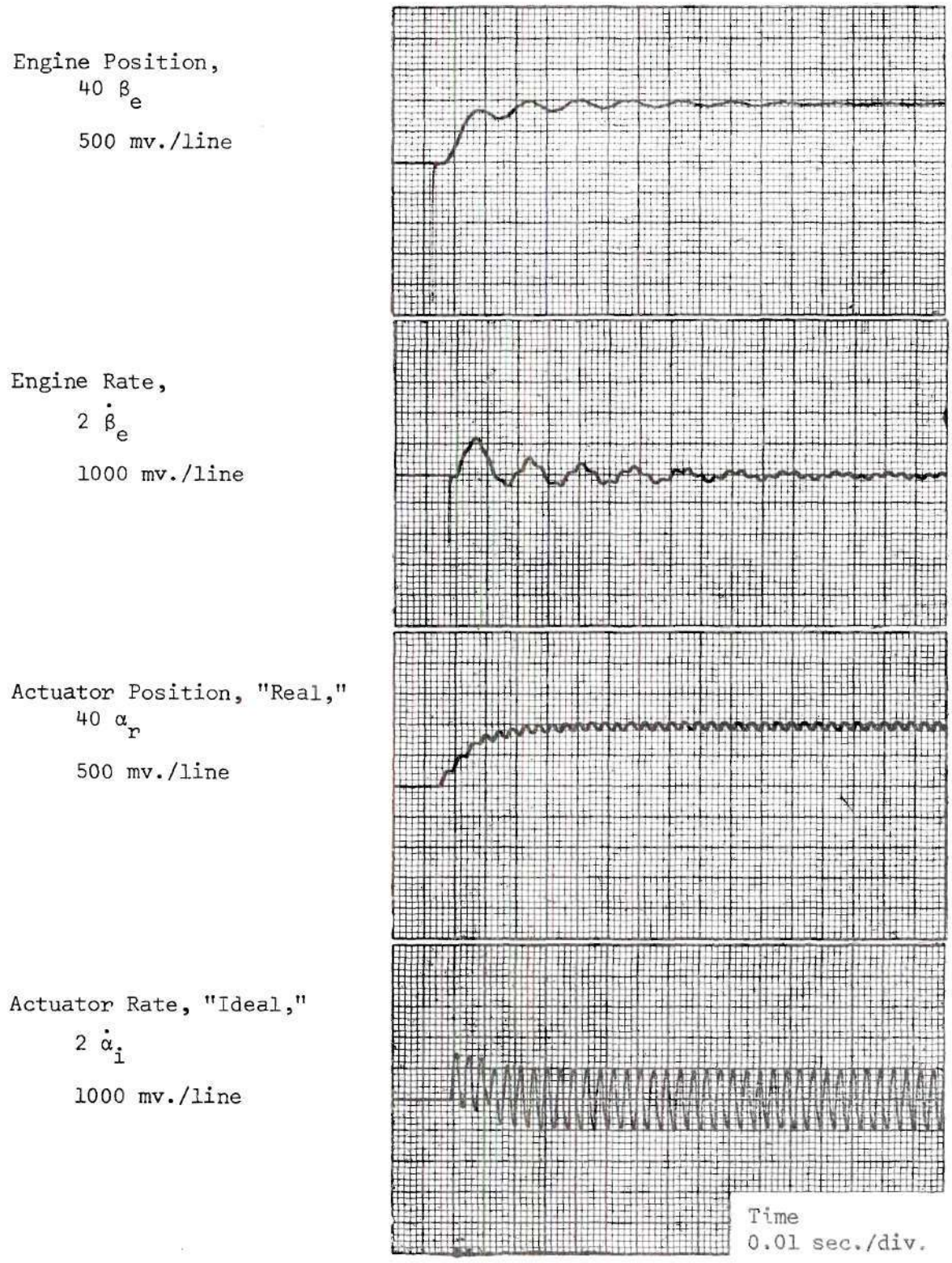

Figure 114. Data Sheet, Analog Simulation: 1/8-in. Step; Rate Coefficient, C_2 = 0.06; DB = 0.031 in.

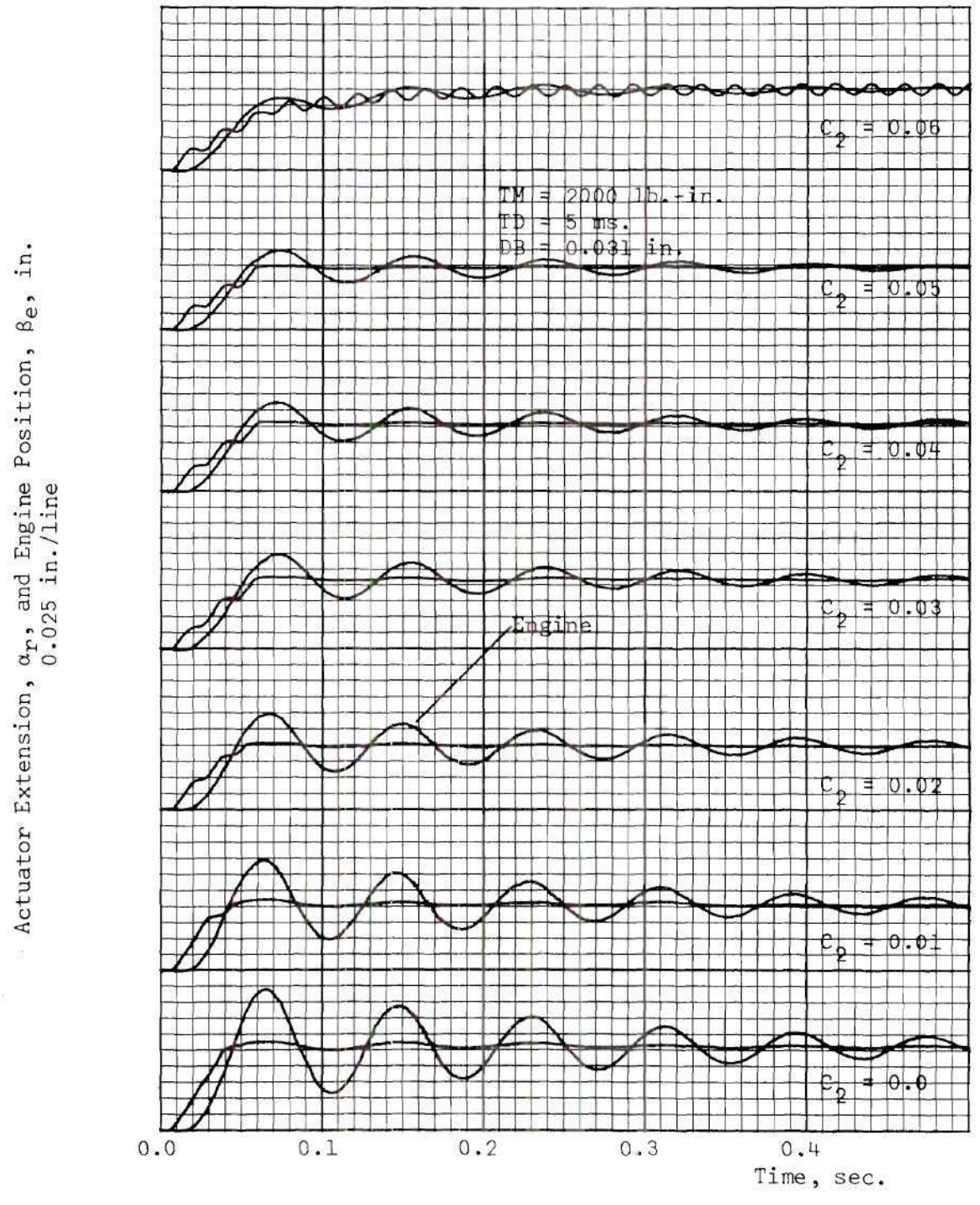

Figure 115. Effect of Variation of Rate Feedback Coefficient, C_2, on Actuator Extension and Engine Position Step Response. Actuation Rate = 4 in./sec., Ref. = 0.125 in.

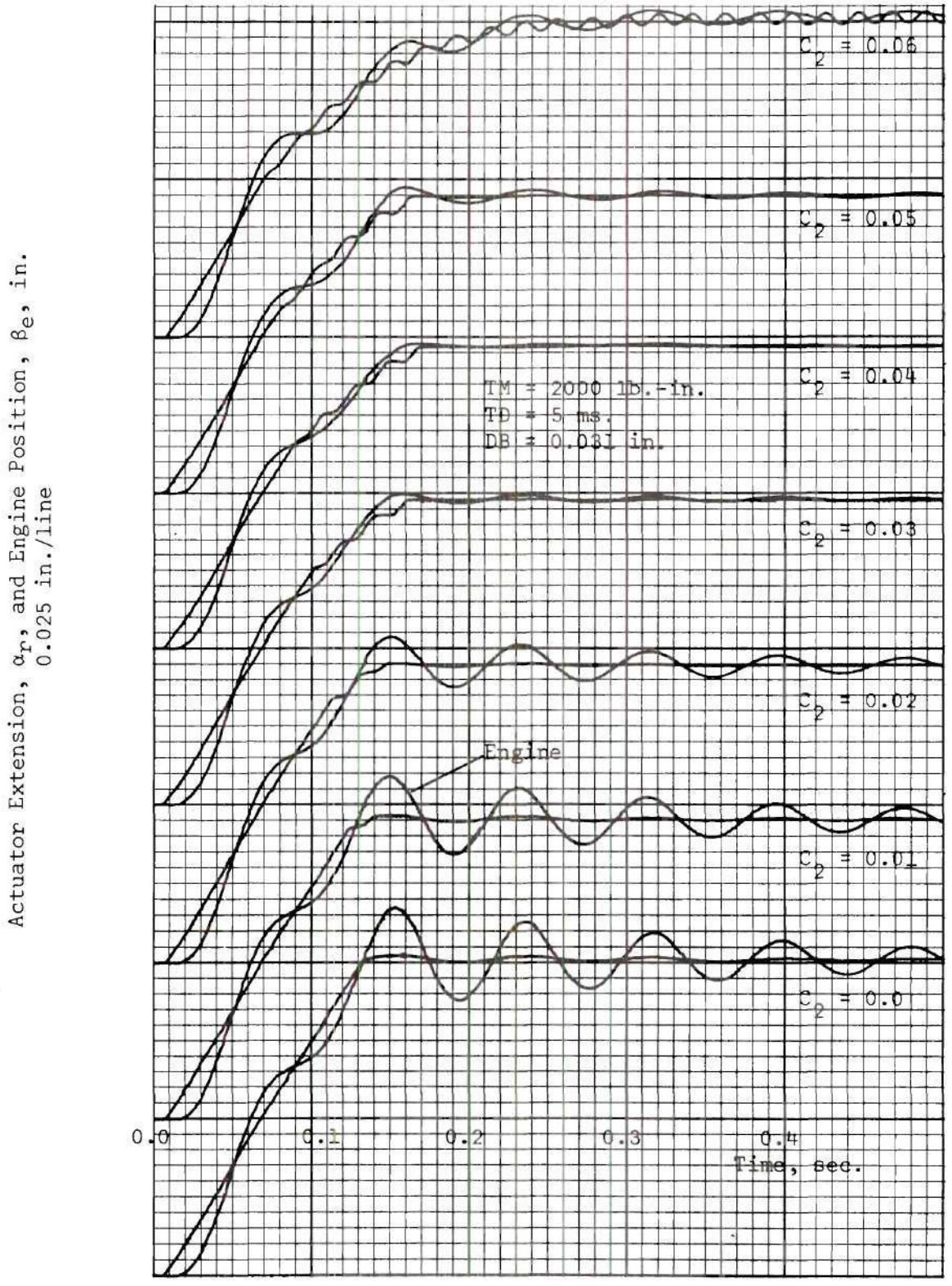

Figure 116. Effect of Variation of Rate Feedback Coefficient, C_2, on Actuator Extension and Engine Position Step Response. Actuation Rate = 4 in./sec., Ref. = 0.50 in.

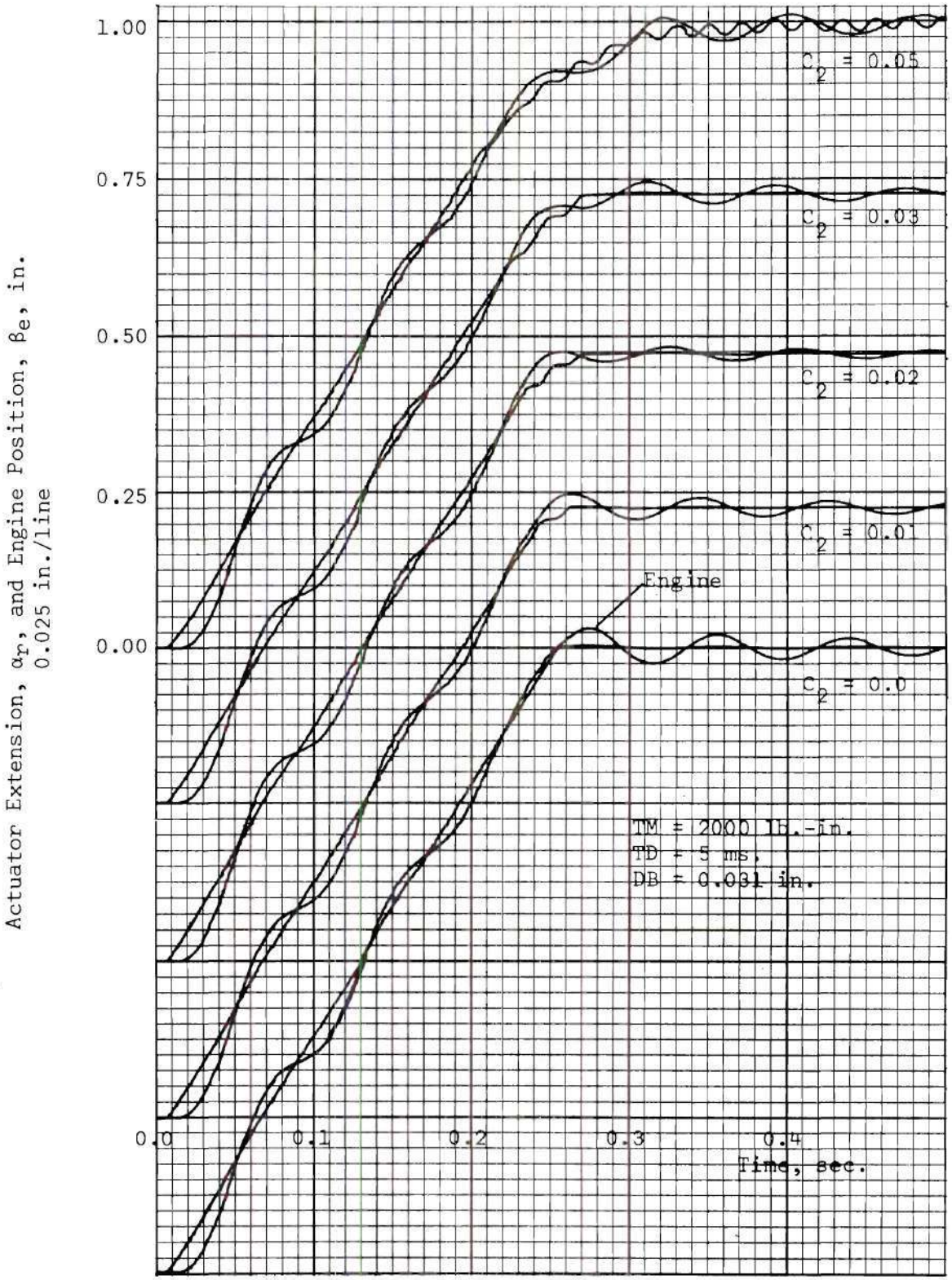

Figure 117. Effect of Variation of Rate Feedback Coefficient, C_2, on Actuator Extension and Engine Position Step Response. Actuation Rate = 4 in./sec., Ref. = 1.0 in.

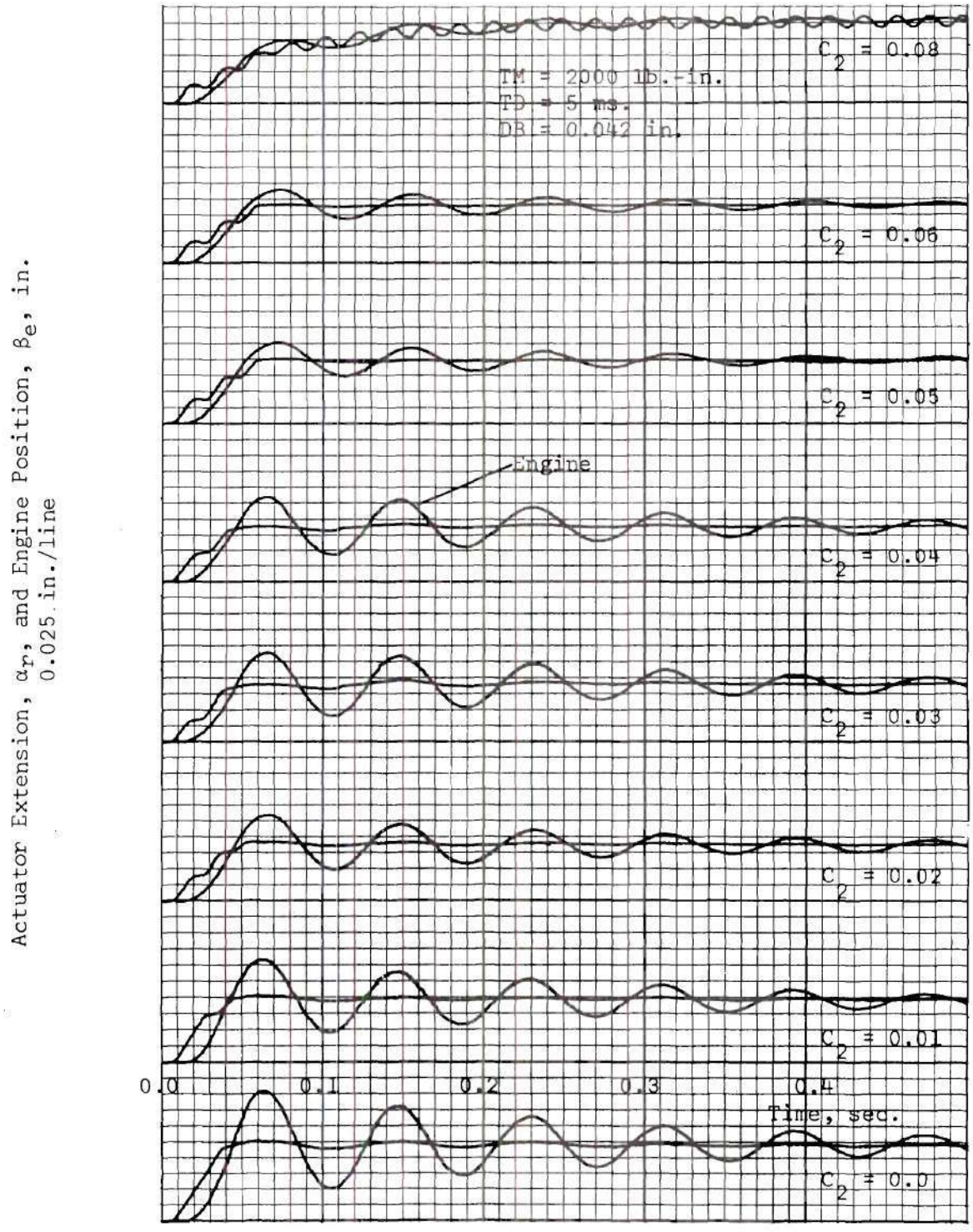

Figure 118. Effect of Variation of Rate Feedback Coefficient, C_2, on Actuator Extension and Engine Position Step Response. Actuation Rate = 4 in./sec., Ref. = 0.125 in., DB = 0.042 in.

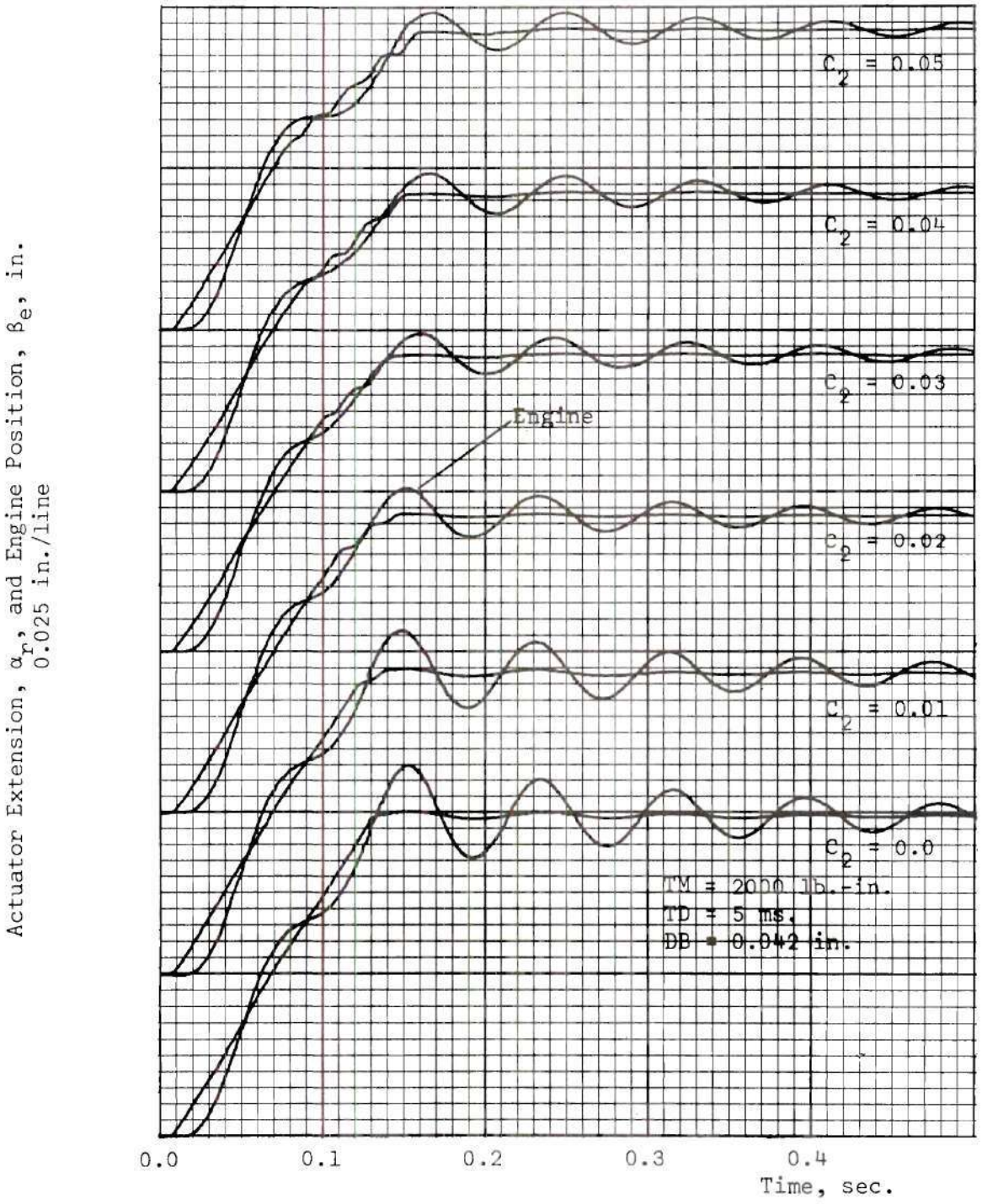

Figure 119. Effect of Variation of Rate Feedback Coefficient, C_2, on Actuator Extension and Engine Position Step Response. Actuation Rate = 4 in./sec., Ref. = 0.50 in., DB = 0.042 in. (Continued)

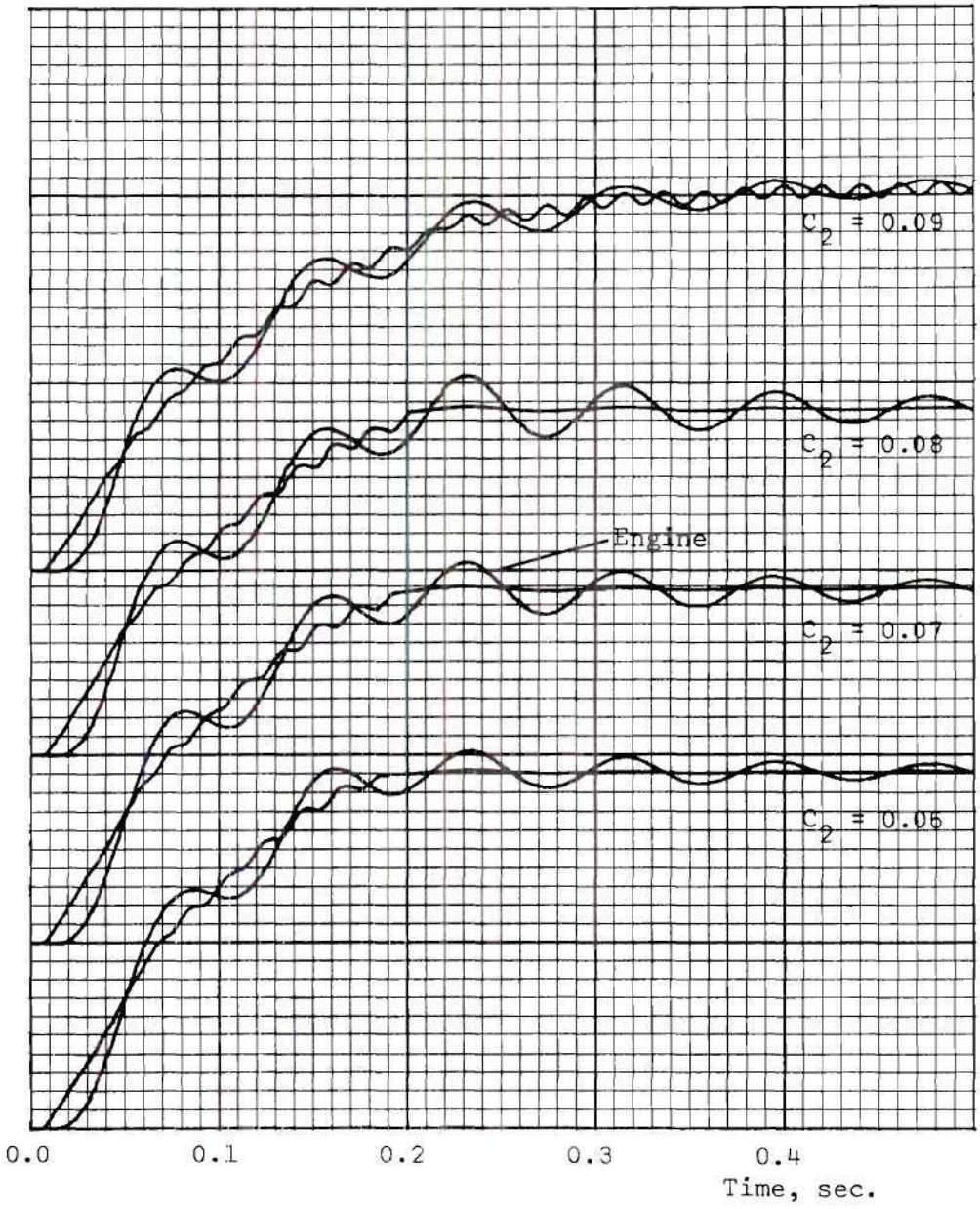

Figure 119. Continued

LITERATURE CITED

1. R. I. Anderson, "Mechanical-Contact Clutches for Space Applications," Master's Thesis, Georgia Institute of Technology, February, 1966.

2. C. A. Depken, "Electro-Magnetic-Flux Clutches for Space Applications," Master's Thesis, Georgia Institute of Technology, July, 1966.

3. "Apollo Servoactuator Design and Performance Data," by the Cadillac Gage Company, West Coast Division, Costa Mesa, California.

4. "Technical Proposal and Program Plan for NASA/MSFC E-M Actuator Study," Proposal No. 677, Fold I, Cadillac Gage Company, West Coast Division, Costa Mesa, California, 1964.

5. Eugene Harrison, "A Survey of Commercially Available Clutches," Final Phase Report--Phase I, Prepared under National Aeronautics and Space Administration Contract No. NAS 8-20071, Georgia Institute of Technology, 1967.

6. W. A. Jones, "An Evaluation of Hydrodynamic Fluid Clutches for Space Applications," Master's Thesis, Georgia Institute of Technology, May, 1966.

7. Depken, pp. 3-4.

8. D. L. Swords, "Magnetic Clutches for Continuous Slip," *Product Engineering*, Vol. 32, Pt. 2, August 28, 1961, pp. 23-28.

9. Depken, pp. 42-45.

10. Anderson, pp. 48-49.

11. Anderson, p. 26.

12. Anderson, pp. 32, 50.

13. J. Kaplan, "Slip Clutches and Brakes," *Machine Design*, pp. 115-117, January 22, 1959.

14. J. Kaplan, "How to Calculate the Dynamic Load Capacity of Spring Clutches," *Machine Design*, pp. 105-109, April 4, 1957.

15. C. R. Schreiber, "The Curtiss 173300 Small Missile Servo System," Report No. PD-511C, Curtiss-Wright Corporation, Curtiss Division, Caldwell, New Jersey, December 7, 1964.

16. J. E. Gibson, *Nonlinear Automatic Control*, McGraw-Hill Book Company, Inc., New York, N. Y., 1963.

17. B. J. Kuo, *Automatic Control Systems*, Prentice-Hall, Inc., Englewood Cliffs, N. J., 1962, pp. 470-474.

18. Anderson, pp. 11-12.

19. Anderson, p. 16.

20. W. B. Duncan and W. V. Surman, Jr., "Analysis of an ON-OFF Modulated Clutch Servomechanism," Master's Thesis, United States Naval Postgraduate School, 1960.

21. K. K. Gowdy, "Design of Third-Order Linear Systems," Paper No. 11, *Proceedings of the Fluid Power Research Conference*, Oklahoma State University, July, 1967.

22. Kuo, pp. 127-130.

23. "Design Guide for Ball Bearing Screws and Splines," Saginaw Steering Gear Division, General Motors Corporation.

OTHER REFERENCES

"A Thrust Vector Control Actuator for Missile Flight Path Control," Report No. GREM-109, Lear, Inc., Grand Rapids, Michigan, 1962.

Chironis, N. P., and Yeaple, F. D., "New Clutch Designs Depend on Spring Windup," *Product Engineering*, May 23, 1966, pp. 52-55.

Churchill, R. V., *Operational Mathematics*, Second Edition, McGraw-Hill Book Company, New York, N. Y., 1958.

Gregory, W. P., and Hungerford, P. C., "A Versatile New Engineering Tool--the Precision Spring Clutch," ASME Paper No. 57-A-244, Presented at ASME Annual Meeting, New York, N. Y., December 1-6, 1957.

Hamilton, M. J., "Design of a Hydraulic Gimbal System for a Moon Mission Booster Stage," *Proceedings of the Aerospace Fluid Power Systems and Equipment Conference*, Los Angeles, California, May 18-20, 1965, pp. 31-39.

Hildebrand, F. B., *Methods of Applied Mathematics*, Prentice-Hall, Inc., Englewood Cliffs, N. J., 1952.

Johnson, C. L., *Analog Computer Techniques*, Second Edition, McGraw-Hill Book Company, Inc., New York, N. Y., 1963.

Kalange, M. A., and Alcott, R. J., "Saturn V S-IC Stage Engine Gimbal Actuation System," *Proceedings of the Aerospace Fluid Power Systems and Equipment Conference*, Los Angeles, California, May 18-20, 1965. pp. 1-20.

Kaplan, J., and Marshall, D., "Design Equations and Nomographs for Self-Energizing Type of Spring Clutches," *Machine Design*, April 19, 1956.

Kaplan, J., "Latest Development in Spring-Wrapped Slip Clutches," *Product Engineering*, August 31, 1959.

Kaplan, J., "You Can Whip the Backlash in Spring Clutches," *Product Engineering*, August 31, 1959.

Katnik, R. L., "Electromagnetic Disc Clutches," *Machine Design*, April 4, 1960, pp. 113-122.

Kohlmeyer, K. W., "5 Clutches for Servomechanisms," *Product Engineering-Design Digest Issue*, Mid-September, 1960, pp. 396-400.

Koester, R. H., "Principles of Non-Linear Servo Operation," Report No. PD-468, Curtiss-Wright Corporation, Curtiss Division, Caldwell, New Jersey, February 14, 1964.

Koester, R. H., "Servo Actuators for Small Missile Steering Controls," Report No. PD-477C, Curtiss-Wright Corporation, Curtiss Division, Caldwell, New Jersey, February 25, 1964.

Leonard, E. V., "Spring Clutches for Faster Response," *Product Engineering*, Vol. 29, No. 15, April 14, 1958, pp. 57-59.

McGillen, V. W., and Jacobs, M. R., "The Saturn S-II Stage Engine Actuation System," *Proceedings of the Aerospace Fluid Power Systems and Equipment Conference*, Los Angeles, California, May 18-20, 1965, pp. 21-30.

"Miniature Magnetic Clutches and Brakes," *Electromechanical Design*, May 1962, pp. 62-78.

Nelson, W. G., "Development of Fluid Power Techniques for Lunar Environments," *Proceedings of the Aerospace Fluid Power Systems and Equipment Conference*, Los Angeles, California, May 18-20, 1965, pp. 40-55.

Pech, J. F., and Miele, J., "Miniature Electric Clutches and Brakes, Part 1--Friction Disc Types," *Machine Design*, April 15, 1965, pp. 150-158.

Pech, J. F., and Miele, J., "Miniature Electric Clutches and Brakes, Part 2--Nonfriction Types," *Machine Design*, April 29, 1965, pp. 223-227.

"Principle of Operation of FORCE Magnetic Particle Clutches," Catalog F-65, Force Limited, Santa Monica, California.

Proctor, J. S., "How to Select Electromagnetic Clutches and Brakes for Automatic Control," *Product Engineering*, December 19, 1960.

Proctor, J. S., "Selecting Clutches for Mechanical Drives," *Product Engineering*, Vol. 32, Pt. 2, June 19, 1961, pp. 43-58.

Rudnirkas, V. W., and Fine, R. A., "Basic Design of Spring Clutches," *Machine Design*, May 13, 1965, pp. 182-186.

Saliatesta, "Realistic Ways to Speed Response of DC Clutches and Brakes," *Product Engineering*, Vol. 32, No. 4, 1961, pp. 41-44.

Thaler, G. J., and Pastel, M. P., *Analysis and Design of Nonlinear Feedback Control Systems*, McGraw-Hill Book Company, Inc., New York, N. Y., 1962.

Wiebusch, C. F., "The Spring Clutch," *Journal of Applied Mechanics*, September, 1939, pp. A-103--A-108.

VITA

James Glynn Wright, Jr. was born in Forsyth, Georgia, on January 1, 1938. In June, 1956, he graduated from Mary Persons High School in Forsyth, Georgia. He entered the Georgia Institute of Technology the same month and graduated in June, 1961, receiving the degree of Bachelor of Mechanical Engineering (Co-operative Plan, With Honor).

In August, 1961, he joined the Georgia Power Company, Macon, Georgia, for three months, after which he resigned to accept employment with the U. S. Naval Ordnance Plant, Macon, Georgia, where he remained until September, 1962. Awarded a National Defense Education Act Fellowship, he returned to Georgia Tech to pursue the Doctorate in Mechanical Engineering. During his graduate study he worked two summers (1963 and 1964) at Lockheed-Georgia Company, Marietta, Georgia, in the Mechanical and Hydraulic Systems Group.

Mr. Wright was married in December, 1961, to the former Geraldine Odessa Neal. They have a son, James Glynn Wright, III.